



UNIVERSIDADE DE BRASÍLIA
INSTITUTO DE GEOCIÊNCIAS

GÊNESE, EVOLUÇÃO E SIGNIFICADO GEOTECTÔNICO DO
COMPLEXO ALCALINO-CARBONATÍTICO TRÊS ESTRADAS,
RS

TESE DE DOUTORADO Nº 167

CIMARA MONTEIRO BOGO

ORIENTADOR: PROF. DR. JOSÉ AFFONSO BROD

BRASÍLIA, 2020



UNIVERSIDADE DE BRASÍLIA
INSTITUTO DE GEOCIÊNCIAS

PROGRAMA DE PÓS-GRADUAÇÃO EM GEOLOGIA

GÊNESE, EVOLUÇÃO E SIGNIFICADO GEOTECTÔNICO DO
COMPLEXO ALCALINO-CARBONATÍTICO TRÊS ESTRADAS,
RS

TESE DE DOUTORADO Nº 167

CIMARA MONTEIRO BOGO

ORIENTADOR: PROF. Dr. JOSÉ AFFONSO BROD (IESA – UFG)

EXAMINADORA INTERNA: PROF^a. Dra. CATARINA LABOURÉ BEMFICA TOLEDO
(IG – UnB)

EXAMINADOR EXTERNO: PROF. Dr. FARID CHEMALE Jr. (PPG – UNISINOS)

EXAMINADOR EXTERNO: PROF. Dr. MARCUS VINICIUS DORNELES REMUS (IGEO
– UFRGS)

BRASÍLIA, Setembro de 2020

BB675g Bogo, Cimara Monteiro
 Gênese, evolução e significado geotectônico do Complexo
 Alcalino-Carbonatítico Três Estradas, RS / Cimara Monteiro
 Bogo; orientador José Affonso Brod. -- Brasilia, 2020.
 179 p.

 Tese (Doutorado - Doutorado em Geologia) -- Universidade
 de Brasilia, 2020.

 1. Complexo Três Estradas. 2. carbonatito. 3. Escudo Sul
 Riograndense. 4. Mesoproterozoico. 5. mineralização em
 fosfato. I. Brod, José Affonso, orient. II. Título.

Dedico essa tese a minha família.

A minha mãe, Maria Nilda, que não me deixou desistir,
Ao meu marido, Allan Bogo, que me apoiou incondicionalmente,
A minha irmã, Nara, minha naninha e minha pessoa nesse mundo, e
Ao Fernando, que está só começando sua caminhada.

AGRADECIMENTOS

Ao Professor Dr. Márcio Martins Pimentel, que me acolheu e se dispôs a me orientar, pelas palavras sempre gentis e por sua disponibilidade em ensinar. Um dos maiores geocientistas do Brasil, reconhecido no mundo e que deixou imenso legado às geociências. Que se registrem meu respeito e deferência a sua pessoa e ao seu trabalho.

Ao Professor Dr. José Affonso Brod, por ter aceitado me orientar após a partida do Professor Márcio Pimentel. Agradeço por compartilhar seu notável conhecimento no campo da geologia de carbonatitos e pela confiança em mim.

À empresa Águia Resources Ltd que, por meio de sua subsidiária Águia Metais Ltda, sob a direção do Dr. Fernando Tallarico e presidência do Sr. Hélio Diniz, me forneceu acesso aos afloramentos, aos testemunhos de sondagem, aos resultados químicos, às análises de DRX e às lâminas petrográficas utilizados na elaboração desta tese.

À CAPES pelo financiamento parcial desta tese. O presente trabalho foi realizado com o apoio da Coordenação de Aperfeiçoamento de Pessoal de Nível Superior - Brasil (CAPES) - Código de Financiamento 001.

Ao Me. Ítalo Lopes de Oliveira e ao Dr. Pedro Cordeiro por terem atuado intensamente como meus coorientadores informais, pelas inúmeras discussões, revisões e correções dos artigos, pela disponibilidade e pelo apoio irrestrito. Um Muito Obrigado especial a vocês!

Ao Me. Érico N. P. Zacchi, sem o qual essa tese não teria nascido, pela execução e processamento de todas as análises geocronológicas U-Pb e Zr-Hf, por todas as explicações e discussões, pela paciência sem tamanho, pelo apoio, pela parceria e por ser minha família.

Ao Dr. Carlos Ganade pelos aportes de conhecimento, pela orientação, por todas as revisões, por todas as dúvidas sanadas, pelo apoio e amizade.

Ao Professor Dr. Reinhardt A. Fuck pela destacada paciência em revisar meu manuscrito todas as vezes que eu solicitei ajuda.

Ao Professor Dr. Elton L. Dantas pelas contribuições que enriqueceram essa tese.

À Dra. Joseneusa B. Rodrigues pelas discussões.

Ao Dr. Rodrigo R. Adôrno, sempre de prontidão a ajudar, pelo imenso trabalho de fazer a primeira tradução dos artigos do português para o inglês.

Ao Me. Noevaldo A. Araujo, chefe do Centro de Desenvolvimento Tecnológico do SGB-CPRM, mestre não só no título acadêmico, mas um dos meus mestres na vida profissional, a

quem agradeço pela troca de ideias no campo desta tese. Meu agradecimento especial por ter me dado a oportunidade de aprender e ganhar tanta experiência com você, sem dúvida alguma um dos maiores geólogos desse país, seja como prospector, seja como gestor.

Ao Sr. Paulo Romano, diretor de Infraestrutura Geocientífica do SGB-CPRM, pela compreensão durante a redação final dessa tese.

Ao Serviço Geológico do Brasil-CPRM pelo incentivo institucional à execução desta tese.

Aos Professores. Dr. Derméval A. do Carmo e a Dra. Roberta Vidotti que, durante a vigência de seus períodos de coordenação à frente do Programa de Pós-Graduação em Geologia, me prestaram todas as informações e me apoiaram para chegar ao fim.

Aos Professores Dra. Adalene Moreira Silva, Dra. Catarina Toledo Bemfica Labourè, Dr. Claudinei Gouveia de Oliveira, Dra. Maria Emilia Schutesky della Giustina, que cada um ao seu jeito, me auxiliaram durante o período do curso de doutorado.

Aos funcionários do Instituto de Geociências da UnB por toda ajuda, nas pessoas da Sra. Francisca e da Sra. Alice.

Aos meus saudosos amigos da Águia Metais Ltda, Alfredo Rossetto Nunes, Lucas Galinari, Daniel Matteo, Luiz Mauro Martins, Willy Hochleitner, Roberto Pinheiro, Wagner Zazá, Carlos Martins e nosso querido mestre José Fanton, pela amizade e pelos aprendizados.

À minha mãe, Maria Nilda Francisca Monteiro, por sempre acreditar em mim, por torcer pelas minhas vitórias, por ter me dado minha irmã e especialmente por ter me incentivado a iniciar e, principalmente, a concluir esta tese. Mãe, muito obrigada!

Ao meu pai, Cincinato Monteiro Neto, por ter investido e acreditado na educação de suas filhas como um bem maior até os seus últimos dias de vida.

À minha irmã, Nara, minha melhor amiga, por estar sempre ao meu lado, por existir e por ter me dado meu sobrinho Fernando que alegra meus dias.

Ao meu marido, Allan Rodrigo Bogo, pela incrível paciência, pelo amor, pelo companheirismo, pelos cafés da manhã, por cuidar de mim, por me incentivar todo o tempo e por ter aceitado caminhar ao meu lado.

Aos meus familiares pela torcida e orações.

E enfim, assim como o fiz na dissertação de mestrado, agradeço a todos os meus amigos, companheiros de vida e de trabalho na pessoa de um grande amigo, Balduíno Neto.

Cimara Monteiro Bogo. Brasília, setembro de 2020.

RESUMO

O Complexo Alcalino-Carbonatítico Três Estradas (CTE) representa a primeira intrusão de carbonatito identificada no Escudo Sul-Riograndense (ESRG), sul do Brasil. É compreendido por calcita metacarbonatitos, dolomita metacarbonatitos, rochas metaultramáficas e metassienitos alojados em gnaisses arqueanos do Terreno Taquarembó, remanescente do Cráton Rio de la Plata. O CTE posiciona-se ao longo da zona de cisalhamento transcorrente sinistral Cerro dos Cabritos, a 800m do Lineamento Ibaré, tido como uma zona de sutura neoproterozoica formada no final da Orogênese Dom Feliciano. Deformação heterogênea e evidências de metamorfismo em fácies xisto verde a anfibolito podem ser encontradas em todo o complexo, com porções preservadas exibindo foliação e bandamento de fluxo ígneos.

As idades U-Pb em zircão revelam que o CTE foi formado no Mesoproterozoico, mostrando idades de cristalização de $1.110 \pm 4,8$ Ma e 1.123 ± 15 Ma em dolomita metacarbonatito e metassienito, respectivamente. Geoquímica de rocha total, dados de isótopos estáveis (C-O) e radiogênicos (Nd-Sr-Hf) indicam que o magma parental das rochas do CTE provavelmente derivou de fonte mantélica heterogênea metassomatizada enriquecida em CO₂. Alguma contribuição menor do Complexo Santa Maria-Chico também pode ter ocorrido, dada a presença de um cristal de zircão paleoproterozoico herdado em dolomita metacarbonatito. Idades-modelo T_{DM}(Nd) para todo o CTE variam entre 1,18 e 1,62 Ga, sendo as idades mais velhas relacionadas aos dolomita metacarbonatitos (1,48 a 1,62 Ga), intermediárias relacionadas às rochas metaultramáficas (1,37 a 1,50 Ga) e as idades-modelo mais jovens associadas à calcita metacarbonatitos (1,18 a 1,55 Ga). A evolução magmática mais provável do CTE envolveu uma relação complicada de processos de cristalização fracionada, imiscibilidade de líquidos e metassomatismo/desgaseificação. Propõe-se que os dolomita carbonatitos derivaram diretamente do magma parental via imiscibilidade de líquidos, enquanto as rochas ultramáficas provavelmente foram formadas por cristalização fracionada do mesmo magma. Os calcita metacarbonatitos podem representar a cristalização de líquido residual após a formação das rochas ultramáficas. Além disso, soluções ricas em K e Na liberadas por magmas carbonatíticos metassomatizaram as rochas ultramáficas e sieníticas, desenvolvendo fenitos potássicos e sódicos.

Curiosamente, há uma similaridade notável entre as assinaturas isotópicas de Nd-Sr dos metacarbonatitos do CTE e carbonatitos mesoproterozoicos da Província Alcalina de Ontário, Canadá. Tal comparação reforça uma hipótese proposta por vários autores recentemente que a Laurentia e o Cráton Rio de la Plata estiveram conectados no fim do Mesoproterozoico, durante a formação do supercontinente Rodínia. Estas intrusões canadenses foram alojadas simultaneamente ao evento magmático extensional Keweenawan (1.110-1.090 Ma), o qual é marcado por vasto vulcanismo basáltico, e à geração do enxame de diques Abitibi (1.160-1.140 Ma), ambos associados a processos de rifteamento intracontinental, os quais podem ser temporalmente relacionados ao CTE. Na história evolutiva do ESRG, a colocação do CTE antecede à formação de crosta oceânica em 920 Ma, que deu origem ao Proto-oceano Adamastor ou Oceano Charrua. Este oceano fechou no final do Neoproterozoico com a formação do supercontinente Gondwana, por volta de 540 Ma, provavelmente culminando na deformação e metamorfismo das rochas do CTE.

A comparação entre feições texturais, composições mineralógicas e assinaturas geoquímicas do CTE com outros carbonatitos do ESRG (i.e. Picada dos Tocos - $603,2 \pm 4,5$ Ma, U-Pb em zircão; e Passo Feio, considerado Neoproterozoico), sugerem mesma fonte de manto astenosférico e processos de fusão semelhantes para essas rochas. Entretanto, idades de cristalização muito distintas foram propostas para esses carbonatitos, sugerindo magmatismo carbonatítico recorrente no sul do Brasil, ao longo do tempo geológico. A recorrência de magmatismo carbonatítico também é reportada em outros terrenos antigos, como Ontário e SW Quebec, no Canadá, Groelândia e Norte da Europa (Península de Kola).

A complexidade petrológica envolvida na gênese de complexos carbonatíticos também é responsável pela geração de ocorrências minerais. O CTE contém recurso mineral medido de 36 Mt @ 4.01% P₂O₅, recurso mineral indicado de 47 Mt @ 4.18% P₂O₅ e recurso mineral inferido de 21.8 Mt @ 3.67% P₂O₅, usando teor de corte de 3.0% de P₂O₅. O fosfato é proveniente da estrutura da apatita, que está hospedada em metacarbonatitos. Embora tenham concentrações consideráveis de P₂O₅, as rochas metaultramáficas não apresentam boa recuperação metalúrgica. O principal controle de ocorrência dos carbonatitos são as zonas de falha/fratura antigas.

Palavras-chave: Complexo Três Estradas; carbonatito; Escudo Sul-Riograndense; Mesoproterozoico; mineralização em fosfato.

ABSTRACT

The Três Estradas Alkaline-Carbonatite Complex (TEC) represents the first carbonatite intrusion discovered in the Sul-Riograndense Shield (SRS), southern Brazil. It comprises calcite metacarbonatites, dolomite metacarbonatites, metaultramafic rocks and metasyenites hosted in archean gneisses of the Taquarembó Terrane, a remnant of the Rio de la Plata Craton. The TEC lies along the sinistral Cerro dos Cabritos transcurrent shear zone, ca. 800m from the Ibaré Lineament, a major neoproterozoic suture zone formed by the end of the Dom Feliciano Orogenesis. Heterogeneous deformation and evidence of greenschist to amphibolite facies metamorphism can be found in the entire complex, with preserved portions showing flow foliation and banding.

The U-Pb ages in zircon reveal that the TEC was formed in the Mesoproterozoic, showing crystallization ages of $1,110 \pm 4.8$ Ma and $1,123 \pm 15$ Ma for dolomite metacarbonatite and metasyenite, respectively. Whole-rock geochemistry, stable (C-O) and radiogenic (Nd-Sr-Hf) isotope data indicate that the parental magma of the TEC rocks probably derived from a metasomatized heterogeneous mantle source enriched in CO₂. Some minor contribution of the Santa-Maria Chico Granulitic Complex also may have occurred given the presence of one inherited paleoproterozoic zircon crystal in dolomite metacarbonatite. TDM (Nd) model-ages for the whole TEC vary between 1.18 and 1.62 Ga, being the oldest ages related to dolomite metacarbonatites (1.48 to 1.62 Ga), intermediate ones related to the metaultramafic rocks (1.37 to 1.50 Ga) and youngest model-ages associated with calcite metacarbonatites (1.18 to 1.55 Ga). The magmatic evolution of the TEC complex most likely involved a complicated relationship of fractional crystallization, liquid immiscibility, and metasomatism/degassing processes. It is proposed that the dolomite carbonatites derived directly from the parental magma via liquid immiscibility, whereas the ultramafic rocks probably were formed by fractional crystallization of the same magma. The calcite metacarbonatites may represent the crystallization of residual liquids after ultramafic rocks formation. Furthermore, K- and Na-rich solutions released by the carbonatite magmas metasomatized the ultramafic and syenitic rocks, developing potassic and sodic fenites.

Interestingly, there is a remarkable similarity between the Nd-Sr isotope signatures of the TEC metacarbonatites and the mesoproterozoic carbonatites from the Alkaline Province of Ontario, Canada. Such comparison reinforces a hypothesis proposed by several authors in the recent years that the Laurentia and the Rio de la Plata Craton were connected at the end of the

Mesoproterozoic, during the formation of the Rodinia supercontinent. These Canadian intrusions were emplaced simultaneously with the Keweenawan extensional magmatic event (1,110-1,090 Ma), which is marked by extensive basaltic volcanism, and to the Abitibi dike swarm (1,160-1,140 Ma), both associated with a major intracontinental rifting process, which can be also temporally related to the TEC. In the evolutionary history of SRS, the placement of the TEC precedes the formation of an oceanic crust in 920 Ma, which gave rise to the Proto-Adamastor Ocean or Charrua Ocean. This ocean closed at the end of the Neoproterozoic with the formation of the supercontinent Gondwana, around 540 Ma, probably culminating in the deformation and metamorphism of the TEC rocks.

A comparison of textural features, mineralogical compositions and geochemical signatures do TEC with the other carbonatites from the SRS (i.e. Picada dos Tocos - 603.2 ± 4.5 Ma, U-Pb in zircon; and Passo Feio - considered as Neoproterozoic) suggest the same source of asthenospheric mantle and similar melting processes for these rocks. However, the very distinct crystallization ages were proposed for these carbonatites, suggesting a recurrent carbonatite magmatism in the southern Brazil along the geological time. The recurrence of carbonatite magmatism is also reported in other ancient terranes such as Ontario and SW Quebec, Canada, Western Greenland, and Northern Europe (Kola Peninsula).

The petrological complexity involved in the genesis of carbonatite complexes is also responsible for the generation of mineral occurrences. The TEC contains a measured mineral resource of 36 Mt @ 4.01% P₂O₅, indicated mineral resource of 47 Mt @ 4.18% P₂O₅ and inferred mineral resource of 21.8 Mt @ 3.67% P₂O₅, using a cut-off grade of 3% P₂O₅. The phosphate comes from the apatite structure, that is hosted in metacarbonatites. Although they have considerable concentrations of P₂O₅, meta-ultramafic rocks do not show good metallurgical recovery. The main control of the occurrence of carbonatites is the ancient fault/fracture zones.

Keywords: Três Estradas Complex; carbonatite; Sul-Riograndense Shield; Mesoproterozoic; phosphate mineralization.

SUMÁRIO GERAL

DEDICATÓRIA	i
AGRADECIMENTOS	ii
RESUMO	iv
ABSTRACT	vi
SUMÁRIO GERAL.....	viii
SUMÁRIO DE FIGURAS	xi
SUMÁRIO DE TABELAS.....	xvi
1. INTRODUÇÃO	1
1.1. APRESENTAÇÃO.....	1
1.2. OBJETIVOS	2
1.2.1. <i>OBJETIVOS ESPECÍFICOS.....</i>	2
1.3. LOCALIZAÇÃO DE VIAS DE ACESSO	3
1.4. HISTÓRICO DA DESCOBERTA DO COMPLEXO ALCALINO-CARBONATÍTICO TRÊS ESTRADAS.....	4
2. GEOLOGIA REGIONAL	6
2.1. INTRODUÇÃO.....	6
2.2. ESCUDO SUL-RIOGRANDENSE	6
2.2.1. <i>TERRENO TAQUAREMBÓ.....</i>	7
2.2.2. <i>TERRENO SÃO GABRIEL.....</i>	8
2.2.3. <i>TERRENO TIJUCAS.....</i>	8
2.2.4. <i>BATÓLITO PELOTAS.....</i>	9
2.2.5. <i>BACIA DO CAMAQUÃ.....</i>	9
2.3. CARBONATITOS DO ESCUDO SUL-RIOGRANDENSE.....	9
2.3.1. <i>METACARBONATITO TRÊS ESTRADAS.....</i>	10
2.3.2. <i>METACARBONATITO SANTA CLARA.....</i>	11
2.3.3. <i>CARBONATITO PICADA DOS TOCOS.....</i>	11
2.3.4. <i>CARBONATITO PASSO FEIO</i>	12
2.3.5. <i>CARBONATITO PORTEIRA.....</i>	12
2.3.6. <i>CARBONATITO SANTA INÉS.....</i>	13
2.3.7. <i>CARBONATITO JOCA TAVARES.....</i>	13
2.3.8. <i>PICRITO DO BOQUEIRÃO</i>	15
3. CARBONATITOS.....	16
3.1. OCORRÊNCIAS DE CARBONATITOS	21
3.2. GÊNESE DE CARBONATITOS	26
3.2.1. <i>FUSÃO DIRETA DO MANTO PERIDOTÍTICO, METASSOMATIZADO, PARCIALMENTE CARBONATADO, COM PRODUÇÃO DE MAGMAS PRIMÁRIOS CARBONATÍTICOS E SILICÁTICOS</i>	30
3.2.2. <i>FRACIONAMENTO A BAIXA PRESSÃO CRUSTAL DE MAGMA PARENTAL DERIVADO DO MANTO</i>	33
3.2.3. <i>SEPARAÇÃO IMISCÍVEL DE LÍQUIDOS CARBONÁTICO E SILICÁTICO, SOB PRESSÃO VARIÁVEL DENTRO DO MANTO OU DA CROSTA, A PARTIR DE MAGMA DERIVADO DO MANTO</i>	34
3.2.4. <i>VISCOSIDADE E DENSIDADE</i>	35

3.3. SOBRE CARBONATITOS E ROCHAS ALCALINAS DEFORMADAS (EM INGLÊS DARC'S) E CARBONATITOS SINTECTÔNICOS.....	35
3.3.1. <i>DARC's</i>	36
3.3.2. <i>CARBONATITOS SIN-TECTÔNICOS</i>	37
3.4. FENITIZAÇÃO.....	41
4. THE MESOPROTEROZOIC TRÊS ESTRADAS ALKALINE-CARBONATITE COMPLEX, BRAZIL: GEOLOGY, MINERALOGY, GEOCHEMISTRY, C-O ISOTOPES AND GENETIC IMPLICATIONS.....	43
ABSTRACT	43
4.1. INTRODUCTION	44
4.2. GEOLOGICAL SETTING	45
4.3. MATERIAL AND METHODS	47
4.3.1. <i>WHOLE-ROCK GEOCHEMISTRY</i>	48
4.3.2. <i>X-RAY DIFFRACTION – XRD</i>	49
4.3.3. $\delta^{13}\text{C}_{\text{PDB}}$ AND $\delta^{18}\text{O}_{\text{V-SMOW}}$	49
4.4. RESULTS	49
4.4.1. <i>GEOLOGY OF THE TRÊS ESTRADAS COMPLEX</i>	49
4.4.2. <i>WHOLE-ROCK GEOCHEMISTRY</i>	61
4.4.3. <i>STABLE $\delta^{13}\text{C}_{\text{V-PDV}}$ AND $\delta^{18}\text{O}_{\text{V-SMOW}}$ ISOTOPES</i>	74
4.5. DISCUSSIONS	75
4.5.1. <i>IMPLICATIONS FOR TEC GENESIS AND EVOLUTION</i>	75
4.5.2. <i>CONSIDERATIONS FOR METASOMATIC CHANGES, METAMORPHISM, AND DEFORMATION</i>	81
4.5.3. <i>RELATIONSHIP BETWEEN TEC AND OTHER CARBONATITE INTRUSIONS IN THE SRS</i>	82
4.5.4. <i>CONSIDERATIONS ABOUT PHOSPHATE MINERALIZATION</i>	85
4.6. CONCLUSIONS	86
ACKNOWLEDGEMENTS	87
REFERENCES	88
5. Nd-Sr-Hf ISOTOPES AND U-Pb AGES OF MESOPROTEROZOIC TRÊS ESTRADAS ALKALINE-CARBONATITE COMPLEX, BRAZIL: IMPLICATIONS FOR SUL- RIOGRANDENSE SHIELD EVOLUTION AND RODINIA BREAK-UP.....	95
ABSTRACT	95
5.1. INTRODUCTION	96
5.2. GEOLOGICAL SETTINGS	97
5.2.1. <i>CARBONATITES OF THE SUL-RIOGRANDENSE SHIELD</i>	99
5.3. PETROGRAPHY OF THE TRÊS ESTRADAS ALKALINE-CARBONATITE COMPLEX 105	
5.3.1. <i>METAULTRAMAFIC ROCKS</i>	105
5.3.2. <i>METACARBONATITE</i>	106
5.3.3. <i>METASYENITE</i>	108
5.4. MATERIALS AND METHODS	109
5.4.1. <i>U-Pb AND Lu-Hf ON ZIRCON</i>	109
5.4.2. <i>Sm-Nd-Sr ISOTOPES</i>	111
5.5. RESULTS	112
5.5.1. <i>U-Pb AND Lu-Hf ON ZIRCON</i>	112
5.5.2. <i>WHOLE-ROCK Nd AND Sr ISOTOPES</i>	121
5.6. DISCUSSION	122
5.6.1. <i>AGE OF CARBONATITE MAGMATISM IN THE SUL-RIOGRANDENSE SHIELD</i> 122	

5.6.2.	<i>GENESIS AND EVOLUTION OF TEC</i>	124
5.6.3.	<i>IMPLICATIONS FOR THE GEOTECTONIC EVOLUTION OF THE SUL-</i> <i>RIOGRANDENSE SHIELD</i>	129
5.6.4.	<i>CONTRIBUTION TO THE PALEOGEOGRAPHIC RECONSTRUCTION OF THE</i> <i>RODINIA SUPERCONTINENT</i>	132
5.7.	CONCLUSIONS	134
	ACKNOWLEDGEMENTS	135
	REFERENCES	136
6.	CONCLUSÕES.....	146
	REFERÊNCIAS BIBLIOGRÁFICAS	150

SUMÁRIO DE FIGURAS

Figura 1.1 - Mapa de localização do Complexo Alcalino-Carbonatítico Três Estradas e demais carbonatitos do Rio Grande do Sul.....	4
Figura 2.1 - Compartimentação tectônica do Escudo Sul-Rio-Grandense (Hartmann <i>et al.</i> , 2007) com a distribuição dos carbonatitos do Rio Grande do Sul.....	7
Figura 2.2 - Feições texturais dos carbonatitos do Rio Grande do Sul. A – Afloramento do Metacarbonatito Três Estradas, foliado; B – Afloramento do Metacarbonatito Santa Clara, foliado; C – Testemunho de sondagem do Metacarbonatito Três Estradas, com bandamento gnáissico; D – Testemunho de sondagem do Carbonatito Picada dos Tocos, com bandamento gnáissico (obtido de Rocha <i>et al.</i> , 2013); E – Afloramento do Carbonatito Passo Feio, foliado (obtido de Morales <i>et al.</i> , 2019); F – Afloramento do Carbonatito Porteira, oxidado, maciço (obtido de Agua Resources Ltd., 2013); G – Afloramento do Carbonatito Santa Inês, maciço (obtido de Agua Resources Ltd., 2017); H – Afloramento do Carbonatito Joca Tavares, maciço, com reação amarela positiva ao molibdato de amônia.....	14
Figura 3.1 - Classificação química de carbonatitos com $\text{SiO}_2 < 20\%$ usando wt% de óxidos (Woolley & Kempe, 1989).....	17
Figura 3.2 - Classificação química de carbonatitos com $\text{SiO}_2 < 20\%$ usando wt% de óxidos de acordo com Gittins & Hamer (1997).....	17
Figura 3.3 - Seção generalizada ilustrando configuração de placas tectônicas e locais de geração de magma, com posicionamento de carbonatitos gerados em ambientes tectônicos distintos (modificado de Winter, 2001).....	21
Figura 3.4 - Distribuição de carbonatitos pelo mundo: ocorrências de carbonatitos magmáticos versus carbonatitos carbohidrotermais (total de 527 ocorrências) (Woolley & Kjarsgaard, 2008).....	23
Figura 3.5 - Distribuição de carbonatitos isotopicamente datados no tempo geológico. Há 192 carbonatitos fanerozoicos e 82 pré-cambrianos (Total de 274 dados) (Woolley & Bailey, 2012).....	23
Figura 3.6 - Idades de carbonatitos em 6 áreas distintas, mostrando repetição de atividade carbonatítica ao longo do tempo, nas seguintes províncias: (1) África Oriental (Quênia, Uganda, Tanzânia e Zâmbia); (2) Namíbia e Angola, (3) Rússia Oriental (East Tuva, Enisei, Oriente Sayan, Baikal, Aldan); (4) Groenlândia; (5) Ontário e sudoeste de Quebec; (6) Norte da Europa (Península de Kola, no norte da Noruega, Suécia, Finlândia) (Woolley & Bailey, 2012).....	24
Figura 3.7 - Ilustração esquemática para mostrar o impacto da pluma mantélica abaixo da litosfera com várias espessuras (modificado de Thompson & Gibson (1991) <i>in</i> Gibson <i>et al.</i> , 1995)....	25
Figura 3.8 - Modelo de intrusão carbonatítica associado a complexo plutônico representativo do Clã- nefelinito (Biondi, 2003 a partir de Le Bas, 1987).....	29
Figura 3.9 - Fluxo esquemático de formação de carbonatitos a partir de fusão parcial de lherzolito rico em CO_2 e processos de diferenciação (ver em associação com a Figura 3.10).....	30
Figura 3.10 - Gráfico de temperatura versus profundidade mostrando a posição do peridotito-C-H-O com razão $\text{CO}_2/\text{CO}_2 + \text{H}_2\text{O}$ igual a 0,8 extrapolada para altas pressões (após Wyllie, 1989).....	32
Figura 3.11 - Corte esquemático de uma pluma do manto astenosférico abaixo de ambiente continental de rife, e a gênese de nefelinito-carbonatitos e kimberlito-carbonatitos (após Wyllie, 1989). Os números correspondem à Figura 3.10	33
Figura 3.12 - Modelo geral de episódios repetidos de magmatismo intracontinental alcalino proposto por Burke & Khan (2006), com base em observações no Malawi, no intervalo de tempo de ~1.0 Ga a 140 Ma. A: Desenho ilustrando como rochas alcalinas e carbonatitos (ARC's).....	33

são expelidos em riftes intracontinentais. B: Desenho ilustrando como essas ARC's podem se posicionar em uma margem continental, enquanto um oceano se desenvolve. C: Desenho ilustrando como os ARC's, antes na margem continental, podem se envolver em uma colisão continental para tornarem-se rochas alcalinas e carbonatitos deformados (DARC's). Alguns desses DARC's são subductados e se tornam parte da litosfera continental, enquanto outros permanecem na crosta. D: Um intervalo de centenas de milhões de anos pode passar sem atividade. E: Um novo rifteamento localizado na antiga zona de sutura pode levar à erupção de novos ARC's por fusão parcial que envolve as fontes de DARC's na litosfera subjacente do manto (Burke & Khan, 2006).....	37
Figura 3.13 - Comparação entre morfologia e dimensões de carbonatitos do tipo “central” e do tipo “linear” (Adaptado de Barbosa, 2009).....	39
Figure 4.1 - Regional geological map of the SRS with the location of the carbonatites discovered in southern Brazil (modified from Ramgrab <i>et al.</i> , 2004; Silva <i>et al.</i> , 2004). Carbonatites: 1 - Três Estradas; 2 - Santa Clara; 3 - Porteira; 4 - Joca Tavares; 5 - Santa Inês; 6 - Passo Feio; and, 7 - Picada dos Tocos (also called Mato Grande Carbonatite by Aguia Resources Ltd, holder of the mining right).....	45
Figure 4.2 - 1:10.000 Geological map of the TEC and representative geological section perpendicular to the TEC axis (Modified from Aguia Resources Ltd., 2018). Datum SAD-69, Zone 21S.	50
Figure 4.3 - NW-SE geological section along TEC from SW (bottom) to NE (top), showing that the complex goes deep in the SW direction.....	51
Figure 4.4 - A to D - Contact features between metaultramafic rock (MUMF) facies, showing absence of alteration or incipient biotitic alteration at the contact edges: A - Contact between MUMF-1 and MUMF-2 facies (TED-12-022, depth 98.30m); B - Contact between coarse and medium-grained MUMF-1 sub-facies (TED-12-022, depth 215.75m); C - Contact between metacarbonatite and MUMF-1 facies (TED-12-022, depth 257.50m); D - Intense biotitization in metaultramafic rock in contact with metasyenite (MSY) (TED-12-023, depth 60.60m).	53
Figure 4.5 - Comparative modal composition between metaultramafic rocks, metacarbonatites and metasyenite. *Main carbonate.....	53
Figure 4.6 - Facies of metaultramafic rocks. A - Top: MUMF-1, undeformed calcite-biotite-titanite metaultramafic rock (Hole TED-12-022, sample 59099, depth 254.40m), Bottom: MUMF-1, banded titanite-calcite-biotite metaultramafic rock (TED-12-022, sample 58857, depth 25.05m); B - Top: MUMF-1, sub-facies with non-deformed beige titanite centimetric porphyroblasts (Hole TED-12-022, sample 58950, depth 107.50m), Bottom: sub-facies with tectonically oriented beige titanite porphyroblasts (TED-12-029, sample 60327, depth 118.15m); C - MUMF-1, magnetite crystals surrounded by carbonate (TED-12-022, sample 58911, depth 73.00m); D - MUMF-2, undeformed biotite-apatite-calcite metaultramafic rock with clusters of white carbonate (TED-11-007, sample 53408, depth 44.60m). E - Photomicrograph of calcite-biotite-titanite metaultramafic rock (MUMF-1) (TED-11-009, sample 53675, depth 69.08m); F - Photomicrograph of biotite-apatite-calcite metaultramafic rock (MUMF-2) (TED-11-007, sample 53408, depth 44.58m). Photomicrographs with crossed polars and objective of 2.5x.....	55
Figure 4.7 - A: Intrusion of calcite metacarbonatite CMC-2 in intermediary host gneiss (GNS), forming locally submilimetric biotitized border (Hole TED-12-022, depth 49.30m); B: Intrusion of dolomite metacarbonatite DMC-2 in MUMF-1, cut by a centimetric quartz vein (Qtz), with development of carbonate submillimetric edge (Hole TED-12-022, depth 67.50m); C: Intrusion of dolomite metacarbonatite DMC-2 in MUMF-1, with generation of biotitized submillimetric border of contact (Hole TED-12-022, depth 24.00m); D: Dolomite metacarbonatite DMC-2 cutting DMC-1 (Hole TED-12-029, depth 191.20m).	57
Figure 4.8 - Metacarbonatite facies. A - CMC-1, banded apatite-biotite-calcite metacarbonatite pink to white (TED-14-044, depth 172m); B - CMC-1, subfacies with higher silicate mineral concentration than average (TED-14-055, depth 154.50m); C - CMC-2, White	

metacarbonatite apatite-calcite with magnetite and oriented apatite (TED-11-006, sample 53320, depth 74.40m); D - DMC-1, Apatite-actinolite-dolomite metacarbonatite (TED-12-022, sample 58888, depth 52.75m); E - DMC-2, Apatite-dolomite white metacarbonatite with incipient foliation (TED-12-022, sample 58871, depth 38.40m); F - Photomicrograph of apatite-biotite-calcite metacarbonatite (CMC-1) (TED-11-010, sample 53761, depth 75.40m); G - Photomicrograph of metacarbonatite apatite-calcite (CMC-2) (TED-11-004, sample 53185, depth 43.40m); H - Photomicrograph of dolomite metacarbonatite apatite (DMC-1) (TED-11-016, sample 54201, depth 73.60m). All photomicrographs were taken with crossed polars and Objective of 2.5x.	58
Figure 4.9 - A: Drill core consisting of metasyenite with potassic feldspar grains showing pressure shadows and fractures filled with carbonate; B: Photomicrograph of metasyenite. Objective of 2.5x, and crossed polars.....	60
Figure 4.10 - Individualization of groups of TEC rocks and their facies based on the chemical composition of major elements.....	61
Figure 4.11 - Box plot with distribution of major element oxides and some minor elements of the different facies in TEC.....	64
Figure 4.12 - Graphic CaO x MgO x FeO+MnO exhibiting contents of these substances in metacarbonatites with levels of SiO ₂ ≤ 20 wt.% based on a diagram proposed by Gittins & Harmer (1997). *FeO and MnO were calculated from Fe ₂ O ₃ e MnO ₂ , respectively.....	65
Figure 4.13 - Spidergram with distribution of minor and trace element in the TEC normalized to the chondrite according to Thompson (1984).....	69
Figure 4.14 - Diagrams of rare earth elements from TEC rocks normalized according to the chondrite according to Boyton (1984)	72
Figure 4.15 - Stable δ ¹³ C versus δ ¹⁸ O isotopes for TEC metacarbonatites and metaultramafic rocks. The light pink field corresponds to the primary igneous carbonatites of Taylor <i>et al.</i> (1967) e Keller & Hoefs (1995). Arrows indicate the main processes in changing the isotopic composition of carbonates (Deines, 1989; Demény <i>et al.</i> , 2004).	74
Figure 4.16 - A: Nb/Ta indicating fractionation probably related to liquid immiscibility; B: Higher concentration of Hf compared to Zr in metaultramafic rocks; C: Zr and Nb correlation that shows higher values in metaultramafic rocks and calcite metacarbonatites; D: La and Yb showing enrichment in ETR in metaultramafic rocks and calcite metacarbonatites compared to dolomite metacarbonatites.	78
Figure 4.17 - Genetic model suggested for TEC.	80
Figure 4.18 - Comparison between geochemical signatures and textures of Três Estradas, Picada dos Tocos and Passo Feio intrusions, showing the similarities between these carbonatites. A: outcrop of calcite metacarbonatite from TEC; B: Calcite metacarbonatite of drill core from TEC (CMC-1 facies); C: calcite carbonatite of drill core form the Picada dos Tocos (Rocha <i>et al.</i> , 2013); D: Outcrop of calcite carbonatite from the Passo Feio (Morales <i>et al.</i> , 2019); E: Spidergram of calcite carbonatite standardized to the chondrite Thompson (1984); F: Spidergram dolomite carbonatite standardized to the chondrite Thompson (1984); G: REE standards of calcite carbonatites normalized to the chondrite (Boyton, 1984); H: REE standards of dolomite carbonatite normalized to chondrite (Boyton, 1984);.....	84
Figure 5.1 - Geological map of the main units of the SRS (dashed boundary), Brazil and Uruguay, showing the locations of carbonatites discovered in southern Brazil (modified from Hartmann <i>et al.</i> , 2007). Carbonatite: 1 – Três Estradas; 2 – Santa Clara; 3 – Porteira; 4 – Joca Tavares; 5 – Santa Inês; 6 – Passo Feio; e, 7 – Picada dos Tocos (also called by Aguiá Resources Ltd, holder of the mining right, as Mato Grande Carbonatite. IL – Ibaré Lineament; CSSZ – Caçapava do Sul Shear Zone; DCSZ – Dorsal de Canguçu Shear Zone.	99
Figure 5.2 - Distribution of carbonatites discovered in Southern Brazil (modified from Ramgrab <i>et al.</i> , 2004; Silva <i>et al.</i> , 2004) regarding the structural configuration of the SRS. Carbonatites: 1 - Três Estradas; 2 - Santa Clara; 3 - Porteira; 4 - Joca Tavares; 5 - Santa Inês; 6 - Passo	

Feio; and, 7 - Picada dos Tocos (also called Mato Grande by Aguia Resources Ltd, holder of the mining rights).....	100
Figure 5.3 - Geological map at 1:10.000 of the TEC with sample locations and schematic NW-SE geological section perpendicular to the complex (Aguia Resources Ltd., 2018). Datum SAD-69, zone 21S.	101
Figure 5.4 - A: Geomorphological expression of the NE portion of the TEC. In the center of the photo, in its highest portion, there are quartz veins that are the core of this elevation. The body continues for another 1.5 km toward SW; B: Typical outcrop of metacarbonatite found in the TEC. Coordinates: 767.719E / 6.577.362N, zone 21S, datum SAD-69; C: Weathered facies of the TEC foliated metacarbonatite.....	102
Figure 5.5 - Representative core samples of the TEC. A: Pink, foliated calcite metacarbonatite intercalated with millimetric bands of biotite-rich metaultramafic rock; B: White to grey, foliated calcite metacarbonatite, with intercalations of millimetric to centimetric bands of biotite-rich metaultramafic rock; C: Dolomite metacarbonatite characterized by the occurrence of disseminated actinolite in the middle of dolomite crystals (sample 58871, borehole TED-12-022, 38.00 m depth); D: Metasyenite core sample with fractures filled with carbonates (sample 59264, borehole TED-12-023, 57.00 m depth); E: Recrystallized metaultramafic rock with pockets of white carbonate and apatite; F: Intrusion of calcite metacarbonatite in the gneiss country-rock (GNS, borehole TED-12-022, 49.30 m depth); G: Late-stage dolomite metacarbonatite cross-cutting early-stage dolomite metacarbonatite interbedded with centimeter-thick metaultramafic bands (borehole TED-12-029, 191.20 m depth); H: Contact between distinct magmatic facies of metaultramafic rocks, one less evolved with little amount of carbonate and the other more differentiated, with carbonate bands; I: Contact between dolomite metacarbonatite and calcite dolomite facies showing flow banding; J: Aggregate of rotated magnetite crystals in calcite metacarbonatite (borehole TED-11-005, 24.80 m depth).....	103
Figure 5.6 - A: Photomicrograph of apatite and carbonate-rich metaultramafic rock (sample 53408, borehole TED-11-007, 44.58 m depth). Mineralogy (sample TEP-12): hornblende (Hb) - 45%; carbonate (Cb) - 20%; apatite (Ap) - 18%; magnetite (Mt) - 4%; biotite-chlorite - 3%; ilmenite - 1.5%; titanite - 1% and pyrite - 1%; B: Photomicrograph of dolomite metacarbonatite (sample 54205, borehole TED-11-016, 77.28 m depth). Mineralogy (sample TEP-25): carbonate (Cb) - 57%; apatite (Ap) - 15%; actinolite (Act) - 14%; pyrite - 8%; ilmenite - 3%; magnetite - 2%; biotite - 1%; titanite, hematite and xenotime (?) – Tr; C: Photomicrograph of metasyenite (sample 53137, borehole TED-11-003, 40.00 m depth). Mineralogy (sample TEP-08): microcline (Mc) - 45%; muscovite (Ms) - 24%; plagioclase (Plag) - 20%; chlorite - 8%; biotite (Bt) - 2%; opaques - 0.7%; titanite - 0.3%; hornblende, carbonate, apatite and rutile – Tr.	106
Figure 5.7 - Metamorphic assemblages of the main TEC units. *Main carbonate mineral.	108
Figure 5.8 - Hand specimens of the samples dated by U-Pb. A: Dolomite metacarbonatite (borehole TED-11-016, 45.0 m depth); B: Metasyenite (borehole TED-11-003, 39.20 m depth); C: Quartz-feldspar gneiss (borehole TED-11-019, 37.0 m depth).....	113
Figure 5.9 - Cathodoluminescence images of zircon crystals analyzed by U-Pb. A: Dolomite metacarbonatite; B: Metasyenite; C: Quartz-feldspar gneiss.....	113
Figure 5.10 - A: U-Pb upper intercept age in $1,110.0 \pm 4.8$ Ma obtained for dolomite metacarbonatite; B; U-Pb upper intercept age in $1,123.0 \pm 15$ Ma obtained for metasyenite. C: U-Pb upper intercept age in $2,022.5 \pm 7.9$ Ma obtained for quartz-feldspar gneiss country rock. In all the graphics, the dashed ellipses represent the rejected zircon crystals.	115
Figure 5.11 - $\epsilon\text{Nd(t)}$ versus $^{87}\text{Sr}/^{86}\text{Sr}_{(i)}$ for metacarbonatites, metaultramafic rocks and metasyenite from the TEC complex. Also plotted are the isotope compositions of Mesoproterozoic Canadian carbonatites (Rukhlov & Bell, 2010; Bell & Blenkinsop, 1987). Bulk Earth composition from Rollinson (1993).....	125
Figure 5.12 - Nd isotope evolution versus time for the TEC rocks.	126

Figure 5.13 - Simple binary mixing modelling showing that the Nd and Sr isotope variations in the TEC complex probably reflects a heterogeneous mantle source signature, possibly with some minor contamination of older continental crust. A - A hypothetical parental magma with 3800 ppm Sr and 238 ppm Nd (average of the TEC rocks); B - Nd and Sr isotope compositions of the country-rock gneiss (TEG-04) calculated at 1.1 Ga. The mixture curve was calculated using well-known equations of mixtures of two components as in Faure (2001).....	126
Figure 5.14 - ϵ Nd(t) variation for different Proterozoic carbonatites in the world. Sources of data: 1 - De Min <i>et al.</i> (2013); 2 - This work; 3 - Antonini <i>et al.</i> (2003); 4 - Bell & Blenkinsop (1987); 5 - Moecher <i>et al.</i> (1997); 6 - Downes <i>et al.</i> (2016); 7 - Ashwal <i>et al.</i> (2016); 8 - Harmer (1999); 9 - Yang <i>et al.</i> (2011); 10 - Ray <i>et al.</i> (2013); 11 - Tichomirova <i>et al.</i> (2006).....	127
Figure 5.15 - $^{87}\text{Sr} / ^{86}\text{Sr}$ ratio variation versus time for the Canadian, Fennoscandian and TEC carbonatites (Modified from Bell & Simonetti, 2010).....	128
Figure 5.16 - ϵ Hf vs. time for the TEC complex and its host rocks.	129
Figure 5.17 - Geotectonic evolution of the SRS from Mesoproterozoic to Neoproterozoic (Modified from Hartmann <i>et al.</i> , 2007; 2019).	131
Figure 5.18 - Paleogeographic reconstruction of Rodinia at 1,100 Ma with three age groups of carbonatites (Modified from Li <i>et al.</i> , 2008). The position of carbonatites is random. 1 - Três Estradas, Brazil: 1,110 Ma (this work); 2 - Carbonatites from the Grenville Province, Canada: 1,155 Ma (Moecher <i>et al.</i> , 1997); 3 - Carbonatites from Ontario Alkaline Province (Prairie Lake, Big Beaver House, Firesand River, Seabrook Lake, Schryburt Lake), Canada: 1,140 to 1,030 Ma (Bell, & Blenkinsop, 1987); 4 - Bull's Run, South Africa: 1,134 Ma (Ashwal <i>et al.</i> , 2016); 5 - Goudini, South Africa: 1,190 Ma (Verwoerd, 2008); 6 - Premier Mine, South Africa: 1,200 Ma (Wooley & Kjarsgaard, 2008); 7 - Epembe, Namibia: 1,184 Ma (Simon <i>et al.</i> , 2017); 8 - Swartbooisdrif, Angola: 1,140 a 1,120 Ma (Drüppel <i>et al.</i> , 2006); 9 - Kalix área, Sweden: 1,142 Ma; 10 - Mountain Pass, USA: 1,415 Ma (Wooley & Kjarsgaard, 2008); 11 – Grønnedal-Íka, Greenland: 1,300 Ma (Ranta <i>et al.</i> , 2018); 12 - Igaliko, Greenland: 1,238 Ma (Wooley & Kjarsgaard, 2008); 13 - Bayan Obo, China: 1,354 Ma (Yang <i>et al.</i> , 2011); 14 - Newania, India: 1,473 Ma (Ray <i>et al.</i> , 2013); 15 - Elchuru, India: 1,242 Ma (Wooley & Kjarsgaard, 2008); 16 - Seis Lagos, Brazil: 1,328 Ma (Rossoni <i>et al.</i> , 2017); 17 - Spitskop, South Africa: 1,341 Ma (Harmer, 1999); 18 - Stukpan, South Africa: 1,357 Ma (Wooley & Kjarsgaard, 2008); 19 - Cummins Range, Australia: 1,009 Ma (Downes <i>et al.</i> , 2016); 20 - Gifford Creek, Australia: 1,075 Ma (Pirajno <i>et al.</i> , 2014); 21 - Glenover, South Africa: 1,000 Ma; 22 - Twareitau, Guyana: 1,025 Ma; 23 - Yenachang, China: 1,048 Ma (Wooley & Kjarsgaard, 2008); 24 - Mutum, Brazil: 1,026 Ma (Oliveira <i>et al.</i> , 1975). Younger carbonatites with positions 19 to 23 estimated in relation to Laurentia at 1,000 Ma.	133

SUMÁRIO DE TABELAS

Tabela 2.1 - Coordenadas e idades definidas e estimadas das intrusões carbonatíticas do ESRG	10
Tabela 3.1 - Classificação de carbonatitos com base em sua composição mineralógica (Streckeisen, 1979 e Le Maitre, 2002).....	16
Tabela 3.2 - Alguns minerais presentes em carbonatitos (Adaptado de Winter, 2001).....	18
Tabela 3.3 - Composições químicas médias representativas de carbonatitos (Woolley & Kempe, 1989; Winter, 2001).	19
Tabela 3.4 - Esquema de classificação das associações entre carbonatitos e rochas silicáticas (elaborada a partir de Woolley & Kjarsgaard, 2008).....	22
Tabela 3.5 - Descrição das associações petrológicas relacionadas a carbonatitos reconhecidas por Mitchell (2005). A coluna “descrição” tem como referência o trabalho supracitado.	27
Tabela 3.6 - Regime geológico-tectônico, deformação dos carbonatitos, e seus tipos morfológico-formacionais (Lapin & Ploshko, 1988 <i>Apud</i> : Lapin <i>et al.</i> , 1999).....	40
Table 4.1 - Analysis of major elements of the TEC rocks. Contents in wt.%. Holes with azimuth 150° and dip varying between -45° and -65° (see Figure 4.2).	62
Table 4.2 - Analysis of minor elements and traces in TEC rocks. Contents are shown in ppm.	68
Table 4.3 - Analysis of rare earth elements in TEC rocks. Contents are in ppm.	73
Table 4.4 - $\delta^{13}\text{C}$ and $\delta^{18}\text{O}$ isotopic data of CTE metacarbonatites and metaultramafic rocks.	75
Table 5.1 - Additional information regarding U-Pb analyses (see also Tables 5.3 to 5.5).	111
Table 5.2 - Additional information regarding Lu-Hf analyses (see also Table 5.6).	111
Table 5.3 - U-Pb analyses of dolomite metacarbonatite zircon crystals (TEG-01).	117
Table 5.4 - U-Pb analyses of metasyenite zircon crystals (TEG-05).....	118
Table 5.5 - U-Pb analyses of zircon crystals of the TEC quartz-feldspar gneiss host rock (TEG-04).	119
Table 5.6 - Lu-Hf isotopes on zircon crystals of the TEC rocks dated by the U-Pb method.....	120
Table 5.7 - Sm-Nd isotopes from TEC rocks.	121
Table 5.8 - Rb-Sr data from TEC rocks.....	122
Table 5.9 - Summary of major tectono-magmatic events related to carbonatites (Rukhlov & Bell, 2010).	134

1. INTRODUÇÃO

1.1. APRESENTAÇÃO

Carbonatitos resultam da cristalização de magmas relativamente raros, originados a partir de fonte mantélica, envolvendo uma variedade de processos (Gittins, 1989; Brooker, 1995; Lee & Wyllie, 1998; Bell *et al.*, 1999; Bell & Simonetti, 1996; Woolley & Bailey, 2012, Kresten & Troll, 2018). Essas rochas ocorrem em restritos ambientes geológicos, preferencialmente extensionais, como áreas estáveis intraplaca e margens divergentes de placas (Bailey, 1974). Esporadicamente, carbonatitos são encontrados em ambientes orogênicos e, raramente, em bacias oceânicas (Bailey, 1974; Burke *et al.*, 2003; Woolley & Kjarsgaard, 2008). Quando localizados em margens continentais ligadas à orogenia podem ter sido colocados antes de uma transição de regime tectônico extensional para compressional ou durante relaxamento extensional pós-orogênico (Simandl & Paradis, 2018).

O Brasil é destacado na literatura científica por suas intrusões carbonatíticas intraplaca, cretáceas, distribuídas na borda da Bacia do Paraná, nas províncias alcalinas do Alto Paranaíba, Goiás, Poxoréu, Ponta Grossa e Serra do Mar (Cretáceo Superior ao Eoceno), às quais se juntam os carbonatitos Lages e Anitápolis e a Suíte Alcalina Piratini (Gibson *et al.*, 1995; Brod *et al.*, 2004). No entanto, no que tange a carbonatitos pré-cambrianos são escassas as ocorrências identificadas, como Angico dos Dias, de idade paleoproterozoica, Maicuru, Mutum e Seis Lagos com idades mesoproterozoicas e Planalto da Serra e Picada dos Tocos, ambos com idades neoproterozoicas. O Complexo Alcalino-Carbonatítico Três Estradas (simplificado como Complexo Três Estradas - CTE) passa a integrar esse grupo de carbonatitos antigos como a primeira ocorrência de carbonatito mesoproterozoico identificada no Escudo Sul-Riograndense (ESRG), sul do Brasil. As intrusões carbonatíticas mesoproterozoicas são raras em todo o mundo com apenas cerca de 30 conhecidas (Oliveira *et al.*, 1975; Drüppel *et al.*, 2006; Woolley & Kjarsgaard, 2008; Yang *et al.*, 2011; Ray *et al.*, 2013; Ashwal *et al.*, 2016; Downes *et al.*, 2016; Rossoni *et al.*, 2017; Simon *et al.*, 2017; Ranta *et al.*, 2018).

Outros seis carbonatitos, Santa Clara, Picada dos Tocos, Passo Feio, Joca Tavares, Porteira e Santa Inês, foram identificados posteriormente ao CTE no ESRG. Os pares de carbonatitos Três Estradas-Santa Clara e Picada dos Tocos-Passo Feio exibem semelhanças mineralógicas e texturais, mas indicam pelo menos duas idades de cristalização U-Pb em zircão distintas, uma Mesoproterozoica (esta tese) e outra Neoproterozoica (Cerva-Alves *et al.*, 2017),

respectivamente. Os demais carbonatitos, em função de suas relações de campo, sugerem, no mínimo, uma outra idade de colocação mais jovem, aventada por Toniolo *et al.* (2013). Situações semelhantes são identificadas em terrenos em Ontário e SW Quebec, no Canadá, Groelândia e Norte da Europa (Península de Kola), onde há a recorrência de magmatismo carbonatítico no espaço e no tempo, através de zonas de fraqueza antigas e outros lineamentos (Woolley & Bailey, 2012).

Pela sua singularidade geológica, carbonatitos permitem inferir condições geotectônicas durante a evolução de um terreno a partir de conteúdos isotópicos de Nd-Sr-Hf. Vários processos, envolvendo fundidos carbonatíticos primários ou derivados de fundidos silicáticos carbonatados podem gerar carbonatitos (Bell *et al.*, 1999, 2004; Bell, 2001) e formar diferentes tipos de depósitos minerais (Mitchell, 2005; Simandl & Paradis, 2018). No CTE, a empresa Agua Resources Ltd cubou recurso mineral medido com 36 Mt @ 4,01% P₂O₅, recurso mineral indicado de 47 Mt com teor médio de 4,18% P₂O₅ e recurso mineral inferido de 21,8 Mt com teor médio de 3,67% P₂O₅, utilizando como teor de corte 3% P₂O₅ (<http://aguairesources.com.au/projects/rio-grande/>).

No ESRG, onde o complexo está encaixado, há raros registros de atividade geológica durante o Mesoproterozoico. Portanto, o CTE adquire importante significado geotectônico na evolução desse escudo, permitindo inferir sobre a configuração paleocontinental no sul do Brasil em ~1,1 Ga. Para tanto, esta tese de doutorado apresenta dados inéditos de geologia de campo, mineralogia, geoquímica de rocha total, isotopia de Nd-Sr-Hf e C-O e geocronologia a partir de idades U-Pb em zircão obtidos acerca do CTE. Estes dados são exibidos no formato de artigos científicos submetidos aos periódicos internacionais Lithos e Precambrian Research.

1.2. OBJETIVOS

Essa tese objetiva contribuir para a compreensão da evolução geotectônica do ESRG, a partir de dados geológicos, geoquímicos, isotópicos e geocronológicos do Complexo Alcalino-Carbonatítico Três Estradas, localizado no Terreno Taquarembó, na borda do Cráton Rio de la Plata.

1.2.1. OBJETIVOS ESPECÍFICOS

Para atingir o objetivo principal foram elencados os seguintes objetivos específicos:

- 1) Estabelecer a composição mineralógica, texturas e relações de contato entre as rochas do CTE;
- 2) Determinar a idade de cristalização das rochas do CTE através de análises geocronológicas U-Pb em zircão de dolomita metacarbonatito e metassienito;
- 3) Sugerir a fonte do magmatismo alcalino-carbonatítico que deu origem ao CTE por meio das assinaturas isotópicas de Nd-Sr-Hf em calcita e dolomita metacarbonatitos, rochas metaultramáficas e metassienitos;
- 4) Sugerir o(s) processo(s) geológico(s) envolvido(s) na formação de rochas carbonatáticas e silicáticas;
- 5) Propor ambiente geotectônico de colocação do CTE;
- 6) Sugerir hipótese sobre como o CTE se encaixa na evolução geotectônica do ESRG;
- 7) Comparar os dados geocronológicos e geoquímicos obtidos para o CTE com os carbonatitos Picada dos Tocos e Passo Feio também localizados no ESRG;
- 8) Comparar os dados geocronológicos e isotópicos obtidos para o CTE com carbonatitos de mesma idade no mundo para contribuir com modelos de reconstrução paleocontinental;
- 9) Identificar potencial para mineralização em fosfato.

1.3. LOCALIZAÇÃO DE VIAS DE ACESSO

O CTE aflora em área de relevo suavemente ondulado nas planícies de clima subtropical úmido no pampa gaúcho, banhadas pelas bacias dos rios Santa Maria e Camaquã, no município de Lavras do Sul, estado do Rio Grande do Sul, sul do Brasil, a 70 km da fronteira Brasil-Uruguai. Distancia-se 360 km a SW da capital estadual, Porto Alegre (**Figura 1.1**). A área pode ser acessada, tendo Porto Alegre como ponto de partida, utilizando-se as BR-116, BR-290 e BR-392 até Caçapava do Sul. A partir dessa cidade toma-se a RS-357 na direção SW, passando por Lavras do Sul, de onde se segue pela mesma rodovia, não asfaltada, até o entroncamento com a RS-473. Seguindo nessa estrada na direção SSW até novo entroncamento com estrada de terra secundária e tomando-se a direção NW por 10 km, é possível alcançar a porteira que dá acesso à porção nordeste do CTE. O percurso dura aproximadamente 04h e 40min.

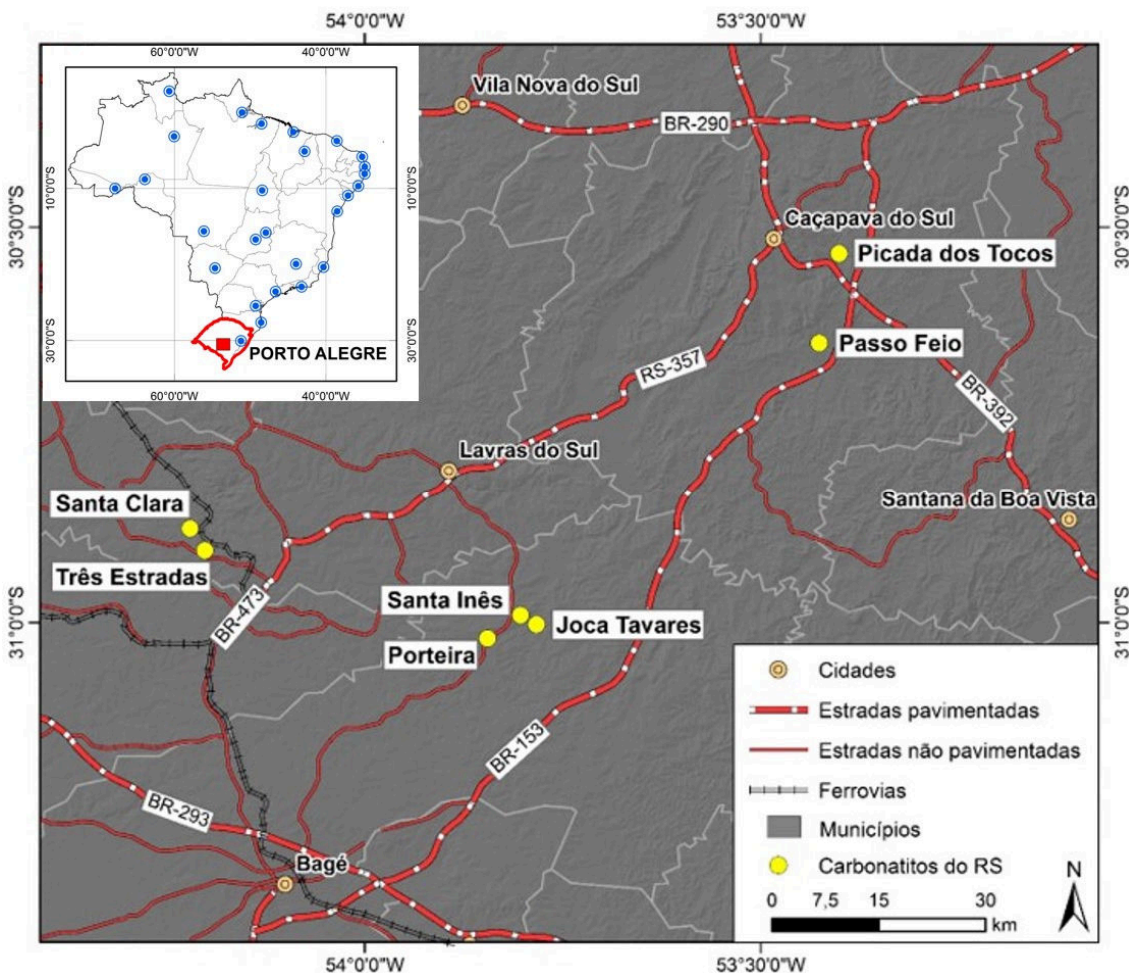


Figura 1.1 - Mapa de localização do Complexo Alcalino-Carbonatítico Três Estradas e demais carbonatitos do Rio Grande do Sul.

1.4. HISTÓRICO DA DESCOBERTA DO COMPLEXO ALCALINO-CARBONATÍTICO TRÊS ESTRADAS

Por várias décadas acreditou-se que o Rio Grande do Sul não tivesse vocação geológica para ocorrências de carbonatito, distintamente dos demais estados que compõem as regiões sul e sudeste do Brasil. Esse quadro começou a ser modificado em 2007/2008, a partir da avaliação de análises químicas de testemunhos de sondagem obtidas pela empresa Santa Elina, em Lavras do Sul (RS), que mantinha uma *joint venture* com a Companhia Brasileira do Cobre (CBC) para prospectar ouro no Processo DNPM nº 810.090/1991, em rochas interpretadas como calcossilicáticas. O Geólogo José Luiz Reischl, consultor da CBC, atentou para os teores de fosfato de até 6,41% em solo e de até 6,64% em testemunhos de sondagem e comunicou ao Serviço Geológico do Brasil-CPRM. A existência do carbonatito foi então confirmada via análise petrográfica pelos geólogos da Superintendência Regional de Porto Alegre (SUREG-

PA), João Ângelo Toniolo e Giovani Parisi, pelo Projeto Agrominerais do Rio Grande do Sul. O Carbonatito Três Estradas começou a ser prospectado meses após a intermediação feita pelo Geol. José Luiz Reischl entre a empresa Aguia Resources Ltd., representada pelos geólogos José Jacob Fanton, Fernando Henrique Bucco Tallarico e Alfredo Rosseto Nunes, e a CBC.

A descoberta do Carbonatito Três Estradas foi publicada em resumos no IV Simpósio de Exploração Mineral (SIMEXMIN), em Ouro Preto (MG), por Toniolo *et al.* (2010) e no 45º Congresso Brasileiro de Geologia, em Belém (PA), por Parisi *et al.* (2010). Quatro trabalhos de conclusão de curso da UFRGS e da UFPEL foram desenvolvidos nos campos da geologia estrutural, mineralogia e da geoquímica, por Senhorinho (2012), Anzolin (2015), Ziebell (2013) e Martinez (2019). Em 2018, Anzolin concluiu dissertação de mestrado com foco em multigerações de apatitas no Carbonatito Três Estradas e publicou os dados em Anzolin *et al.* (2019).

A identificação do Carbonatito Três Estradas impulsionou a pesquisa por novas intrusões. Ao todo já foram descobertos 7 carbonatitos no Rio Grande do Sul: Três Estradas (Toniolo *et al.*, 2010), em Lavras do Sul, pela CBC e SGB/CPRM; Santa Clara (Aguia Resources Ltd., 2016), também em Lavras do Sul, pela Aguia Resources Ltd.; Joca Tavares (Toniolo *et al.*, 2010), em Bagé, pelo SGB-CPRM; Porteira (Aguia Resources Ltd., 2013, Monteiro *et al.*, 2016) e Santa Inês (Aguia Resources Ltd., 2014), ambos em Bagé, pela Aguia Resources Ltd; e, Passo Feio e Picada dos Tocos (Rocha *et al.*, 2013), ambos em Caçapava do Sul, pela Mining Ventures. As intrusões Três Estradas, Passo Feio e Picada dos Tocos são semelhantes entre si em termos de assembleias mineralógicas, associações petrológicas e assinaturas geoquímicas (Monteiro *et al.*, 2016). Monteiro *et al.* (2016) levantaram a possibilidade desses carbonatitos terem idade neoproterozoica, talvez sin-tectônicos à Orogênese Brasiliiana. Cerva-Alves (2017) concluiu dissertação de mestrado sobre a geologia dos carbonatitos de Caçapava do Sul e apontou idade neoproterozoica ($603,2 \pm 4,5$ Ma – U-Pb em zircão) para a intrusão Picada dos Tocos, publicada em Cerva-Alves *et al.* (2017). Morales *et al.* (2019) apresentam dados de mineralogia, geoquímica de rocha total e isótopos de ^{13}C e ^{18}O , e sugerem idade neoproterozoica para o Carbonatito Passo Feio. Laux *et al.* (2019), por sua vez, levantam a possibilidade de o Carbonatito Três Estradas ter se cristalizado no Triássico Superior (233 Ma – U-Pb em zircão).

2. GEOLOGIA REGIONAL

2.1. INTRODUÇÃO

Gnaisses com composição intermediária e retrometamorfizados para a fácie anfibolito na borda de terreno remanescente do Cráton Rio de la Plata no ESRG, serviram como hospedeiros para a intrusão do CTE em posição próxima a intersecção entre as zonas de cisalhamento transcorrentes Ibaré e Cerro dos Cabritos.

2.2. ESCUDO SUL-RIOGRANDENSE

O CTE está alojado no ESRG, porção sul do Cinturão Dom Feliciano, formado durante a Orogenia Brasiliiana (Hartmann *et al.*, 2007, 2008; Philipp *et al.*, 2016, 2018; Toni *et al.*, 2020). Este complexo alcalino-carbonatítico intrude gnaisses intermediários atribuídos ao Complexo Santa Maria-Chico, principal unidade geológica do Terreno Taquarembó, tido como remanescente Arqueano a Paleoproterozoico do Cráton Rio de la Plata (Chemale Jr., 2000; Girelli *et al.*, 2018), próximo ao Lineamento Ibaré (Ruppel, 2016).

Para muitos autores, o Terreno Taquarembó representa a extensão para norte do Terreno Nico Pérez, posicionado no centro do Uruguai (e.g. Bossi & Campal, 1992; Bossi & Cingolani, 2009; Philipp *et al.*, 2016, 2018). Hartmann *et al.* (2007, 2008) individualizaram as principais unidades do ESRG, com base nas associações de rochas, feições tectônicas, assinaturas geoquímica e isotópica e geofísica aérea, subdividindo-o nos terrenos Taquarembó, São Gabriel, Tijucas, Batólito Pelotas e Bacia do Camaquã (**Figura 2.1**).

A construção do ESRG envolveu o fechamento do oceano Charrua durante a Orogenese São Gabriel (900-680 Ma), com posterior colisão entre os crâtons Rio de la Plata e Kalahari, envolvendo o Terreno Nico Perez, durante a Orogenese Dom Feliciano (650-550 Ma), com a formação do terreno acrecionário Tijucas (Philipp *et al.*, 2016). Ao final da evolução da Orogenia Brasiliiana houve a geração da granitogênese do Batólito Pelotas e deposição das rochas sedimentares e vulcânicas da Bacia do Camaquã (Chemale Jr., 2000; Hartmann *et al.*, 2008).

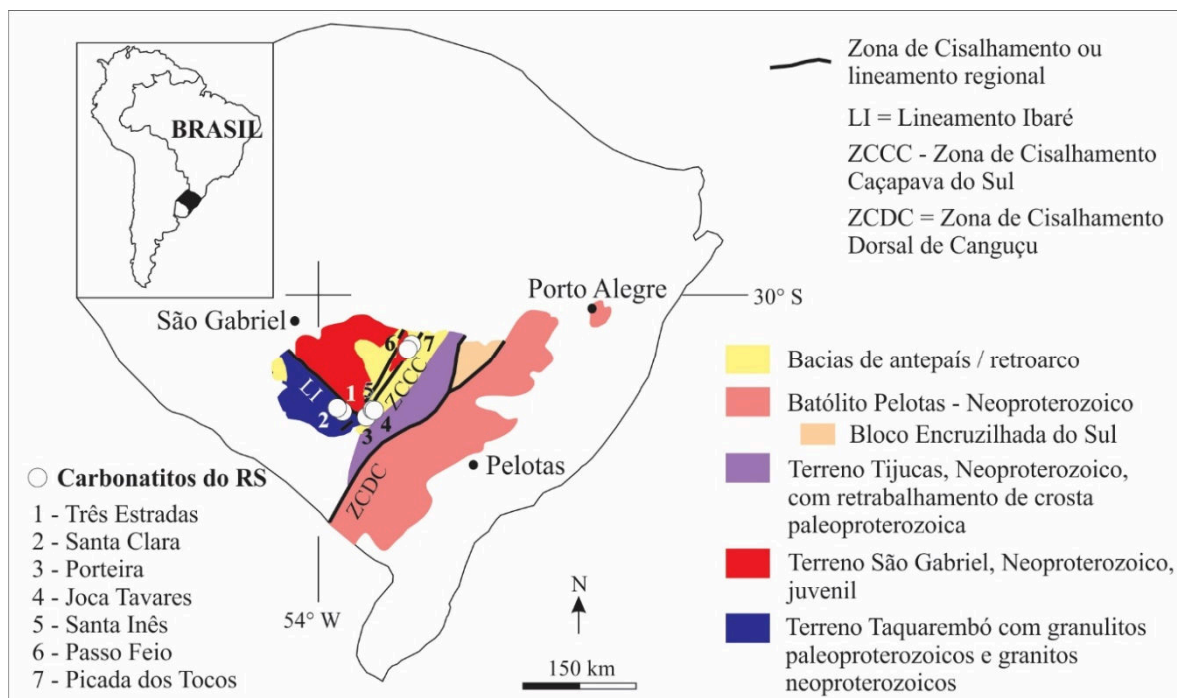


Figura 2.1 - Compartimentação tectônica do Escudo Sul-Rio-Grandense (Hartmann *et al.*, 2007) com a distribuição dos carbonatitos do Rio Grande do Sul.

2.2.1. TERRENO TAQUAREMBÓ

O Terreno Taquarembó é constituído por rochas paleopreterozoicas metamorfizadas em fácies granulito, parcialmente retrabalhadas durante a Orogenia Brasiliana, no Neoproterozoico, e coberturas metavulcano-sedimentares e granitos gerados na mesma Era (Nardi & Hartmann, 1979; Chemale Jr., 2000; Hartmann *et al.*, 2008). O terreno é limitado a norte e nordeste pelo Lineamento Ibaré, a leste, pela Zona de Cisalhamento de Caçapava do Sul e para sul e oeste desaparece sob a cobertura sedimentar da Bacia do Paraná (Costa *et al.*, 1995). Encontra-se localizado no sudoeste do ESRG e representa a extensão para o norte do Terreno Nico Pérez, no Uruguai (Bossi & Campal, 1992; Bossi & Cingolani, 2009).

Os granulitos do Terreno Taquarembó constituem o Complexo Granulítico Santa Maria-Chico (CGSMC), composto essencialmente por intercalações em escala métrica de rochas básicas granadíferas e tonalitos e, subordinadamente, anortositos, lherzolitos e rochas metassedimentares (Hartmann, 1987; 1998). As idades U-Pb em zircão obtidas para os protólitos das rochas datadas por Hartmann *et al.* (2008) foram de 2.366 ± 8 Ma para o protólito do gnaisse granodiorítico e 2.489 ± 6 Ma para o protólito do granulito, as quais são menores do que o intervalo de idades Sm-Nd (>2.510 - 2.555 Ma) obtidas por Hartmann (1987). Os dados obtidos por Girelli *et al.* (2018) apontam para a formação dos protólitos das rochas do CGSMC

em arcos vulcânicos de múltiplos estágios, posteriormente metamorfizados em ambiente de colisão continental em intervalo de 370 Ma (2.430 a 2.060 Ma, U-Pb em zircão).

Hartmann *et al.* (2008) obtiveram idades de metamorfismo U-Pb em zircão de 2.035 ± 9 Ma e 2.006 ± 3 Ma em gnaisse granodiorítico e granulito do CGSMC, respectivamente, em concordância com idades U-Pb em zircão de 2.022 ± 18 Ma e 2.031 ± 40 Ma reportados por Hartmann (1987) para granulitos básicos e intermediários, respectivamente. Girelli *et al.* (2018) obteve idade U-Pb em titanita metamórfica de $1.018 \pm 9,9$ Ma em anortosito do CGSMC, sugerindo a ocorrência de evento metamórfico adicional atuante sobre essas rochas no final do Mesoproterozoico.

2.2.2. TERRENO SÃO GABRIEL

O Terreno São Gabriel se justapõe ao Terreno Taquarembó por meio do Lineamento Ibaré e constitui-se de unidades de acreção juvenil representadas por associações petrotectônicas de ambientes de margem passiva e de retro-arco, ofiolitos e arcos magmáticos constituídos por rochas vulcano-sedimentares e plutônicas (Babinski *et al.*, 1996; Leite *et al.*, 1998; Chemale Jr. 2000; Hartmman *et al.*, 2008, Philipp *et al.*, 2016; 2018). É neste terreno que se encontra o Complexo Passo Feio, onde foram intrudidos os carbonatitos Picada do Tocos e Passo Feio (Cerva-Alves *et al.*, 2017). Este complexo é formado por uma sequência de metapelitos, mármore, rochas calcossilicáticas, quartzitos, anfibolitos, rochas metavulcanoclásticas e xistos magnesianos (Bitencourt, 1983) que ocorrem margeando o Granito Caçapava do Sul com idade U-Pb em zircão de 562 ± 8 Ma (Remus *et al.*, 2000). A idade mínima do Complexo Passo Feio é de 774 ± 8 Ma em albita-muscovita-clorita xisto (Remus *et al.*, 2000) e a idade máxima de $3.367 \pm 7,8$ Ma em clorita-muscovita filito (Lopes, 2014), ambas obtidas pelo método U-Pb em zircão detritico. Goulart *et al.* (2013) apresenta estimativa de períodos de deposição das rochas carbonáticas da Formação Passo Feio entre 770 e 730 Ma.

2.2.3. TERRENO TIJUCAS

Ocupando a porção central do ESRG ocorrem as rochas do Terreno Tijucas, conforme definido por Jost & Bitencourt (1980) e Chemale Jr. *et al.*, (1995a, b). Este cinturão estende-se desde Santa Catarina ao Uruguai, em faixa alongada N 20° -45°E/S 20° -45°W. No Rio Grande

do Sul é representado pelo Grupo Porongos, constituído por rochas supracrustais e plutônicas cálcio-alcalinas neoproterozoicas, e Complexo Encantadas, composto por rochas granito-gnáissicas e anfibolíticas paleoproterozoicas (Chemale Jr. 2000).

2.2.4. BATÓLITO PELOTAS

O Batólito Pelotas é formado por complexo granítico-gnáissico e sete suítes, seis graníticas e uma sienítica, a saber: Suíte Intrusiva Pinheiro Machado (Complexo granito-gnáissico), Suíte Intrusiva Erval, Suíte Granítica Cordilheira, Suíte Intrusiva Viamão, Suíte Intrusiva Encruzilhada do Sul, Suíte Granítica Dom Feliciano e Suíte Intrusiva Piquiri (Suíte sienítica) (Hartmann *et al.*, 2007). Os granitos sin-colisionais ocorrem na porção noroeste do batólito e estão representados por granítóides de afinidade cálcico-alcalina alto-K, fracamente peraluminosos, com principal período de geração entre 650 e 620 Ma (Frantz *et al.*, 2003). O batólito está constituído predominantemente por suítes graníticas de natureza pós-colisional, com ocorrência subordinada de uma associação vulcanosedimentar, preservada essencialmente em enxames de diques ácidos e básicos (Chemale Jr. 2000, Philipp *et al.*, 2016, 2018).

2.2.5. BACIA DO CAMAQUÃ

A sequência sedimentar da Bacia do Camaquã (Ribeiro & Fantinel, 1978; Paim *et al.*, 2000; Chemale Jr., 2000; Hartmann *et al.*, 2007) é composta predominantemente por siltitos, arenitos com aumento na abundância de conglomerados e arenitos em direção ao topo da sequência. Representa evolução de ambientes marinhos rasos para continentais, onde dominam os ambientes flúvio-lacustres e desérticos. Os ciclos vulcânicos foram individualizados em: (i) vulcanismos Maricá, Hilário e Acampamento Velho, associados às formações homônimas; (ii) vulcanismo Rodeio Velho, vinculado ao Membro Rodeio Velho da Formação Guaritas.

2.3. CARBONATITOS DO ESCUDO SUL-RIOGRANDENSE

Sete intrusões carbonatíticas foram identificadas no ESRG entre 2010 até o momento (**Tabela 2.1, Figura 2.1**), todas com teores de P₂O₅ superiores a 3% denotando potencial para

ocorrência de depósitos de fosfato. Em termos de grau de deformação e textura é possível separar essas intrusões em pelos menos dois grupos: carbonatitos foliados com ocorrência de bandamento gnáissico e carbonatitos não foliados ou com foliação incipiente. Dentre os carbonatitos foliados com bandamento estão as intrusões Três Estradas, Santa Clara, Picada dos Tocos e Passo Feio. Joca Tavares, Santa Inês e Porteira apresentam deformação fraca ou incipiente. Ocorre ainda picrito permiano/mesozoico possivelmente relacionado as 3 últimas intrusões ou pelo menos uma delas.

Tabela 2.1 - Coordenadas e idades definidas e estimadas das intrusões carbonatíticas do ESRG.

Carbonatito	UTM E	UTM N	Datum/ Zona	Referência Bibliográfica ¹	Idade
Três Estradas	767.719	6.577.362	SAD-69/ 21S	Esta tese	$1.110 \pm 4,8$ Ma, U-Pb em zircão (esta tese)
Santa Clara	763.221	6.579.044	SAD-69/ 21S	Aguia Resources Ltd. 2017	Sem datação. Estimada nesta tese como Mesoproterozoico
Picada dos Tocos	269.457	6.619.303	SAD-69/ 22S	Aguia Resources Ltd., 2018b	$603,2 \pm 4,5$ Ma, U-Pb em zircão (Cerva-Alves <i>et al.</i> , 2017)
Passo Feio	267.530	6.607.080	SAD-69/ 22S	Estimado a partir de Morales <i>et al.</i> (2019)	Sem datação. Estimada como Neoproterozoico (Cerva-Alves <i>et al.</i> , 2017; Morales <i>et al.</i> , 2019)
Porteira	228.612	6.564.885	SAD-69/ 22S	Aguia Resources Ltd. 2017	Sem datação. Estimada nesta tese como Neoproterozoico ou mais jovem
Santa Inês	231.006	6.566.546	SAD-69/ 22S	Aguia Resources Ltd. 2017	Sem datação. Estimada nesta tese como Neoproterozoico ou mais jovem
Joca Tavares	234.096	6.566.729	SAD-69/ 22S	Esta tese	Sem datação. Estimada nesta tese como Neoproterozoico ou mais jovem
Picrito do Boqueirão	229.537	6.566.502	Córrego Alegre / 22S	Goulart (2014)	292 ± 10 Ma (borda da intrusão) e 119 ± 10 Ma (centro da intrusão), K-Ar em rocha total (Ribeiro e Teixeira, 1970)

¹ Referência bibliográfica das coordenadas UTM.

2.3.1. METACARBONATITO TRÊS ESTRADAS

O Metacarbonatito Três Estradas, descoberto pela Companhia Brasileira do Cobre (CBC) e SGB-CPRM (Toniolo *et al.*, 2010) e prospectado pela Aguaia Resources Ltd (Aguia Resources Ltd., 2018a), possui formato linear segundo a direção NE com mergulho subvertical preferencial para NW. Apresenta desde foliação incipiente (**Figura 2.2A**) até bandamento gnáissico com alternância de bandas milimétricas a centimétricas de biotita metaultramáfica e dobras parasíticas fechadas observadas em testemunhos de sondagem (**Figura 2.2C**) e

afloramentos. O metacarbonatito faz parte do CTE, onde se associa a metaultramáficas e metassienitos intrudidos em rochas paleoproterozoicas/arqueanas do Complexo Santa Maria-Chico, no Terreno Taquarembó, na borda do Cráton Rio de la Plata. São individualizados dois tipos de metacarbonatito em função do mineral de carbonato dominante: calcita metacarbonatitos e dolomita metacarbonatitos. Localmente ocorrem metaultramáficas ricas em titanita com textura porfírica e cogenéticos ao metacarbonatito. Essas rochas se encontram recristalizadas e metamorfizadas em fácies xisto verde a anfibolito. Datação U-Pb em zircão indica que dolomita metacarbonatitos se cristalizaram em $1.110 \pm 4,8$ Ma (esta tese).

A Agua Resources Ltd cubou reserva medida com 36 Mt @ 4,01% P₂O₅, reserva indicada de 47 Mt com teor médio de 4,18% P₂O₅ e reserva inferida de 21,8 Mt com teor médio de 3,67% P₂O₅, utilizando como teor de corte 3% P₂O₅ (<http://aguairesources.com.au/projects/rio-grande/>).

2.3.2. METACARBONATITO SANTA CLARA

O Metacarbonatito Santa Clara, descoberto pela Agua Resources Ltd, é muito semelhante ao Metacarbonatito Três Estradas e está situado a 4,5 km a NW deste, também intrudindo rochas paleoproterozoicas/arqueanas do Complexo Santa Maria-Chico, no Terreno Taquarembó. Possui formato linear com direção NE. Em afloramentos também são distinguidos foliação (**Figura 2.2B**) e bandamento com alternância entre bandas centimétricas de metacarbonatito e bandas milimétricas a centimétricas de biotita metaultramáfica, metamorfizados em fácies xisto verde a anfibolito. Estima-se que esse carbonatito tenha a mesma idade Mesoproterozoica obtida para o CTE. A Agua Resources Ltd obteve teores de até 6,38% P₂O₅ em afloramento de metacarbonatito (Aguia Resources Ltd., 2017).

2.3.3. CARBONATITO PICADA DOS TOCOS

O Carbonatito Picada dos Tocos, identificado pela Mining Ventures Ltd durante programa de exploração para Cobre, apresenta formato linear, com direção N-S, e está alojado no Terreno São Gabriel, no Complexo Passo Feio, com idade Neoproterozoica Inferior (Rocha *et al.*, 2013). Este carbonatito é semelhante ao Três Estradas em termos texturais, mineralógicos, tipo de deformação e assinaturas geoquímicas (esta tese). Cerva-Alves *et al.*

(2017) individualizou calcita e dolomita carbonatitos bandados com intercalações de bandas maficas, interpretadas pelos autores como pertencentes à rocha encaixante (**Figura 2.2D**), e obtiveram idade de cristalização fornecida pelo método U-Pb em zircão de $603,2 \pm 4,5$ Ma para o Carbonatito Picada dos Tocos.

Durante campanha de sondagem da Mining Ventures Ltd foram interceptados 14,37m @ 3,21% P₂O₅, além de amostras de rocha em afloramento com até 8,38% de P₂O₅ (Rocha *et al.*, 2013). A Mining Ventures perdeu o prazo de renovação do direito de propriedade mineral e a Aguaia Resources fez o requerimento da área, adquirindo o direito de pesquisa e passou a chamar essa intrusão como Carbonatito Mato Grande (Aguia Resources Ltd., 2017). Em sondagem a tradô motorizado, a Aguaia Resources obteve 9,0m @ 7,37% P₂O₅ com teor de até 11,71% P₂O₅ (Aguia Resources Ltd., 2018b).

2.3.4. CARBONATITO PASSO FEIO

O Carbonatito Passo Feio, descoberto pela Mining Ventures Ltd, aflora a aproximadamente 12 km a SSW do Carbonatito Picada dos Tocos, e também intrude o Complexo Passo Feio. Morales *et al.* (2019) descrevem as amostras de afloramento estudadas como calcita carbonatitos com dolomita e relatam foliação (**Figura 2.2E**). Cerva-Alves (2017) descreve na intrusão Passo Feio uma rocha encaixante classificada como titanita-hornblenda granofels localmente porfirítica, com megacristais centimétricos de hornblenda e titanita. Este carbonatito possui características texturais, mineralógicas, tipo de deformação e assinaturas geoquímicas semelhantes ao Três Estradas (esta tese).

Em amostras de rocha em afloramento foram identificados teores de até 12,85% de P₂O₅ (Rocha *et al.*, 2013).

2.3.5. CARBONATITO PORTEIRA

Essa intrusão, descoberta pela Aguaia Resources Ltd (Aguia Resources Ltd., 2013), está localizada 35 km a SE do CTE e apresenta formato linear, com dimensão de 1 km x 70 m, orientado segundo a direção NE e bordejado a norte e nordeste por brechas ígneas carbonatíticas, carbonáticas e hematíticas e a sul por silexitos. Em afloramento apresenta-se

texturalmente maciço (**Figura 2.2F**). Carbonatitos e brechas estão encaixados próximo ao contato entre metassiltitos neoproterozoicas da Formação Arroio Marmeiro e vulcânicas e piroclásticas da Bacia do Camaquã. Junto ao carbonatito ocorrem arenitos líticos com teores ao redor de 5% P₂O₅.

Teores de até 14,57% P₂O₅ foram verificados em afloramentos de carbonatito (Aguia Resources Ltd., 2017).

2.3.6. CARBONATITO SANTA INÊS

O Carbonatito Santa Inês dista aproximadamente 4,5 km do Carbonatito Porteira e 2,5 km do Carbonatito Joca Tavares e ocorre encaixado em rochas metassedimentares da Formação Arroio Marmeiro. Assim como o Porteira, o Santa Inês possui formato linear com direção NE e ocorre bordejado por brechas carbonatíticas e carbonáticas. Sua textura em afloramento é maciça (**Figura 2.2G**). Também estão presentes ao redor do Santa Inês arenitos e siltitos mineralizados em P₂O₅ com concentrações ao redor de 10% (Aguia Resources Ltd., 2017). Observam-se nas rochas sedimentares concreções fosfáticas com diâmetro desde milimétrico até 10 cm.

A Aguia Resources obteve teores de até 13,99% P₂O₅ em carbonatito rico em Fe (32,6% Fe₂O₃) (Aguia Resources Ltd., 2017).

2.3.7. CARBONATITO JOCA TAVARES

O Carbonatito Joca Tavares está localizado 6 km a NE do Carbonatito Porteira. Dentre todas as intrusões é a única com morfologia aproximadamente circular, com aproximadamente 320m de diâmetro. A rocha é maciça, com granulação fina, pouca magnética (**Figura 2.2H**). Essa intrusão foi alojada próximo a zona de contato entre conglomerados e arenitos da Formação Cerro do Bugio, Bacia do Camaquã, e metassiltitos da Formação Arroio Marmeiro (Toniolo *et al.*, 2013) e é bordejado a sul e sudoeste por brechas ígneas carbonatíticas e carbonáticas ricas em magnetita e, menos frequentemente, por fenitos. A anomalia magnetométrica está associada principalmente a essas brechas. As brechas são similares àquelas observadas margeando o Carbonatito Porteira. Ocorrem xenólitos de siltito de suas encaixantes no Carbontito Joca Tavares e cristais de dolomita neoformados com até 1 cm.

A Aguia Resources obteve intercepto mineralizado de até 14,7 m @ 10,8% P₂O₅ (Aguia Resources Ltd., 2017) por meio de sondagem com trado motorizado e concentrações em rocha de até 12,45% P₂O₅ (Aguia Resources Ltd., 2013).



Figura 2.2 - Feições texturais dos carbonatitos do Rio Grande do Sul. A – Afloramento do Metacarbonatito Três Estradas, foliado; B – Afloramento do Metacarbonatito Santa Clara, foliado; C – Testemunho de sondagem do Metacarbonatito Três Estradas, com bandamento gnáissico; D – Testemunho de sondagem do Carbonatito Picada dos Tocos, com bandamento gnáissico (obtido de Rocha *et al.*, 2013); E – Afloramento do Carbonatito Passo Feio, foliado (obtido de Morales *et al.*, 2019); F – Afloramento do Carbonatito Porteira, oxidado, maciço (obtido de

Aguia Resources Ltd., 2013); G – Afloramento do Carbonatito Santa Inês, maciço (obtido de Aguia Resources Ltd., 2017); H – Afloramento do Carbonatito Joca Tavares, maciço, com reação amarela positiva ao molibdato de amônia.

2.3.8. PICRITO DO BOQUEIRÃO

O Picrato do Boqueirão ocorre há 2,5 km dos carbonatitos Porteira a SW e Santa Inês a ENE e a 4,5 km do Carbonatito Joca Tavares a ESE. Trata-se de pequena intrusão tabular (200 x 40m) encaixada em rochas metapelíticas da Formação Arroio Marmeiro, com direção E-W, localizada próxima a interseção das falhas Porteira - ENE-WSW e Graciano – NNE-SSW (Goulart, 2014). Segundo Goulart (2014), a rocha é composta por olivina serpentinizada, ortopiroxênio, diopsídio, kaesurtita, flogopita e vidro, tendo apatita como mineral acessório, sendo descartada pelo autor a possibilidade de metamorfismo e deformação. Ribeiro & Teixeira (1970) apresentam duas idades K-Ar em rocha total obtidas para o Picrato do Boqueirão de 292 ± 10 Ma (borda de intrusão) e 119 ± 10 Ma (centro da intrusão), que devem ser avaliadas com cuidado, embora Ribeiro (1980) assuma que essa intrusão seja Mesozoica.

3. CARBONATITOS

O termo carbonatito foi introduzido na literatura por Brögger (1921) ao denominar rochas de origem magnética com composição carbonática na área de Fen, localizada a 119 km a sudoeste de Oslo, na Noruega. Este termo é utilizado tanto para definir um tipo particular de rocha, quanto o nome de um grupo dado a rochas carbonáticas e silicáticas inter-relacionadas em um complexo magmático ou extrusivo (Mitchell, 2005). Enquanto tipo de rocha, Le Maitre (2002) considera carbonatito como um termo coletivo para rochas ígneas em que o conteúdo modal de minerais carbonatados primários é maior que 50%. Na **Tabela 3.1** é apresentada classificação de carbonatitos com base em Streckeisen (1979) e Le Maitre (2002).

Tabela 3.1 - Classificação de carbonatitos com base em sua composição mineralógica (Streckeisen, 1979 e Le Maitre, 2002).

Carbonato dominante	Nome da rocha	Outros nomes reconhecidos
Calcita	Calcita carbonatito	Sovito (granulação grossa)
		Alvikito (granulação média a fina)
Dolomita	Dolomita carbonatito	Beforsito
Carbonatos ricos em Fe	Ferrocarbonatito	-
Carbonatos de Na, K e Ca	Natrocarbonatito (ex. Oldoinyo Lengai, na Tanzânia)	-

Considerando a composição química de carbonatitos com granulação muito fina, teores de $\text{SiO}_2 < 20\%$ e soluções sólidas complexas de carbonatos de Ca-Mg-Fe+Mn, estas rochas podem ser classificadas como calciocarbonatito, magnesiocarbonatito e ferrocarbonatito (Woolley & Kempe, 1989) (**Figura 3.1**). Gittins & Harmer (1997) consideram que o sistema IUGS trata FeO , Fe_2O_3 e MnO como um componente único, incapaz de distinguir carbonatitos de calcita ou dolomita que contenham hematita ou magnetita, e carbonatitos compostos principalmente de ankerita rica em Fe, ou de calcita e siderita. Estes autores propõem o uso de proporções molares ao invés de peso, nas quais o campo de ferrocarbonatito seja dividido em duas partes, de modo a reconhecer um grupo de rochas como calciocarbonatitos ferruginosos e restringir o termo ferrocarbonatito a rochas muito mais ricas em Fe (**Figura 3.2**). Carbonatitos com conteúdo de $\text{SiO}_2 > 20\%$ são denominados pelos autores como silicocarbonatito.

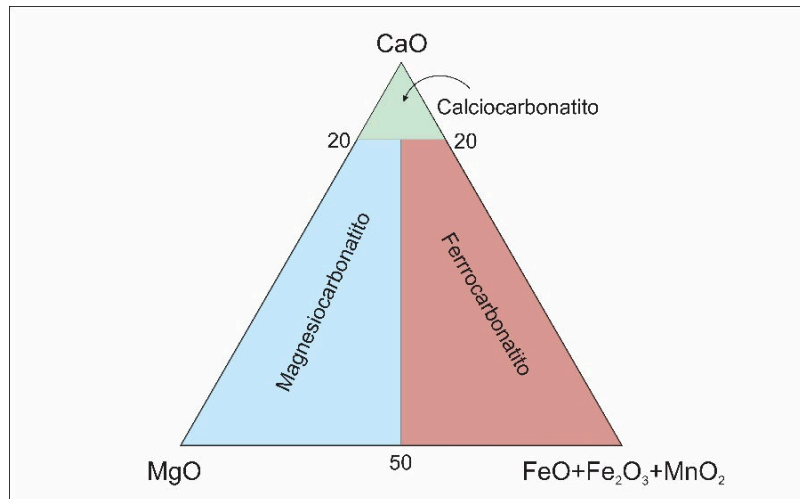


Figura 3.1 - Classificação química de carbonatitos com $\text{SiO}_2 < 20\%$ usando wt% de óxidos (Woolley & Kempe, 1989).

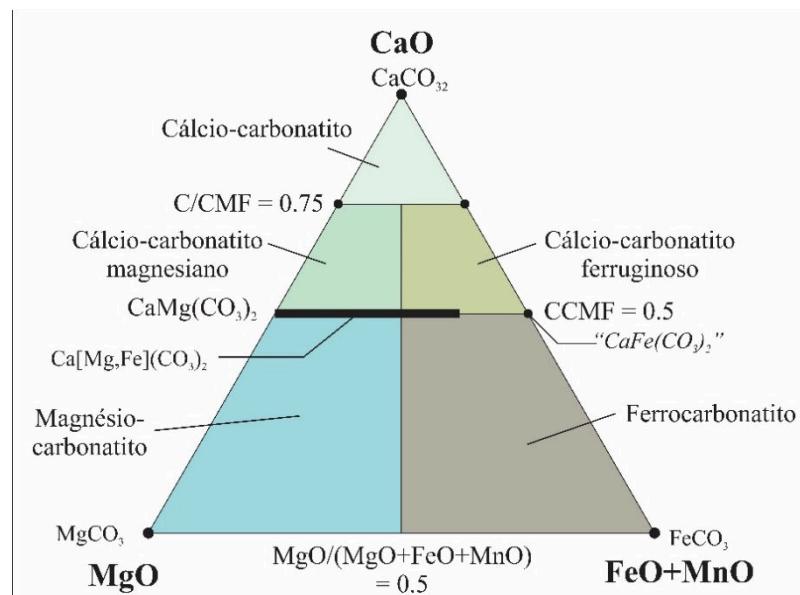


Figura 3.2 - Classificação química de carbonatitos com $\text{SiO}_2 < 20\%$ usando wt% de óxidos de acordo com Gittins & Hamer (1997).

Mitchell (1995, 2005) e Gittins *et al.* (2005) consideram, no entanto, que devido à alta variação dos percentuais modais dos minerais constituintes de rochas geneticamente relacionadas em complexos carbonatíticos, as classificações apresentadas por Streckeisen (1979), Woolley & Kempe (1989) e Le Maitre (2002) não seriam adequadas. Mitchell (2005) alega que a classificação de carbonatitos com conteúdo de $\text{SiO}_2 > 20\%$ como simplesmente silicocarbonatitos, por exemplo, é insatisfatória, pois, não especifica o silicato presente (piroxênios, anfibólios, micas etc) e não considera que um magma que forma carbonatito, por diferenciação magmática, gera um conjunto de rochas em que o teor de carbonato varia

significativamente. O autor vai além das objeções científicas e aponta que o uso de um termo único para “carbonatito” pode resultar em esforços mal direcionados na exploração mineral, quanto à pesquisa de metais raros e outros depósitos minerais, pois, cada tipo genético de carbonatito tem características geoquímicas particulares. Mitchell (2005) sugere, enfim, a adição de prefixos mineralógicos ao nome da rocha, como piroxênio-calcita carbonatito, calcita piroxenito, flogopita-dolomita carbonatito, calcita flogopitito etc.

De acordo com Winter (2001), sabe-se que mais de 280 minerais ocorrem em vários carbonatitos, refletindo a química diversa e exótica dessa rocha. A **Tabela 3.2** lista alguns dos minerais que ocorrem em carbonatitos.

Tabela 3.2 - Alguns minerais presentes em carbonatitos (Adaptado de Winter, 2001).

Carbonatos	Silicatos	Sulfetos	Óxidos-hidróxidos	Halogenetos	Fosfatos
Calcita CaCO_3	Olivina $(\text{Mg},\text{Fe})_2\text{SiO}_4$	Pirrotita $\text{Fe}(1-x)\text{S}$ ($x=0-0.17$)	Magnetita $\text{Fe}^{3+}_2\text{Fe}^{2+}\text{O}_4$	Fluorita CaF_2	Apatita $\text{Ca}_5(\text{PO}_4)_3(\text{OH}, \text{F}, \text{Cl})$
Dolomita $\text{CaMg}(\text{CO}_3)_2$	Monticellita CaMgSiO_4	Pirita FeS_2	Pirocloro $(\text{Na},\text{Ca})_2\text{Nb}_2\text{O}_6(\text{OH},\text{F})$		Monazita $(\text{La},\text{Ce},\text{Nd})\text{PO}_4$
Siderita $\text{Fe}^{2+}(\text{CO}_3)_2$	Alanita $\text{Ca}(\text{REE},\text{Ca})\text{Al}_2(\text{Fe}^{2+},\text{Fe}^{3+})(\text{SiO}_4)$ $(\text{Si}_2\text{O}_7)\text{O}(\text{OH})$	Galena PbS	Perovskita CaTiO_3		
Ankerita $\text{Ca}(\text{Fe}^{2+},\text{Mg},\text{Mn})$ $(\text{CO}_3)_2$	Andradita $\text{Ca}_3\text{Fe}^{3+}_2(\text{SiO}_4)_3$	Esfalerita $(\text{Zn},\text{Fe})\text{S}$	Hematita $\text{Fe}^{3+}_2\text{O}_3$		
Estroncianita SrCO_3	Flogopita $\text{KMg}_3\text{AlSi}_3\text{O}_{10}(\text{F},\text{OH})_2$		Ilmenita $\text{Fe}^{2+}\text{TiO}_3$		
Bastnaesita $(\text{Ce},\text{La})\text{FCO}_3$	Zircão ZrSiO_4		Rutile TiO_2		
Nyerereita $(\text{Na},\text{K})_2\text{Ca}(\text{CO}_3)_2$	<i>Piroxênios (clinopyroxênios):</i>			Badeleita ZrO_2	
Gregoryita $(\text{Na},\text{K})_2\text{CO}_3$	Aegerina-augita $(\text{Ca},\text{Na})(\text{Mg},\text{Fe}^{2+},\text{Fe}^{3+})[\text{Si}_2\text{O}_6]$		Pirolusita Mn^{4+}O_2		
	Diopsídio $\text{CaMgSi}_2\text{O}_6$				
	Augita $(\text{Ca},\text{Na})(\text{Mg},\text{Fe},\text{Al},\text{Ti})(\text{Si},\text{Al})_2\text{O}_6$				
	<i>Anfíbolios alcalinos:</i>				
	Glaucofana $\text{Na}_2(\text{Mg}_3\text{Al}_2)\text{Si}_8\text{O}_{22}(\text{OH})_2$				
	Riebequita $\text{Na}_2(\text{Fe}^{2+}_3\text{Fe}^{3+}_2)\text{Si}_8\text{O}_{22}(\text{OH})_2$				
	Arfvedsonita $\text{Na}_3\text{Fe}^{2+}_4\text{Fe}^{3+}_4(\text{Si}_8\text{O}_{22})(\text{OH})_2$				

Quimicamente, carbonatitos são caracterizados por baixos teores de SiO_2 e elevados conteúdos de Sr, ETR e voláteis. Os carbonatitos têm o maior conteúdo de Sr dentre quaisquer rochas na Terra (pelo menos 2000 ppm) e altas concentrações de ETR (várias centenas de ppm) (Rukhlov & Bell, 2010). Concentrações de Ba, P, Nb e ETR leves são anomalamamente altos

(Winter, 2001). A **Tabela 3.3** apresenta a composição química de tipos diferentes de carbonatitos como referência.

Tabela 3.3 - Composições químicas médias representativas de carbonatitos (Woolley & Kempe, 1989; Winter, 2001).

%	Calcita-carbonatito	Intervalo	Dolomita-carbonatito	Intervalo	Ferro-carbonatito	Intervalo	Natró-carbonatito
SiO ₂	2,72	0,0 – 8,93	3,63	0,6 – 9,40	4,7	0,36 – 9,0	0,16
TiO ₂	0,15	0,0 – 1,09	0,33	0,0 – 1,98	0,42	0,0 – 2,30	0,02
Al ₂ O ₃	1,06	0,0 – 6,89	0,99	0,0 – 4,41	1,46	0,01 – 5,60	0,01
Fe ₂ O ₃	2,25	0,0 – 9,28	2,41	0,0 – 9,57	7,44	0,46 – 17,84	0,05
FeO	1,01	0,0 – 4,70	3,93	0,0 – 10,40	5,28	0,0 – 20,28	0,23
MnO	0,52	0,0 – 2,57	0,96	0,02 – 5,47	1,65	0,23 – 5,53	0,38
MgO	1,80	0,0 – 8,11	15,06	9,25 – 24,82	6,05	0,10 – 14,50	0,38
CaO	49,1	39,24 – 55,40	30,1	20,8 – 47,0	32,8	9,20 – 46,43	14,0
Na ₂ O	0,29	0,0 – 1,73	0,29	0,0 – 2,23	0,39	0,0 – 1,52	32,2
K ₂ O	0,26	0,0 – 1,47	0,28	0,0 – 1,89	0,39	0,0 – 2,80	8,38
H ₂ O+	0,76	0,0 – 4,49	1,20	0,0 – 9,61	1,25	0,04 – 4,52	0,56
P ₂ O ₅	2,10	0,0 – 10,41	1,90	0,0 – 11,30	1,97	0,0 – 11,56	-
CO ₂	36,6	11,02 – 47,83	36,8	16,93 – 47,88	30,7	20,56 – 41,81	31,6
BaO	0,34	0,0 – 5,0	0,64	0,01 – 4,30	3,25	0,02 – 20,60	1,66
SrO	0,86	0,0 – 3,29	0,69	0,06 – 1,50	0,88	0,01 – 5,95	1,42
F	0,29	0,0 – 2,66	0,31	0,03 – 2,10	0,45	0,02 – 1,20	2,50
Cl	0,08	0,0 – 0,45	0,07	-	0,02	0,01 – 0,04	3,40
S	0,41	0,02 – 2,29	0,35	0,03 – 1,30	0,96	0,12 – 5,40	
SO ₃	0,88	0,02 – 3,87	1,08	0,06 – 2,86	4,14	0,06 – 17,10	3,72
ppm							
Li	0,1	-		-	10	-	
Be	2	0,4 – 8	<5	-	12	-	
Sc	7	0,6 – 18	14	10 – 17	10	9 – 14	
V	80	0 – 300	89	7 – 280	191	56 – 340	116
Cr	13	2 – 479	55	2 – 175	62	15 – 135	0
Co	11	2 – 26	17	4 – 39	26	11 – 54	
Ni	18	5 – 30	33	21 – 60	26	10 – 63	1
Cu	24	4 – 80	27	4 – 94	16	4 – 45	
Zn	188	20 – 1120	251	15 – 851	606	35 – 1800	88
Ga	<5	-	5	-	12	-	<20
Rb	14	4 – 35	31	2 – 80		-	178
Y	119	25 – 346	61	5 – 120	204	28 – 535	7
Zr	189	4 – 2320	165	0 – 550	127	0 – 900	0
Nb	1204	1 – 15000	569*	10 – 3000	1292	10 – 5033	28
Mo	-	-	12	-	71	26 – 94	125
Ag		-		3,2 – 3,3		3,4 – 3,5	
Cs	20	-	31	-	31	-	6
Hf	-	-	3	-	-	-	0
Ta	5	-	21	4 – 34	1	-	0
W	-	-	10	-	20	-	49
Au	-	-	-	-	12	10 – 15	-
Pb	56	30 – 108	89	30 – 244	217	46 – 400	-
Th	52	5 – 168	93	4 – 315	276	100 – 723	4

U	9	0,3 – 29	13	1 – 42	7	1 – 20	11
La	608	90 – 1600	764	95 – 3655	2666	95 – 16883	545
Ce	1687	74 – 4152	2183	147 – 8905	5125	1091 – 19457	645
Pr	219	50 – 389	560	-	550	141 – 1324	-
Nd	883	190 – 1550	634	222 – 1755	1618	437 – 3430	102
Sm	130	95 – 164	45	33 – 75	128	30 – 233	8
Eu	39	29 – 48	12	3 – 20	34	11 – 78	2
Gd	105	91 – 119	-	-	130	31 – 226	-
Tb	9	9 – 10	5	0,9 – 8	16	4 – 36	-
Dy	346	22 – 46	-	-	526	11 – 105	2
Ho		3 – 9		-		1 – 9	
Er	4	-	-	-	17	3 – 35	-
Tm	1	-	-	-	2	0,3 – 3	-
Yb	5	1,5 – 12	10	1 – 52	16	1 – 16	-
Lu	1	-	0	-		-	0

Na literatura sobre carbonatitos, destaca-se o trabalho seminal publicado por Wyllie & Tuttle (1960). Com caráter experimental, esse trabalho mostrou que a calcita pode se cristalizar como fase *liquidus* em temperaturas de aproximadamente 650 °C e pressões em torno de 0,1 GPa, subsidiando a teoria de origem ígnea de carbonatitos discutida à época. Até a década de 1960, carbonatitos eram considerados calcários remobilizados, xenólitos de mármore ou precipitados de soluções hidrotermais (Shand, 1943). Desde então, e com a descoberta do vulcão de lavas carbonatíticas Oldoinyo Lengai, na Tanzânia, importantes trabalhos foram apresentados sobre o caráter ígneo desse tipo de rocha. Destacam-se Tuttle & Gittins (1966), que publicaram o livro *Carbonatites*, no qual reuniram uma série de artigos sobre estudos de campo e laboratório de carbonatitos e rochas associadas; Heinrich (1966), que no mesmo ano publicou o livro *The geology of carbonatites*, com destaque para a descrição de carbonatitos em todos os continentes, à exceção da Oceania; Kapustin (1980), autor do livro *Mineralogiya karbonatitov* (Mineralogia de carbonatitos), apresenta resultados de investigações mineralógicas de maciços de rochas básicas e ultrabásicas e carbonatitos da Província de Kola e Sibéria, na Rússia; Bell (1989), traz ao público um compêndio de artigos em seu livro *Carbonatites: genesis and evolution*, que discutem, entre outros, que carbonatitos podem se originar das mesmas fontes que rochas silicáticas associadas, não sendo a recíproca verdadeira; Woolley (1987; 2001) traz em seus livros, *Alkaline Rocks and Carbonatites of the World: Part 1: North and South America* e *Part 3: Africa*, respectivamente, uma reunião de dados sobre rochas alcalinas e carbonatitos conhecidos até então, com breves descrições geológicas, coordenadas geográficas e referências bibliográficas originais; Kogarko *et al.* (1995) ficaram responsáveis pelo livro *Alkaline Rocks and Carbonatites of the World: Part 2: Former USSR*.

(antiga União Soviética, 1922-1991); e, Wall & Zaitsev (2004), que publicaram o livro *Phoscorites and carbonatites from mantle to mine: the key example of the Kola Alkaline Province*, no qual essas rochas são analisadas, buscando entender como magmas carbonáticos e magmas ricos em carbonatos ascendem até a crosta e à superfície, colocando também em evidência trabalhos de pesquisadores russos sobre o tema. Woolley (2019), lançará neste 2º semestre o quarto livro da série: *Alkaline Rocks and Carbonatites of the World: Part 4: Antarctica, Asia and Europe, Australasia and Oceanic Islands*.

3.1. OCORRÊNCIAS DE CARBONATITOS

A maioria dos carbonatitos ocorre preferencialmente em ambientes intraplaca estáveis e em ambientes de rifte em estágio inicial onde há litosfera espessa ou manto litosférico a ser fundido, sob condições de pressão ou temperatura elevadas (Bailey, 1974). Carbonatitos ocorrem sob a forma de complexos plutônicos, *plugs*, diques, *cone sheets*, tefra, derrames e raros *sills* (Barker, 1989). As ocorrências em margens continentais ligadas à orogenia e em bacias oceânicas são bastante raras (**Figura 3.3**).

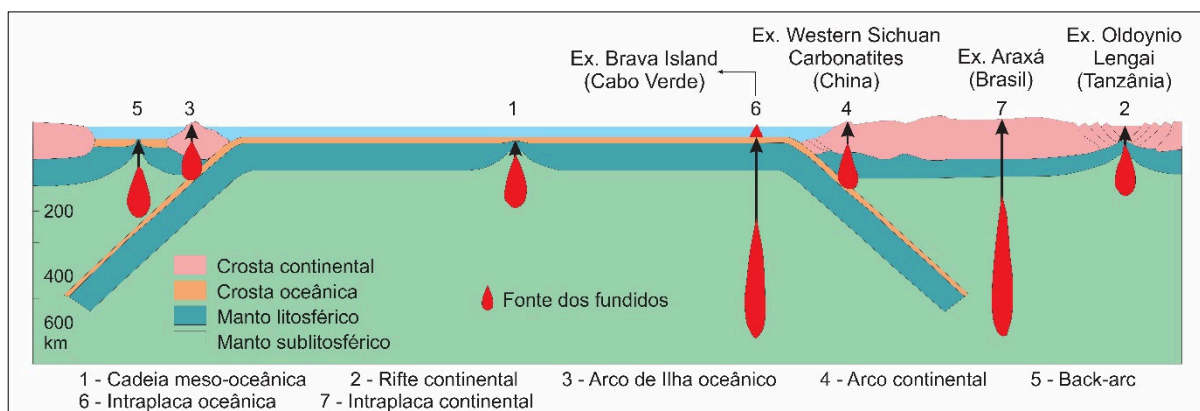


Figura 3.3 - Seção generalizada ilustrando configuração de placas tectônicas e locais de geração de magma, com posicionamento de carbonatitos gerados em ambientes tectônicos distintos (modificado de Winter, 2001).

Woolley & Kjarsgaard (2008) discorrem sobre 527 intrusões carbonatíticas conhecidas no mundo, até a publicação daquele trabalho, geradas em variados ambientes e com diversas associações petrológicas. Em geral, os carbonatitos ocorrem em complexos intrusivos relativamente pequenos junto a rochas alcalinas silicáticas (tipicamente sienitos, nefelinitos, ijolitos e urtitos). Associações menos comuns incluem piroxenitos, peridotitos, kimberlitos do grupo I ou lamprófiros (Bell *et al.*, 1999). Utilizando o critério de tipo de rocha silicática

associada à ocorrência de carbonatito, Woolley & Kjarsgaard (2008) propuseram um esquema de classificação dessas associações, levando em consideração a distinção entre carbonatitos magmáticos de alta temperatura e carbonatitos carbohidrotermais de baixa temperatura, e definiram 8 grupos de rochas silicáticas (**Tabela 3.4, Figura 3.4**). Dentre as 527 ocorrências de carbonatitos, 78% estão relacionadas às rochas silicáticas, deixando clara a predominância da relação genética entre elas frente à ocorrência de carbonatitos isolados.

Tabela 3.4 - Esquema de classificação das associações entre carbonatitos e rochas silicáticas (elaborada a partir de Woolley & Kjarsgaard, 2008).

Rochas silicáticas associadas à carbonatitos	Nº de associações com carbonatitos magmáticos de alta temperatura	Nº de associações com carbonatitos carbohidrotermais de baixa temperatura	Total
Carbonatito somente	96	20	116
Carbonatito com <1% (raro) de rochas silicáticas, tipicamente diques de lamprófiros	10		10
Lamprófiro (tipicamente ultrabásica, i.e. alnoito, ailikito, damtjernito)	20	2	22
Kimberlito	5		5
Nefelinito +/- Melteigito/Ijolito/Urtito +/- rochas ultramáficas cumuláticas (sem rochas ricas em melilita)	112	12	124
Melilitito +/- Melilitolito +/- rochas ultramáficas cumuláticas	27	3	30
Fonolito +/- Sienito feldspatoidal	58	10	68
Traquito +/- Sienito	33	10	43
Basanito +/- Gабro	3	2	5
Rochas ultramáficas cumuláticas (dunito ou peridotito ou piroxenito) +/- sienito	39	14	53
Sem dados para classificar	51		51
Total geral	454	73	527

Em negrito está destacada a associação mais comum.

Com base na distribuição de carbonatitos pelo mundo (Woolley & Kjarsgaard, 2008), nota-se que estão preferencialmente intrudidos em rochas proterozoicas, que representam aproximadamente 2/3 das rochas encaixantes desse tipo de intrusão (**Figura 3.4**). Entretanto, com base em um total de 274 carbonatitos datados, dentre os 527 cadastrados, Woolley & Bailey (2012) mostram que 64% das ocorrências são do Fanerozoico, isto é, mais jovens que 542 M.a. (**Figura 3.5**). Estes dados revelam que existe uma grande concentração de

carbonatitos em áreas pré-cambrianas cratônicas, a maioria das quais é elevada topograficamente (Woolley & Kjarsgaard, 2008). Há, portanto, uma notável tendência para rochas hospedeiras terem idade proterozoica.

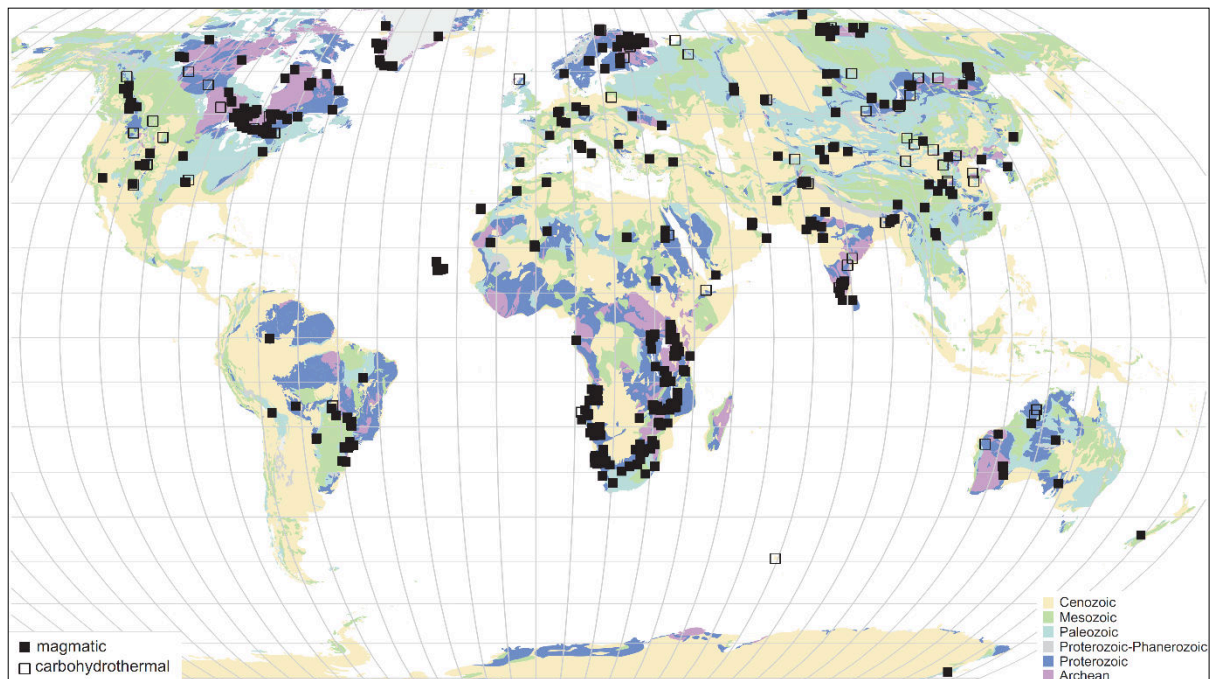


Figura 3.4 - Distribuição de carbonatitos pelo mundo: ocorrências de carbonatitos magmáticos versus carbonatitos carbohidrotermais (total de 527 ocorrências) (Woolley & Kjarsgaard, 2008).

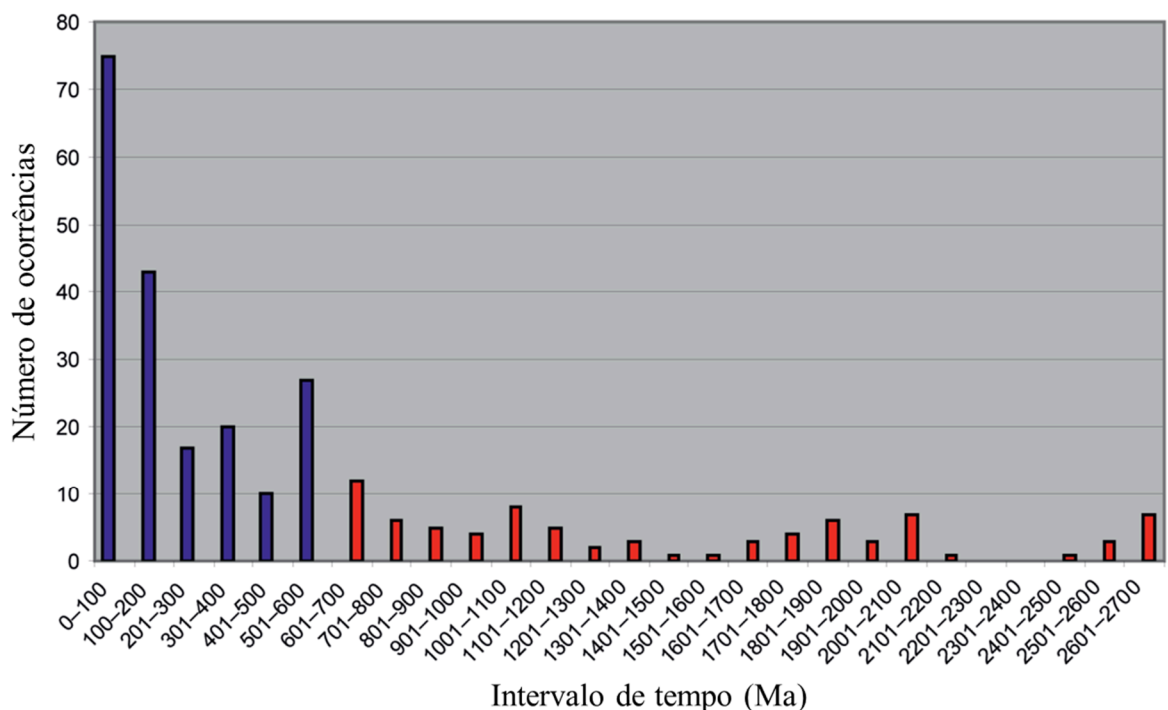


Figura 3.5 - Distribuição de carbonatitos isotopicamente datados no tempo geológico. Há 192 carbonatitos fanerozoicos e 82 pré-cambrianos (Total de 274 dados) (Woolley & Bailey, 2012).

Idades obtidas com datação isotópica mostram que muitas províncias carbonatíticas foram afetadas por repetidas intrusões, com até 5 episódios separados por centenas de milhões de anos. Pelo menos três províncias no mundo tiveram atividade desse tipo desde o Arqueano até o recente: Península de Kola, no norte da Noruega, Suécia e Finlândia, no norte da Europa; Ontário e Sudoeste de Quebec, no Canadá; e Groenlândia (**Figura 3.6**).

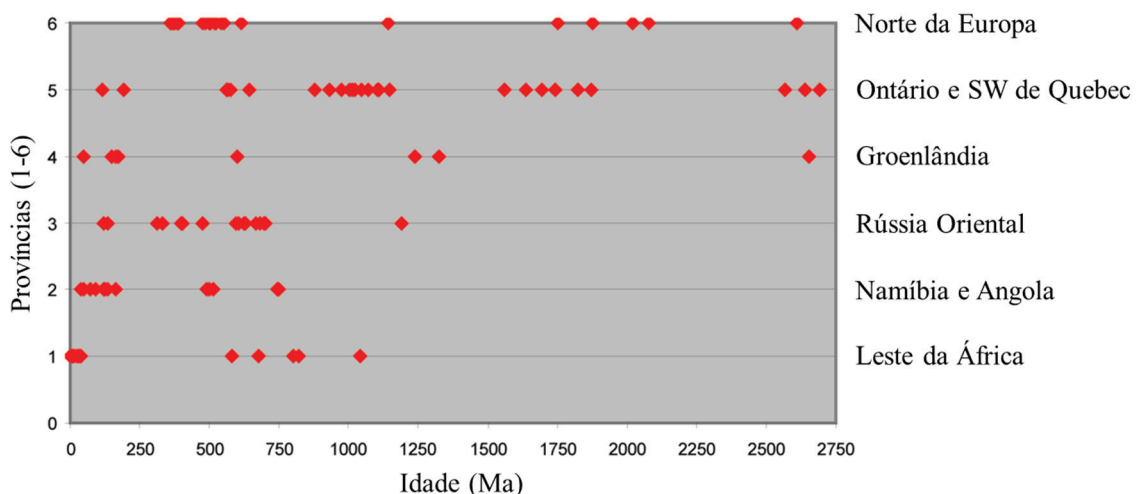


Figura 3.6 - Idades de carbonatitos em 6 áreas distintas, mostrando repetição de atividade carbonatítica ao longo do tempo, nas seguintes províncias: (1) África Oriental (Quênia, Uganda, Tanzânia e Zâmbia); (2) Namíbia e Angola, (3) Rússia Oriental (East Tuva, Enisei, Oriente Sayan, Baikal, Aldan); (4) Groenlândia; (5) Ontário e sudoeste de Quebec; (6) Norte da Europa (Península de Kola, no norte da Noruega, Suécia, Finlândia) (Woolley & Bailey, 2012).

Bell (2001) defende que a repetitividade de intrusões carbonatíticas em uma mesma província ao longo de milhares de milhões de anos esteja relacionada a plumas mantélicas. O papel da litosfera seria agir como uma camada limítrofe mecanicamente resistente durante a atuação da pluma (Bell & Simonetti, 1996; Rukhlov & Bell, 2010). Bell (2001) se baseou em estudos de isótopos de Sr, Nd e Pb, que sugerem que carbonatitos derivem de fonte mantélica para desenvolver sua hipótese. Segundo o autor, uma pluma localizada na base da litosfera se aproveita de zonas de fraqueza, podendo estar associada a rifteamento continental, e estaria envolvida na concentração de elementos voláteis e incompatíveis durante a migração ascendente do magma. O calor gerado pela pluma penetra na litosfera, tanto por condução como por advecção, por fusões a partir de descompressão astenosférica, e promove a fusão de porções do manto litosférico e a gênese de magmas potássicos (Gibson *et al.*, 1995), carbonatíticos e silicáticos carbonatados. Como exemplo desse modelo, Herz (1977), Toyoda *et al.* (1994), VanDercar *et al.* (1995), Gibson *et al.* (1995) e outros apresentam a relação

genética entre a Província Ígnea do Alto Paranaíba (APIP, sigla em inglês), no estado de Minas Gerais, Brasil, e a Pluma de Trindade.

A APIP consiste de um volumoso magmatismo máfico ultrapotássico (kamafugitos, olivina lamproítos madupíticos e kimberlitos, quantidades menores de melilitito e complexos alcalinos contendo carbonatito) (Gibson *et al.*, 1995; Brod *et al.*, 2000, 2004). Os autores consideram que nas reconstruções dos movimentos das placas há aproximadamente 85 Ma (idade de formação da APIP), a localização da APIP coincidia com a posição postulada da atual pluma de Trindade (ou Martin Vaz) (**Figura 3.7**). Gibson *et al.* (1995) propõem que o generalizado magmatismo alcalino do Cretáceo Superior no sudeste do Brasil possa ter sido causado pelo impacto desta pluma na base da litosfera subcontinental.

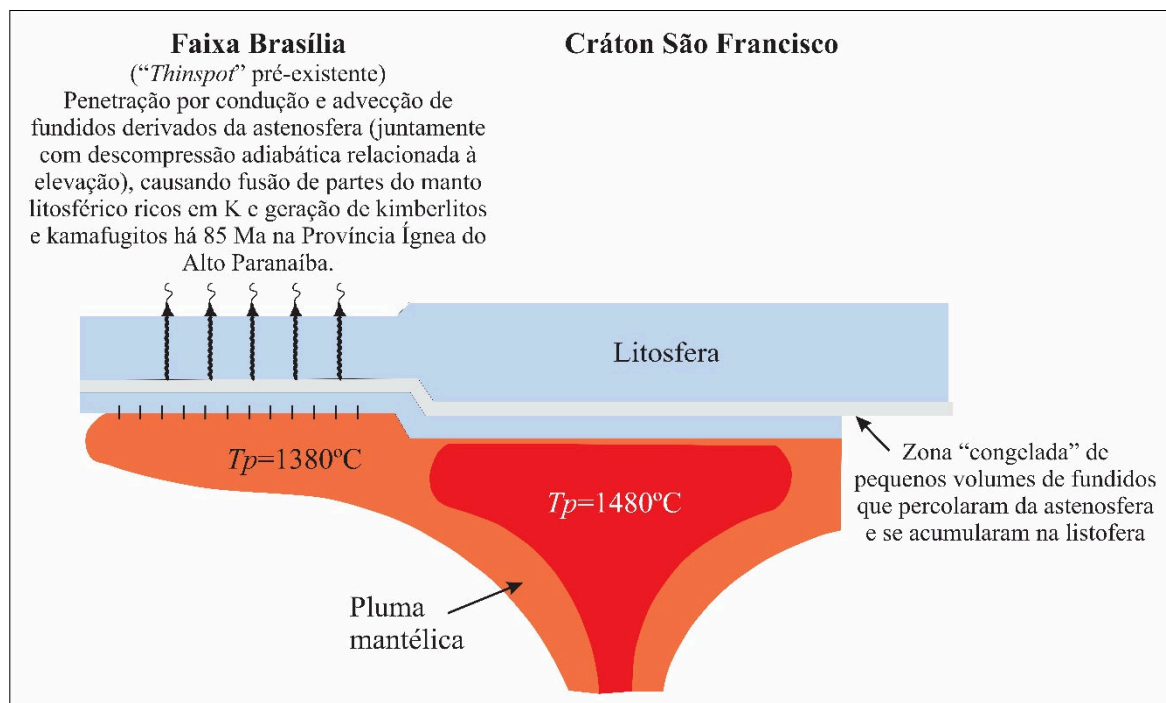


Figura 3.7 - Ilustração esquemática para mostrar o impacto da pluma mantélica abaixo da litosfera com várias espessuras (modificado de Thompson & Gibson (1991) *in* Gibson *et al.*, 1995).

Alguns autores (Bailey, 1987, 1993; Woolley, 2003; Woolley & Bailey, 2012), no entanto, descartam o envolvimento de plumas na gênese de carbonatitos baseados em: 1) repetida atividade carbonatítica em um mesmo segmento crustal ao longo de extensos períodos de tempo; 2) sincronicidade de ocorrência de carbonatitos em toda placa; 3) rara progressão de idade ao longo de falhas ou lineamentos, como seria de se esperar se fossem produzidos em pontos quentes (*hot spots*); 4) baixos gradientes geotérmicos requeridos para a formação destes fundidos próximos ao solidus para o peridotito na presença de voláteis; e, 5) aumento da

degaseificação do manto profundo e metassomatismo na base da litosfera ao longo do tempo geológico. Para Woolley & Bailey (2012), o magmatismo é ativado quando fraturas profundas na litosfera são reabertas em resposta a grandes mudanças nos padrões globais de movimento das placas tectônicas.

De acordo com Winter (2001), independentemente do processo exato (fusão parcial direta do manto, cristalização fracionada ou imiscibilidade de líquidos), a astenosfera parece ser o contribuinte predominante para os magmas de carbonatito e *hot spots* ou plumas associadas a voláteis podem desempenhar papel importante em sua gênese. Por fim, Kresten & Troll (2018) concluem que, embora o modelo de pluma associado à gênese de carbonatito seja o mais aceito, estudos de controles litosféricos tem sido aprofundados, ou seja, ainda não há consenso sobre o assunto.

3.2. GÊNESE DE CARBONATITOS

Diversos autores discutem a origem de carbonatitos. Durante a década de 1960, quando o manto passou a ser reconhecido como a fonte da maioria dos magmas e quando os estudos sobre a lava do vulcão Oldoinyo Lengai (Dawson, 1962), na Tanzânia, foram aprofundados, é que carbonatitos passaram a ser vistos como tendo suas origens a partir do manto também. Nos últimos 60 anos a pesquisa de carbonatitos progrediu nas áreas de estudos experimentais e isotópicos. No entanto, questões genéticas levantadas por Heinrich (1966) ainda continuam em debate. O relacionamento entre carbonatitos e rochas alcalinas altamente insaturadas (nefelinitos, melilititos) e outros magmas contendo carbonatos (aillikitos, kimberlitos), por exemplo, ainda é controverso (Downes *et al.*, 2012).

A hipótese mais aceita, baseada em evidências isotópicas (Sr e Nd), sugere que carbonatitos são formados a partir de fontes astenosféricas profundas (Bell, 2001; Bell *et al.*, 2004), com contribuições litosféricas de acordo com estudos isotópicos de Nd, Pb e Sr (Bell & Tilton, 2001). Evidências mostraram que os carbonatitos podem ser gerados por uma variedade de processos, envolvendo tanto os fundidos primários quanto os diferenciados (Bell *et al.*, 1999, 2004; Bell, 2001), caracterizando carbonatitos, portanto, como grupo de rochas com multiplicidade de origens (Mitchell, 2005).

Woolley & Bailey (2012) consideram que uma das características mais controversas de modelos propostos para a petrogênese do carbonatito tem sido o papel relativo desempenhado

pela litosfera e astenosfera. Com base em dados geoquímicos e isotópicos de Sr, Nd, Pb, C e O, Nelson *et al.* (1988) argumentaram que fundidos carbonatíticos são gerados na astenosfera, enquanto outros pesquisadores, como Kalt *et al.* (1997) interpretaram seus dados isotópicos de Sr, Nd e Pb como indicadores de fonte em manto litosférico heterogêneo. Outros modelos, também baseados em dados isotópicos Sr, Nd e Pb, propõem mistura entre a litosfera e astenosfera (Bell & Simonetti, 1996). A maioria dos modelos exige algum grau de metassomatismo, geralmente da litosfera (Woolley & Bailey, 2012).

Mitchell (2005) reconhece dois grandes grupos de carbonatito (*sensu lato*) a partir do conceito de clã petrológico (Daly, 1914) e utilizando abordagem mineralógica-genética (Mitchell, 1995): i) calcita e/ou dolomita carbonatitos primários, geneticamente relacionados a nefelinito, melilitito, kimberlito e outras rochas cristalizadas a partir de magmas derivados do manto, e ii) resíduos carbotermais derivados de ampla variedade de magmas, sendo carbotermal um termo referente a fluidos de baixa temperatura derivados de magmas fracionados dominados por CO₂, mas também contendo F e H₂O em quantidades variáveis. Os resíduos carbotermais podem representar tanto a continuidade da diferenciação de um magma carbonatítico primário, quanto a fusão de determinadas rochas crustais sob condições de P e T específicas, neste último caso gerando rochas modalmente semelhantes a carbonatitos, mas distintas geneticamente.

Dentro desses 2 grandes grupos, Mitchell (2005) individualizou tipos geneticamente distintos de carbonatito, cada qual relacionado a um tipo específico de magma (**Tabela 3.5**).

Tabela 3.5 - Descrição das associações petrológicas relacionadas a carbonatitos reconhecidas por Mitchell (2005). A coluna “descrição” tem como referência o trabalho supracitado.

Gr.	Clã/associação petrológica	Descrição (Mitchell, 2005)
Primário	Carbonatito do clã-nefelinito	Provavelmente a associação mais comum. É representada por carbonatitos associados a rochas intrusivas (suite melteigito-ijolito-urtito, nefelina sienito) e rochas extrusivas (nefelinito, suite fonolito). Formam complexos plutônicos de nefelina sienito-ijolito-carbonatito. Ex.: Fen (Noruega), Alnö (Suécia), Spitzkop (África do Sul), Tororo e Napak (Uganda), Lackner Lake (Canadá) (Figura 3.8).
	Carbonatito do clã-melilitito	Esta associação inclui carbonatitos associados a rochas plutônicas (melilitolitos, <i>i.e.</i> , okaíto, turjaíto, afrikandito, uncompahgrito, perovskita piroxenito, dunito, etc). Também estão incluídos neste grupo os carbonatitos e lamprófiros ultramáficos associados à facies hipoabissal do clã melilitito, ou seja, alnöito, polzenito, etc. Formam depósitos de Ti, Nb, Fe, ETR e P. Ex.: Araxá, Catalão, Tapira (Brasil), Kovdor, Turja (Kola, Rússia), Iron Hill (EUA), Oka (Canadá), Gardiner (Groenlândia).
	Clã kimberlito – calcita kimberlito	Carbonatitos, no sentido modal do IUGS, estão associados a kimberlitos <i>bona fide</i> (fidedignos) e representam diferenciais tardios do magma kimberlítico e são denominados

Carbohidrotermal		calcita kimberlitos, em reconhecimento desta afinidade genética. No entanto, eles não possuem qualquer relação genética com carbonatitos associados a magmas dos clãs nefelinito ou melilitito. Ex.: Benfontein, Wesselton sills, Premier (África do Sul), Internationalya (Sibéria), Jos & Nikos (Canadá).
	Associação ailikito-carbonatito	Ailikitos consistem em proporções modais variáveis de olivina, flogopita e calcita e/ou dolomita. Podem incluir espinélio magnesiano e perovskita junto a clinopiroxênio e anfibólio menos comuns, embora em mela-alkilito sejam mais frequentes (Tappe <i>et al.</i> , 2005). A ausência de feldspatoídes serve para separar os ailikitos dos lamprófiros ultramáficos modalmente similares associados com melilitolito ou nefelinito. Ex.: Torngat-Abloviak (Canadá), Sarfartoq, Sisimiut-Maniitsoq (Groenlândia).
	Associação peralcalina nefelinito-natrocobonatito	As lavas natrocobonatíticas de Oldoinyo Lengai são tidas como únicas. Consistem de fenocristais de gregoryita (carbonato de Na, K, Ca) e nyerereita (carbonato de Na e Ca) em matriz composta predominantemente por carbonato semelhante a gregoryita, nyerereita rica em Ba, silvita sódica e fluorita. Calcita e dolomita são ausentes em rochas sem alteração. O natrocobonatito é considerado derivado de magma residual e não tem relação parental com calcita carbonatitos encontrados no clã nefelinito, ao contrário do que foi sugerido por Le Bas (1981).
	Carbonatitos sem associação com rochas silicáticas	Woolley & Kjarsgaard (2008) observaram que existem pelo menos 116 ocorrências de carbonatito sem associação com rochas silicáticas, excluindo os fenitos relacionados. Os complexos Bulhoek (África do Sul) e Laiwu Zibu (China), por exemplo, não apresentam rochas silicáticas associadas pertencentes a suítes ijolito-nefelina sienito e melilitolito. Uma possibilidade é a não exposição das partes mais profundas de um complexo plutônico parental (ex.: Kangankunde, Malawi).
	“Carbonatitos” suíte potássica	As características da maioria das ocorrências aqui são sua associação com diversas rochas sieníticas potássicas saturadas a insaturadas, alta abundância de carbonatos ricos em ETR e barita e a ausência total de membros das suítes ijolito e melilitolito. Os magmas parentais para os complexos potássicos plutônicos não são bem caracterizados, mas parecem ter sido derivados do manto litosférico metassomatizado antigo (Mitchell, 1995). Ex.: Mountain Pass, Rocky Boy (EUA), Dunkeldyksky (Tajiquistão) e Loch Borrallan (Escócia).
	“Carbonatitos” suíte sódica	Esta classe tem como exemplo o complexo Khibina (Rússia), em que os carbonatitos estão associados a sienitos peralcalinos sódicos. Embora existam pequenas quantidades dessa rocha em relação às demais rochas silicáticas em Khibina, elas demonstram que magmas peralcalinos sódicos podem se diferenciar até fluidos residuais que cristalizam carbonatos de ETR, Ca, Na.
	Rochas carbonatadas ricas em ETR-F não relacionadas a rochas alcalinas subsaturadas	Este grupo de rochas carbonadas ricas em ETR e F não possui relação óbvia com quaisquer rochas alcalinas insaturadas. De acordo com Gittins (1978), veios carbonatados ricos em Sr e ETR não deveriam ser automaticamente classificados como carbonatitos. Partindo do fato que alguns magmas formadores de carbonatitos se diferenciam até resíduos tardios ricos em fluorocarbonatos de ETR (ex. Fen, Noruega e Saint Honoré, Canadá), alguns autores visualizam que ocorrências de fluorocarbonatos de ETR semelhantes em outros ambientes também sejam derivadas de carbonatito, o que leva a especulação genética inapropriada. Ex.: Ravelli-Lemhi, Goldie (EUA), Rock Canyon Creek (Canadá) e Bayan Obo (China).
	Pseudo-carbonatitos anatáticos	Em geral são rochas ricas em carbonato, mas com mineralogia e associação geológica com outras rochas distinta de carbonatitos fidedignos, sendo resultados de fusões anatáticas de rochas crustais sem qualquer relação com magmas alcalinos derivados do manto. Ex.: área de Haliburton – Bancroft (Canadá) e partes do norte do estado de Nova York (EUA).

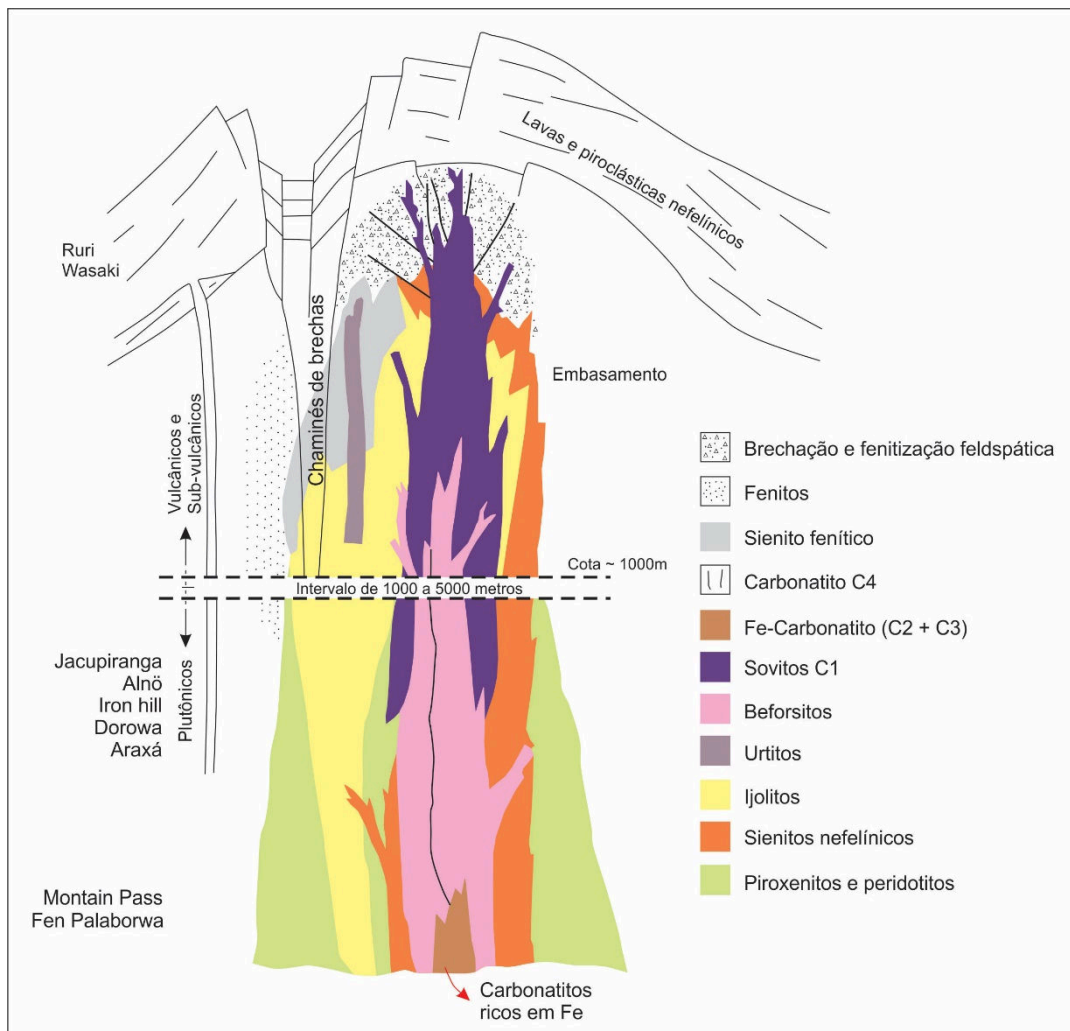


Figura 3.8 - Modelo de intrusão carbonatítica associado a complexo plutônico representativo do Clá-nefelinito (Biondi, 2003 a partir de Le Bas, 1987).

Os estudos experimentais, até a década de 1990, tomaram como base a relação espacial entre rochas silicáticas e carbonatitos, desconsiderando as mais de 116 ocorrências de carbonatitos como intrusões isoladas (Woolley & Kjaarsgard, 2008).

A discussão sobre a geração de fundidos carbonatíticos aborda três possibilidades (Gittins, 1989; Harmer & Gittins; 1998, Winter, 2001; Jones *et al.*, 2013): i) fusão direta do manto metassomatizado, parcialmente carbonático, para produzir magmas primários separados de carbonato e silicato; ii) fracionamento a baixa pressão crustal de magma parental derivado do manto; e, iii) separação imiscível de líquidos carbonático e silicático (nefelinítico ou fonolítico), sob pressão variável dentro do manto ou da crosta, a partir de magma derivado do manto. Na **Figura 3.9** é apresentado um fluxo simplificado para a geração de carbonatitos.

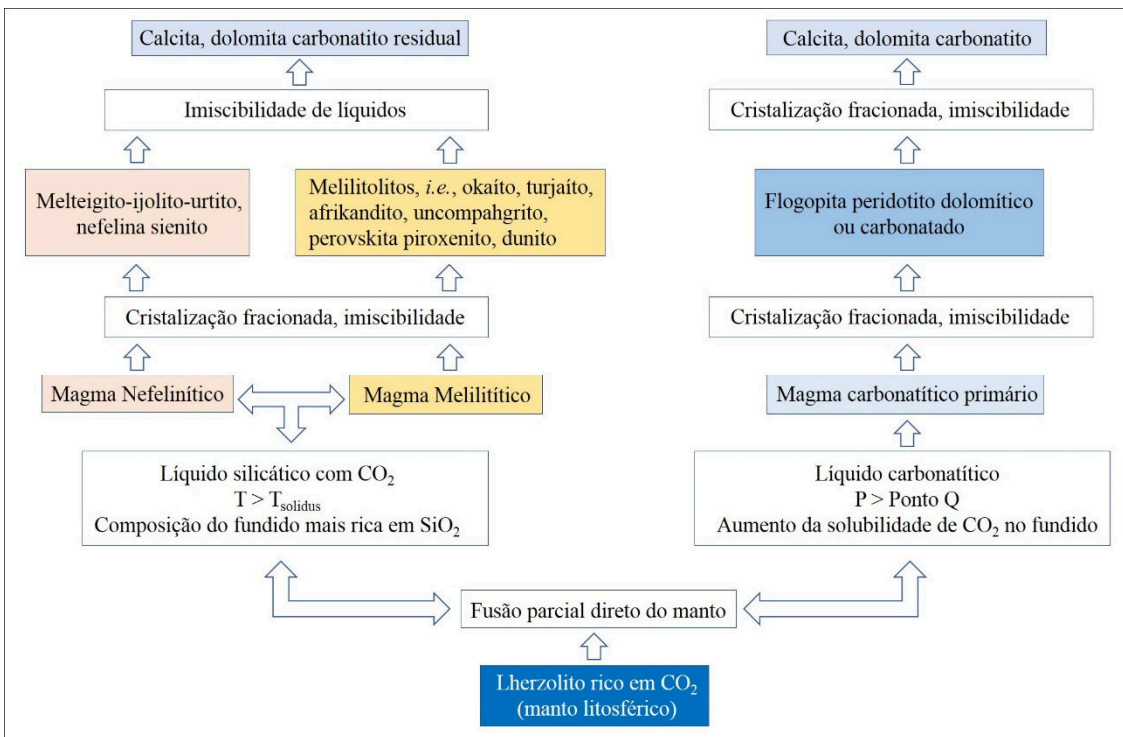


Figura 3.9 - Fluxo esquemático de formação de carbonatitos a partir de fusão parcial de lherzolito rico em CO₂ e processos de diferenciação (ver em associação com a **Figura 3.10**).

3.2.1. FUSÃO DIRETA DO MANTO PERIDOTÍTICO, METASSOMATIZADO, PARCIALMENTE CARBONATADO, COM PRODUÇÃO DE MAGMAS PRIMÁRIOS CARBONATÍTICOS E SILICÁTICOS

A íntima associação dos carbonatitos e magmas silicáticos alcalinos, assim como muitas semelhanças químicas entre os dois tipos de magma, sugere que os carbonatitos se formam em associação com rochas silicáticas alcalinas (Gittins, 1989; Winter, 2001).

A **Figura 3.10** mostra as relações de fase no sistema peridotito-H₂O-CO₂ de acordo com Wyllie (1989), baseado em experimentos de Olafsson e Eggler (1983), as quais ajudam a explicar a formação de fundidos ricos em carbonato no manto. A fusão de lherzolito (peridotito composto por olivina e quantidades subordinadas de clinopiroxênio e ortopiroxênio) é função da temperatura, pressão e conteúdos de H₂O e CO₂ e outros voláteis como S, F e Cl (Winter, 2001), cuja variação reflete diretamente na composição dos fundidos gerados.

Segundo Eggler (1989), a fusão de peridotito-lherzolito, quando livre de voláteis e sob variadas pressões e frações de fusão, produz líquidos que variam de komatiítos, picrítos, toleítos a basaltos alcalinos. Composições mais exóticas, como carbonatitos, requerem voláteis

na fonte de fusão ou material mantélico afetado por metassomatismo, seja SCLM (sub-continental lithospheric mantle) ou astenosfera enriquecida (Winter, 2001).

Sob condições oxidantes, assumidas para entendimento do diagrama da **Figura 3.10**, as fases C-O-H podem existir como mistura de fluidos contendo H₂O e CO₂, que gerarão manto lherzolítico com quantidades menores de hornblenda (Hbl), flogopita (Phlog), dolomita (Do) e/ou magnesita (Mc). Sob baixas pressões, em profundidades de até aproximadamente 60 km, a assembleia solidus é composta de fundido mais anfibólio-espinélio lherzolito e vapor rico em CO₂ (V). Nessas condições a posição do solidus (curva roxa) se situa entre o solidus para o peridotito seco e o solidus saturado em H₂O (curvas vermelhas).

Com o aumento da pressão, em profundidades em torno de 70 km, começa a se desenvolver uma fase sub-solidus rica em CO₂, em que dolomita começa a ser gerada junto ao anfibólio. Nessa situação a temperatura diminui consideravelmente (~150 °C) em direção ao ponto Q, enquanto a pressão se mantém quase constante. A formação de magnesita (MgCO₃) no fundido após a dolomita se tornar uma fase do manto incorre na continuidade da queda de temperatura com o aumento da pressão, em função da dissolução de CO₂ no líquido, o que leva a sua estabilização a temperaturas mais baixas. Com o aumento da pressão ainda sob condições de queda da temperatura, o anfibólio atinge sua estabilidade e uma nova assembleia solidus composta por flogopita-magnesita lherzolito rico em CO₂ passa a se formar. Nesse ponto, em profundidade aproximada de 100 km associada ao aumento de P e T, o solidus com carbonato novamente deflete, sobrepondo-se ao solidus para lherzolito saturado em H₂O, o que permite que fundidos primários de carbonatito sejam gerados.

A composição de líquidos quase solidificados (baixa percentagem de fusão parcial) a pressões superiores ao ponto Q na **Figura 3.10** (a primeira aparição de um carbonato no solidus com pressão crescente) reflete o aumento da solubilidade do carbonato no fundido (Winter, 2001). Ainda de acordo com Winter (2001), a predominância de calcita carbonatito e sua ocorrência como primeiro carbonatito em localidades onde uma sequência de líquidos carbonatíticos é colocada, sugere-se que magma carbonatítico rico em carbonato de cálcio possa ser o líquido carbonatítico inicial e parental para os outros tipos de carbonatito. No entanto, dolomita carbonatito parece ser o tipo formado por fusão parcial de lherzolitos mantélicos tipicamente ricos em Mg (**Figura 3.9**).

Quanto a temperaturas acima do solidus (aumento da porcentagem de fusão parcial), Eggler (1989) considera que as composições dos fundidos tornam-se mais ricas em SiO₂ e

incluem melilititos e nefelinitos, dando condições para a formação de complexos alcalino-carbonatíticos (**Figura 3.9**).

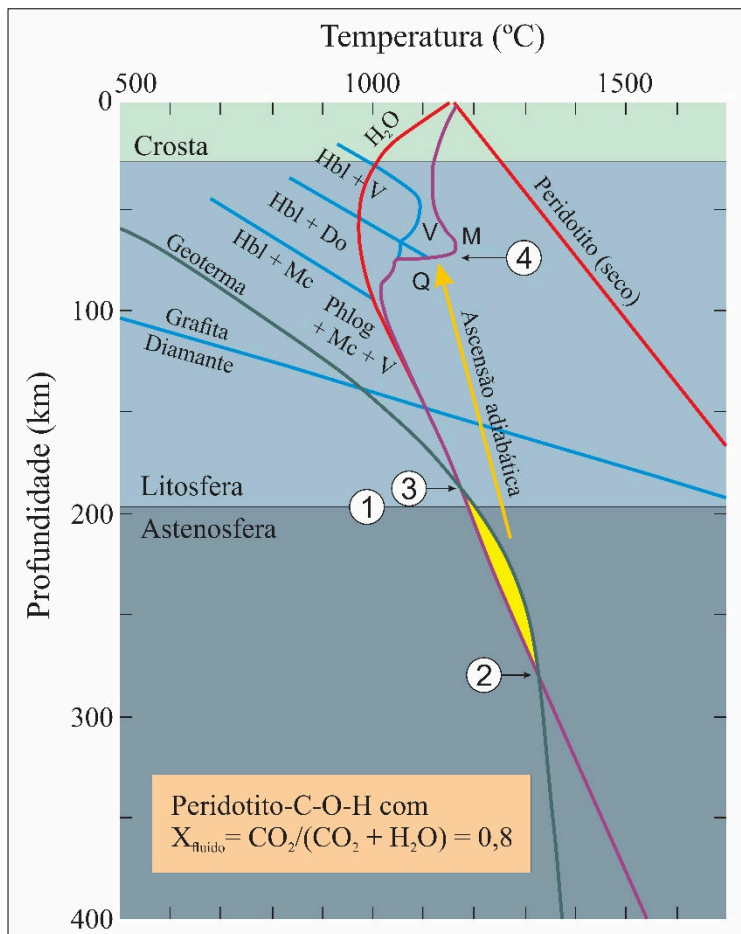


Figura 3.10 - Gráfico de temperatura versus profundidade mostrando a posição do peridotito-C-H-O com razão $\text{CO}_2/\text{CO}_2 + \text{H}_2\text{O}$ igual a 0,8 extrapolada para altas pressões (após Wyllie, 1989).

Se houver suficientes CO_2 e H_2O disponíveis em uma pluma no manto astenosférico que ascende ao longo da geotermia, a fusão do lherzolito ocorrerá no momento em que a temperatura solidus no ponto 2 for excedida (**Figuras 3.10 e 3.11**). Líquidos carbonatíticos primários podem se acumular no limite litosfera-astenosfera (ponto 1, **Figuras 3.10 e 3.11**), onde encontram alguma resistência mecânica devido à natureza mais rígida da litosfera (Winter, 2001). Outros líquidos carbonatíticos podem penetrar no manto litosférico, seguindo o gradiente geotérmico, até encontrarem o solidus novamente no ponto 3 e começarem a solidificar sob temperaturas sub-solidus (**Figuras 3.10 e 3.11**). A cristalização dos líquidos carbonatíticos saturados em voláteis gera degaseificação levando a metassomatismo das rochas adjacentes. Os vapores liberados se aproveitam de zonas de fraqueza na litosfera, permitindo que o fundido suba ainda mais antes de se cristalizar completamente (**Figura 3.11**).

Se a astenosfera se elevar sob uma zona rifte (para a qual a **Figura 3.11** foi projetada), a pluma astenosférica crescente pode resultar em graus mais altos de fusão parcial e produzir fusões silicáticas alcalinas, como nefelinitos ou melilititos, além de carbonatitos e kimberlitos (Winter, 2001). Se os fundidos se elevarem adiabaticamente, eles podem atingir o nível 4 em uma profundidade de cerca de 75 km, onde encontrarão o solidus na **Figura 3.10**. Neste ponto eles devem cristalizar, liberando novamente os voláteis, metassomatizando e fraturando as rochas da parede do conduto (Winter, 2001).

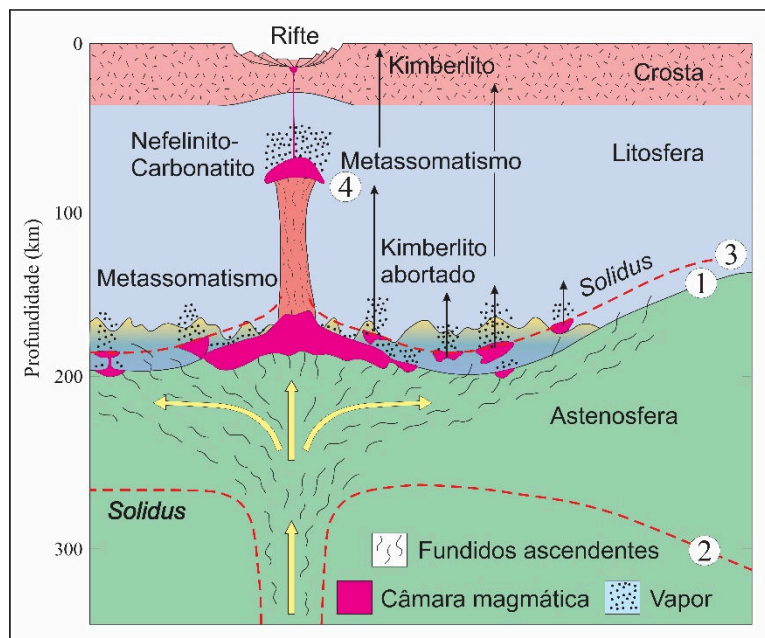


Figura 3.11 - Corte esquemático de uma pluma do manto astenosférico abaixo de ambiente continental de rifte, e a gênese de nefelinito-carbonatitos e kimberlito-carbonatitos (após Wyllie, 1989). Os números correspondem à **Figura 3.10**.

3.2.2. FRACIONAMENTO A BAIXA PRESSÃO CRUSTAL DE MAGMA PARENTAL DERIVADO DO MANTO

Magmas alcalino-silicáticos parentais derivados do manto podem gerar carbonatitos por cristalização fracionada quando enriquecidos em CO_2 e H_2O (**Figura 3.9**). A entrada de H_2O na estrutura de anfibólios alcalinos no manto peridotítico hidratado causa a fusão precoce desses minerais e liberação de álcalis na faixa de profundidade de 65 a 80 km (Eggler, 1989), tendo como produtos primários da fusão nefelinitos e melilititos. De acordo com Gittins (1989) e Winter (2001), a adição de CO_2 e/ou fonte mantélica metassomatizada enriquecida tornaria a geração de fundidos alcalinos ainda mais provável em faixa mais ampla de condições de P e T.

A partir de magmas parentais nefeliníticos e melilitíticos, são gerados complexos de rochas silicáticas alcalino-carbonatíticas. A cristalização fraccionada de fases não carbonatadas de um magma Ne-normativo (nefelina normativa) carbonatado poderia concentrar CO₂ no fluido restante até o ponto de saturação de carbonato, resultando em líquido carbonatítico residual (Lee e Wyllie, 1994).

3.2.3. SEPARAÇÃO IMISCÍVEL DE LÍQUIDOS CARBONÁTICO E SILICÁTICO, SOB PRESSÃO VARIÁVEL DENTRO DO MANTO OU DA CROSTA, A PARTIR DE MAGMA DERIVADO DO MANTO

Juntamente com a fusão parcial, o fracionamento de cristais e a degaseificação / metassomatismo, a imiscibilidade líquida é considerada um dos mais importantes mecanismos de diferenciação em magmas alcalinos e carbonatíticos (Brod *et al.*, 2013).

Experimentos em diferentes sistemas compostionais provam que existe imiscibilidade entre certos líquidos carbonáticos e silicáticos separados de magma parental comum (Gittins, 1989). Os magmas carbonatíticos podem representar uma das frações imiscíveis que coexistirão com uma fração de silicato também carbonatada, sendo que esta última também teria o potencial de diferenciar por cristalização fracionada para um fundido rico em carbonato (Mitchell, 2005).

Com base em estudos experimentais a partir de nefelinito e melilitito carbonatados sintéticos, Brooker (1998) demonstrou que a imiscibilidade pode ocorrer nas partes superiores do manto litosférico ou na crosta, já que o tamanho do campo de miscibilidade entre os líquidos silicático e carbonatítico é fortemente dependente de mudanças na pressão de CO₂. Evidências isotópicas e geoquímicas registradas nos líquidos parentais e nas rochas carbonatíticas e silicáticas demonstram a atuação do processo de imiscibilidade em sua formação (Harmer & Gittins, 1998, Brod *et al.*, 2013).

O sistema Na₂O-CaO-Al₂O₃-SiO₂-CO₂ tem importância para a origem dos carbonatitos, pois ilustra as lacunas de imiscibilidade determinadas experimentalmente nesse sistema sob condições de P e T variáveis. No entanto, ele não é relevante para a maioria dos processos e produtos do manto, mas inclui composições que representam alguns nefelinitos e fonolitos evoluídos, calciocarbonatitos e natrocarbonatitos (Lee & Wyllie, 1997).

Três fases não sólidas imiscíveis coexistem em equilíbrio nesse sistema: um líquido alcalino silicático, um líquido carbonatítico sódico e um fluido alcalino volátil, sendo este último possivelmente relacionado à fenitização.

3.2.4. VISCOSIDADE E DENSIDADE

Os carbonatitos estão entre os magmas de menor viscosidade na Terra (Dobson *et al.*, 1996), com valores estimados (η) em fundidos carbonáticos, sob condições de manto litosférico cratônico, variando de 0,005 a 0,065 Pa s, comparáveis à viscosidade da água (Sharygin *et al.*, 2017). A viscosidade tende a diminuir com o aumento da pressão e com o decréscimo do conteúdo de sílica, principalmente em magmas polimerizados (Junqueira-Brod *et al.*, 2005). A partir de trabalho experimental, Dobson *et al.* (1996) concluem que a viscosidade extremamente baixa dos fundidos carbonatíticos indica que a variação dessa propriedade não é um fator tão importante para modelar o fluxo de carbonatito no manto quanto as variações na densidade.

A densidade é controlada basicamente pela composição do magma e a ascensão dele frequentemente depende desta propriedade. Para uma composição fixa, a densidade varia inversamente com a temperatura e diretamente com a pressão (Junqueira-Brod *et al.*, 2005).

A ascenção de fundidos carbonatíticos é rápida em função de sua baixa viscosidade, tendo a capacidade de se moldar facilmente aos condutos pelos quais ascendem, além de criar novos devido ao fraturamento hidráulico da encaixante causado por sua degaseificação. Ao encontrar uma barreira de densidade entre o manto e a crosta, o fundido começa a estacionar e se solidificar. Junqueira-Brod *et al.* (2005) mostram a importância do controle de barreiras de densidade sobre a profundidade de intrusões alcalinas e carbonatíticas na Província Alcalina de Goiás como exemplo.

3.3. SOBRE CARBONATITOS E ROCHAS ALCALINAS DEFORMADAS (EM INGLÊS DARC'S) E CARBONATITOS SINTECTÔNICOS

Novas descobertas geológicas sobre carbonatitos ainda estão sendo feitas e compreendem, por exemplo, o vulcanismo silicático-carbonatítico transportando xenólitos de

manto, carbonatitos em extensas zonas de cisalhamento e carbonatitos associados com cinturões de ofiolito (Jones *et al.*, 2013).

3.3.1. DARC's

As associações de rochas alcalinas e carbonatitos (ARC's) com áreas cratônicas estáveis e riftes intracontinentais são os tipos clássicos de instalação de carbonatitos na crosta. No entanto, rochas alcalinas deformadas e carbonatitos (DARC's), que formam um pequeno subconjunto (<10%) de ARC's, tornaram-se foco de atenção, pois foi reconhecido que em alguns lugares estão associadas a zonas de sutura (Burke *et al.*, 2003, 2008; Burke & Khan, 2006; Attoh *et al.*, 2007; Ashwal *et al.*, 2016).

Bailey (1974) enfatiza a repetição de alojamento de carbonatitos, aproveitando uma mesma estrutura em intervalos variados ao longo do tempo. Tem-se como exemplo a região do Malawi, Groenlândia, Ontário e sudoeste de Quebec e Norte da Europa (Península de Kola). Burke *et al.* (2003) notam a mesma repetição no que tange a DARC's em zonas de suturas.

Burke *et al.* (2003) registraram ocorrências de rochas alcalinas e carbonatitos deformados na África (sigla em inglês, DARC's), os quais estão concentrados em zonas de suturas de idades variadas. Os autores defendem a utilização de DARC's para mapear antigas zonas de colagem. Essa hipótese considera a intrusão de rochas alcalinas como indicativas de episódio de extensão litosférica que precedem orogenias, enquanto a deformação evidente em DARC's registra o evento colisional, ou seja, seria possível datar início e fim de um Ciclo de Wilson (**Figura 3.12**).

No entanto, com base em estudos geocronológicos em DARC's na zona de sutura Pan-Africana Dahomeyide, no oeste da África, Attoh *et al.* (2007) demonstram que nem sempre essas rochas podem ser usadas para restringir o início de um Ciclo de Wilson, pois, não necessariamente intrusões de DARC's ocorrem durante o rompimento da litosfera. No caso das rochas estudadas pelos autores, as intrusões são sin-orogênicas, datadas em 592 ± 2 Ma e estão associadas a rochas de ultra alta pressão (eclogitos) (Ganade de Araújo *et al.*, 2014).

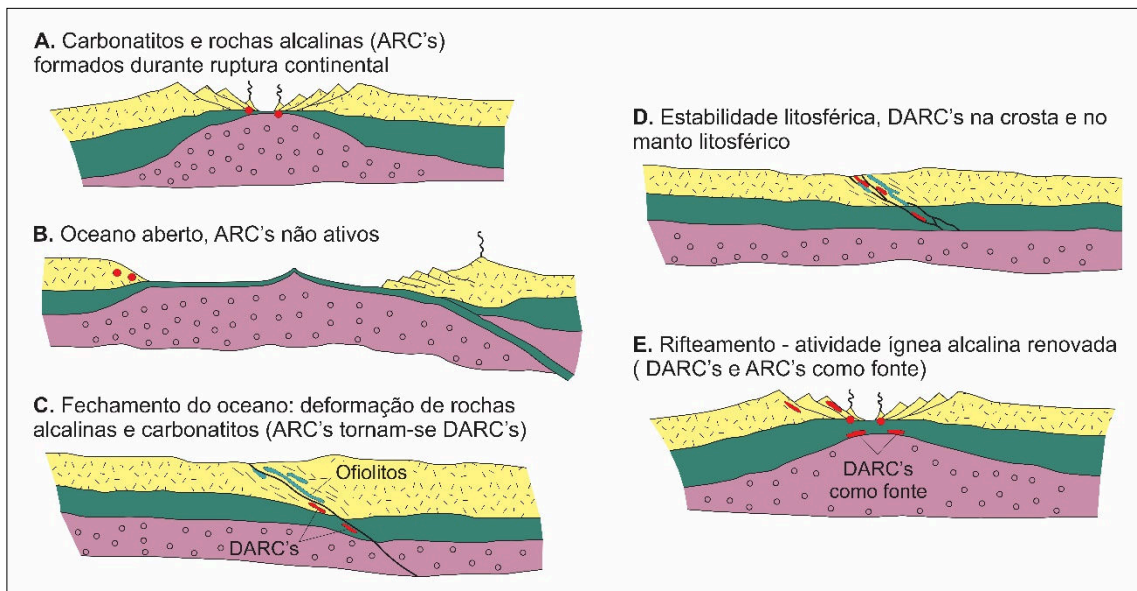


Figura 3.12 - Modelo geral de episódios repetidos de magmatismo intracontinental alcalino proposto por Burke & Khan (2006), com base em observações no Malawi, no intervalo de tempo de ~1.0 Ga a 140 Ma. A: Desenho ilustrando como rochas alcalinas e carbonatitos (ARC's) são expelidos em riftes intracontinentais. B: Desenho ilustrando como essas ARC's podem se posicionar em uma margem continental, enquanto um oceano se desenvolve. C: Desenho ilustrando como os ARC's, antes na margem continental, podem se envolver em uma colisão continental para tornarem-se rochas alcalinas e carbonatitos deformados (DARC's). Alguns desses DARC's são subducidos e se tornam parte da litosfera continental, enquanto outros permanecem na crosta. D: Um intervalo de centenas de milhões de anos pode passar sem atividade. E: Um novo rifteamento localizado na antiga zona de sutura pode levar à erupção de novos ARC's por fusão parcial que envolve as fontes de DARC's na litosfera subjacente do manto (Burke & Khan, 2006).

3.3.2. CARBONATITOS SIN-TECTÔNICOS

Porque eram tidos como raros, carbonatitos sintectônicos foram considerados durante muito tempo como meras curiosidades geológicas. Nos últimos vinte anos complexos com essa origem foram descobertos e estudados (principalmente na Rússia, Ucrânia, Índia, China e Canadá), verificando-se serem mais comuns que inicialmente imaginado, ganhando com isso uma nova dimensão, não só científica como econômica.

O que torna os carbonatitos sin-tectônicos singulares é a sua colocação na crosta terrestre durante a evolução de cinturões móveis, em ambiente que precede a compressão e o dobramento dos mesmos. Carbonatitos desse tipo se destacam pela morfologia linear, localizando-se ao longo de zonas de falhas profundas e, em geral, estendendo-se por dezenas de quilômetros, chegando por vezes a se prolongar por mais de 100 km (Levin *et al.*, 1978 in Lapin *et al.*, 1999). São constituídos por sistemas de intrusões lineares ou encurvados e que se

alternam com as rochas encaixantes, com as quais se dispõem concordantemente (Lapin *et al.*, 1999).

Ao examinarmos a morfologia dos complexos carbonatíticos, de imediato distinguimos dois tipos extremos: um deles é representado por complexos intrusivos do *Tipo “Central”*, os quais se caracterizam pela sua forma arredondada ou oval e com frequente distribuição anelar zonal das rochas constituintes e o outro é representado por *Zonas Lineares de Carbonatitos e Fenitos* (**Figura 3.13**).

Os complexos carbonatítico-feníticos situam-se em cinturões orogênicos atuais (Carbonatito Loe Shilman), em cinturões do Neógeno e em seus análogos do Paleozoico e Pré-Cambriano (Angico dos Dias, Chernigov, etc.). Como regra, estão desconectados no espaço e no tempo de complexos carbonatíticos do *Tipo Central*, os quais intrudem predominantemente ortoplataformas.

Nos casos em que os complexos carbonatítico-feníticos se localizam nas partes internas das plataformas, apresentam idades muito antigas. As idades desses complexos mostram que eles se formaram antes da estabilização protoplataformal e instalação do regime plataformal (Lapin *et al.*, 1999).

As diferenças entre o regime geológico-tectônico, o caráter deformacional dos carbonatitos, e seus diferentes tipos morfológico-formacionais são apresentados na **Tabela 3.6**.

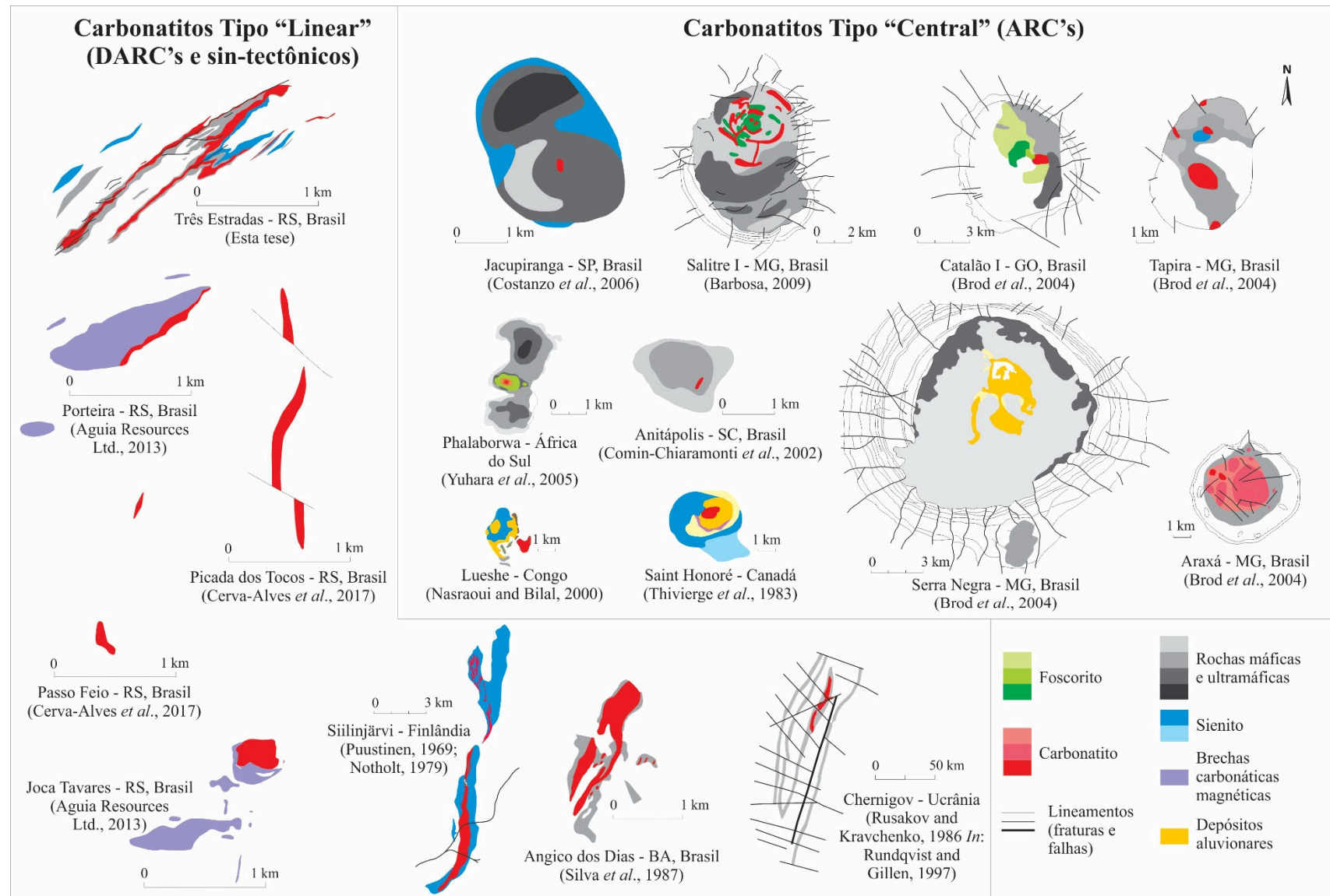


Figura 3.13 - Comparação entre morfologia e dimensões de carbonatitos do tipo “central” e do tipo “linear” (Adaptado de Barbosa, 2009).

Tabela 3.6 - Regime geológico-tectônico, deformação dos carbonatitos, e seus tipos morfológico-formacionais (Lapin & Ploshko, 1988 *Apud*: Lapin *et al.*, 1999).

Tipos morfológico-formacionais de Complexos Carbonatíticos	Ambiente Geológico-tectônico de formação e disposição espacial dos Complexos Carbonatíticos	Relação geológica e temporal dos Complexos Carbonatíticos com as rochas encaixantes	Profundidade de intrusão, idade absoluta dos Complexos Carbonatíticos	Características energéticas do regime de formação dos Complexos Carbonatíticos	Forma e dimensão dos Complexos Carbonatíticos	Rochas magmáticas e metassomáticas que acompanham os carbonatitos	Grau de diferenciação dos carbonatitos
Zonas lineares de carbonatitos e metassomatitos alcalinos	Falhas profundas de faixas móveis em estruturas dobradas do futuro embasamento plataforma, que herdaram a estruturação tectônica deformacional da faixa. A intrusão dos carbonatitos ocorre antes da estabilização das faixas móveis e instalação do regime plataforma	Os carbonatitos se dispõem de modo concordante ou subparalelo às rochas encaixantes	Predominam complexos de grande e média profundidade. Idades antigas do Paleoproterozoico (em sua maioria)	Grande dissipação de energia ao longo da falha profunda, ausência de grandes anomalias térmicas locais nas rochas encaixantes, que tem por característica alto fluxo térmico	As zonas de carbonatitos e de metassomatitos alcalinos podem ter extensão de dezenas a centenas de km, e largura variando até 5-10 km; no âmbito das zonas os carbonatito formam corpos tabulares ou lenticulares, que por vezes podem constituir corpos sinuosos, encurvados com dimensões de até 2 x 0,2 km	Rochas magmáticas normalmente estão ausentes, às vezes elas são representadas por eutéticos (sienitos e nefelina sienitos) de baixo ponto de fusão, desenvolvem-se amplamente metassomatitos alcalinos (albititos, rochas semelhantes a carbonatitos, etc.)	Os carbonatitos são pouco diferenciados, normalmente constituem intrusões de um único estágio (são monofásicos)
Complexos Carbonatíticos tipo “Central”	Regiões de reativação tectono-magmática em crâtons estáveis e em faixas de dobramentos estabilizadas, que estão há longo tempo em regime plataforma	Os complexos carbonatíticos apresentam contatos discordantes em relação às rochas encaixantes. O diapirismo é uma característica do magmatismo, presença de estruturas cupoliformes nas encaixantes	Predominantemente complexos superficiais, de baixa profundidade e idade variada	Os complexos carbonatíticos exibem nitidamente excesso de energia termal, formam grandes anomalias térmicas nas rochas encaixantes, que apresentam baixo fluxo térmico	Os complexos carbonatíticos constituem “stocks” de forma circular, oval ou isométrica, com área de 1-2 até 40-50 km ² . No âmbito de cada complexo, os carbonatitos formam “stocks”, veios, diques anelares, radiais e cônicos	As rochas magmáticas estão representadas por uma série de diferenciação magmática, desde rochas ultramáficas até nefelina sienitos. Desenvolvem-se amplamente metassomatitos alcalinos (aegirina-albiticos e outros.)	Os carbonatitos estão representados por uma série de diferenciação, com vários estágios de intrusão. São polifaciais e polifásicos.

3.4. FENITIZAÇÃO

Fenitos são auréolas de rochas metassomaticamente alteradas de alta temperatura devido a intrusões de rochas carbonatíticas e alcalinas (Elliot *et al.*, 2018). A fenitização é geralmente vista como resultado de múltiplos pulsos de fluidos ricos em álcalis gerados a partir do resfriamento e cristalização do fundido alcalino ou carbonatítico, sendo difícil distinguir em muitas ocorrências, no entanto, se os fenitos produzidos são o resultado da intrusão do silicato alcalino ou dos magmas carbonatíticos (Le Bas, 2008).

Heinrich (1985) identificou três tipos de fenitos: potássico, potássico-sódico e sódico. Todos são de aparência sienítica e alguns são facilmente confundidos com sienitos ígneos, a menos que seja dada atenção especial à mineralogia, composição química e relações de campo (Le Bas, 2008).

Por muito tempo fenitos sódicos eram atribuídos ao magmatismo silicático alcalino e fenitos potássicos às intrusões carbonatíticas, mas Le Bas (2008) relata carbonatitos associados tanto a fenitização potássica, quanto sódica.

De acordo com Zharikov *et al.* (2007), fenitos são caracterizados pela presença de K-feldspato, albita, piroxênios alcalinos e/ou anfibólios alcalinos. Fenitos potássicos mostram alta proporção de ortoclásio rico em K ou microlínio ou em alguns casos concentrações de flogopita com abaixo Al ou biotita (Le Bas, 2008). Por sua vez, a fenitização sódica é caracterizada pela abundância de anfibólios sódicos e alguns piroxênios acompanhados por feldspatos ricos em K e Na (Le Bas, 2008).

A perda ou mobilização de sílica ainda é motivo de discussão. Le Bas (2008) define como uma feição importante de fenitos a perda de sílica seguida pelo aumento de álcalis. Bardina e Popov (1994), no entanto, argumentam que a fenitização é marcada por aumento do teor de álcalis ($\text{Na}_2\text{O} + \text{K}_2\text{O}$), independente do conteúdo de sílica ou sua mobilidade. Com base em análises de dados de vários complexos, Elliot *et al.* (2018) reportam que a maioria mostra aumento substancial nos álcalis entre 0,5 e 10% em peso e diminuição na sílica entre 0,5 e 29% em peso. Enquanto os protólitos com baixo teor inicial de sílica podem experimentar enriquecimento em sílica durante a fenitização, Elliot *et al.* (2018) afirmam que este não é o caso quando as rochas circundantes possuem conteúdo inicialmente altamente alcalino e citam como exemplo um granito aplítico, consistindo apenas de feldspato e quartzo (Le Maitre, 2002), que perde até 2,3% em peso de álcalis durante a fenitização em Meech Lake, Canadá.

A fenitização pode ocorrer de forma pervasiva ou como veios, com intensidade diminuindo com a distância da origem da intrusão, e ainda como brechas. Kresten (1988) interpretou a brechação em torno dos carbonatitos como resultado do aumento de volume durante o processo de fenitização. Verplanck *et al.* (2014), consideram que a presença de brechas está relacionada a liberação explosiva de fluidos e voláteis de um magma em desenvolvimento abaixo.

Le Bas (1981) e Woolley (1982) propuseram zonação química vertical de fenitos, com a hipótese de que ocorram composições mais sódicas em profundidade e fenitos potássicos em níveis mais rasos da crosta. K é mais móvel a baixas temperaturas que Na, permitindo que K seja transportado por fluidos até profundidades menores (Elliot *et al.*, 2018). Fenitos potássicos tendem a se formar em halo mais proximal em relação à intrusão, enquanto fenitos sódicos ocupariam porção mais distal Woolley (1982).

4. THE MESOPROTEROZOIC TRÊS ESTRADAS ALKALINE-CARBONATITE COMPLEX, BRAZIL: GEOLOGY, MINERALOGY, GEOCHEMISTRY, C-O ISOTOPES AND GENETIC IMPLICATIONS

Cimara Francisca Monteiro^{a,b}, José Affonso Brod^c, Pedro Cordeiro^d, Ítalo Lopes de Oliveira^a

^a University of Brasilia, Institute of Geosciences, Campus Darcy Ribeiro, Asa Norte, Brasília, DF. Brazil, Postal Code: 70.910-900.

^b Geological Survey of Brazil (SGB-CPRM), Center for Technological Development (CEDES), Setor Bancário Norte, Brasília, DF, Brazil. Postal Code: 70.040-904.

^c Federal University of Goiás, Faculty of Sciences and Technology, Campus Aparecida de Goiânia, Aparecida de Goiânia, GO, Brazil. Postal Code: 74.968-755

^d Pontifical Catholic University of Chile, Vicuña Mackenna 4860, Santiago, Chile, Postal Code: 78.204-36

Corresponding author: cimara.monteiro@cprm.gov.br

ABSTRACT

The Três Estradas Alkaline-Carbonatitic Complex (TEC) was the first Mesoproterozoic intrusion of the type identified in the Rio de la Plata Craton, in southern Brazil. The TEC has a linear shape consisting of ultramafic rocks, carbonatites, and metasomatized syenites, metamorphosed into amphibolite facies, and subjected to intense ductile deformation, intruded into the Taquarembó Terrane, a remnant of the Rio de la Plata Craton. Geochemical and isotopic signatures suggest that it evolved from the partial fusion of a metasomatized mantle source enriched in LREE, through liquid immiscibility and fractional crystallization of silicate liquid CO₂ rich. K and Na rich solutions were released by carbonatites and caused the metasomatism of ultramafic rocks and syenites. Similar genesis and evolution are identified in the Neoproterozoic Picada dos Tocos and Passo Feio carbonatites, emplaced in accretional terrane of the Sul Riograndense Shield (SRS), suggesting that this shield has lodged carbonatite intrusions of recurrent magmatic episodes over time in areas of weakness. Isotopic ¹³C and ¹⁸O signatures similar to TEC are found in Mesoproterozoic carbonatites from the Alkaline Province of Ontario, which reinforces that these intrusions originated from a primitive mantle

and provides one more clue to the hypothesis that Laurentia and the Rio de la Plata Craton were linked at the end of the Mesoproterozoic. At the end of the Dom Feliciano orogeny, during the Ediacaran, the TEC rocks were subjected to deformation caused by the development of a sinistral Cerro dos Cabritos shear zone and as more recent processes were subjected to low temperature alterations. O TEC forms phosphate deposit with measured and inferred mineral resources 83 Mt @ 4.1% P₂O₅ and inferred mineral resources 21.8 Mt @ 3.67% de P₂O₅, using a cut-off grade of 3% P₂O₅.

Keywords: Três Estradas Complex, Carbonatite, Sul-Riograndense Shield, phosphate mineralization.

4.1. INTRODUCTION

Carbonatites can be generated by a variety of processes, involving both primary and differentiated melt (Kjarsgaard & Hamilton, 1989b; Bell *et al.*, 1999, 2004; Mitchell, 2005). Among these processes there are: i) mantle origin from a partial fusion of the carbonate-containing metasomatized mantle (Eagler, 1989; White & Wyllie, 1992; Harmer & Gittins, 1998; Hammouda & Keshav, 2015); ii) originated by fractional crystallization at low crustal pressure of parental magma derived from the mantle (Simonetti & Bell, 1994; Lee & Wyllie, 1994, 1998; Guzmics *et al.*, 2015); e, iii) origin by separation of immiscible carbonate and silicate liquids, under variable pressure within the mantle or crust, from magma derived from the mantle (Kjarsgaard & Hamilton, 1989a; Brooker, 1995, 1998; Wyllie & Lee, 1998; Halama *et al.*, 2005; Brod *et al.*, 2013; Novella *et al.*, 2014; Potter *et al.*, 2017).

The detailing of the relevant mineralogical and geological characteristics of the TEC would provide scientific data for the discussion of the genesis and evolution of parental magma, which can help in the geotectonic understanding of the SRS. These rocks were crystallized under pressure relief conditions in a deep fracture zone at the edge of the Rio de la Plata Craton, at 1.1 Ga, subjected to intense metasomatism, metamorphism under greenschist to amphibolite facies and heterogeneous deformation in unknown age between 1.1 Ga and 0.54 Ga.

Allied to isotopic studies, interpretations of field, petrological and geochemical evidence are widely used in the discussion of carbonatite genesis and evolution (Bell, 1989; Bailey, 1993; Toyoda *et al.*, 1994; Bell & Keller, 1995; Lee & Wyllie, 1997; Dunworth *et al.*, 2001;

Podborodnikov *et al.*, 2019) and contribute substantially to the understanding of TEC, include considerations about phosphate mineralization. This paper presents first whole-rock geochemistry and $\delta^{13}\text{C}$ and $\delta^{18}\text{O}$ isotope data of the rocks that make up the TEC and additional data on its geology and mineralogy.

4.2. GEOLOGICAL SETTING

TEC is located in the extreme south of Brazil, in the southwest of the Sul-Rio-Grandense Shield (SRS), in the southern portion of the Dom Feliciano Belt. The host rocks of the TEC are gneisses of the Paleoproterozoic Taquarembó Terrane, part of the Rio de la Plata Craton (**Figure 4.1**).

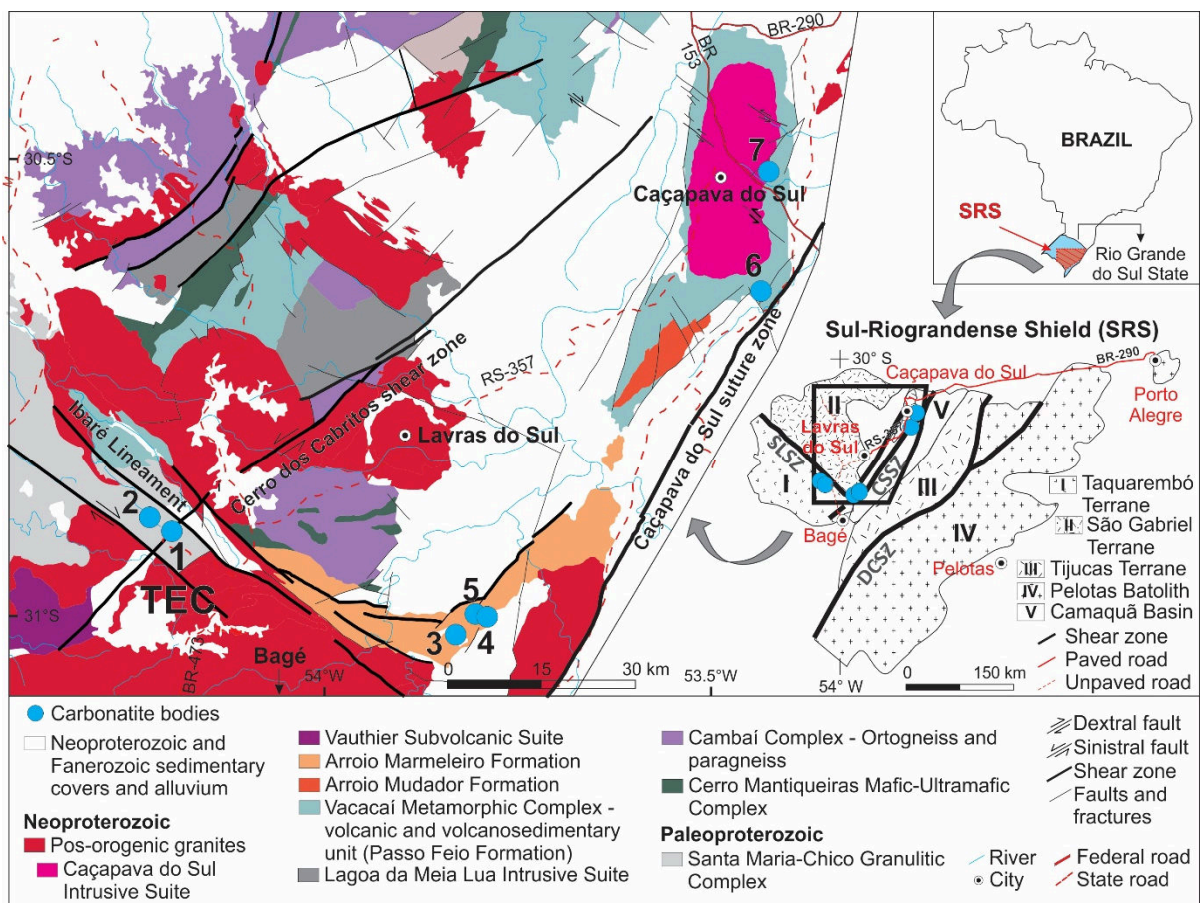


Figure 4.1 - Regional geological map of the SRS with the location of the carbonatites discovered in southern Brazil (modified from Ramgrab *et al.*, 2004; Silva *et al.*, 2004). Carbonatites: 1 - Três Estradas; 2 - Santa Clara; 3 - Porteira; 4 - Joca Tavares; 5 - Santa Inês; 6 - Passo Feio; and, 7 - Picada dos Tocos (also called Mato Grande Carbonatite by Aguiar Resources Ltd, holder of the mining right).

The granulites of the Taquarembó Terrane constitute the Santa Maria-Chico Granulitic Complex (CGSMC) (Hartmann, 1987; 1998), composed essentially by metric intercalations of garnet-bearing basic rocks and tonalites, with indications of bimodal magmatism. Subordinate anorthosites, Iherzolites, metapelitic rocks, BIF and microcline gneisses occur. Ages of granulitic metamorphism obtained recently are 2035 ± 9 Ma and 2006 ± 3 Ma (Hartmann *et al.*, 2008), 2055-2060 Ma (Girelli *et al.*, 2018) and 2022.5 ± 7.9 Ma (Monteiro *et al.*, unpublished).

There are few records of mesoproterozoic tectonics in the SRS. Girelli *et al.* (2018) mention Mesoproterozoic crustal fragments located on Uruguay and south Brazil outcropping in small portions in the Capivarita Anortosite (Chemale *et al.*, 2011), Tupi Silveira Amphibolite (Philipp *et al.*, 2016), Rocha Group (Basei *et al.*, 2000) and Parque UTE Group (Gaucher *et al.*, 2011). The TEC represents the only rocks dated around 1.1 Ga in the SRS so far, indicating crustal extension at the edge of the Rio de la Plata Craton (Monteiro *et al.*, unpublished), when it was juxtaposed with Laurentia (Li *et al.*, 2008). At 920 Ma, an oceanic crust begins to form, the Proto-Adamastor ocean (Hartmann *et al.*, 2019), also called Charrua Ocean by several authors (Fragoso César, 1991; Chemale Jr., 2000; Philipp *et al.*, 2016), recorded by the occurrence of ophiolites in the São Gabriel Terrane.

The Neoproterozoic is marked by the Brasiliano Orogen, which started with the formation of oceanic arcs (890-860 Ma) and continental arcs (770-680 Ma) that form the São Gabriel Terrane, juxtaposed to the Taquarembó Terrane through the Ibaré Lineament (Fragoso-César, 1991; Toniolo *et al.*, 2007, Ruppel, 2016). The Ibaré Lineament is considered as a transforming fault and lateral ramp. Metavolcanic and metasedimentary rocks that form the Tijucas Terrane (Camozzato *et al.*, 2013), juxtaposed to the São Gabriel Terrane through the Caçapava do Sul suture zone, began to form between 700 e 680 Ma. Collisional metamorphism is recorded throughout the SRS between 650 and 620 Ma (Philipp *et al.*, 2016). Between 650 and 550 Ma the main granitic magmatic event occurred with intense crustal anatexis promoted by the injection of mantle magmas (Philipp *et al.*, 2016), registered mainly in Pelotas Batholith, in contact with the Tijucas Terrane through the Dorsal Shear Zone of Canguçu. The post-collisional Camaquã basin was formed almost coeval, between 600 and 540 Ma. This basin consists of a sequence of volcanic and sedimentary rocks submitted to a low-grade metamorphism (Hartmann *et al.*, 2007).

Carbonatitic magmatism at SRS was identified in the early 2010's and scientific research has developed in recent years. Altogether seven intrusions have been discovered: Três Estradas (Toniolo *et al.*, 2010; Parisi *et al.*, 2010; Grazia *et al.*, 2011; Anzolin *et al.*, 2019; Monteiro *et al.*, unpublished), Santa Clara (Aguia Resources Ltd., 2016), Passo Feio (Rocha *et al.*, 2013; Cerva-Alves *et al.*, 2017; Morales *et al.*, 2019), Picada dos Tocos (Rocha *et al.*, 2013; Cerva-Alves *et al.*, 2017), Joca Tavares (Toniolo *et al.*, 2010; Parisi *et al.*, 2010), Porteira (Aguia Resources Ltd., 2013, Monteiro *et al.*, 2016) and Santa Inês (Aguia Resources Ltd., 2014).

Três Estradas and Santa Clara carbonatites are located approximately 100 km SW from Picada dos Tocos and Passo Feio carbonatites. These four intrusions have textural and petrographic similarities to each other and, with the exception of Santa Clara, for which there is no data, they also have similar geochemical and isotopic signatures ($\delta^{13}\text{C}$ e $\delta^{18}\text{O}$). Intrusions are composed of different facies of calcite metacarbonatite, calcite magnesian metacarbonatite, dolomite metacarbonatite and metaultramafic rocks, which often intersect in millimeter to metric bands. These rocks are metamorphosed into greenschist to amphibolite facies and show heterogeneous deformation suggested by closed folds with subvertical plunge, gneissic banding and flow banding locally preserved.

The geochronological context of these intrusions is still poorly known with two zircon U-Pb ages (Monteiro *et al.*, unpublished) of $1,110.0 \pm 4.8$ Ma in metacarbonatite and $1,123 \pm 15$ Ma in metasyenite, distinct from the proposed age for carbonatite from the Picada dos Tocos intrusion of 603.2 ± 4.5 Ma, also by U-Pb in zircon (Cerva-Alves *et al.*, 2017). Joca Tavares, Porteira and Santa Inês carbonatites, located approximately 45 km to SE from Três Estradas and 140 km to SW from Picada dos Tocos, have no published date, but field observations indicate that these intrusions are more young. Monteiro *et al.* (unpublished) suggest that the extreme south of Brazil has been the target of repeated carbonatitic magmatism over time, as recorded in various parts of the World, such as the Kola Province, in northern Europe, Ontario and SW Quebec, Canada, and the eastern Africa (Woolley & Bailey, 2012).

4.3. MATERIAL AND METHODS

The TEC area was mapped on a 1: 10,000 scale from the available outcrops and the subsurface geology observed in more than 5,000 m of diamond drilling cores placed mainly in the central-northeast portion of the TEC. Altogether, 31 thin sections, of which 6 are polished

sections, were described at the Petrography Laboratory of UnB. From these, samples were selected for whole-rock geochemistry, X-ray diffraction (XRD), scanning electron microscopy (SEM) and $\delta^{13}\text{C}$ and $\delta^{18}\text{O}$ isotopic analyses.

4.3.1. WHOLE-ROCK GEOCHEMISTRY

The exploration geochemistry results presented in this work come from analyzing half of the drilling cores cut along the core axis, with an average length of 1.0m. These results were provided by Agua Resources Ltd, which drilled the diamond drill holes in 2011 and 2012. 49 representative samples were studied with the most homogeneous features and textures possible, avoiding carbonate veins and mixtures with other rocks, 21 calcite metacarbonatites, 10 dolomite metacarbonatites, 16 metaultramafic rocks and 2 metasyenites.

All samples were prepared and analyzed by ALS Chemex Minerals to analyze major, minor, trace, and rare earth elements. The quality assurance and quality control materials used include coarse and fine blank white certified by ACME Analytical, standards GRE-03 and GRE-04. Both standards were generated from Tanzanian carbonatites, certified for ETR, P, Zr, Sc and Ti and produced by GEOSTATS PTY Ltd, duplicates, 5% reanalysis and 5% coarse reject analysis at the SGS Geosol Laboratory. In each batch of 44 samples, 1 pair composed of 1 fine blank and 1 coarse blank, 1 to 2 reference materials GRE-03 or GRE-04 and up to 2 duplicates were inserted. ALS Minerals also inserted its internal reference materials for analytical quality control, SARM-32 and SARM-39, from flotation product from the carbonatite phosphate beneficiation from Phalaborwa, South Africa, NCSDC79001 and NCSDC79003 generated from phosphorites, blanks and duplicates. The batch results were validated immediately after being received and before being integrated into the database. In case of identified inconsistencies, corrective actions were performed.

The analysis of major elements in ALS Minerals was carried out according to the analytical package ME-XRF12pt, which consists of the fusion of the sample aliquot prepared with 12:22 lithium metaborate-lithium tetraborate, followed by analysis on a fluorescence spectrometer. Analytes: Al_2O_3 , CaO , Fe_2O_3 , K_2O , MgO , MnO_2 , Na_2O , P_2O_5 , SiO_2 and TiO_2 . The determination of loss on ignition was made under 1,000°C, according to the analytical method OA-GRA05. Analysis of minor elements and traces were performed in ALS Minerals according to the analytical package ME-MS81. This method consists of fusing the sample

aliquot prepared with lithium metaborate, followed by analysis in an inductively coupled plasma spectrometer. Analytes: Ba, Ce, Cr, Cs, Dy, Er, Eu, Ga, Gd, Hf, Ho, La, Lu, Nb, Nd, Pr, Rb, Sm, Sn, Sr, Ta, Tb, Th, Tl, Tm, U, V, W, Y, Yb and Zr.

4.3.2. X-RAY DIFFRACTION – XRD

Analyses of quantitative mineralogical composition were made at the Technological Characterization Laboratory of the University of São Paulo (LCT-USP). Detailed mineralogical analyses were performed using X-ray diffraction (XRD), carried out by the powder method, in an PANalytical X-ray diffractometer, model X'Pert PRO with X'Celerator detector. The identification of the crystalline phases was obtained by comparing the diffractograms with the ICDD database - International Center for Diffraction Data (2003).

4.3.3. $\delta^{13}\text{C}_{\text{PDB}}$ AND $\delta^{18}\text{O}_{\text{V-SMOW}}$

$\delta^{13}\text{C}_{\text{PDB}}$ and $\delta^{18}\text{O}_{\text{V-SMOW}}$ isotopic data of whole-rock were obtained from 15 samples (eight calcite metacarbonatites, five dolomite metacarbonatites, and two metaultramafic rocks), using a GAS BENCH II analyzer with autosampler, coupled with delta five, after reaction with phosphoric acid (H_3PO_4) at 100%, in helium atmosphere for 1 hour. All analyses were performed at the Laboratory of Geochronology, Geodynamic, and Environmental Studies at the University of Brasília (UnB).

4.4. RESULTS

4.4.1. GEOLOGY OF THE TRÊS ESTRADAS COMPLEX

The TEC is 2.35 km long and up to 400 m wide along with a linear structure, in the N50°-60°E direction, with a preferential plunge to the NW (**Figures 4.2 and 4.3**) which forms small and sparse outcrops with evident foliation. This structure generated a gently undulating hill

with its highest central portion (altitude of ca. of 365 m) when compared to the margins (altitude of ca. of 315 m).

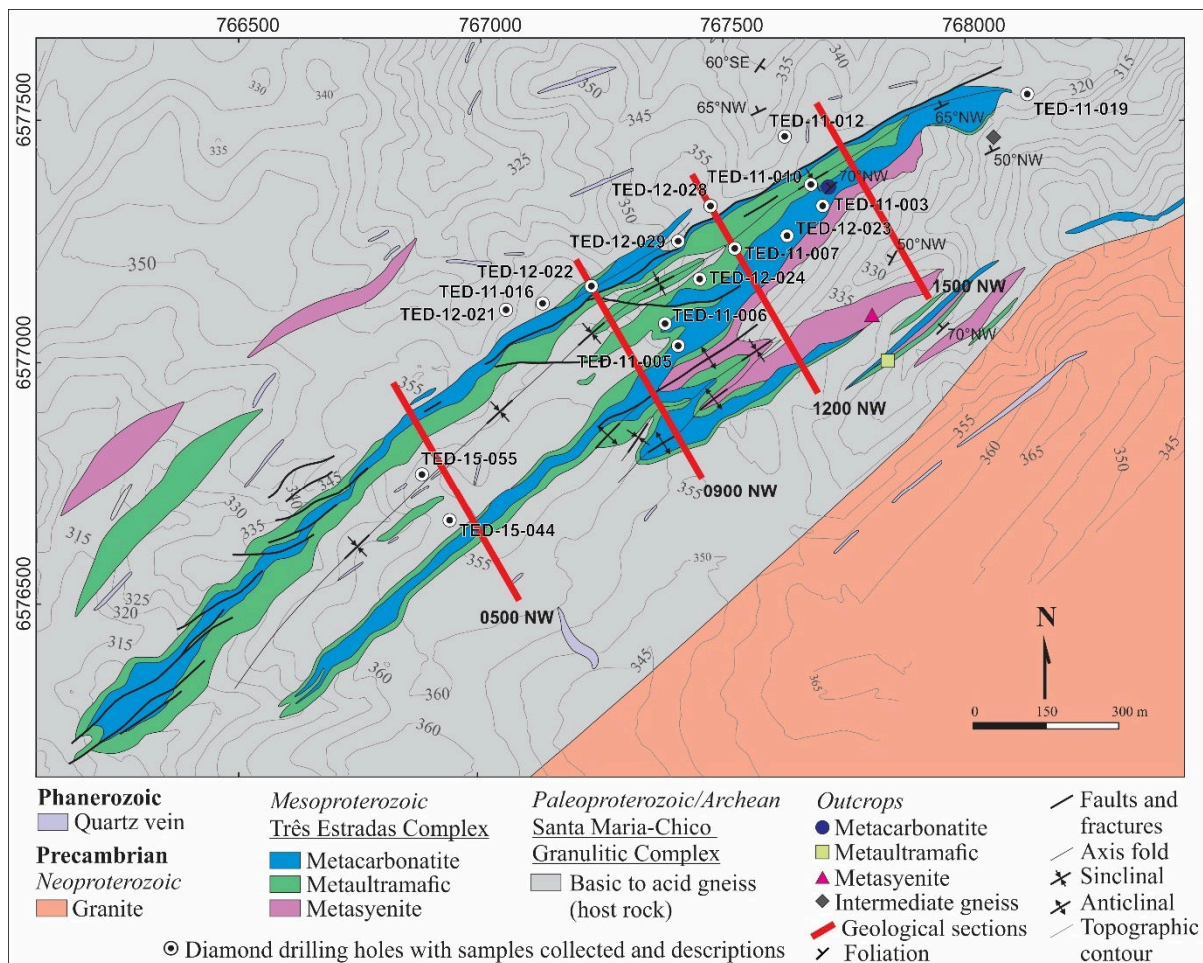


Figure 4.2 - 1:10.000 Geological map of the TEC and representative geological section perpendicular to the TEC axis (Modified from Aguia Resources Ltd., 2018). Datum SAD-69, Zone 21S.

The complex consists of three mapping units metamorphosed into greenschist to amphibolite facies: metacarbonatites, metaultramafic rocks and metasyenites. These units were deformed under a ductile-brittle regime with flow structures locally preserved. The geological units are formed by different facies often folded. The Três Estradas Complex forms a closed syncline with host gneisses and metaultramafic rock at its center and metacarbonatite in the flanks. However, even under intense tectonic action, there are rare portions of the metaultramafic rock that are not deformed or show only incipient deformation. Contacts between the rocks in the complex range from gradational to sharp. The rocks of the TEC are marked by heterogeneity. There are few intervals with more than 2 meters of homogeneous rocks with massive texture and which do not have lithological intercalations, xenoliths,

parasitic folds, faults that juxtapose different lithologies, and late cluster or veins of carbonatites. This heterogeneity makes it difficult to individualize different types of metacarbonatite on a map.

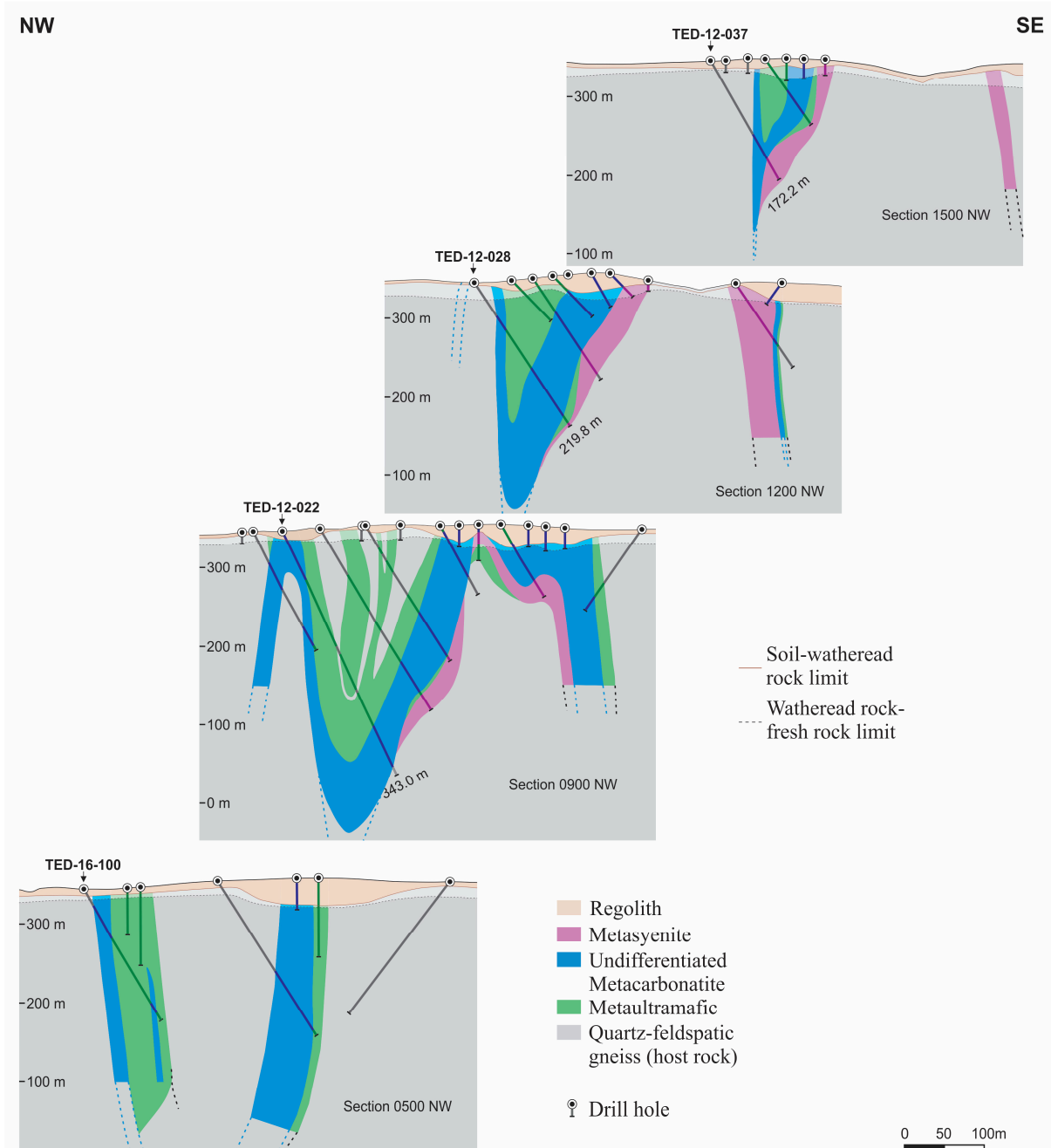


Figure 4.3 - NW-SE geological section along TEC from SW (bottom) to NE (top), showing that the complex goes deep in the SW direction.

In addition to the lithologies widely prevalent in the TEC, some more rare lithologies deserve mention. Foscorite occurs between the middle portion and at the NE end of the TEC

in an interval of 1.45 m (TED-11-016). It presents granoblastic texture, gradual contact with apatite-dolomite metacarbonatite, reaching 12.90% P₂O₅. Albite occurs punctually throughout the TEC (TED-11-009, TED-11-014, TED-11-019, TED-12-022, TED-12-036, TED-12-039), with granoblastic texture and irregular contact, usually with metaultramafic rocks and host gneisses. Magnetite occurs in rare centimetric levels in the southwest portion of the TEC (TED-14-055), with centimeter magnetite crystals bordered by clusters of carbonate and granoblastic texture. Finally, younger undeformed trachybasalt to trachyandesite and tefrite-basanite cut the TEC rocks.

4.4.1.1. METAULTRAMAFIC ROCK UNIT

This unit contains medium to coarse-grained dark-green alkaline ultramafic rocks. These are often magnetic, and intensely recrystallized and metamorphized into greenschist to amphibolite facies, subjected to potassic and sodic metasomatism. Metaultramafic rocks occur interspersed with metacarbonatites and metasyenites throughout the main intrusion, preferentially occupying its central portion consistent with the closed synclinal fold core. They occur as centimetric to decametric layers subjected to ductile deformation, but locally preserved from this, often subjected to potassium and sodium metasomatism with intense biotitization/glimeritization. The outcrops of metaultramafic rocks are restricted to *in situ* small blocks. The interaction features between the metaultramafic rock facies with other TEC rock types and with the host rock show generally incipient, submillimetric alteration edges, sometimes with biotite and/or carbonate (**Figures 4.4A and 4.4C**). In **Figure 4.4D** emphasis is placed on the contact zone between metaultramafic rock and metasyenite, with associated biotitization.

The Metaultramafic Rock unit is composed by varying amounts of hornblende, calcite, dolomite, apatite, biotite, chlorite, titanite, magnetite and, subordinately, plagioclase (**Figure 4.5**). The most common accessory minerals are pyrite, chalcopyrite, hematite, and quartz. X-ray diffraction analysis showed that epidote, zircon, barite, anatase, pyrochlore, and monazite occur as trace minerals.

The Metaultramafic Rock unit was divided into two facies: MUMF-1 and MUMF-2, based on the significant variation of the mineralogical content and of the mineralization in apatite. In both facies, medium to coarse grain varieties is observed. The rock is dominantly

nematoblastic, with subordinate granoblastic and lepidoblastic texture. Crystals are generally subhedral to anhedral, except for apatite, titanite and magnetite, that vary between subhedral and euhedral.

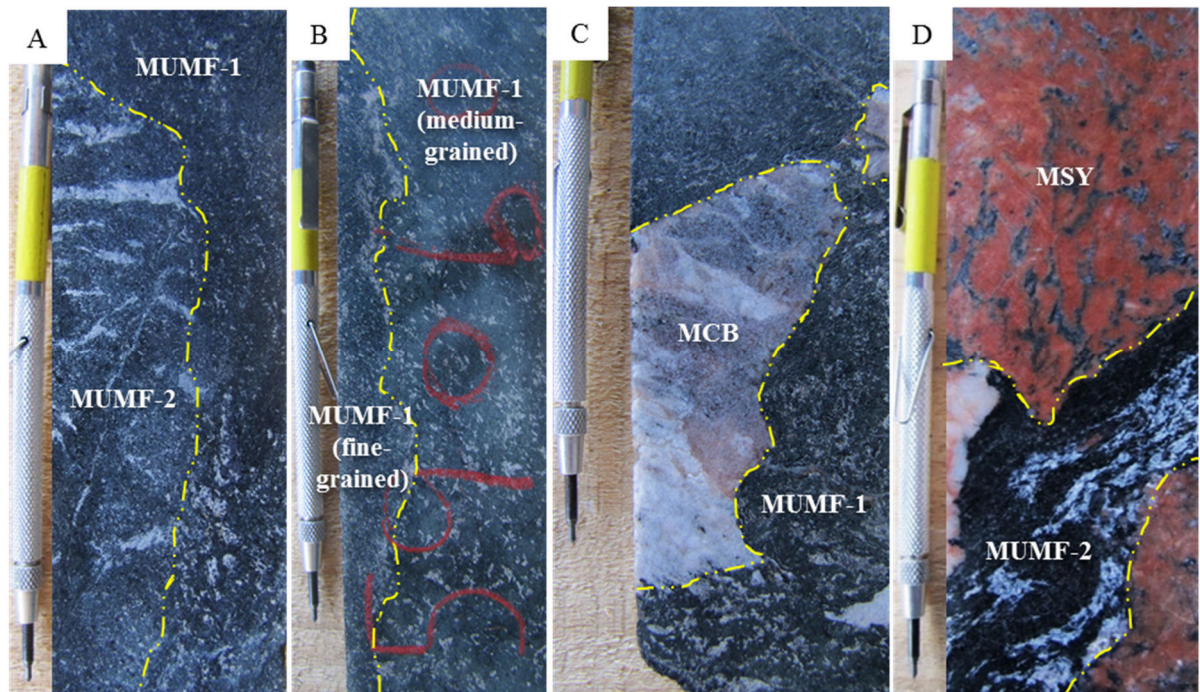


Figure 4.4 - A to D - Contact features between metaultamafic rock (MUMF) facies, showing absence of alteration or incipient biotic alteration at the contact edges: A - Contact between MUMF-1 and MUMF-2 facies (TED-12-022, depth 98.30m); B - Contact between coarse and medium-grained MUMF-1 sub-facies (TED-12-022, depth 215.75m); C - Contact between metacarbonatite and MUMF-1 facies (TED-12-022, depth 257.50m); D - Intense biotitization in metaultamafic rock in contact with metasyenite (MSY) (TED-12-023, depth 60.60m).

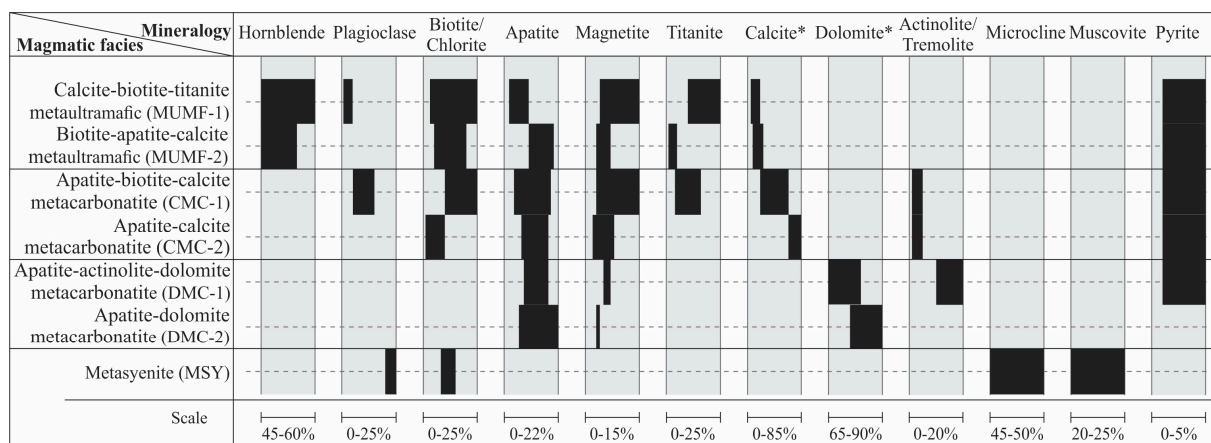


Figure 4.5 - Comparative modal composition between metaultamafic rocks, metacarbonatites and metasyenite.
*Main carbonate.

MUMF-1 Facies - Calcite-biotite-titanite Metaultramafic Rock

The MUMF-1 facies classified as dark green calcite-biotite-titanite metaultramafic rock, occurs both as a banded rock, where hornblende and biotite bands alternate with subordinate carbonatite bands, and as a rock with only incipient foliation (**Figure 4.6A**). It occurs throughout the complex, and sub-facies can be differentiated according to the grain size. A sub-facies with centimeter sized crystals of titanite and hornblende is locally found (**Figure 4.6B**).

This facies is composed of hornblende (45-60%), titanite (10-25%), biotite locally changing to chlorite (3-25%), calcite as the predominant carbonate (5-20%), magnetite (4-15%), apatite (2-10%) and subordinate plagioclase (1-5%) and pyrite (1-5%) (**Figure 4.6E**). Chalcopyrite, hematite, and ilmenite occur as trace minerals. The biotite content, as well as the presence of interstitial carbonate, increase proportionally to the intensity of the hydrothermal alteration that affected the amphiboles due to carbonatite intrusions, which is more frequent in the foliated rock compared to the non-deformed type. Apatite often occurs as disseminated granoblastic aggregates, preferably associated with calcite, and, occasionally, as inclusions in the hornblende. Magnetite is also widespread, locally surrounded by calcite (**Figure 4.6C**), interspersed with pyrite or changing to hematite.

Fácies MUMF-2 Facies - Biotite-apatite-calcite Metaultramafic Rock

Dark green rock, coarse-grained, with a texture varying between nematoblastic and granoblastic, subordinately lepidoblastic. When preserved from deformation, it exhibits clusters of cumulus hornblende with intercumulus white calcite and when affected by tectonic processes, it shows hornblende and biotite bands alternating with subordinate calcite and apatite bands (**Figure 4.6D**). It has a very restricted geographic occurrence, and was only identified punctually, in the NE portion of the TEC.

This facies is composed of hornblende (45-55%), calcite as the main carbonate (8-25%), apatite (10-20%), biotite (5-20%), magnetite (3-7%) and titanite (1-5%), with accessory pyrite, chalcopyrite, hematite and ilmenite (**Figure 4.6F**). The MUMF-2 facies is distinguished from MUMF-1 by higher contents of apatite and calcite and smaller amounts of titanite. Apatite is concentrated in the calcite pockets, occurring as dispersed granoblastic aggregates. Biotite content increases with the intensity of deformation.

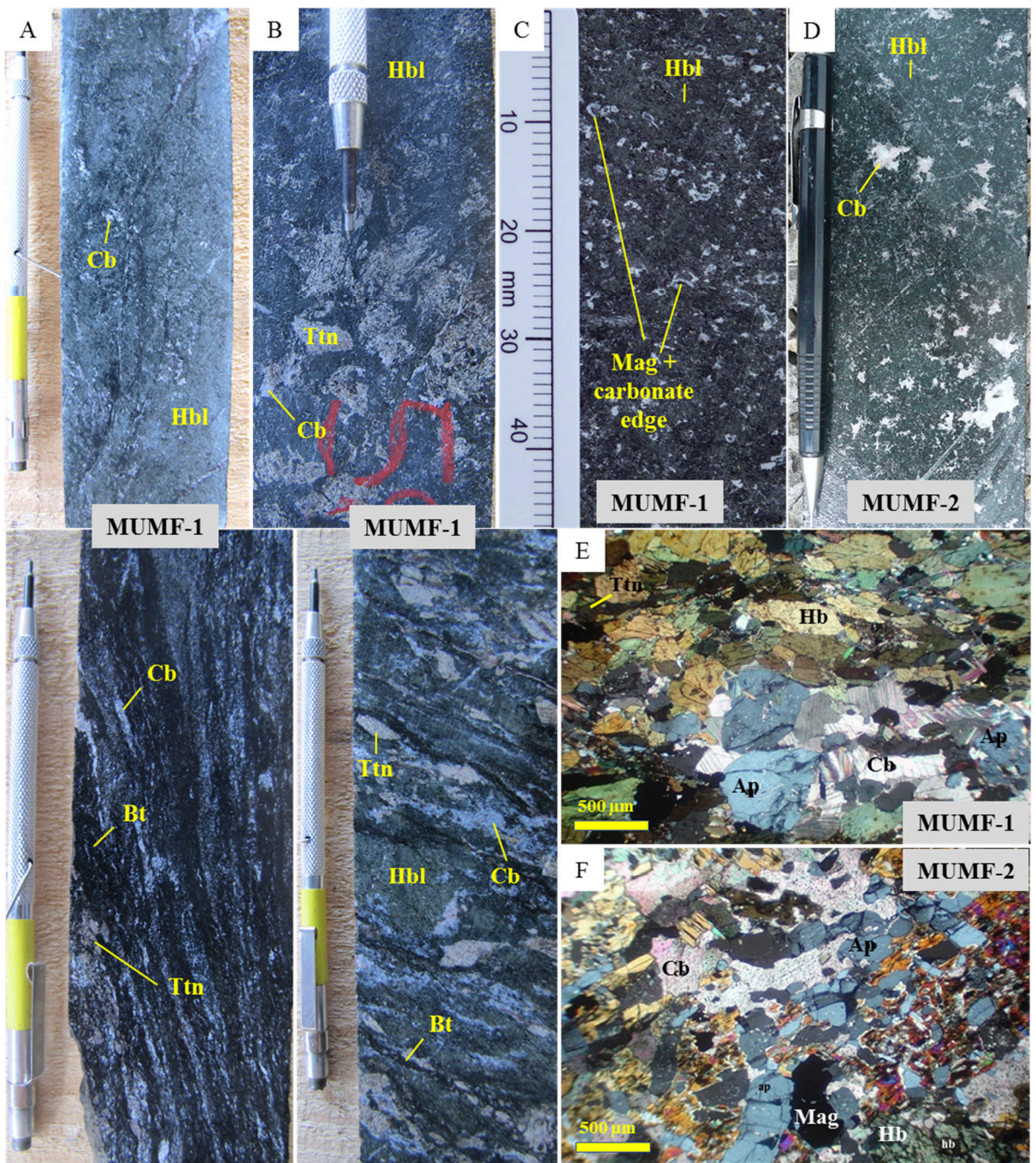


Figure 4.6 - Facies of metaultramafic rocks. A - Top: MUMF-1, undeformed calcite-biotite-titanite metaultramafic rock (Hole TED-12-022, sample 59099, depth 254.40m), Bottom: MUMF-1, banded titanite-calcite-biotite metaultramafic rock (TED-12-022, sample 58857, depth 25.05m); B - Top: MUMF-1, sub-facies with non-deformed beige titanite centimetric porphyroblasts (Hole TED-12-022, sample 58950, depth 107.50m), Bottom: sub-facies with tectonically oriented beige titanite porphyroblasts (TED-12-029, sample 60327, depth 118.15m); C - MUMF-1, magnetite crystals surrounded by carbonate (TED-12-022, sample 58911, depth 73.00m); D - MUMF-2, undeformed biotite-apatite-calcite metaultramafic rock with clusters of white carbonate (TED-11-007, sample 53408, depth 44.60m). E - Photomicrograph of calcite-biotite-titanite metaultramafic rock (MUMF-1) (TED-11-009, sample 53675, depth 69.08m); F - Photomicrograph of biotite-apatite-calcite metaultramafic rock (MUMF-2) (TED-11-007, sample 53408, depth 44.58m). Photomicrographs with crossed polars and objective of 2.5x.

4.4.1.2. METACARBONATITE UNIT

Metacarbonatite Unit is composed of white to pink rocks, medium to coarse-grained, with centimetric to decametric banding, cropping out as small and sparse blocks. Metacarbonatites are the most abundant geologic Unit and occur interspersed with metaultramafic rocks and metasyenites throughout the main intrusion, preferably occupying the outermost flanks of the closed syncline fold (**Figure 4.2**). The rocks in this unit show intense deformation with the development of protomylonitic foliation, gneissic banding, smooth to tight folds and micro-faults. Preserved or slightly deformed nucleus occur sporadically without an apparent pattern. Rocks from the Metacarbonatite Unit are essentially composed of varying amounts of calcite, dolomite, apatite, biotite, actinolite, titanite and magnetite, and, subordinately, plagioclase (**Figure 4.5**). Trace minerals include allanite, zircon, microcline, chlorite, quartz, pyrite, chalcopyrite, ilmenite, anatase, barite, monazite, pyrochlore, plagioclase, microcline and epidote.

Two varieties are individualized: calcite metacarbonatites and dolomite metacarbonatites. Each one was subdivided into two facies, based on their mineralogy and textural relationships, the first type being more abundant than the second. In the four facies, medium to coarse grain size is observed, texture is predominantly granoblastic and, subordinately, lepidoblastic, in biotite-rich calcite metacarbonatites. The crystals are generally subhedral to anhedral, with the exception of apatite, titanite, and magnetite that vary between subhedral and euhedral. All facies have significant concentrations of apatite that may reach up to 22% of the rock.

The interaction features of the various metacarbonatite facies with other types of TEC rocks and with the host-rocks show, as in the metaultramafic rocks, submillimetric contact borders with incipient alteration, usually formed by carbonate (**Figures 4.7A to 4.7D**).

CMC-1 Facies - Apatite-biotite-calcite Metacarbonatite

This facies is formed by alternating millimeter to centimeter-thick, white to pink bands, rich in calcite and millimeter to centimeter-thick dark gray bands, rich in biotite and actinolite. The rocks have medium grain size, and granoblastic to lepidoblastic texture (**Figure 4.8A**). Sub-facies can be differentiated according to the amount of silicate minerals present, such as biotite, plagioclase and actinolite (**Figure 4.8B**).

The modal composition is calcite (20-65 wt.%), biotite (10-25 wt.%), apatite (4-19 wt.%), titanite (4-16 wt.%), magnetite (3-15 wt.%), plagioclase (5-15 wt.%) and actinolite (1-5 wt.%) (**Figure 4.8F**). Monazite, pyrite, chalcopyrite and hematite occur as trace minerals. Biotite forms continuous bands and is also disseminated in carbonatite bands, locally altered to chlorite. Apatite is widespread as millimetric granoblastic aggregates, preferably in carbonatite bands, often fractured with calcite filling. Titanite occurs in in biotite- and actinolite-rich bands.

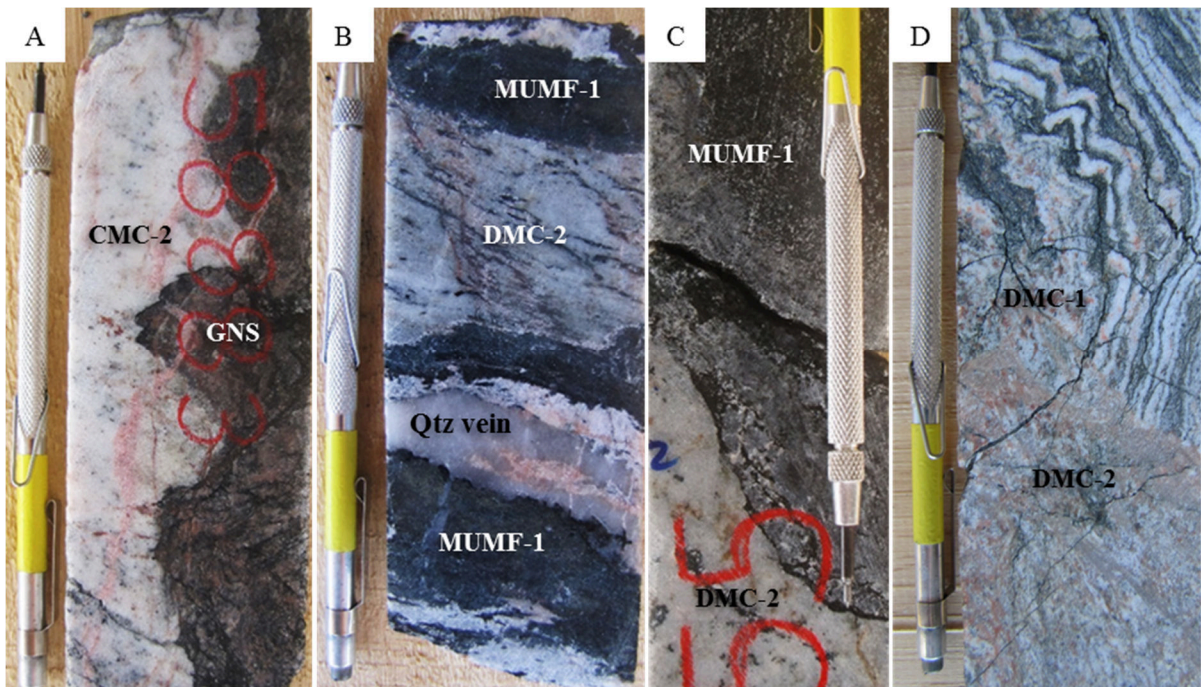


Figure 4.7 - A: Intrusion of calcite metacarbonate CMC-2 in intermediary host gneiss (GNS), forming locally submillimetric biotitized border (Hole TED-12-022, depth 49.30m); B: Intrusion of dolomite metacarbonate DMC-2 in MUMF-1, cut by a centimetric quartz vein (Qtz), with development of carbonate submillimetric edge (Hole TED-12-022, depth 67.50m); C: Intrusion of dolomite metacarbonate DMC-2 in MUMF-1, with generation of biotitized submillimetric border of contact (Hole TED-12-022, depth 24.00m); D: Dolomite metacarbonate DMC-2 cutting DMC-1 (Hole TED-12-029, depth 191.20m).

CMC-2 Facies - Apatite-calcite Metacarbonate

This consists of centimetric white/pink calcite-rich bands, alternating with dark gray, biotite-rich bands. Incipient deformation, with disseminated magnetite and biotite and slightly oriented through the mass of predominantly granoblastic, medium-grained calcite (**Figure 4.8C**).

The modal composition comprises calcite (65-85 wt.%), apatite (7-18 wt.%), biotite (1-10 wt.%), magnetite (2-8 wt.%) and actinolite (1-5 wt.%). Titanite, pyrochlore, monazite, allanite, pyrite, chalcopyrite, ilmenite and hematite occur as trace minerals. This facies has

lower silicate and titanite mineral content than the CMC-1 facies, due to the increased concentration of calcite. The amount of apatite between the CMC-1 and CMC-2 facies does not change significantly oscillation. The microfractures filled with calcite in the apatite crystals observed in the CMC-1 facies persist. A subfacies with slightly lower concentrations in pyrochlore and slightly higher in magnetite occurs locally.

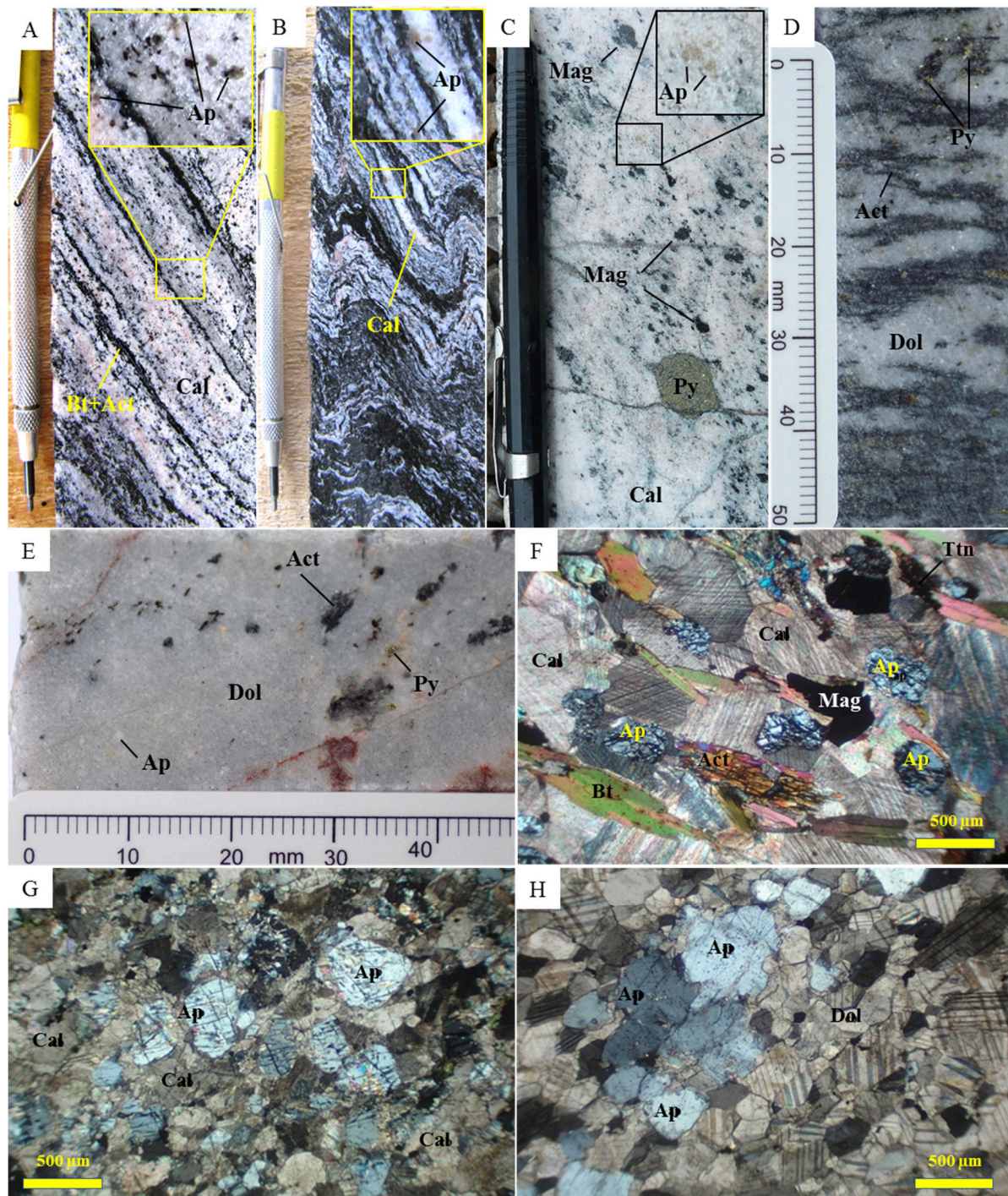


Figure 4.8 - Metacarbonate facies. A - CMC-1, banded apatite-biotite-calcite metacarbonate pink to white (TED-14-044, depth 172m); B - CMC-1, subfacies with higher silicate mineral concentration than average (TED-

14-055, depth 154.50m); C - CMC-2, White metacarbonate apatite-calcite with magnetite and oriented apatite (TED-11-006, sample 53320, depth 74.40m); D - DMC-1, Apatite-actinolite-dolomite metacarbonate (TED-12-022, sample 58888, depth 52.75m); E - DMC-2, Apatite-dolomite white metacarbonate with incipient foliation (TED-12-022, sample 58871, depth 38.40m); F - Photomicrograph of apatite-biotite-calcite metacarbonate (CMC-1) (TED-11-010, sample 53761, depth 75.40m); G - Photomicrograph of metacarbonate apatite-calcite (CMC-2) (TED-11-004, sample 53185, depth 43.40m); H - Photomicrograph of dolomite metacarbonate apatite (DMC-1) (TED-11-016, sample 54201, depth 73.60m). All photomicrographs were taken with crossed polars and Objective of 2.5x.

DMC-1 Facies - Apatite-actinolite-dolomite Metacarbonate

This facies is characterized by the alternation between white centimeter-thick, dolomite- and apatite-rich bands and millimeter-thick dark green, sometime discontinuous, actinolite-rich bands. Medium grain size and predominantly granoblastic texture are typical.

Modally the rock in this facies consist of dolomite as the main carbonate (65-80 wt.%), actinolite (10-20 wt.%), apatite (8-18 wt.%), magnetite (5-7 wt.%) and pyrite (1-5 wt.%). Chalcopyrite, ilmenite and hematite occur as trace minerals. Apatite occurs as disseminated granoblastic aggregates associated with dolomite, while magnetite appears associated with pyrite.

Fácies DMC-2 - Apatite-dolomite metacarbonate

These rocks have medium grain size, granoblastic texture and incipient foliation. They are formed by dolomite (75-90 wt.%), apatite (6-22 wt.%) and magnetite (3-4 wt.%). Actinolite, pyrite and ilmenite occur as trace minerals.

The rocks of this facies contain the highest concentrations of apatite in the TECs. The only phoscorite sample identified in the complex was found in gradational contact with rocks of this facies between the intermediate portion and the NE end of the carbonatite intrusion. It contains approximately 30 wt.% apatite, occurring as disseminated and poorly fractured granoblastic aggregates.

4.4.1.3. METASYENITE UNIT

This unit contains red-pink coarse-grained rocks with granoblastic texture, bordering the SE portion of the TEC, and, unlike the other units, it consists of one single facies. It is intensely

potassified. The metasyenite is intruded in sharp contact in metaultramafic rock (**Figure 4.4D**), causing the biotitization of amphiboles. Secondary carbonate veins and veins cut the metasyenite (**Figure 4.9A**).

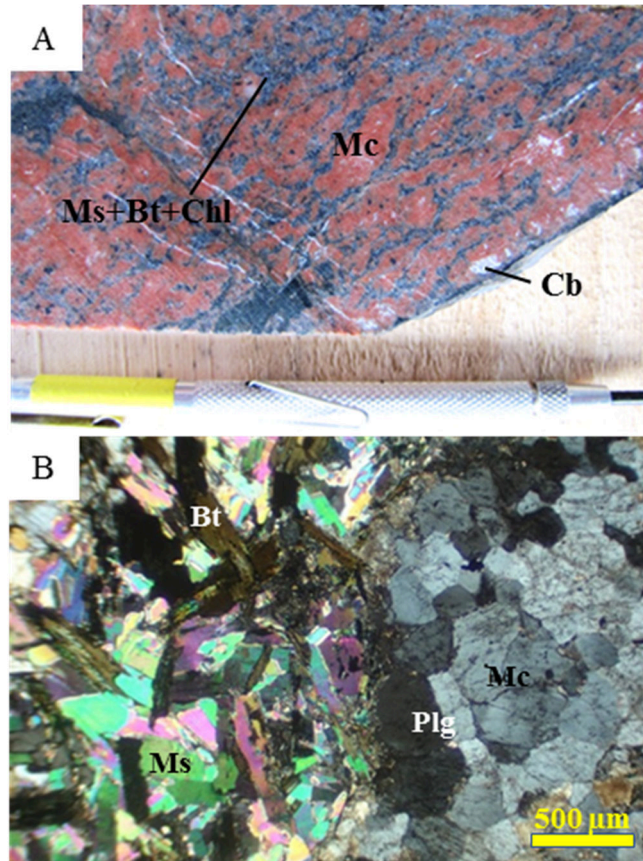


Figure 4.9 - A: Drill core consisting of metasyenite with potassic feldspar grains showing pressure shadows and fractures filled with carbonate; B: Photomicrograph of metasyenite. Objective of 2.5x, and crossed polars.

Metasyenites contain centimetric, red-pink K-feldspar porphyroblasts, oriented according to banding/foliation, sometimes exhibiting pressure shadows, and aggregates composed of black biotite lamellae, green chlorite, and abundant muscovite (**Figure 4.9A**). The rock is composed of microcline (45-50 wt.%) weakly altered to kaolinite, in addition to a second generation of polygonal millimeter-sized post-tectonic crystals, muscovite (20-25 wt.%), plagioclase with intense kaolinization (20-25 wt.%) and biotite (8-15 wt.%) partially altered to chlorite (**Figure 4.9B**). Hornblende, titanite, apatite, carbonate, rutile and opaque occur as trace minerals.

4.4.2. WHOLE-ROCK GEOCHEMISTRY

4.4.2.1. MAJOR ELEMENTS

Variations in the concentration of major elements allow of the study of TEC lithologies and their facies (**Figure 4.10, Table 4.1**) in greater detail. Metaultramafic rocks, metacarbonatites and metasyenites have clear differences in the abundance of SiO_2 , CaO , MgO , TiO_2 and P_2O_5 , elements that can be used to discriminate them into groups of chemical affinity (**Figure 4.10**). Chemical variations between facies of each lithological unit, such as metaultramafic rocks are also notable. Some subtle among the metacarbonatites are seen in the case of the contents of TiO_2 and P_2O_5 .

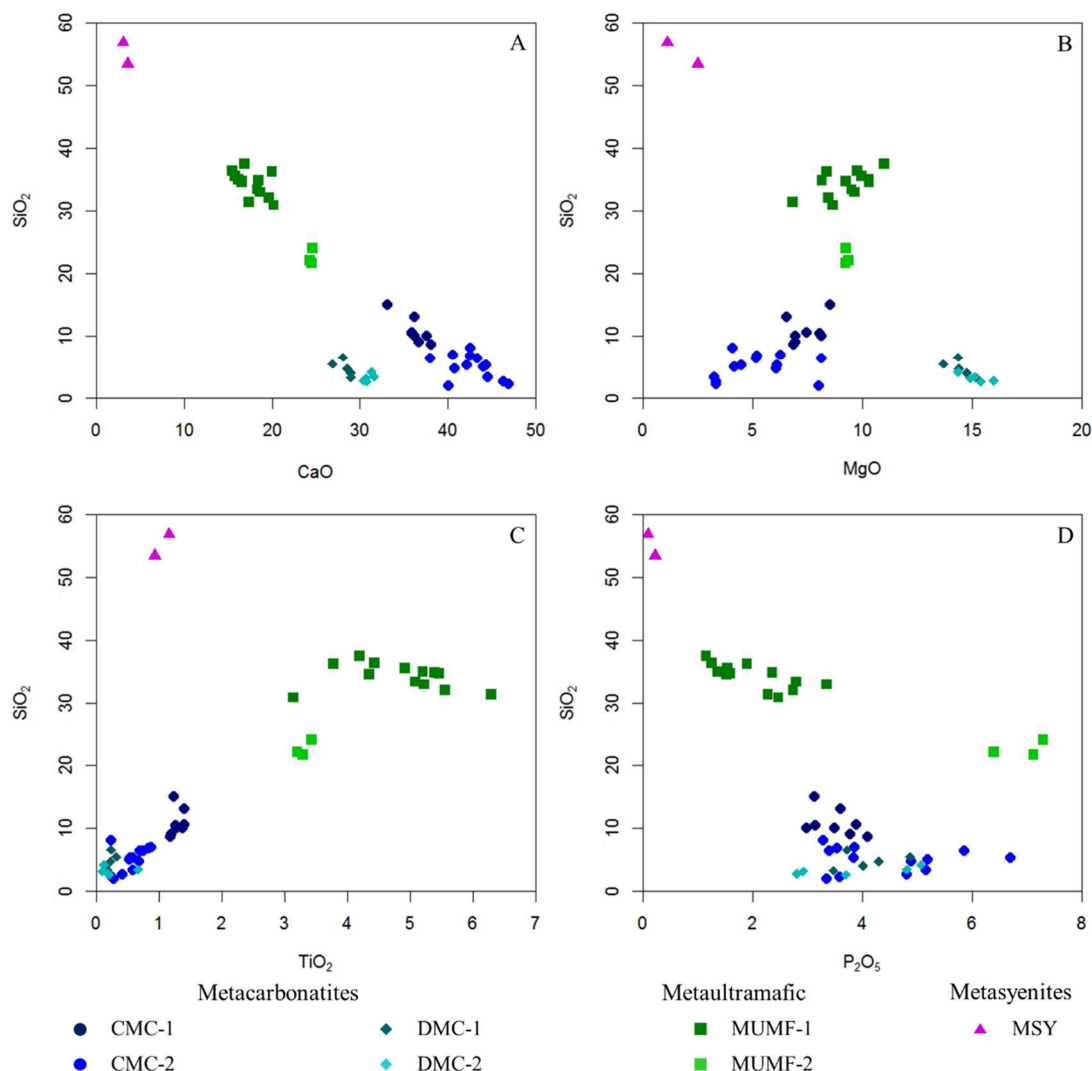


Figure 4.10 - Individualization of groups of TEC rocks and their facies based on the chemical composition of major elements.

Table 4.1 - Analysis of major elements of the TEC rocks. Contents in wt.%. Holes with azimuth 150° and dip varying between -45° and -65° (see **Figure 4.2**).

Sample	Hole	Facies	SiO ₂	TiO ₂	Al ₂ O ₃	Fe ₂ O ₃	MnO ₂	MgO	CaO	Na ₂ O	K ₂ O	P ₂ O ₅	LOI	Total
53939	TED-11-13	MUMF-1	37.50	4.19	4.71	15.70	0.28	11	16.90	1.14	0.70	1.15	5.71	100.70
53940	TED-11-13	MUMF-1	35	5.20	5.15	18.80	0.31	10.30	16.20	0.99	1.05	1.36	5.41	101.40
58911	TED-12-22	MUMF-1	33	5.22	4.14	20.21	0.31	9.64	18.65	0.96	0.39	3.35	3.47	101.55
58912	TED-12-22	MUMF-1	33.40	5.08	4.16	19.74	0.31	9.50	18.30	1.06	0.40	2.79	4.06	100.90
53667	TED-11-09	MUMF-1	31.40	6.29	6.17	15.40	0.34	6.84	17.35	0.69	2.91	2.28	6.04	101.80
53668	TED-11-09	MUMF-1	36.20	3.78	5.30	14.25	0.36	8.37	20	1.29	0.93	1.90	6.94	100.30
58950	TED-12-22	MUMF-1	32.10	5.55	4.98	17.76	0.34	8.44	19.65	1.40	0.75	2.74	5.14	100.85
60327	TED-12-29	MUMF-1	34.90	5.39	5.26	16.21	0.34	8.15	18.45	1.46	1.60	2.36	5.21	102.20
53654	TED-11-09	MUMF-1	35.60	4.92	5.66	17.50	0.46	9.96	15.75	1.18	2	1.54	5.19	101.45
53655	TED-11-09	MUMF-1	36.40	4.43	5.35	18.50	0.49	9.75	15.45	1.40	1.54	1.25	4.82	101.45
53813	TED-11-11	MUMF-1	34.60	4.35	4.68	16.85	0.44	10.30	16.60	1.10	1.99	1.52	6.12	100.55
53821	TED-11-11	MUMF-1	34.70	5.46	4.52	18.65	0.41	9.24	16.60	1.52	1.28	1.59	4.95	101.50
53798	TED-11-11	MUMF-1	30.90	3.14	6.27	11.50	0.33	8.64	20.20	1.59	2.40	2.47	10.31	100.65
53400	TED-11-07	MUMF-2	21.70	3.29	5.62	13.40	0.25	9.23	24.50	0.56	1.98	7.12	9.82	99.95
53408	TED-11-07	MUMF-2	24	3.43	5.52	14.05	0.25	9.26	24.60	0.85	1.26	7.29	8.90	101.50
53409	TED-11-07	MUMF-2	22.10	3.20	5.26	13.75	0.27	9.37	24.30	0.52	1.74	6.40	10.42	100.35
53732	TED-11-10	CMC-1	10.40	1.26	2.01	6.65	0.33	8.06	35.90	0.06	1.34	3.15	28.51	100.05
53735	TED-11-10	CMC-1	15.05	1.24	3.60	6.63	0.27	8.52	33.10	0.21	2.35	3.13	24.37	100.35
53861	TED-11-11	CMC-1	10	1.38	1.80	6.77	0.32	8.14	36.20	0.13	1.26	2.98	28.82	100.20
53787	TED-11-11	CMC-1	10	1.28	1.86	7.26	0.31	6.95	37.60	0.14	1.36	3.49	27.28	99.74
53870	TED-11-11	CMC-1	10.60	1.40	1.78	8.09	0.29	7.45	35.90	0.27	1.26	3.89	25.47	98.92
55986	TED-11-12	CMC-1	13	1.40	2	7.53	0.33	6.55	36.20	0.47	0.74	3.60	26.03	100.10
54343	TED-11-18	CMC-1	8.64	1.18	1.58	7.64	0.30	6.88	38.10	0.20	1.14	4.09	28.65	100.10
54344	TED-11-18	CMC-1	9.07	1.20	1.68	7.47	0.29	6.93	36.70	0.22	1.26	3.78	28.22	98.41
53265	TED-11-06	CMC-2	4.96	0.53	0.82	4.79	0.26	4.16	44	0.01	0.02	5.19	31.76	99.37
53343	TED-11-06	CMC-2	4.78	0.68	0.81	7.31	0.35	6.07	40.80	0.20	0.41	4.89	31.06	99.75
53838	TED-11-11	CMC-2	6.35	0.75	0.98	5.04	0.32	5.15	43.30	0.04	0.70	3.39	31.63	100.30
53839	TED-11-11	CMC-2	6.88	0.83	1.18	5.69	0.30	5.21	42.60	0.11	0.84	3.54	30.98	100.40
53865	TED-11-11	CMC-2	6.96	0.87	1.11	6.73	0.32	6.29	40.60	0.03	0.63	3.86	30.65	100.60
53336	TED-11-06	CMC-2	2.26	0.25	0.10	5.15	0.36	3.33	46.90	0.04	0.02	3.58	35.77	99.96
53713	TED-11-10	CMC-2	5.28	0.59	0.90	5.24	0.29	4.48	44.30	0.01	0.67	3.84	32.11	99.55
53724	TED-11-10	CMC-2	2	0.28	0.21	5.83	0.38	8.01	40.10	0.01	0.12	3.35	36.90	99.61
53727	TED-11-10	CMC-2	8.09	0.24	0.35	4.03	0.27	4.09	42.60	0.01	0.13	3.29	33.96	99.67
53412	TED-11-07	CMC-2	5.27	0.54	0.70	7.13	0.36	6.10	42.20	0.01	0.02	6.70	29.09	99.59
53414	TED-11-07	CMC-2	6.44	0.70	0.53	10.30	0.45	8.15	38	0.02	0.15	5.85	28.50	100.05
53418	TED-11-07	CMC-2	2.68	0.42	0.27	6.52	0.30	3.32	46.30	0.01	0.07	4.81	32.63	99.30
53419	TED-11-07	CMC-2	3.38	0.59	0.46	9.48	0.39	3.27	44.50	0.03	0.14	5.16	30.51	99.73
54204	TED-11-16	DMC-1	4.75	0.23	0.08	11.50	0.48	14.40	28.60	0.12	0.01	4.30	32.58	99.85
54209	TED-11-16	DMC-1	5.48	0.32	0.07	14.10	0.42	13.70	26.90	0.11	0.01	4.87	28.47	98.44
54226	TED-11-16	DMC-1	6.60	0.24	0.25	11.85	0.49	14.35	28.10	0.17	0.08	3.72	31.84	99.62
54227	TED-11-16	DMC-1	4.06	0.16	0.05	10.05	0.48	14.75	29	0.08	0.01	4.01	34.81	99.02
54229	TED-11-16	DMC-1	3.29	0.18	0.03	10	0.51	15.15	29	0.09	0.01	3.47	36.11	99.41
54214	TED-11-16	DMC-2	3.15	0.10	0.01	5.78	0.57	14.90	30.70	0.01	0.01	2.92	39.31	98.45
54216	TED-11-16	DMC-2	2.60	0.21	0.05	6.06	0.55	15.40	30.80	0.01	0.01	3.70	38.11	98.96
54217	TED-11-16	DMC-2	3.43	0.67	0.09	6.26	0.54	15.10	31.60	0.03	0.03	4.81	36.59	100.30
54218	TED-11-16	DMC-2	2.80	0.19	0.03	6.58	0.57	16	30.40	0.02	0.01	2.81	39.15	99.67
54232	TED-11-16	DMC-2	4.17	0.13	0.22	7.83	0.47	14.35	31.30	0.07	0.07	5.07	33.34	99.89
53135	TED-11-03	MSY	56.80	1.16	19.65	3.13	0.08	1.10	3.04	7.32	3.13	0.09	3.05	100.60
53137	TED-11-03	MSY	53.40	0.93	19.45	4.46	0.14	2.51	3.55	4.95	5.44	0.22	4.01	100.85

SiO₂ concentrations in the TEC metaultramafic rocks vary between 21.70 wt.% and 37.50 wt.%, and are inversely proportional to CaO contents which vary between 15.45 wt.% and 24.60 wt.% (**Figure 4.10A**). The concentrations of SiO₂, CaO and MgO vary in each

metaultramafic rock facies, sometimes with a predominance of contents above the median value, sometimes below (**Figure 4.11**). MgO behaves distinctly between MUMF-1 (6.84 wt.% to 11 wt.%) and MUMF-2 (9.23 wt.% to 9.37 wt.%), showing a direct proportionality relationship with SiO₂ in the first facies, whereas in MUMF-2 the variation in MgO content does not change significantly with the increase of silica (**Figure 4.10B**).

The combined Na₂O and K₂O concentrations vary between 1.35 wt% and 3.99 wt% in metaultramafic rocks, with an average of 2.54 wt%. Starting from the chemical composition of MUMF-1 towards MUMF-2 there is an increase in the amount of carbonates, indicated by average LOI of 5.64 wt.% and 9.71 wt.%, respectively, and a decrease in silicate minerals reflected by average levels of SiO₂ that changes from 34.29 wt.% in MUMF-1 to 22.60 wt.% in MUMF-2, respectively. The content of Fe₂O₃ are higher in MUMF-1 facies compared to MUMF-2 facies, varying between 11.50 wt.% and 20.21 wt.% with predominance of contents below the median value and between 13.40 wt.% and 14.05 wt.% with predominance of contents above the median value, respectively (**Figure 4.11**). The concentrations of Al₂O₃ do not vary significantly between the two facies, being around 5 wt%. The metaultramafic rocks of the MUMF-1 facies are the rocks with the highest concentrations of TiO₂ in the complex, varying between 3.14 wt.% and 6.29 wt.% with predominance of contents below the median value, and around 3 wt.% in MUMF-2, with a set of contents revealing contents usually above the median value (**Figure 4.11**). There is a negative correlation between TiO₂ and SiO₂ in MUMF-1 facies, whereas in MUMF-2 facies, a positive correlation trend is observed (**Figure 4.10C**). P₂O₅ levels increase with decreasing silica in metaultramafic rocks (**Figure 4.10D**). The MUMF-2 facies, with occasional occurrence in the northeast portion of TEC, concentrate the highest levels of P₂O₅, varying between 6.40 wt.% and 7.29 wt.%, with predominance of contents below the median value, whereas the average content of P₂O₅ in the MUMF-1 facies is 2.02 wt.% (up to 3.35 wt.%), with contents usually above the median value (**Figure 4.11**). The phosphate concentrations observed in MUMF-2 are expressive and higher than those observed in calcite and dolomite metacarbonatites.

The chemical results of metacarbonatites from undifferentiated facies with SiO₂ content <20 wt.% reveal that, chemically, there is a predominant occurrence of calciocarbonatite and its magnesian and ferruginous calciocarbonatite variants according to the classification diagram proposed by Gittins & Harmer (1997) (**Figure 4.12**). Samples from the CMC-1 facies fall on the magnesian calciocarbonatite field, very close to the ferruginous calciocarbonatite

field, whereas CMC-2 facies samples fall predominantly on the calciocarbonatite field, with a sample incorporated into the ferruginous calciocarbonatite field, enriched in magnetite.

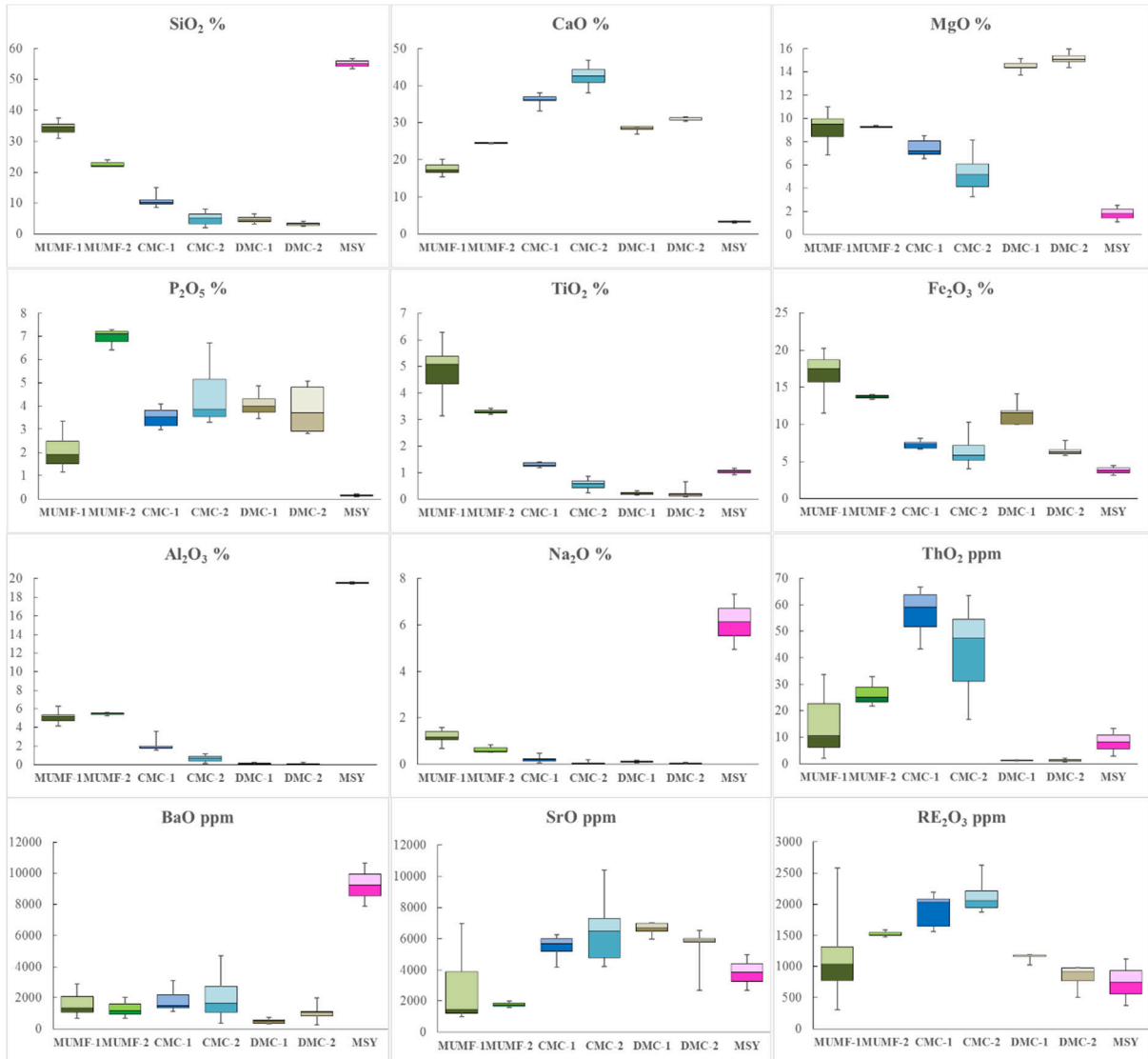


Figure 4.11 - Box plot with distribution of major element oxides and some minor elements of the different facies in TEC.

Mineralogically, two large groups of metacarbonatite were recognized: calcite metacarbonatites and dolomite metacarbonatites. The former may be further divided in a facies rich in magnesian silicates (CMC-1) and a facies rich in apatite and magnetite (CMC-2). The dolomite metacarbonatite facies are divided into actinolite-rich dolomite metacarbonatite (DMC-1) and pure dolomite metacarbonatite (DMC-2).

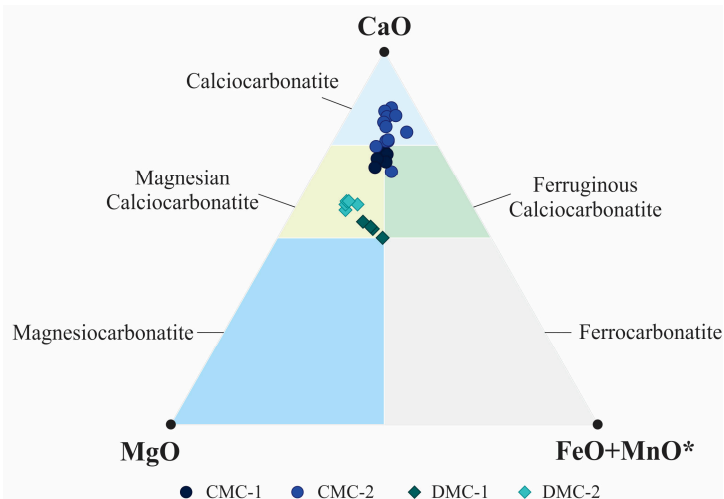


Figure 4.12 - Graphic $\text{CaO} \times \text{MgO} \times \text{FeO} + \text{MnO}^*$ exhibiting contents of these substances in metacarbonatites with levels of $\text{SiO}_2 \leq 20$ wt.% based on a diagram proposed by Gittins & Harmer (1997). * FeO and MnO were calculated from Fe_2O_3 e MnO_2 , respectively.

The CMC-1 facies is silicate rich, with concentrations of 11.40 wt.% to 19.89 wt.% of SiO_2 and lower calcium carbonate contents, reflected by contents of 33.10 wt.% to 38.10 wt.% of CaO and 24.37 wt.% to 28.82 wt.% of LOI (**Table 4.1**), whereas the CMC-2 facies have much lower silica concentrations, between 2 wt.% and 8.09 wt.%, and high concentrations of CaO and LOI ranging from 38 wt.% to 46.90 wt.% and 28.50 wt.% to 36.90 wt.%, respectively. Similar behavior is observed in the DMC-1 and DMC-2 facies, in which the first presents higher SiO_2 contents (3.29 wt.% to 6.60 wt.%) and lower CaO contents (26.90 wt.% to 29 wt.%) and LOI (28.47 wt.% to 36.11 wt.%), in contrast to the second showing SiO_2 levels ranging from 2.60 wt.% to 4.17 wt.%, between 30.40 wt.% to 31.60 wt.% CaO and 33.34 wt.% to 39.31 wt.% LOI. The highest variability of SiO_2 and CaO contents in metacarbonatites are observed in the CMC-2 facies, where they show predominance of values above the median, whereas in CMC-1 the concentrations of these oxides show values below the median (**Figure 4.11**). The negative correlation between CaO and SiO_2 in metaultramafic rocks and calcite metacarbonatites follows the same trend, whereas dolomite metacarbonatites, although they also show a negative correlation between both oxides, do not follow the same alignment and form a distinct group (**Figure 4.10A**). Similar behavior is observed when opposing MgO and SiO_2 with metaultramafic rocks and calcite metacarbonatites showing a positive correlation trend and dolomite metacarbonatites forming a distinct group outside this arrangement showing a negative correlation (**Figure 4.10B**). MgO contents are usually below 9 wt.% in calcite metacarbonatite, varying between 3.27 wt.% and 8.52 wt.%, whereas in dolomite carbonatite

MgO ranges between 13.70 wt.% and 16 wt.%. The CMC-2 facies show the highest variability of levels with slight predominance of concentrations below the median value, whereas the other metacarbonatites facies show most of the contents above the median (**Figure 4.11**).

The alkali content is higher in the CMC-1 facies, with an average concentration of Na₂O and K₂O added to 1.55 wt.%, reaching up to 2.56 wt.%. In the other facies, these concentrations do not exceed 1 wt.%, with an average value of 0.23 wt.%, with DMC-2 being the poorest facies. Al₂O₃ and TiO₂ are present in concentrations below 1 wt.% in facies CMC-2, DMC-1 and DMC-2 and show low variability in all facies (**Figure 4.11**). In CMC-1, Al₂O₃ varies between 1.58 wt.% and 3.60 wt.% and TiO₂ between 1.18 wt.% and 1.40 wt.%. TiO₂ and SiO₂ positively correlate in calcite metacarbonatites, but in dolomite metacarbonatites TiO₂ does not vary significantly with the increase in silica (**Figure 4.10C**). Fe₂O₃ concentrations in metacarbonatites are generally lower than 10 wt.%, reaching a range between 10 wt.% and 14.10 wt.% in DMC-1, which, together with CMC-2, are the facies with the greatest variability (**Figure 4.11**).

Among the calcite metacarbonatite facies, the CMC-2 facies is the most P₂O₅-rich, with an average content of 4.42 wt.%, reaching up to 6.70 wt.%, with significant variability of contents in relation to the other facies and usually with concentrations above the median value, whereas in CMC-1 the contents vary between 2.98 wt.% to 4.09 wt.%, with distribution of concentrations above and below the average content of 3.51 wt.% almost equal (**Figure 4.11**). P₂O₅ concentrations tend to increase with the decrease of SiO₂ concentrations in calcite metacarbonatite, as opposed to dolomite metacarbonatites in which there is a slightly positive correlation between them (**Figure 4.10D**). In dolomite metacarbonatite, the DMC-1 and DMC-2 facies present P₂O₅ concentrations varying between 3.47 wt.% to 4.87 wt.% and between 2.81 wt.% to 5.07 wt.%, respectively, with DMC-1 tending towards slight predominance of values below the median value and DMC-2 showing usually contents above the median (**Figure 4.11**).

The metasyenite have SiO₂ concentrations varying between 53.40 wt.% and 56.80 wt.%. In terms of the oxides major elements, TEC syenites are characterized by Al₂O₃ varying between 19.45 wt.% and 19.65 wt.%, K₂O between 3.13 wt.% and 5.44 wt.% and very high Na₂O between 4.95 wt.% and 7.32 wt.%. CaO and MgO contents vary between 3.04 wt.% and 3.55 wt.% and between 1.10 wt.% and 2.51 wt.%, respectively, and are negatively correlated with SiO₂ (**Figures 4.10A e 4.10b**). TiO₂ varies between 0.93 wt.% and 1.16 wt.% and

increases with the increase in SiO₂ (**Figure 4.10C**). The concentration of P₂O₅ is very low and varies from 0.09 wt.% to 0.22 wt.%, showing negative correlation with silica (**Figure 4.10D**), whereas Fe₂O₃ varies between 3.13 wt.% and 4.46 wt.%, and LOI varies between 3.05 wt.% and 4.01 wt.% (**Table 4.1**).

4.4.2.2. MINOR ELEMENTS AND TRACE ELEMENTS

Concentrations of minor elements and traces in metaultramafic rocks and calcite metacarbonatite (**Table 4.2**), when normalized to the chondrite according to Thompson (1984), show geochemical patterns with similarities to each other and distinct from that observed in dolomite metacarbonatite (**Figure 4.13**). The greater amplitude of geochemical patterns of calcite metacarbonatite stands out in relation to metaultramafic rocks.

The facies of metaultramafic rocks and calcite metacarbonatite show slight Ba enrichment (>10000 ppm in MUMF-1 and even 4210 ppm in CMC-2), Nb (up to 333 ppm in MUMF-1 and up to 572 ppm in CMC-2), Th (up to 29.60 ppm in MUMF-1 and up to 58.60 ppm in CMC-1) and ΣREO (up to 2209 ppm in MUMF-1 and 2246.74 ppm in CMC-2) and depletion in Rb, K, Ta, Sr and Ti in relation to the chondrite in most of the analyzed samples (**Figures 4.13A to 4.13D**). Metasyenites are enriched in Ba (samples with 7060 ppm and 9520 ppm) in relation to metaultramafic rocks, calcite metacarbonatites and dolomite metacarbonatites, which have average concentrations of 2078.17 ppm, 1731.86 ppm and 702.60 ppm.

Positive Th anomalies in metacarbonatites are more expressive when compared to metaultramafic rocks, mainly in CMC-2 facies, whereas in metasyenites there is a tendency for Th flat behavior to a negative anomaly (**Figures 4.13A to 4.13G**). Anomalies of Rb and K are, in general, negative, with the exception of metasyenites, where there is a flat tendency to negative anomaly with respect to Rb and slightly positive anomalies of K (**Figure 4.13G**). Sr negative anomalies in metaultramafic rocks are more prominent than in calcite metacarbonatite. However, the occurrence, even if sporadic, of positive Sr anomaly, observed in two samples, stands out (**Figure 4.13A**). Dolomite metacarbonatites exhibit flat pattern to slightly positive Sr anomalies (**Figures 4.13E and 4.13F**). The two metasyenite samples show contradictory results of Sr, sometimes with a positive anomaly, sometimes with a negative anomaly (**Figure 4.13G**).

Table 4.2 - Analysis of minor elements and traces in TEC rocks. Contents are shown in ppm.

Sample	Rock	Ba	Rb	Sr	Cs	Ga	Ta	Nb	Hf	Zr	Y	Th	U	Cr	Co	V	Mo	W	Sn	Tl	Nb/Ta	Zr/Hf	Zr/Nb
53939	MUMF-1	1010	13.30	5880	0.26	16.80	1.10	22.10	7.30	185	19.40	1.88	0.58	130	60.40	414	3	4	3	<0.5	20.09	25.34	8.37
53940	MUMF-1	795	24.90	3280	0.52	19.20	6.60	93.80	9.70	292	32.90	5.03	0.97	240	64.50	503	4	4	4	<0.5	14.21	30.10	3.11
53667	MUMF-1	>10000	87.20	1110	2.31	19.80	6.90	333	9.90	386	110.50	29.60	5.37	60	48	370	2	4	5	<0.5	48.26	38.99	1.16
53668	MUMF-1	2280	14.30	1035	0.28	14.60	14.90	272	8.90	385	77.40	20.10	2.43	30	39.10	337	2	4	4	<0.5	18.26	43.26	1.42
53654	MUMF-1	1340	43.50	871	1.18	15.20	8.90	179	11.10	438	48.80	6.38	0.83	300	52.10	380	2	4	3	<0.5	20.11	39.46	2.45
53655	MUMF-1	1100	33	835	0.89	15.10	7.60	159	11.50	413	45.20	5.35	0.73	350	51.30	407	2	4	3	<0.5	20.92	35.91	2.60
53813	MUMF-1	1735	54	2000	0.99	16.90	11	209	10.20	383	52.60	9.22	1.67	370	54.10	422	2	4	5	<0.5	19	37.55	1.83
53821	MUMF-1	609	30.80	1235	0.72	15.50	13.20	203	10.90	384	54.10	9.88	1.43	270	62.40	485	4	4	4	<0.5	15.38	35.23	1.89
53798	MUMF-1	2590	73.40	3370	2.14	21.10	11	254	13	525	61.10	19.95	9.26	250	37.40	232	109	6	5	<0.5	23.09	40.38	2.07
53400	MUMF-2	1805	50.70	1675	1.31	19.10	5.60	116	17.90	1100	97.70	19.05	4.41	30	50.10	223	2	2	5	<0.5	20.71	61.45	9.48
53408	MUMF-2	619	28.10	1505	0.90	19.50	3.60	103.50	17.40	1130	104.50	22	4.03	30	50.80	235	2	10	6	<0.5	28.75	64.94	10.92
53409	MUMF-2	1055	42	1325	1.32	18	9.10	173.50	17.40	1300	98.90	28.90	8.26	30	47.70	213	2	3	5	<0.5	19.07	74.71	7.49
53732	CMC-1	1210	36.60	5280	0.81	8.50	0.20	248	4.10	236	84.20	54.80	36.80	230	27.30	150	3	2	3	<0.5	1240	57.56	0.95
53735	CMC-1	1200	49.60	4650	1.27	9.10	5.90	308	4	257	80.30	58.60	30.80	230	23.90	178	2	3	4	<0.5	52.20	64.25	0.83
53861	CMC-1	1025	34.80	4870	0.92	9.70	3	321	3.60	220	83.50	56.50	19.25	230	25.50	127	3	4	4	<0.5	107	61.11	0.69
53787	CMC-1	2150	35.40	5000	1.13	9.20	3.90	347	5.30	312	92.60	47.80	20.10	220	25.70	144	3	5	3	<0.5	88.97	58.87	0.90
53870	CMC-1	1880	34.20	5270	0.72	11.20	3.90	330	5.50	375	90.20	49.20	14.50	200	30.80	150	2	3	4	<0.5	84.62	68.18	1.14
55986	CMC-1	2780	20.60	4720	0.99	9.70	8.60	329	5.30	359	94.50	55.80	19.55	210	24.90	141	5	4	3	<0.5	38.26	67.74	1.09
54343	CMC-1	1320	28	3640	0.85	10.50	11.90	285	5.50	396	99.40	38.20	9.97	140	23.40	156	2	4	2	<0.5	23.95	72	1.39
54344	CMC-1	1360	30.40	3540	0.89	10.40	13.70	352	5.30	350	94	38.40	12.90	170	23.60	157	2	4	2	<0.5	25.69	66.04	0.99
53265	CMC-2	1695	0.80	3550	0.08	6.30	8.70	78.30	5.50	474	119	44	6.37	70	19	53	159	5	1	<0.5	9	86.18	6.05
53343	CMC-2	2670	8	6190	0.23	7.10	7.30	258	5.90	377	84.20	26.30	4.37	100	22.50	79	3	9	3	<0.5	35.34	63.90	1.46
53838	CMC-2	2450	17.90	5930	0.48	6.80	0.50	284	2.90	222	87	50.60	18.70	110	16.20	117	2	4	3	<0.5	568	76.55	0.78
53839	CMC-2	1485	19.90	4960	0.47	7.50	3.50	316	3.10	230	87.60	55.80	22.40	120	20.30	111	2	2	3	<0.5	90.29	74.19	0.73
53865	CMC-2	1285	15.70	5480	0.43	8	2.60	315	3.90	300	86.50	55.80	16.65	140	21.70	134	2	4	4	<0.5	121.15	76.92	0.95
53336	CMC-2	4210	0.70	6110	<0.01	5	1.50	56.60	4.10	303	128.50	14.65	0.41	30	14.70	81	3	1	1	<0.5	37.73	73.90	5.35
53713	CMC-2	1300	16.40	6270	0.28	5.70	5.60	258	2.90	215	100.50	47.80	20.10	90	17.40	120	3	3	2	<0.5	46.07	74.14	0.83
53724	CMC-2	3370	3.10	8780	0.06	5.90	3.30	572	1.90	145	86.90	41.70	8.41	60	17.50	87	3	4	3	<0.5	173.33	76.32	0.25
53727	CMC-2	2270	4.30	6490	0.08	4.70	1.30	300	1.50	103	95.60	41.60	11.30	30	15.70	62	11	3	2	<0.5	230.77	68.67	0.34
53412	CMC-2	944	0.90	4040	0.05	7.80	5.80	45.90	9.90	693	133	29.90	4.22	20	20.60	105	2	1	2	<0.5	7.91	70	15.10
53414	CMC-2	967	4.40	3620	0.11	7.20	4	70.50	9.50	728	103.50	36.90	1.78	<10	19.60	138	2	2	4	<0.5	17.63	76.63	10.33
53418	CMC-2	455	2.30	4910	0.06	6.30	4.80	51.70	9.50	771	121	27.30	3.61	<10	14.50	120	2	2	3	<0.5	10.77	81.16	14.91
53419	CMC-2	343	4.10	4020	0.14	8.10	4.10	35.30	6.40	500	120.50	23.60	1.97	<10	24.20	158	2	3	4	<0.5	8.61	78.13	14.16
54204	DMC-1	518	0.30	5490	0.05	4.60	29	88.90	6.10	341	35.40	1.29	39.20	40	33.90	134	26	2	1	<0.5	3.07	55.90	3.84
54209	DMC-1	480	0.40	5060	0.06	5.40	10	47.70	2.30	115	38.10	1.06	8.24	40	38.60	199	5	4	3	<0.5	4.77	50	2.41
54226	DMC-1	660	3.50	5660	0.17	6.60	86.10	192	0.40	13	35.20	1	87.60	50	26.80	179	2	2	2	<0.5	2.23	32.50	0.07
54227	DMC-1	317	0.80	5930	0.13	5.10	24.30	61.90	0.90	28	33.60	0.97	30.80	40	23	104	2	8	<1	<0.5	2.55	31.11	0.45
54229	DMC-1	285	0.40	5940	0.02	4.50	45.80	108	1.90	105	30.40	1.14	57.10	40	31.40	106	2	5	1	<0.5	2.36	55.26	0.97
54214	DMC-2	756	0.30	4900	0.10	2.60	22.40	77.30	0.30	6	27.10	1.17	34.90	40	13.80	28	5	6	<1	<0.5	3.45	20	0.08
54216	DMC-2	983	0.50	5000	0.04	3.10	52.50	159	0.20	4	31.40	1.72	59.10	40	16.70	32	141	2	<1	<0.5	3.03	20	0.03
54217	DMC-2	247	0.60	2290	0.04	2	19.90	89.50	<0.2	4	19.90	0.72	9.32	40	7.70	30	120	1	<1	<0.5	4.50	40	0.04
54218	DMC-2	1000	0.20	5110	0.06	2.80	136.50	313	0.20	7	27.60	1.29	147.50	40	13.30	34	4	2	1	<0.5	2.29	35	0.02
54232	DMC-2	1780	2.90	5510	0.11	3.70	9.80	27.90	0.80	43	42.30	0.77	7.39	40	23	59	22	6	<1	<0.5	2.85	53.75	1.54
53135	MSY	7060	45.20	4210	0.26	17.30	4.20	128	2.30	102	13.10	2.57	0.77	20	5.90	70	3	7	1	<0.5	30.48	44.35	0.80
53137	MSY	9520	82.90	2270	0.78	21.60	3.20	129.50	3.60	189	16.70	11.75	0.71	70	10.10	100	3	5	2	<0.5	40.47	52.50	1.46

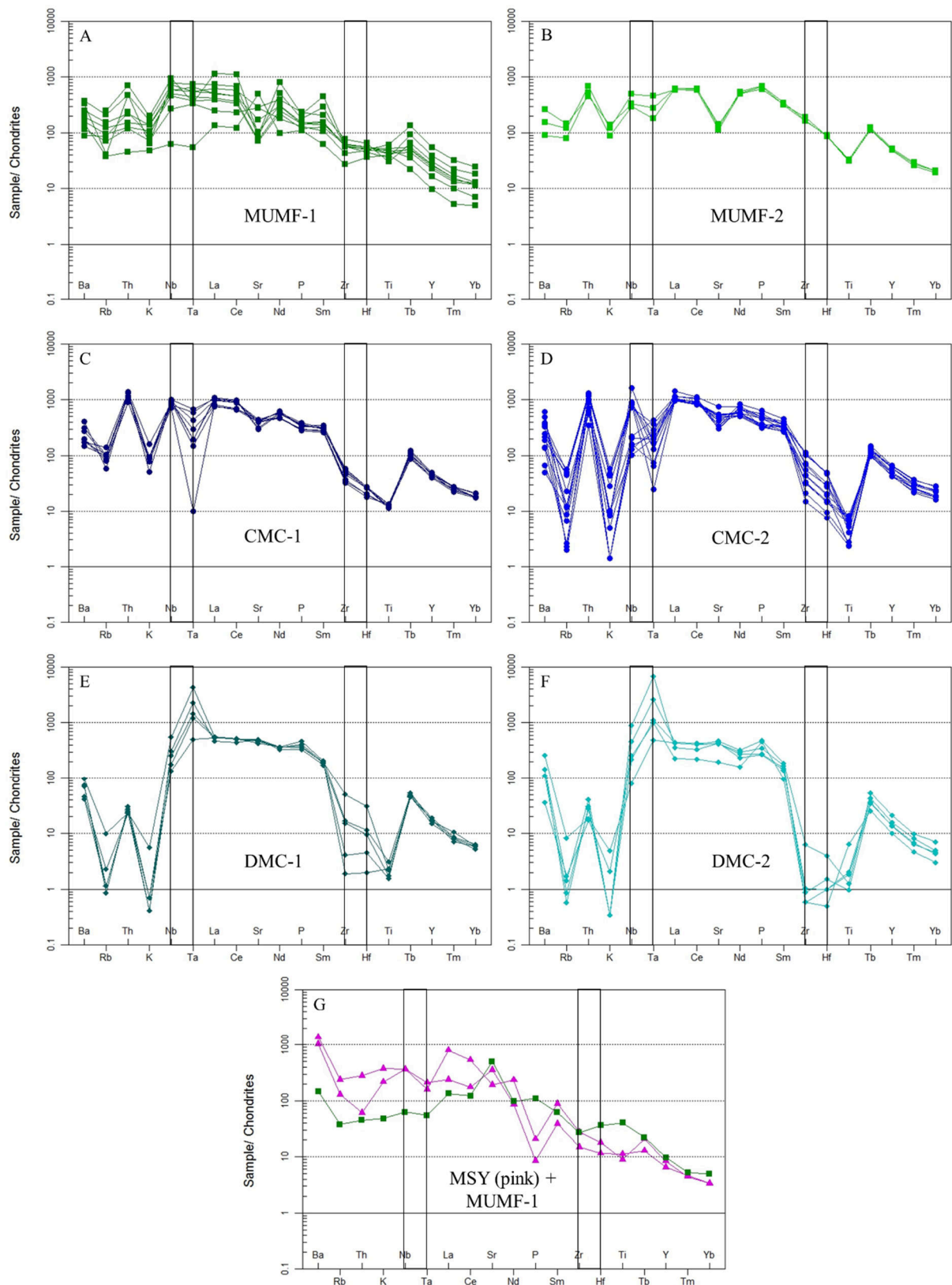


Figure 4.13 - Spidergram with distribution of minor and trace element in the TEC normalized to the chondrite according to Thompson (1984).

The behavior of Ti is similar to Sr, with the exception that the most prominent negative anomalies are associated with calcite metaultramafic rocks and that there is a sample with a positive anomaly in the facies MUMF-1, in which, sometimes Ti tends to flat (**Figures 4.13A to 4.13D**). Dolomite metacarbonatites also exhibit Ti anomalies, in general, pronounced, mainly in DMC-1 (**Figures 4.13E and 4.13F**), whereas in metasyenites the Ti it presents a flat pattern varying to negative anomaly (**Figure 4.13G**). As for P, each facies present a behavior. The anomalies are predominantly negative in MUMF-1, with restricted occurrences of flat patterns and positive anomalies, whereas all samples of MUMF-2 show P with a flat pattern. CMC-1 shows a consistent pattern of slightly positive anomalies of P, and CMC-2 shows variation between a flat pattern and anomalies, sometimes slightly negative, sometimes slightly positive. Dolomite metacarbonatites diverge from this picture and present positive P anomalies in both facies, whereas metasyenites exhibit strongly negative anomalies (**Figures 4.13A to 4.13G**).

Nb and Ta are little fractionated in relation to each other in metaultramafic rocks. The Nb/Ta ratios (MUMF-1: 14.21-48.26; MUMF-2: 19.07-28.75) do not vary significantly between both facies, ranging from slightly positive in two samples in MUMF-1 to predominantly negative, reflecting slight enrichment in Nb in relation to Ta in metaultramafic rocks in general (**Figures 4.13A and 4.13B, Table 4.2**). In calcite metacarbonatite Nb and Ta are extremely fractionated from each other with Nb showing strong enrichment compared to Ta. A few samples in the CMC-2 facies, however, exhibit Ta enrichment in relation to the Nb. More pronounced variations in the ratio Nb/Ta are observed in CMC-2 (7.91 a 568) when compared to CMC-1 (23.95 to 107, occasionally reaching up to 1240) (**Figures 4.13C and 4.13D, Table 4.2**). In dolomite metacarbonatite the inverse occurs with enrichment in Ta in relation to Nb with ratios Nb/Ta varying between 2.23 and 4.77 in DMC-1 and 2.29 and 4.50 in DMC-2 (**Figures 4.13E and 4.13F, Table 4.2**). The Nb/Ta ratios in metasyenite (30.48-40.47) show fractionation with enrichment of Nb compared to Ta (**Figure 4.13G, Table 4.2**).

The Zr/Hf ratios vary little in metaultramafic rocks (MUMF-1: 25.34-43.26; MUMF-2: 61.45-74.71), sometimes with enrichment in Zr, sometimes in Hf in the MUMF-1 facies, whereas in the MUMF-2 facies, a higher degree of fractionation is observed between Hf and Zr with enrichment in Zr (**Figures 4.13A and 4.13B, Table 4.2**). In both calcite metacarbonatite facies there is depletion in Zr and Hf in relation to the metaultramafic rocks of the facies CMC-1, without significant changes in Zr/Hf ratios (CMC-1: 57.56-72; CMC-2:

63.90-86.18) (**Figures 4.13C and 4.13D, Table 4.2**). In dolomite metacarbonatite, however, the Zr/Hf ratio apparently decreases as the degree of Zr and Hf depletion increases, from > 1 in less depleted rocks to < 1 in two of the three most depleted rock samples (**Figures 4.13E and 4.13F, Table 4.2**). The Zr/Hf ratios in these rocks also do not vary significantly (DMC-1: 31.11-55.90; DMC-2: 20-53.75). The Zr/Hf ratios in metasyenite (44.35-52.50) show fractionation with enrichment of Zr in relation to Hf (**Figure 4.13G, Table 4.2**).

4.4.2.3. RARE EARTH ELEMENTS – REE

The REE pattern normalized to the chondrite (Boyton, 1984) of all TEC rocks shows enrichment of light REE compared to heavy REE (**Figure 4.14**).

The La/Yb ratios vary between 40.64 to 72.28 in MUMF-1 and between 43.32 and 48.22 in MUMF-2 indicating little difference in degree fractionation between the metaultramafic rock facies (**Table 4.3**). The lowest mean of Σ REO concentration is found in MUMF-1 (960.66 ppm), whereas the highest mean is found in MUMF-2 (1304.06 ppm) (**Table 4.3**).

In metacarbonatites, the La/Yb ratios vary between 62.31 and 91.47 in CMC-1, 51.85 and 134.28 in CMC-2, 127.34 and 142.25 in DMC-1 and between 91.61 and 143 in DMC-2 indicating greater REE fractionation in CMC-2 and DMC-2 facies (Table 3). The highest average concentrations of Σ REO are found in calcite metacarbonatite (1633.35 ppm in CMC-1 and 1839.01 ppm in CMC-2), whereas the lowest average contents are found in dolomite metacarbonatite (977.76 ppm in DMC-1 and 709.16 ppm in DMC-2) (**Table 4.3**).

The degree of fractionation observed in metasyenites is more pronounced than that observed in metaultramafic rocks and metacarbonatites with La/Yb ratio ranging from 106.22 to 352 (**Figure 4.14, Table 4.3**). The average concentration of Σ REO in metasyenites, of 638.95 ppm, is lower than that observed in other rocks of the TEC.

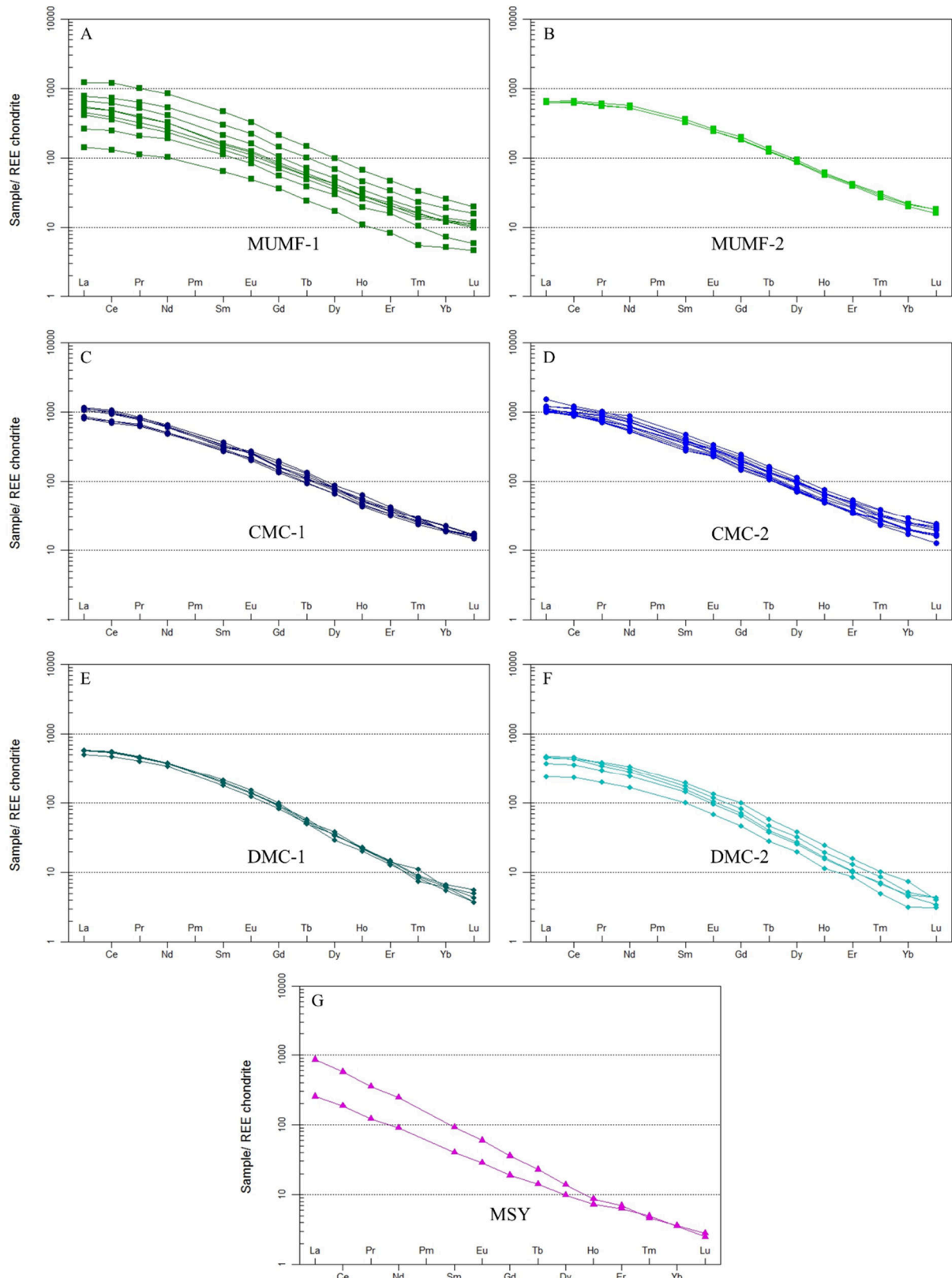


Figure 4.14 - Diagrams of rare earth elements from TEC rocks normalized according to the chondrite according to Boyton (1984).

Table 4.3 - Analysis of rare earth elements in TEC rocks. Contents are in ppm.

Amostra	Rocha	La	Ce	Pr	Nd	Sm	Eu	Gd	Tb	Dy	Ho	Er	Tm	Yb	Lu	ΣREE	La/Yb	La/Sm	Sm/Yb
53939	MUMF-1	44.30	105.50	13.65	61.60	12.55	3.67	9.44	1.15	5.60	0.79	1.76	0.18	1.09	0.15	261.43	40.64	3.53	11.51
53940	MUMF-1	81.30	201	25.40	114	21.70	6.14	14.30	1.84	9.56	1.40	3.39	0.34	1.53	0.19	482.09	53.14	3.75	14.18
53667	MUMF-1	378	968	122	510	91.30	24	54.90	7	32	4.83	9.89	1.09	5.35	0.64	2209	70.65	4.14	17.07
53668	MUMF-1	242	592	77.80	323	58.90	16.50	37.50	4.82	22.30	3.30	7.13	0.76	3.99	0.51	1390.51	60.65	4.11	14.76
53654	MUMF-1	139.50	317	39.10	158	28.80	8.16	19.90	2.61	12.70	2.05	4.44	0.48	2.71	0.36	735.81	51.48	4.84	10.63
53655	MUMF-1	128	289	34.80	140.50	25.90	7.27	18.10	2.34	11.30	1.84	3.99	0.45	2.60	0.37	666.46	49.23	4.94	9.96
53813	MUMF-1	169	390	47.20	192	30.70	8.91	20.90	2.67	13.65	2.05	4.37	0.52	2.56	0.34	884.87	66.02	5.50	11.99
53821	MUMF-1	164.50	394	48.50	195	31.50	9.22	22.50	2.87	13.75	2.10	4.75	0.53	2.52	0.32	892.06	65.28	5.22	12.50
53798	MUMF-1	206	495	63	247	41.90	11.80	27.10	3.40	16.80	2.55	5.28	0.60	2.85	0.39	1123.67	72.28	4.92	14.70
53400	MUMF-2	203	520	69.50	318	64.10	17.95	47.10	5.85	27.90	4.04	8.34	0.88	4.21	0.52	1291.39	48.22	3.17	15.23
53408	MUMF-2	203	538	73.90	343	70.40	19.35	51.90	6.41	30.50	4.42	8.95	1	4.60	0.59	1356.02	44.13	2.88	15.30
53409	MUMF-2	194.50	500	68	318	64.60	18.05	48.20	6.04	28.40	4.21	8.73	0.95	4.49	0.59	1264.76	43.32	3.01	14.39
53732	CMC-1	267	605	81	304	57.30	15.35	37.40	4.59	21.30	3.28	7.09	0.81	4.13	0.52	1408.77	64.65	4.66	13.87
53735	CMC-1	255	564	76.50	293	55	14.85	35	4.47	21.30	3.12	6.66	0.76	3.91	0.47	1334.04	65.22	4.64	14.07
53861	CMC-1	248	604	78.50	301	53.20	16	37.30	5.08	23.70	3.42	7.14	0.86	3.98	0.53	1382.71	62.31	4.66	13.37
53787	CMC-1	332	758	94.10	373	65.30	18.45	41.30	5.32	24.90	3.69	7.72	0.82	4.02	0.51	1729.13	82.59	5.08	16.24
53870	CMC-1	354	787	96.90	368	60.20	19.10	42.60	5.59	25.80	3.85	7.89	0.95	3.87	0.56	1776.31	91.47	5.88	15.56
55986	CMC-1	327	756	100.50	391	71.30	18.75	42.30	5.20	25.80	3.68	8.51	0.91	3.96	0.50	1755.41	82.58	4.59	18.01
54343	CMC-1	356	855	102.50	378	64	20.20	50.90	6.35	28.10	4.57	9.03	0.95	4.72	0.54	1880.86	75.42	5.56	13.56
54344	CMC-1	344	823	97.30	357	61.40	19.30	47.20	6.08	25.80	4.04	8.41	0.93	4.56	0.53	1799.55	75.44	5.60	13.46
53265	CMC-2	377	894	115.50	468	83.70	22.80	57.90	7.04	33.20	4.87	10.10	1.01	5.38	0.67	2081.17	70.07	4.50	15.56
53343	CMC-2	344	779	95.30	368	60.20	17.85	42.20	5.36	24.50	3.80	7.76	0.78	4.02	0.52	1753.29	85.57	5.71	14.98
53838	CMC-2	324	722	87.10	317	54.80	16.70	38.20	5.06	23.10	3.55	7.66	0.90	4.23	0.54	1604.84	76.60	5.91	12.96
53839	CMC-2	325	727	88.80	326	54.70	17.25	39.40	5.21	23.90	3.64	7.21	0.90	4.18	0.55	1623.74	77.75	5.94	13.09
53865	CMC-2	312	719	89	336	57.40	17.30	39.60	5.21	23.40	3.55	7.59	0.88	4.01	0.52	1615.46	77.81	5.44	14.31
53336	CMC-2	323	745	91.20	375	67.10	21.20	50.10	6.59	30.70	4.75	10.65	1.24	6.23	0.74	1733.50	51.85	4.81	10.77
53713	CMC-2	313	710	94	368	69.60	18.20	42.50	5.69	25.80	3.98	8.76	1	4.94	0.63	1666.10	63.36	4.50	14.09
53724	CMC-2	474	977	125	478	77.60	20.40	47.50	5.70	25.90	3.73	7.23	0.74	3.53	0.41	2246.74	134.28	6.11	21.98
53727	CMC-2	350	755	100.50	375	70.30	19.15	42.90	5.49	25.10	3.59	7.69	0.86	4.22	0.51	1760.31	82.94	4.98	16.66
53412	CMC-2	379	920	119.50	530	92.70	24.70	63.10	7.66	36.90	5.48	11.35	1.26	6.03	0.77	2198.45	62.85	4.09	15.37
53414	CMC-2	323	801	106.50	425	72.50	20.80	51.30	6.30	30.40	4.44	8.92	0.89	4.17	0.52	1855.74	77.46	4.46	17.39
53418	CMC-2	332	798	107.50	430	73.50	21.80	52.40	6.43	31.80	4.84	9.82	1.05	5.28	0.71	1875.13	62.88	4.52	13.92
53419	CMC-2	324	813	109.50	434	74.70	21.90	54.30	6.58	32.50	4.92	10.35	1.10	5.09	0.66	1892.60	63.65	4.34	14.68
54204	DMC-1	179	442	55	224	39.20	10.25	23.40	2.35	11.35	1.58	2.99	0.28	1.30	0.14	992.84	137.69	4.57	30.15
54209	DMC-1	177	451	56.40	231	41.80	11.25	25.90	2.57	12.40	1.63	3.11	0.29	1.39	0.18	1015.92	127.34	4.23	30.07
54226	DMC-1	183.50	454	57.20	229	39.30	10.35	24.50	2.48	11.05	1.59	2.91	0.24	1.29	0.12	1017.53	142.25	4.67	30.47
54227	DMC-1	179.50	435	55.20	228	38	10.15	23.80	2.78	10.90	1.66	2.97	0.36	1.29	0.16	989.77	139.15	4.72	29.46
54229	DMC-1	155	380	49.60	205	35	9.16	21.50	2.40	9.42	1.45	2.69	0.27	1.15	0.12	872.76	134.78	4.43	30.43
54214	DMC-2	143	352	42.40	172	30.70	7.64	18.30	1.89	8.78	1.17	2.21	0.22	1	0.14	781.45	143	4.66	30.70
54216	DMC-2	147	371	46.20	187.50	34.20	8.73	21.40	2.21	10.35	1.38	2.73	0.28	1.09	0.14	834.21	134.86	4.30	31.38
54217	DMC-2	74.10	189	24.30	100.50	19.50	5.01	12.05	1.32	6.34	0.82	1.81	0.16	0.66	0.10	435.67	112.27	3.80	29.55
54218	DMC-2	116.50	288	36.30	146.50	28.30	7.11	16.75	1.79	8.32	1.13	2.14	0.23	0.95	0.11	654.13	122.63	4.12	29.79
54232	DMC-2	142	352	47.50	203	37.90	9.81	26	2.78	12.25	1.77	3.30	0.33	1.55	0.13	840.32	91.61	3.75	24.45
53135	MSY	78.60	151.50	14.80	54.20	7.86	2.11	4.91	0.67	3.18	0.52	1.32	0.16	0.74	0.08	320.65	106.22	10	10.62
53137	MSY	264	463	43	147	18	4.37	9.29	1.08	4.44	0.62	1.46	0.15	0.75	0.09	957.25	352	14.67	24

4.4.3. STABLE $\delta^{13}\text{C}_{\text{V-PDV}}$ AND $\delta^{18}\text{O}_{\text{V-SMOW}}$ ISOTOPES

Figure 4.15 and **Table 4.4** show the results of isotopic analyses of $\delta^{13}\text{C}_{\text{V-PDV}} (\text{\textperthousand})$ and $\delta^{18}\text{O}_{\text{V-SMOW}} (\text{\textperthousand})$. This graph also contains samples of calcite carbonatite from Passo Feio Carbonatite (Morales *et al.*, 2019) and some Mesoproterozoic carbonatites for comparison, from Greenville Province in Canada (Moecher *et al.*, 1997) and the Alkaline Province of Ontario (Bell & Blenkinsop, 1987).

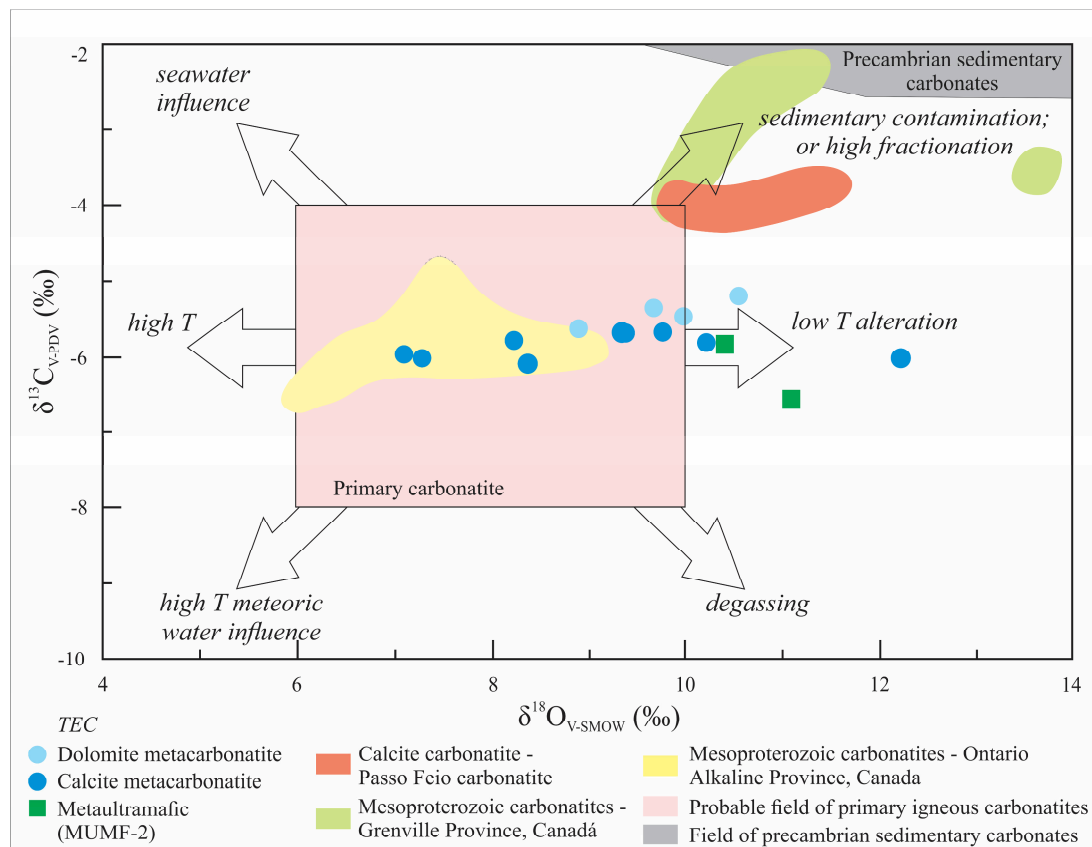


Figure 4.15 - Stable $\delta^{13}\text{C}$ versus $\delta^{18}\text{O}$ isotopes for TEC metacarbonatites and metaultramafic rocks. The light pink field corresponds to the primary igneous carbonatites of Taylor *et al.* (1967) e Keller & Hoefs (1995). Arrows indicate the main processes in changing the isotopic composition of carbonates (Deines, 1989; Demény *et al.*, 2004).

The $\delta^{13}\text{C}_{\text{V-PDV}}$ and $\delta^{18}\text{O}_{\text{V-SMOW}}$ values of TEC metaultramafic rocks and metacarbonatites show values compatible with primary igneous carbonatites and very little variation in terms of $\delta^{13}\text{C}$. Greater isotopic fractionation occurs with respect to $\delta^{18}\text{O}$ towards the low temperature change (**Figure 4.15**), similar to the isotopic signature of Passo Feio Carbonatite, which is distinguished by presenting higher $\delta^{13}\text{C}$ values.

Part of the TEC calcite metacarbonatite coincides with the isotope signatures of the Mesoproterozoic carbonatites in the Alkaline Province of Ontario, which fall almost entirely within the probable field of primary igneous carbonatites. In turn, the Mesoproterozoic carbonatites from the Grenville Province show high isotopic fractionation of $\delta^{13}\text{C}$ and $\delta^{18}\text{O}$.

Table 4.4 - $\delta^{13}\text{C}$ and $\delta^{18}\text{O}$ isotopic data of CTE metacarbonatites and metaultramafic rocks.

Analysis	num. BSB	Sample	Rock	Carbonate		
				V-PDB	V-PDB	V-SMOW
1	11933	TEG-01	Dolomite metacarbonatite	-5.48	-20.22	10.01
2	11934	TEG-02	Calcite metacarbonatite	-5.99	-23.03	7.12
3	11935	TEG-03	Metaultramafic rock	-6.59	-19.15	11.12
4	11936	TEG-06	Dolomite metacarbonatite	-5.69	-20.45	9.78
5	11937	TEG-07	Calcite metacarbonatite	-6.10	-21.80	8.39
6	11938	TEG-08	Metaultramafic rock	-5.86	-19.83	10.42
7	11939	TEG-11	Calcite metacarbonatite	-5.70	-20.84	9.37
8	11940	TEG-12	Calcite metacarbonatite	-6.03	-22.84	7.32
9	11941	TEG-13	Calcite metacarbonatite	-6.03	-18.05	12.25
10	11942	TEG-14	Dolomite metacarbonatite	-5.65	-21.28	8.92
11	11943	TEG-15	Dolomite metacarbonatite	-5.20	-19.68	10.58
12	11944	TEG-16	Calcite metacarbonatite	-5.83	-20.01	10.23
13	11945	TEG-17	Calcite metacarbonatite	-5.80	-21.92	8.26
14	11946	TEG-18	Dolomite metacarbonatite	-5.37	-20.54	9.69
15	11947	TEG-19	Calcite metacarbonatite	-5.71	-20.81	9.40

4.5. DISCUSSIONS

4.5.1. IMPLICATIONS FOR TEC GENESIS AND EVOLUTION

In the last 60 years, carbonatite research has progressed in the areas of isotopic and experimental studies. However, the genesis of carbonatites is still controversial (Downes *et al.*, 2012). The main issues under discussion include the generation of carbonatite from carbonate-rich magmas or carbonated silicate magmas, formed from mantle melting, their modification as they are transported to the crust, and their differentiation within the crust before being placed in subvolcanic structures (Lee & Wyllie, 1998).

Although TEC rocks are affected by metasomatic changes and metamorphism of greenschist to amphibolite facies, they preserve many of the textural and isotopic, geochemical signatures of the original magmatic protolith (for example, cumulates, flow banding, trace

element, and REE patterns, and mantle-like isotopic compositions), allowing to make several considerations about its genesis and evolution.

Metaultramafic rocks and metacarbonatites provide the best available approximation of the magmas involved in the generation and evolution of the Três Estradas Complex. Based on isotopic signatures of Nd-Sr in whole-rock and Hf in zircon, Monteiro *et al.* (unpublished) suggest that TEC rocks are derived from a metasomatized, isotopically depleted heterogeneous mantle source with some minor influence from the ancient continental crust, and were crystallized around 1.1 Ga (U-Pb in zircon age). The ^{13}C and ^{18}O isotopic signatures reported in this work corroborate this proposal and show compatibility with the primitive mantle signature (**Figure 4.15**).

In the TEC, the similar geochemical signature patterns of calcite metacarbonatite and metaultramafic rock and the generally gradual contact between both suggest that they are cogenetic rocks. Such cogeneticity among the rocks that make up the TEC was pointed out by Monteiro *et al.*, (unpublished) from similar isotopic signatures of Nd-Sr and can be corroborated by the little variation of the carbon isotopes in metaultramafic rocks and calcite and dolomite metacarbonatites, which suggests similarities between these rocks (**Figure 4.15**). Dolomite metacarbonatites, on the other hand, are geochemically distinct and indicate a different evolution from calcite metacarbonatites and metaultramafic rocks.

Chemical evidence such as high levels of MgO, Cr, and Sr and extreme undersaturation in SiO₂ and high concentrations of igneous calcite suggest that metaultramafic rocks are the least evolved rocks identified in TEC and that are derived from carbonated silicate liquid. The major elements indicate that the total content of Fe₂O₃, TiO₂ and SiO₂ decreases with the evolution of the complex from the MUMF-1 facies to the facies CMC-2 (**Figure 4.11**), suggesting a path of magmatic differentiation involved in the generation of metaultramafic rocks and calcite metacarbonatites. The CMC-1 facies, chemically classified as magnesian calcium carbonate (**Figure 4.12**), is rich in magnesian silicate minerals and appears to represent the gradual transition between metaultramafic rocks and calcium carbonate from facies CMC-2 (**Figure 4.8B**).

The normalized multielement diagram shown in **Figure 4.13**, highlights similar geochemical patterns between MUMF and CMC. The Sr shows predominantly negative anomalies in metaultramafic rocks, gradually becoming slightly negative in calcite metacarbonatite, probably due to the gradual increase in calcite crystallization in the direction

MUMF-1 to CMC-2. The content of P varies in relation to the crystallization of apatite. Starting from MUMF-1, P show negative anomalies becoming slightly positive in MUMF-2. MUMF-2 has high average content of P_2O_5 when compared to other TEC rocks (**Figure 4.10D and Figure 4.11**). This greater availability of P in the liquid allowed the crystallization of larger amounts of apatite in these facies, which occurs closely associated with white calcite intercumulus. In calcite metacarbonatite, P anomalies range from slightly negative in CMC-1 to slightly positive in CMC-2 sub-facies, showing that the fractionated crystallization residue had greater availability of P and Ca, thus forming more apatite than in CMC-1.

The decoupling of the Nb-Ta and Zr-Hf geochemical pairs in magmas that originate carbonatites is discussed by several authors (Veksler *et al.*, 1998; Brod, 1999; Thompson *et al.*, 2002; Chakhmouradian, 2006; Barbosa *et al.*, 2012; Brod *et al.*, 2013; Barbosa *et al.*, 2020). Chakhmouradian (2006) proposes that such decoupling occurs due to the fractionation of minerals that have these elements in their constitution. On the other hand, there are authors who suggest that this type of behavior results from the immiscibility of carbonated silicate liquid (Veksler *et al.*, 1998). In TEC, it is observed that during the crystallization of the liquid that generated calcite, metacarbonatites and metaultramafic rocks, Zr and Hf had a preference for silicate liquid much more than Nb and Ta (**Figures 4.16A and 4.16B**). Titanite, which occurs in higher amounts in metaultramafic rocks, concentrates Hf in its structure, which justifies lower Zr / Hf ratios in these rocks, mainly in MUMF-1, facies richer in titanite, which presents discrete inversions of ratio, sometimes > 1 , or < 1 (**Figures 4.13A and 4.13B**), whereas the ratios are higher in MBH-2 probably due to the lower amount of titanite (**Figures 4.10C, 4.13A, 4.13B and 4.16B**). The fractionation between Nb and Ta tends to be greater than that observed between Zr and Hf, mainly in calcite metacarbonatites in relation to metaultramafic rocks, probably due to the crystallization of a greater amount of accessory pyrochlore, which concentrates Nb, in the first type of rock. It is observed in CMC-2 inversion of Nb/Ta (< 1) coinciding with sub-facies richer in apatite, calcite, and REE, with lower concentrations of Nb and fewer silicate minerals. Veksler *et al.* (1998) suggest that carbonatites rich in Zr and Nb, as in the case of TEC metacarbonatites calcite (**Figure 4.16C**), they originate as residual liquids formed from fractional crystallization, and not as immiscibility products. Slightly greater fractionation of LREE compared to HREE, in calcite metacarbonatites compared to metaultramafic rocks (**Figures 4.14A to 4.14D**), reinforces that these rocks evolved through different degrees of fractional crystallization, according to the proposition made by Barbosa *et al.* (2009) for carbonatites of the Salitre I Alkaline-Carbonatitic Complex.

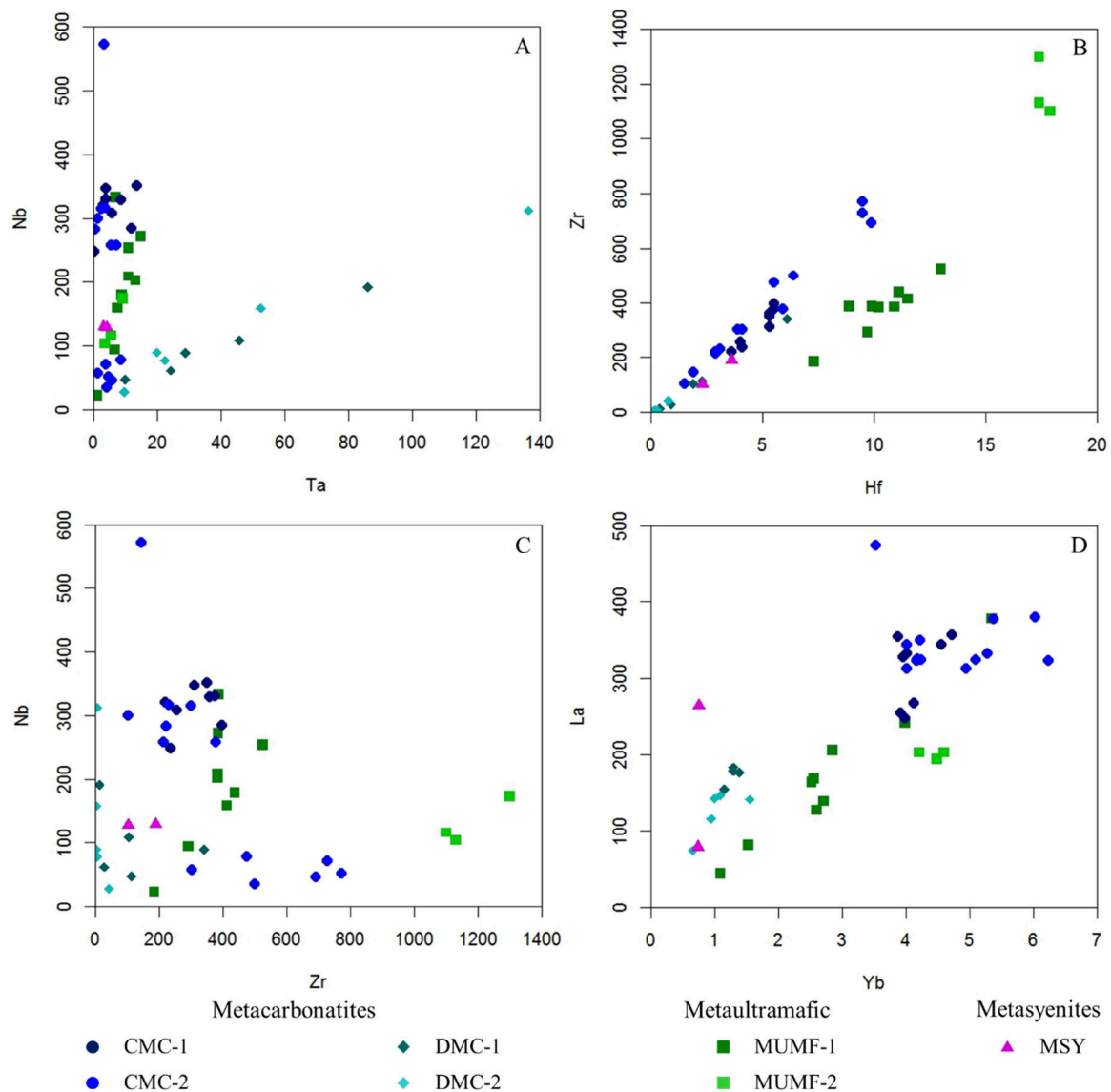


Figure 4.16 - A: Nb/Ta indicating fractionation probably related to liquid immiscibility; B: Higher concentration of Hf compared to Zr in metaultramafic rocks; C: Zr and Nb correlation that shows higher values in metaultramafic rocks and calcite metacarbonatites; D: La and Yb showing enrichment in ETR in metaultramafic rocks and calcite metacarbonatites compared to dolomite metacarbonatites.

On the other hand, dolomite metacarbonatites point to a distinct evolution of these rocks. There is a clear inversion of reason Nb/Ta (<1) in dolomite metacarbonatites (**Figures 4.13E and 4.13F**) with strong enrichment in Ta, whereas Nb does not vary significantly in relation to metaultramafic rocks and metacarbonatites. Studies show that Ta has an even greater preference for silicate liquids than Nb (Veksler *et al.*, 1998; Chakhmouradian, 2006; Brod *et al.*, 2013), therefore, the Nb/Ta ratio would be expected to increase as instead of decreasing as it happens in metacarbonatite dolomites. A possible interpretation for these variations in the Nb/Ta ratio may be the fractionation of pyroclore with enrichment of Ta in dolomite

metacarbonatites (Brod *et al.*, 2013; Barbosa *et al.*, 2020). Zr and Hf are depleted in dolomite metacarbonatites (**Figure 4.16B**) and the ratio between them tends to decrease with an increase in the degree of depletion of Zr and Hf, from >1 in less depleted rocks to <1 in more depleted rocks (**Figures 4.13E and 4.13F**), suggesting that Hf is slightly less incompatible than Zr in these rocks, similar to the situation observed by Brod *et al.* (2013) in carbonatites of the Alkaline Carbonatitic Complex of Salitre. The higher La/Yb ratio in dolomite metacarbonatites (Figure 16D) reflects greater fractionation between LREE in relation to HREE than in metaultramafic rocks and calcite metacarbonatite.

When comparing the geochemical patterns of dolomite metacarbonatites in relation to metaultramafic rocks and calcite metacarbonatites, the analysis of CaO and MgO concentrations in relation to SiO₂ (**Figures 4.10A and 4.10B**), the mirrored behavior of Sr, Nd and P (**Figures 4.13E and 4.13F**), the inverse Nb/Ta (<1) ratio (**Figure 4.16A**) and the lower Hf incompatibility suggest that dolomite metacarbonatites may have been formed by immiscibility of liquids (Brod *et al.*, 2013). However, among the dolomite metacarbonatite group, the DMC-1 and DMC-2 facies differed by fractional crystallization, similar to what occurs in Mesoproterozoic dolomite metacarbonatite from Newania, India (Ray *et al.*, 2013). DMC-1, which has pockets of immiscible meta-ultramafic, evolves to form DMC-2 more enriched in CaO, MgO, Ba, Nb and Ta and depleted in Al₂O₃, Fe₂O₃, SiO₂, Zr, Hf and ΣREE.

Therefore, the mineralogical, textural, type of contact, and chemical characteristics of TEC calcite metacarbonatite suggest that they can represent fractional crystallization residues of parental carbonated silicate magma that initially formed the metaultramafic rocks, whereas dolomite metacarbonatite may have been generated through the immiscibility of liquids and if differentiated by fractional crystallization (**Figure 4.17**). In immiscibility events in carbonated silicate liquid, the most common is the generation of liquid with calciocarbonatite composition (Kjaarsgard & Hamilton, 1989; Lee & Wyllie, 1997). However, at greater depths and in less differentiated stages, a liquid with magnesium-carbonatitic composition can be formed (Le Bas, 1989; Lee *et al.*, 2000). This situation can be used to explain the occurrence of dolomite metacarbonatites in TEC. The isotopic data presented by Monteiro *et al.* (unpublished), that indicate metasomatized mantle as a source of the carbonated silicate liquid that generated these rocks, are corroborated by their enrichment in LREE, as suggested by Roden & Murty (1985).

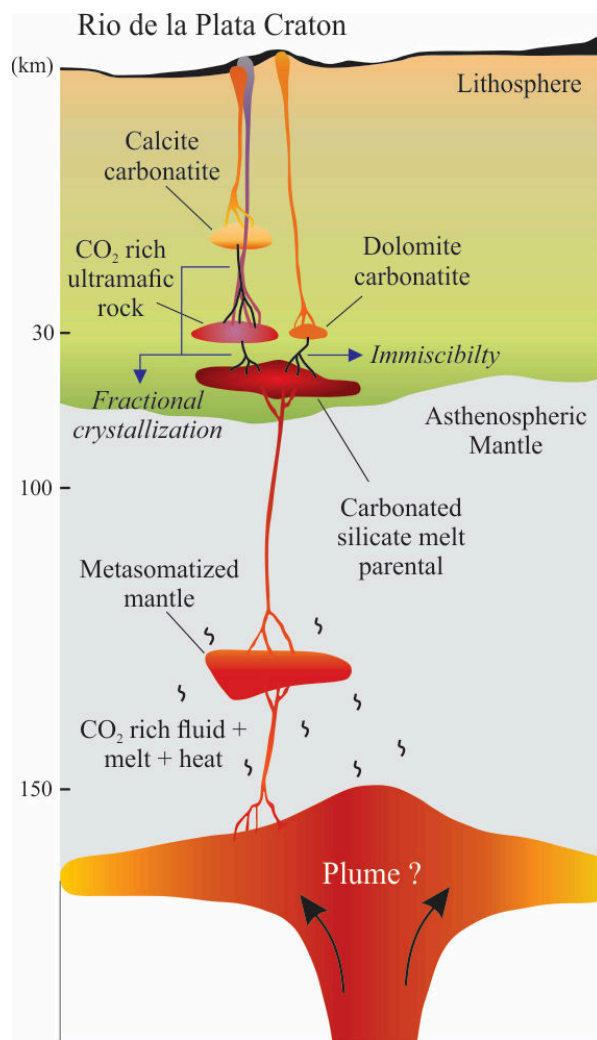


Figure 4.17 - Genetic model suggested for TEC.

The metasyenite was affected by high degree of metasomatism, which may have altered its geochemical signature, impairing the interpretation of the data. The geochemical patterns of traces and minor elements of metasienite have some similarity with MUMF-1 metaultramafic rocks (**Figure 4.13G**), as for Rb, Th, K, REE, Sr and Nb/Ta, whereas P and Zr/Hf show different signatures. From the geochemical patterns in metasienite allied to its occurrence located only in the NE portion of the TEC and its almost exclusive contact relationship with metaultramafic rocks, it is possible to speculate that this rock may have derived from the parental silicate magma from fractional crystallization and evolved in a chamber distinct from that which generated metaultramafic rocks and calcite metacarbonatites.

4.5.2. CONSIDERATIONS FOR METASOMATIC CHANGES, METAMORPHISM, AND DEFORMATION

In the proximity of calcite metacarbonatites, intense fenitization develops. Similar to other alkaline-carbonatitic complexes, such as Cambrian intrusions in the Omineca Crystalline Belt, Canada (Pell & Höy, 1989), at least three types of metasomatic alterations in the TEC are individualized. The most common alteration is observed in metaultramafic rocks with the formation of biotite-rich mafic fenite with high concentrations of K₂O (up to 1.99 wt.% K₂O), due to the release of potassium solutions associated with metacarbonatites. Martinez (2019) identifies the formation of glimerites associated with this type of fenitization. Locally these fenites are interspersed with thin bands of fenite rich in albite, which justifies the significant Na₂O levels found in metaultramafic rocks (up to 1.59 wt.%). The third type comprises sodic-potassic fenitization and predominantly targets metasyenites with up to 5.44 wt.% of K₂O and 7.32 wt.% of Na₂O and hosting gneisses. In fenitized metasyenites, barium is characteristically enriched, with up to 9,520 ppm, as suggested by Le Bas (2008). Both calcite metacarbonatite and dolomite metacarbonatite may have induced potassium and sodium fenitization in their margins (Le Bas, 2008), not having been distinguished in TEC. Even though, due to the geological contact relationships, it is possible to assume that most of the potassium metasomatism in metaultramafic rocks is due to fluids from calcite metacarbonatite. According to Elliot *et al.* (2018), fluids derived from the cooling of alkaline magmas or carbonatite intrusions carry large amounts of alkalis and volatiles, which were originally constituents of the parental magma. The intrusion of TEC in the Santa Maria-Chico Complex caused a propylitic alteration in these gneisses with amphibole and biotite chloritization and sulfidation with formation of pyrite and chalcopyrite (Senhorinho *et al.*, 2016). Both chloritization and sulfidation also affected TEC rocks.

TEC was subjected to metamorphism into greenschist to amphibolite facies identified by the presence of actinolite and recrystallized hornblende. These rocks are submitted to heterogeneous deformation with flow foliation and banding locally preserved. The age of metamorphism and deformation not were determined. Based on Monteiro *et al.* (unpublished), the folding and faulting of the Três Estradas Carbonatite may be related to deformation generated in the final stages of the agglutination of Rodinia, in Mesoproterozoic, or to one of the three major deformational events: the Passinho Event at 900 Ma (Hartmann *et al.*, 2000), the São Gabriel Event (750-690 Ma) or the Dom Feliciano Event (640-590 Ma) (Chemale Jr.,

2000). As for metaultramafic rocks, it is not easy to identify their protolith for sure. No remnants of pyroxene or igneous amphibole were found that allow it to be accurately determined. However, it is possible to presume that it is an alkaline ultramafic rock, given the very low amount of silica and concentrations of alkalis above 2 wt.%, when preserved from sodic-potassic metasomatism. Few occurrences of carbonatite affected by metamorphism are described as such in the scientific literature, and references in Angico dos Dias, Brazil can be highlighted (Silva *et al.*, 1987), Newania, India (Ray *et al.*, 2013), Vesely, Russia (Lastochkin *et al.* 2011) and carbonatite intrusions in the Olmineca Crystalline Belt, Canada (Pell & Höy, 1989).

^{13}C and ^{18}O isotopes evidence that low temperature changes affected the TEC, as indicated by the calcite carbonatite isotopic signature of Passo Feio carbonatite, Brazil, although this intrusion shows a high degree of isotopic fractionation of both ^{13}C , well as ^{18}O (Morales *et al.*, 2019), whereas TEC fractionates more the ^{18}O than ^{13}C (**Figure 4.15**). When comparing the signatures of ^{13}C - ^{18}O of TEC with Mesoproterozoic carbonatites Alkaline Complex of Ontario, Canada (Bell & Blenkinsop, 1987), note that these were also generated from primitive mantle, which reinforces the proposition made by Monteiro *et al.* (unpublished), that TEC can be correlated to these Canadian intrusions in time and space. There are no relevant secondary processes in the carbonatites of the Alkaline Complex of Ontario that have significantly affected the composition of these isotopes. Mesoproterozoic carbonatites from Greenville Province, Canada, indicate strong sediment assimilation or high degree of C and O fractionation (Moecher *et al.*, 1997).

4.5.3. RELATIONSHIP BETWEEN TEC AND OTHER CARBONATITE INTRUSIONS IN THE SRS

The formation of carbonated silicate magma under the Rio de la Plata Craton in the SRS during the Mesoproterozoic ($1,110 \pm 4.8$ Ma, U-Pb in zircon age) had not yet been registered, having first been defended by Monteiro *et al.* (unpublished). Another period of formation of this type of magma was verified by Cerva-Alves *et al.* (2017), that admit Neoproterozoic age (603 Ma, U-Pb in zircon age) for the crystallization of Carbonatite Picada do Tocos emplaced in orogenic terrane of the SRS. This Neoproterozoic age is assumed by the authors and by Morales *et al.* (2019) for the Passo Feio Carbonatite intrusive in the same host rock, 12 km to

SSW from Picada dos Tocos. Although the Três Estradas and Picada dos Tocos intrusions have been dated in different eras, they have geochemical signatures and textural similarity with each other and with the Passo Feio Carbonatite (**Figures 4.18A to 4.18H**). The geochemical signatures discussed in this work and the Nd-Sr isotopic data presented by Monteiro *et al.* (unpublished) show that the metaultramafic rocks found in TEC, sometimes as massive intrusions, sometimes as banding (**Figure 4.18B**), identified in this work as metaultramafic rocks subjected to intense biotitization, are cogenetic to metacarbonatites. Similar mafic bands are found in drill holes of the Picada dos Tocos intrusion (**Figure 4.18C**) and are attributed to the enclosing biotite amphibolite, belonging to the Passo Feio Complex, dated by Remus *et al.* (2000) e Lopes (2014) with minimum neoproterozoic age. Metasyenites and potassic fenitization have only been described in TEC (Monteiro *et al.*, unpublished), whereas sodic fenitization was observed in TEC and in the Passo Feio carbonatite (Cerva-Alves, 2017).

When comparing the geochemical signatures of calcite carbonatites of the Picada dos Tocos (Cerva-Alves *et al.*, 2017) and Passo Feio (Morales *et al.*, 2019) and TEC calcite metacarbonatite, very similar patterns can be seen, mainly between TEC and Passo Feio (**Figure 4.18E**). The calcite carbonatite from Picada do Tocos is more fractionated than the calcite metacarbonatite from TEC with greater enrichment in Th and Nb, greater depletion in Sr, Zr, Hf and Ti and enriched concentrations of P, now depleted in the first two (**Figure 4.18E**). It is not possible to compare the Nb/Ta ratios between these two intrusions, due to the lack of analysis of Ta in the literature. However, when comparing the Nb/Ta ratios between TEC calcite metacarbonatites and the calcite carbonatite from Passo Feio, there is compatibility between them, mainly with the CMC-2 facies, where the Nb/Ta ratios are > 1 , or sometimes < 1 (**Figures 4.13D and 4.18E**). As in CMC-2 there is a subfacies with inverse Nb/Ta ratio enriched in apatite and REE, a similar situation is observed in Passo Feio, where slightly positive anomalies of P and La are observed. The fractionation between Zr and Hf in all compared calcite carbonatites is very similar (**Figure 4.18E**).

The comparison between the geochemical signatures of dolomite carbonatite from Picada dos Tocos (10.70 wt.% to 17.50 wt.% MgO) and TEC dolomite metacarbonatite is hampered by the lack of Ta analysis, however, it is possible to notice similarities between both. It is noteworthy that the dolomite carbonatite signature of Picada dos Tocos analyzed by Cerva Alves *et al.* (2017) shows a pattern very close to that observed in calcite carbonatite from this same intrusion (**Figure 4.18F**).

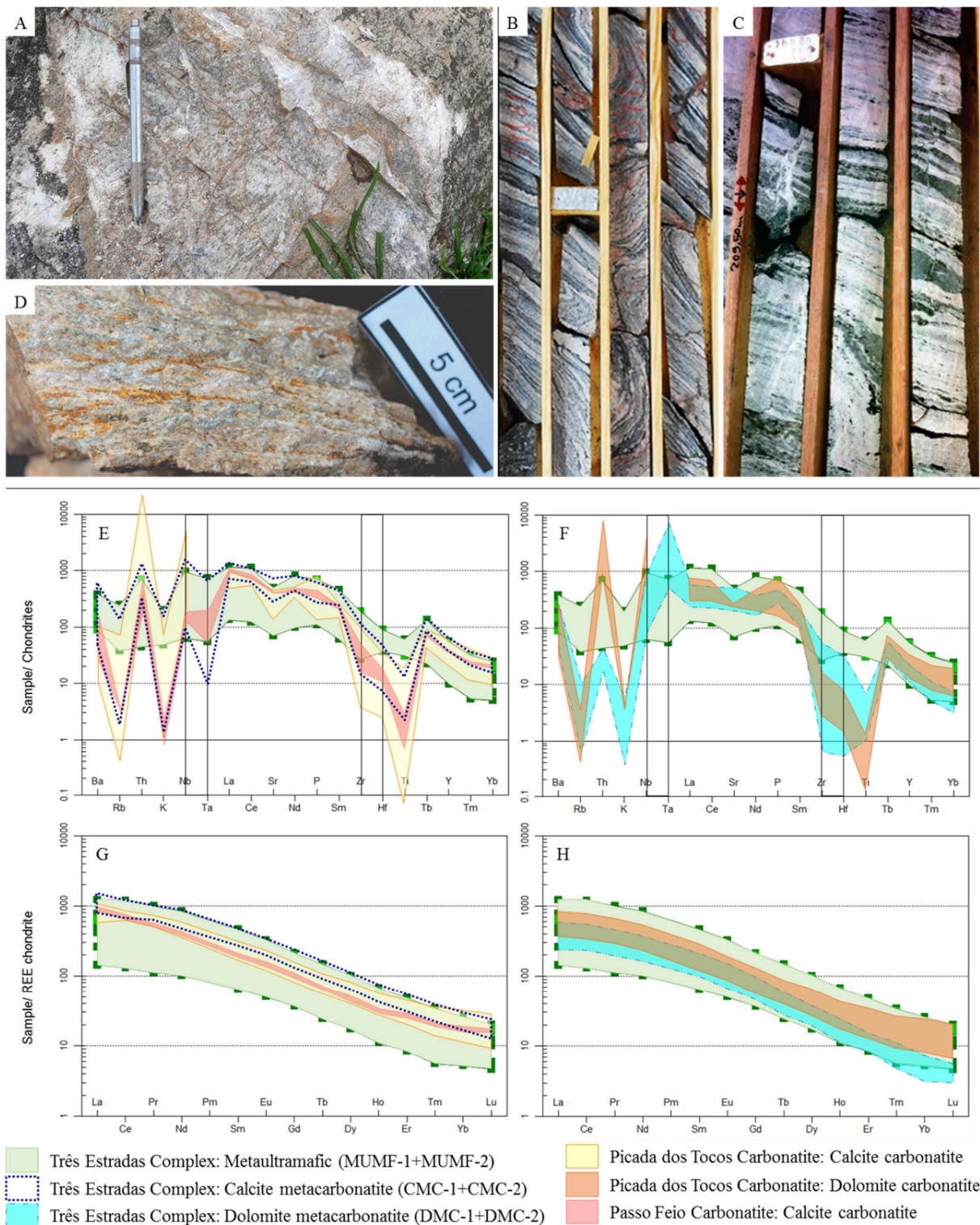


Figure 4.18 - Comparison between geochemical signatures and textures of Três Estradas, Picada dos Tocos and Passo Feio intrusions, showing the similarities between these carbonatites. A: outcrop of calcite metacarbonatite from TEC; B: Calcite metacarbonatite of drill core from TEC (CMC-1 facies); C: calcite carbonatite of drill core form the Picada dos Tocos (Rocha *et al.*, 2013); D: Outcrop of calcite carbonatite from the Passo Feio (Morales *et al.*, 2019); E: Spidergram of calcite carbonatite standardized to the chondrite Thompson (1984); F: Spidergram dolomite carbonatite standardized to the chondrite Thompson (1984); G: REE standards of calcite carbonatites normalized to the chondrite (Boyton, 1984); H: REE standards of dolomite carbonatite normalized to chondrite (Boyton, 1984);

In the three carbonatites there is enrichment in LREE in relation to HREE. The degree of ETR fractionation observed in TEC calcite metacarbonatite is slightly higher than that observed in calcite carbonatite from Picada dos Tocos and Passo Feio (**Figure 4.18G**). The La/Yb ratios vary between 43.70 and 81.11 and between 67.07 and 84.86 in calcite carbonatite from the Picada dos Tocos and Passo Feio, respectively, the latter being closer to the degree of fractionation observed in CMC-2. The dolomite carbonatite analyzed by Cerva-Alves *et al.* (2017) present a La/Yb ratio varying between 30.63 and 105.56, showing a degree of fractionation also lower than that observed in TEC dolomite metacarbonatites (**Figure 4.18H**).

In Ontario and SW Quebec, Canada, Greenland and Northern Europe (Kola Peninsula) there is a recurrence of carbonatitic magmatism in space and time, through ancient crustal weakness zones and other lineaments (Woolley & Bailey, 2012). The same situation may have occurred in the SRS with the intrusions of TEC, Picada dos Tocos and Passo Feio, in the space of approximately 500 Ma. Due to similar geochemical signatures and texture, it's possible suggest that these intrusions were originated from the fusion of the same REE enriched asthenospheric mantle and were subjected to similar petrogenetic processes, corroborating the hypothesis raised by Monteiro *et al.*, (unpublished) of origin for the TEC from enriched asthenosphere. Outcrops of Boqueirão Picrite occur 2.5 km from the carbonatites Porteira, towards SW, and Santa Inês, towards ENE, and 4.5 km from Joca Tavares Carbonatite. In alkaline-carbonatite complexes such as those in Alto Paranaíba, picrites represent primitive parental magmas (Brod *et al.*, 2000, 2004). It is plausible, therefore, to raise the possibility that Boqueirão Picrite is related to the genesis of Joca Tavares, Porteira and Santa Inês carbonatites, probably younger than the other carbonatitic intrusions. Ribeiro & Teixeira (1970) present two K-Ar ages in whole-rock obtained for Boqueirão Picrite of 292 ± 10 Ma (intrusion edge) and 119 ± 10 Ma (intrusion center), which must be carefully evaluated, although Ribeiro (1980) assume that this intrusion is Mesozoic. Therefore, a possible third age of placing carbonatites in the SRS may be associated with the Joca Tavares, Porteira and Santa Inês intrusions, texturally different from the other carbonatites and probably younger with or without tectonic deformation.

4.5.4. CONSIDERATIONS ABOUT PHOSPHATE MINERALIZATION

Nine percent of carbonatites and alkaline-carbonatite complexes contain active or historic mines, showing the relevance of this type of magmatism in the formation of mineral deposits

(Simandl & Paradis, 2018). The TEC and the other carbonatite intrusions identified in the SRS have P₂O₅ contents above 3%, denoting the potential for occurrence of phosphate deposits. The economic content of phosphate found in metacarbonatites and metaultramafic rocks TEC, form a phosphate deposit with measured mineral resources of 36 Mt @ 4.01% P₂O₅, indicated mineral resources of 47 Mt @ 4.18% P₂O₅ and inferred mineral resources of 21.8 Mt @ 3.67% P₂O₅, using a cut-off grade of 3% P₂O₅ (Aguia Resources Ltd., 2018).

P₂O₅ in TEC comes from apatite. Anzolin *et al.* (2019) defined four types of apatite: a primary one associated with the crystallization of rocks and another three subsequent ones associated with weathering processes. In fresh rock, enrichment in primary apatite is closely associated with the fractionation of this mineral in magma, with higher concentrations in CMC-2, DMC-2 and MUMF-2 facies. Although MUMF-2 concentrates the highest average content of P₂O₅ in TEC, the metaultramafic rocks do not show good metallurgical recovery (Aguia Resources Ltd., 2018).

All carbonatites emplaced in SRS are clearly controlled for deep fault/fracture zones. The shape of these carbonatites is predominantly linear, and they are often magnetic, therefore, one should look not only for circular magnetometric anomalies, as is the case of the Joca Tavares Carbonatite, but also for linear anomalies. Although the average levels of P₂O₅ are not so high, the occurrence of several small carbonatites nearby helps to improve the economy.

4.6. CONCLUSIONS

Available field, petrographic, chemical, mineralogical and isotopic evidence indicates that TEC resulted from the interaction of several different petrogenetic processes, such as fractional crystallization, liquid immiscibility and metasomatism, and was also subjected to metamorphism into greenschist to amphibolite facies and heterogeneous deformation with flow foliation and banding locally preserved. Geochemical patterns and isotopic compositions of ¹³C and ¹⁸O compatible with the primitive mantle signature show that TEC evolved from a metasomatized mantle rich CO₂ source and LREE. The partial melting of this mantle generated silicate carbonate liquid that evolved through at least two processes. By fractional crystallization, ultramafic rocks rich in calcite may have been generated and calcite carbonatites may have been formed from the residual liquid. The immiscibility of liquids

secreted carbonatite magma, from which dolomite metacarbonatite would have crystallized with clusters of ultramafic rock.

TEC ^{13}C and ^{18}O isotopic compositions were identified, similar to those of the Mesoproterozoic carbonatites of the Alkaline Province of Ontario emplaced in Laurentia, which reinforces that Laurentia and the Rio de la Plata Craton were linked to the end of the Mesoproterozoic and that these carbonatites shared probably the same mantle source. When comparing mineralogical and textural features and geochemical signatures between TEC, crystallized in Mesoproterozoic, and Picada dos Tocos carbonatites, dated as Neoproterozoic, and its similar Passo Feio, there is a strong affinity. These rocks' similarities indicate that they had very similar genesis and evolution, although with hundreds of millions of years between their crystallizations. As with other terranes in the world, there seems to have been a recurrence of carbonatitic magmatism in space and time over areas of weakness in the SRS.

Although it is not ruled out that these rocks may have been metamorphosed and deformed still in the Mesoproterozoic, it is observed that these processes were intensely active on these rocks at the Neoproterozoic. Although not common, metamorphosed and deformed carbonatites are found in the world, but it is not yet known how these processes can alter chemical signatures. However, in TEC, some minor and trace elements signatures and REE patterns were preserved, making it possible to make the inferences presented here.

In addition to contributing to the understanding of the geotectonic evolution of the SRS, the TEC also reveals economic importance for phosphate, raising the possibility that new deposits of the type may be found in the other carbonatites emplaced in the SRS, having as its main prospective guide its location along zones of deep fault/fracture.

ACKNOWLEDGEMENTS

The authors would like to thank Aguia Resources Ltd mining company for supporting field work, accessing core samples and for assigning geochemistry, DRX and petrography data, to the Laboratório de Estudos Ambientais e Geodinâmicos from the Instituto de Geociências of the Universidade de Brasília for isotopic analyses and to the Centro de Desenvolvimento Tecnológico (CEDES) of the Serviço Geológico do Brasil-CPRM. We thank Professor Márcio M. Pimentel (*in memorian*) for their contributions and Dr. Rodrigo R. Adôrno for English text formatting.

REFERENCES

- Aguia Resources Ltd. 2013. Key phosphate tenements granted at Três Estradas South and Joca Tavares in southern Brazil. 5p. <http://aguiaresources.com.au/site/wp-content/uploads/20130501.pdf>
- Aguia Resources Ltd. 2014. Annual Report. 74p. http://aguiaresources.com.au/site/wp-content/uploads/11202014_agr_final_full_annual_report_20142.pdf.
- Aguia Resources Ltd. 2016. Aguia signs option agreement on property adjacent Três Estradas and secures new carbonatite occurrence. 3p. <https://www.asx.com.au/asxpdf/20160608/pdf/437rv1w13f05f8.pdf>.
- Aguia Resources Ltd. 2018. Três Estradas Phosphate Project, Rio Grande do Sul, Brazil. Preparado por Millcreek Mining Group. 591p. <http://aguiaresources.com.au/site/wp-content/uploads/Tres-Estradas-JORC-Report-4.11.18.pdf>.
- Anzolin, H.M., Dani, N., Remus, M.V.D., Ribeiro, R.R., Nunes, A.R., Ruppel, K.M.V. 2019. Apatite multi-generations in the Três Estradas Carbonatite, Southern Brazil: physical and chemistry meaning and implications to phosphate ore quality. *Brazilian Journal of Geology*, 49(2): 17p. DOI: 10.1590/2317-4889201920180092.
- Bailey, D.K. 1993. Carbonate magmas: *Journal of the Geological Society*, 150(4):637-651. DOI: 10.1144/gsjgs.150.4.0637.
- Barbosa, E.S.R. 2009. Mineralogia e petrologia do Complexo Carbonatítico-Foscorítico de Salitre – MG. Tese de Doutorado, Universidade de Brasília, Brasília, 432p.
- Barbosa, E.S.R., Brod, J.A., Junqueira-Brod, T.C., Dantas, E.L., Cordeiro, P.F.O., Gomide, C.S. 2012. Bebedourite from its type area (Salitre I complex): a key petrogenetic series in the Late-Cretaceous Alto Paranaíba kamafugite–carbonatite–phoscorite association, Central Brazil. *Lithos*, 144-145:56-72. DOI:10.1016/j.lithos.2012.04.013.
- Barbosa, E.S.R., Brod, J.A., Cordeiro, P.F.O., Junqueira-Brod, T.C., Santos, R.V., Dantas, E.L. 2020. Phoscorites of the Salitre I complex: Origin and petrogenetic implications. *Chemical Geology*, 535-119463. DOI: 10.1016/j.chemgeo.2020.119463.
- Basei, M.A.S., Peel, E., Sánchez Bettucci, L., Preciozzi, F., Nutman, A.P. 2011. The basement of the Punta del Este Terrane (Uruguay): an African Mesoproterozoic fragment at the eastern border of the South American Río de la Plata Craton. *International Journal of Earth Sciences*, 100(2-3):289-304. DOI: 10.1007/s00531-010-0623-1.
- Bell, K., (ed). 1989. Carbonatites: Genesis and Evolution. Chapman & Hall, London, U.K.
- Bell, K., Blenkinsop, J. 1987. Archean depleted mantle: Evidence from Nd and Sr initial isotopic ratios of carbonatites. *Geochimica Cosmochimica Acta*, 51(2):291-298. DOI 10.1016/0016-7037(87)90241-9.
- Bell, K., Keller, J. 1995. Carbonatite Volcanism Oldoinyo Lengai and the Petrogenesis of Natrocarbonatites. IAVCEI Proceedings in Volcanology Series Volume 4. xi + 210 pp. Berlin, Heidelberg, New York, Barcelona, Budapest, Hong Kong, London, Milan, Paris, Tokyo: Springer-Verlag. DOI: 10.1017/S0016756800007913.
- Bell, K., Simonetti, A. 1996. Carbonatite magmatism and plume activity: implications from the Nd, Pb and Sr isotope systematics of Oldoinyo Lengai. *Journal of Petrology*, 37(6):1321-1339. DOI: 10.1093/petrology/37.6.1321.
- Bell, K., Kjarsgaard, B.A., Simonetti, A. 1999. Carbonatites Into the twenty-first century. *Journal of Petrology*, 39(11-12):1839-1845. DOI: 10.1093/petroj/39.11-12.1839.

- Bell, K., Castorina, F., Lavecchia, G., Rosatelli, G., Stoppa F. 2004. Is there a mantle plume below Italy? *EOS, Transactions American Geophysical Union*, 85(50):541-546. DOI: 10.1029/2004EO500002.
- Bossi, J., Campal, N., 1992. Magmatismo y tectónica transcurrente durante el Paleozoico Inferior en Uruguay. In: Gutierrez- Marco, J.G., Saavedra, J., Rabano, I. (Editors): *Paleozoico Inferior de Iberoamérica*. Universidad de Extremadura, Mérida, pp 343- 356.
- Bossi, J., Cingolani, C.A. 2009. Extension and general evolution of the Rio de la Plata Craton. In: Gaucher, C., Sial, A.N., Halverson, G.P., Frimmel, H.E. (Eds.), *Neoproterozoic-Cambrian tectonics, global change and evolution: a focus on southwestern Gondwana. Developments in Precambrian Geology*, 16:73-85. DOI: 10.1016/S0166-2635(09)01604-1.
- Boynton, W.V. 1984. Cosmochemistry of the rare-earth elements: meteorite studies. In: Henderson, P. ed. *Rare-earth Elements Geochemistry*. Amsterdam, Elsevier. p.63-114.
- Brod, J.A. 1999. Petrology and Geochemistry of the Tapira Alkaline Complex, Minas Gerais State, Brazil. PhD Thesis, University of Durham, UK.
- Brod, J.A., Gibson, S.A., Thompson, R.N., Junqueira-Brod, T.C., Seer, H.J., Moraes, L.C., Boaventura, G.R. 2000. Kamafugite affinity of the Tapira alkaline-carbonatite complex (Minas Gerais, Brazil). *Revista Brasileira de Geociências*, 30:404-408.
- Brod, J.A., Ribeiro, C.C., Gaspar, J.C., Junqueira-Brod, T.C., Barbosa, E.S.R., Riffel, B.F., Silva, J.F., Chaban, N., Ferrari, A.L.D. 2004. Excursão 1: Geologia e Mineralizações dos Complexos Alcalino-Carbonatíticos da Província Ígnea do Alto Paranaíba. In: 42 Congresso Brasileiro de Geologia, Guias de Excursões. 1-29. (CD-ROM).
- Brod, J. A., Junqueira-Brod, T.C., Gaspar, J.C., Petrinovic, I.A., Valente, S.C., Corval, A. 2013. Decoupling of paired elements, crossover REE patterns, and mirrored spider diagrams: Fingerprinting liquid immiscibility in the Tapira alkaline-carbonatite complex, SE Brazil. *Journal of South American Earth Sciences*, 41:41-56. DOI: 10.1016/j.jsames.2012.04.013.
- Brooker, R.A. 1995. Carbonatite genesis: the role of liquid immiscibility to 25 kb. PhD thesis, University of Manchester, Manchester.
- Brooker, R.A. 1998. The effect of CO₂ saturation on immiscibility between silicate and carbonate liquids: an experimental study. *Journal of Petrology*, 39(11-12):1905-1915. DOI: 10.1093/petroj/39.11-12.1905.
- Camozzato, E., Philipp, R.P., Chemale Jr., F. 2013. Idades estaterianas e calimianas no domo da Vigia: Complexos Vigia e Porongos, metagranito Seival e anfibolito Tupi Silveira, Bagé, RS. In: XIV Simpósio Nacional de Estudos Tectônicos, Cuiabá, Sociedade Brasileira de Geologia, CD ROM, 1 p.
- Cerva-Alves, T., Remus, M.V.D., Dani N., Basei, M.A.S. 2017. Integrated field, mineralogical and geochemical characteristics of Caçapava do Sul alvikite and beforsite intrusions: A new Ediacaran carbonatite complex in southernmost Brazil. *Ore Geology Reviews*, 88:352-369. DOI: 10.1016/j.oregeorev.2017.05.017.
- Chakhmouradian, A.R., 2006. High-field-strength elements in carbonatitic rocks: geochemistry, crystal chemistry and significance for constraining the sources of carbonatites. *Chemical Geology*, 235:138-160. DOI: 10.1016/j.chemgeo.2006.06.008.
- Chemale Jr., F. 2000. Evolução Geológica do Escudo Sul-rio-grandense. In: Holz, M. De Ros, L.F. (eds). *Geologia do Rio Grande do Sul*. Porto Alegre, CIGO/UFRGS. pp. 13-52.
- Chemale Jr., F., Philipp, R.P., Dussin, I., Formoso, M.L., Kawashita, K., Bertotti, A.L. 2011. Lu-Hf and U-Pb age determination of the Capivarita Anorthosite, Dom Feliciano belt, RS, Brazil. *Precambrian Research*, 186(1-4):117-126. DOI: 10.1016/j.precamres.2011.01.005.

- Comin-Chiaromonti, P., Cundari, A., Piccirillo, E.M., Gomes, C.B., Castorina, F., Censi, P., De Min, A., Marzoli, A., Speziale, S., Velazquez, V.F. 1997. Potassic and sodic igneous rocks from Eastern Paraguay: their origin from the lithospheric mantle and genetic relationships with the associated Paraná flood tholeiites. *Journal of Petrology*, 38:495–528. DOI: 10.1093/petroj/38.4.495.
- Deines, P. 1989. Stable isotope variations in carbonatites. In: Bell, K. (ed.). *Carbonatites: Genesis and Evolution*. Chapman & Hall, London, U.K. p.301-359.
- Demény, A., Sitnikova, M.A., Karchevsky, P.I. 2004. Stable C and O isotope compositions of carbonatite complexes of the Kola Alkaline Province: phoscorite-carbonatite relationships and source compositions. In: Wall, F., Zaitsev A.N, (eds). *Phoscorites and Carbonatites from Mantle to Mine: the Key Example of the Kola Alkaline Province*. Mineralogical Society Series nº 10, p.407-431.
- Downes, H., Wall, F., Demény, A., Szabo, C. 2012. Continuing the carbonatite controversy: preface. *Mineralogical Magazine*, 76(2):255-257. DOI: 10.1180/minmag.2012.076.2.01.
- Dunworth, E.A., Bell, K. 2001. The Turiy massif, Kola Peninsula, Russia: Isotopic and geochemical evidence for multi-source evolution. *Journal of Petrology*, 42(2):377-405. DOI: 10.1093/petrology/42.2.377.
- Eggler, D.H. 1989. Carbonatites, primary melts, and mantle dynamics. In: Bell, K. (ed.). *Carbonatites: Genesis and Evolution*. Chapman & Hall, London, U.K. p.561-579.
- Elliott, H.A.L., Wall, F., Chakhmouradian, A.R., Siegfried, P.R., Dahlgren, S., Weatherley, S., Finch, A.A., Marks, M.A.W., Dowman, E., Deady, E. 2018. Fenites associated with carbonatite complexes: A review. *Ore Geology Reviews*, 93:38-59. DOI: 10.1016/j.oregeorev.2017.12.003.
- Fragoso-César, A.R.S. 1991. Tectônica de Placas no Ciclo Brasiliano: as orogenias dos cinturões Dom Feliciano e Ribeira no Rio Grande do Sul. Unpublished PhD Thesis, IGC-USP, São Paulo, 367 pp.
- Gaucher, C., Frei, R., Chemale Jr., F., Bossi, J., Martínez, G., Chiglino, L., Cernuschi, F. 2011. Mesoproterozoic evolution of the Río de la Plata Craton in Uruguay: at the heart of Rodinia? *International Journal of Earth Sciences*, 100(2):273-288. DOI: 10.1007/s00531-010-0562-x.
- Girelli, T.J., Chemale Jr., F., Lavina, E.L.C., Laux, J.H., Bongiolo, E.M., Lana, C. 2018. Granulite accretion to Rio de la Plata Craton, based on zircon U-Pb-Hf isotopes: Tectonic implications for Columbia Supercontinent reconstruction. *Gondwana Research*, 56:105-118. DOI: 10.1016/j.gr.2017.12.010.
- Gittins, J., Harmer, R. 1997. What is ferrocarbonatite? A revised classification. *Journal of African Earth Sciences*, 25(1):159-168. DOI: 10.1016/S0899-5362(97)00068-7.
- Grazia, C.A.; Toniolo, J.A.; Parisi, G.N.; Muller, E.I.; Dressler, V.L. 2011. Prospecção hidrogeoquímica no carbonatito Três Estradas, RS. In: XIII Congr. Bras. Geoq. e III Simp. Geoq. Países do Mercosul. Gramado, RS. p.1769-1772.
- Guzmics, T., Zajacz, Z., Mitchell, R.H., Szabó, C., Wälle, M. 2015. The role of liquid–liquid immiscibility and crystal fractionation in the genesis of carbonatite magmas: insights from Kerimasi melt inclusions. *Contributions to Mineralogy and Petrology*, 169:17. DOI: 10.1007/s00410-014-1093-4.
- Halama, R., Vennemann, T., Siebel, W., Markl, G. 2005. The Gronnedal-Ika carbonatite-syenite complex, South Greenland: carbonatite formation by liquid immiscibility. *Journal of Petrology*, 46(1):191-217. DOI: 10.1093/petroj/egh069.
- Hammouda, T., Keshav, S., 2015. Melting in the mantle in presence of carbon; review of experiments and discussion on the origin of carbonatites. *Chemical Geology*, 418:171-188. DOI: 10.1016/j.chemgeo.2015.05.018.
- Harmer, R.E., Gittins, J. 1998. The case for primary, mantled-derived carbonatite magma. *Journal of Petrology*, 39(11-12):1895-1903. DOI: 10.1093/petroj/39.11-12.1895.

- Hartmann, L.A. 1987. Isócrona Sm-Nd de 2,1 Ga em minerais de duas amostras do Complexo Granulítico Santa Maria Chico, RS. In: Anais of I Congresso Brasileiro de Geoquímica, Porto Alegre, pp. 105-111.
- Hartmann, L.A. 1998. Deepest exposed crust of Brazil – Geochemistry of Paleo-proterozoic depleted Santa Maria Chico granulites. *Gondwana Research*, 1(3-4):331-341. DOI: 10.1016/S1342-937X(05)70849-2.
- Hartmann, L.A., Leite, J.A.D., Silva, L.C., Remus, M.V.D. Advances in SHRIMP geochronology and their impact on understanding the tectonic and metallogenic evolution of southern Brazil. *Australian Journal of Earth Sciences*, 47(5):829-844. DOI: 10.1046/j.1440-0952.2000.00815.x.
- Hartmann, L.A., Chemale Jr., F., Philipp R.P. 2007. Evolução geotectônica do Rio Grande do Sul no Pré-Cambriano. In: 50 Anos de geologia no Rio Grande do Sul. Editora Comunicação e Identidade, Porto Alegre, 97-123p.
- Hartmann, L. A., Liu, D., Wang, Y., Massonne, H. J., & Santos, J. O. S. 2008. Protolith age of Santa Maria Chico granulites dated on zircons from an associated amphibolite-facies granodiorite in southernmost Brazil. *Anais da Academia Brasileira de Ciências*, 80(3):543-551. DOI: 10.1590/S0001-37652008000300014.
- Hartmann, L. A., Werle, M., Michelin, C.R.L., Lana, C., Queiroga, G.N., Castro, M.P., Arena, K.R. 2019. Proto-Adamastor ocean crust (920 Ma) described in Brasiliano Orogen from coextensive zircon and tourmaline. *Geoscience Frontiers*, 10(4):1623-1633. DOI: 10.1016/j.gsf.2018.09.018.
- Keller, J., Hoefs, J. 1995. Stable isotope characteristics of recent natrocarbonatites from Oldoinyo Lengai. In: Bell, K., Keller, J. (eds). Carbonatite volcanism: Oldoinyo Lengai and the petrogenesis of natrocarbonatites. Springer, Berlin, p.113-123.
- Kjarsgaard, B.A., Hamilton, D. L. 1989a: The genesis of carbonatites by immiscibility. In: Bell, K. (ed.). Carbonatites: Genesis and Evolution. Chapman & Hall, London, U.K. p.388-404.
- Kjarsgaard, B.A., Hamilton, D.L. 1989b. Carbonatite origin and diversity. *Nature* 338:547-548. DOI: 10.1038/338547d0.
- Lastochkin, E.I., Ripp, G.S., Doroshkevich, A.G. 2011. Mineralogy of Metamorphosed Carbonatite of the Vesely Occurrence, Northern Transbaikal Region, Russia. *Geology Ore of Deposits*, 53(3):236-247. DOI: 10.1134/S107570151102005X.
- Le Bas, M.J. 1989. Diversification of carbonatite. In: Bell, K. (ed.). Carbonatites: Genesis and Evolution. Chapman & Hall, London, U.K. p.428-447.
- Le Bas, M.J., 2008. Fenites associated with carbonatites. *The Canadian Mineralogist*, 46(4):915-932. DOI: 10.3749/canmin.46.4.915.
- Lee, W.J., Wyllie, P.J. 1994. Experimental data bearing on liquid immiscibility, crystal fractionation, and the origin of calciocarbonatites and natrocarbonatites. *International Geology Review*, 36(9):797-819. DOI: 10.1080/00206819409465489.
- Lee, W.J., Wyllie, P.J. 1997. Liquid Immiscibility in the Join NaAlSiO₄-NaAlSi₃O₈-CaCO₃ at 1 GPa: Implications for Crustal Carbonatites. *Journal of Petrology*, 38(9):1113-1135. DOI: 10.1093/petroj/38.9.1113.
- Lee, W.J., Wyllie, P.J. 1998. Petrogenesis of carbonatite magmas from mantle to crust, constrained by the system CaO-(MgO+FeO*)(Na₂O+K₂O)-(SiO₂+Al₂O₃+TiO₂)-CO₂. *Journal of Petrology* 39(3):495-517. DOI: 10.1093/petroj/39.3.495.
- Lee, W.J., Fanelli, M.F., Cava, N., Wyllie, P.J. 2000. Calciocarbonatite and magnesiocarbonatite rocks and magmas represented in the system CaO-MgO-CO₂-H₂O at 0.2 GPa. *Mineralogy and Petrology*, 68:225-256. DOI: 10.1007/s007100050011.

- Li, Z.X., Bogdanova, S.V., Collins, A.S., Davidson, A. De Waele, B., Ernst, R.E., Fitzimons, I.C.W., Fuck, R.A., Gladkochum, D.P., Jacobs, J., Karlstrom, K.E., Lu, S., Natapov, L.M., Pease, V., Pisarevsky, S.A., Thrane, K., Vernikovsky, V. 2008. Assembly, configuration, and break-up history of Rodinia: a synthesis. *Precambrian Research*, 160(1-2):179-210. DOI: 10.1016/j.precamres.2007.04.021.
- Lopes, C.G. 2014. Análises de U-Pb por LA-ICP-MS e SHRIMP em zircões detriticos do Complexo Passo Feio, Terreno São Gabriel: implicações geotectônicas para a evolução do Cinturão Dom Feliciano. Dissertação de mestrado, Universidade Federal do Rio Grande do Sul, Porto Alegre, 51p.
- Martinez, G.A. 2019. Caracterização petrográfica e geoquímica das rochas glimeríticas do complexo alcalino-carbonatítico Três Estradas, Lavras do Sul, RS. Trabalho de Conclusão de Curso de Graduação em Geologia - Universidade Federal do Rio Grande do Sul, Porto Alegre, 73p.
- Mitchell, R.H., 2005. Carbonatites and carbonatites and carbonatites. *Canadian Mineralogist*, 43(6):2049-2068. DOI: 10.2113/gscanmin.43.6.2049.
- Monteiro, C.F., Toniolo, J.A., Bastos Abram M. 2016. Carbonatitos associados ao Escudo Sul-Riograndense, Rio Grande do Sul. In: Bastos Abram M. Projeto Fosfato Brasil – Parte II, CPRM, Salvador.
- Monteiro, C.F., Oliveira, I.L. de, Brod, J.A., Dantas, E.L., Ganade de Araujo, C.E., Zacchi, E.N.P., Fuck, R.A. Unpublished. Nd-Sr-Hf isotopes and U-Pb ages of Mesoproterozoic Três Estradas Alkaline-Carbonatite Complex, Brazil: implications for Sul-Riograndense shield evolution and Rodinia Break-up.
- Moecher, D.P., Anderson, E.D., Cook, C.A., Mezger, K. 1997. The petrogenesis of metamorphosed carbonatites in the Grenville Province, Ontario. *Canadian Journal of Earth Sciences*, 34(9):1185-1201. DOI: 10.1139/e17-095.
- Morales, B.A.A., Almeida, D.P.M., Koester, E., Rocha, A.M.R., Dorneles, N.T., Rosa, M.B., Martins, A.A. 2019. Mineralogy, whole-rock geochemistry and C, O isotopes from Passo Feio Carbonatite, Sul-Riograndense Shield, Brazil. *Journal of South American Earth Sciences*, 94:102-208. DOI: 10.1016/j.jsames.2019.05.024.
- Novella, D., Keshav, S., Gudfinnsson, G.H., Ghosh, S., 2014. Melting phase relations of model carbonated peridotite from 2 to 3GPa in the system CaO-MgO-Al₂O₃-SiO₂-CO₂ and further indication of possible unmixing between carbonatite and silicate liquids. *Journal of Geophysical Research: Solid Earth*, 119(4):2780-2800. DOI: 10.1002/2013JB010913.
- Parisi, G.N., Toniolo, J.A., Grazia, C.A., Pinto, L.G. 2010. Prospecção de fosfato no Rio Grande do Sul. In: Anais of 45º Congresso Brasileiro de Geologia, Belém.
- Pell, J., Hoy, T. 1989. Carbonatites in a Continental Margin Environment – the Canadian Cordillera. In: Bell, K. (ed.). *Carbonatites: Genesis and Evolution*. Chapman & Hall, London, U.K. p. 200–217.
- Philipp, R.P., Pimentel, M.M., Chemale Jr., F. 2016. Tectonic evolution of the Dom Feliciano belt in Southern Brazil: geological relationships and U-Pb geochronology. *Brazilian Journal of Geology*, 46(1):83-104. DOI: 10.1590/2317-4889201620150016.
- Podborodnikov, I.V., Shatskiy, A., Arefiev, A.V., Litasov, K.D. 2019. Phase relations in the system Na₂CO₃-CaCO₃-MgCO₃ at 3 GPa with implications for carbonatite genesis and evolution. *Lithos*, 330-331:74-89. DOI: 10.1016/j.lithos.2019.01.035.
- Potter, N.J., Kamenetsky, V.S., Simonetti, A., Goemann, K. 2017. Different types of liquid immiscibility in carbonatite magmas: A case study of the Oldoinyo Lengai 1993 lava and melt inclusions. *Chemical Geology*, 455:376-384. DOI: 10.1016/j.chemgeo.2016.09.034.
- Ramgrab, G.E., Wildner, W., Lopes, R.C., Favilla, C.A.C., Silva, M.A.S., Sachs, L.L.B., Silva, V.A., Batista, I.H. 2004. Folha SH.22-Porto Alegre. In: Schobbenhaus, C., Gonçalves, J.H., Santos,

- J.O.S., Abram, M.B., Leão Neto, R., Matos, G.M.M., Vidotti, R.M, Ramos, M.A.B., Jesus, J.D.A. de. (eds.). Carta Geológica do Brasil ao Milionésimo, Sistema de Informações Geográficas. Programa Geologia do Brasil. CPRM, Brasília. CD-ROM.
- Ray, J.S., Pande, K., Bhutani, R., Shukla, A.D., Rai V.K., Kumar, A., Awasthi, N., Smitha, R.S., Panda, D.K. 2013. Age and geochemistry of the Newania dolomite carbonatites, India: implications for the source of primary carbonatite magma. *Contributions to Mineralogy and Petrology*, 166:1613-1632. DOI 10.1007/s00410-013-0945-7.
- Remus, M.V.D., Hartmann, L.A., McNaughton, N.J., Groves, D.I., Fletcher, I.R. 2000. The link between hydrothermal epigenetic copper mineralization and the Caçapava Granite of the Brasiliano Cycle in Southern Brazil. *Journal of South American Earth Sciences*, 13(3):191-216. DOI: 10.1016/S0895-9811(00)00017-1.
- Ribeiro, M., Teixeira, C.A.S. 1970. Datações de rochas do Rio Grande do Sul e sua influência nos conceitos estratigráficos e geotectônicos locais. *Iheringia, Série Geologia* 3:109-120.
- Ribeiro, M. 1980. Geossuturas do Escudo do Rio Grande do Sul. In: Anais do 31º Congresso Brasileiro de Geologia, Balneário Camboriú.
- Rocha, A.M.R., Dorneles, N.T., Gindri, M.D., Vargas, J.M., Alves, T.C., Benetti F.A. 2013. Descoberta dos carbonatitos Picada dos Tocos e Passo Feio e o potencial para fosfato e ETR's, Caçapava do Sul, Rio Grande do Sul. In: Anais do III Simpósio Brasileiro de Metalogenia, Gramado.
- Roden, M.F., Murthy, V.R. 1985. Mantle Metasomatism. *Annual Review of Earth and Planetary Sciences*, 13:269-296. DOI: 10.1146/annurev.ea.13.050185.001413.
- Senhorinho, E.M., Remus, M.V.D., Dani, N., Ruppel, K. 2016. Características da alteração propilítica das rochas encaixantes do Carbonatito Três Estradas – Lavras do Sul, RS. In: Anais of 48º Congresso Brasileiro de Geologia, Porto Alegre.
- Silva A.B.; Liberal G.S.; Issa Filho A.; Rodrigues C.S.; Riffel B.F. 1987. Depósito de fosfato em carbonatito pré-cambriano Angico dos Dias- BA. Sociedade Brasileira de Geologia, Núcleo da Bahia, Salvador, 15 p. (inédito).
- Silva, M.A.S., Favilla, C.A.C., Wildner, W., Ramgrab, G.E., Lopes, R.C., Sachs, L.L.B., Silva, V.A., Batista, I.H. 2004. Folha SH.21-Uruguaiana. In: Schobbenhaus, C., Gonçalves, J.H., Santos, J.O.S., Abram, M.B., Leão Neto, R., Matos, G.M.M., Vidotti, R.M, Ramos, M.A.B., Jesus, J.D.A. de. (eds.). Carta Geológica do Brasil ao Milionésimo, Sistema de Informações Geográficas. Programa Geologia do Brasil. CPRM, Brasília. CD-ROM.
- Simandl, G.J., Paradis, S. 2018. Carbonatites: related ore deposits, resources, footprint, and exploration methods. *Applied Earth Science*, 127(4):123-152. DOI: 10.1080/25726838.2018.1516935.
- Taylor, H.P. Jr., Frechen, J., Degens, E.T. 1967. Oxygen and carbon isotope studies of carbonatites from the Laacher See District, West Germany and the Alno District Sweden. *Geochimica et Cosmochimica Acta*, 31(3):407-430. DOI: 10.1016/0016-7037(67)90051-8.
- Thompson, R.N., Morrison, M.A., Hendry, G.L., Parry, S.J., Simpson, P.R., Hutchison, R., O'Hara, M.J. 1984. An assessment of the relative roles of crust and mantle in magma genesis: an elemental approach [and discussion]. *Philosophical Transactions of the Royal Society of London. Series A, Mathematical and Physical Sciences*, 310(1514):549-590. DOI: 10.1098/rsta.1984.0008.
- Thompson, R., Smith, P., Gibson, S., Mattey, D., Dickin, A. 2002. Ankerite carbonatite from Swartbooisdrif, Namibia: the first evidence for magmatic ferrocarbonatite. *Contributions to Mineralogy and Petrology*, 143:377-396. DOI: 10.1007/s00410-002-0350-0.
- Toniolo, J.A., Gil, C.A.A., Sander, A. 2007. Metalogenia das bacias neoproterozoicas-eopaleozoicas do Sul do Brasil: Bacia do Camaquã. CPRM, Porto Alegre, 154p.
- Toniolo, J.A., Parisi, G.N., Grazia, C.A., Reischl, J.L. 2010. Prospecção de fosfato na região de Três Estradas, Lavras do Sul, RS. In: IV Simpósio de Exploração Mineral, Ouro Preto.

- Toyoda, K., Horiuchi, H., Tokonami, M. 1994. Dupal anomaly of Brazilian carbonatites - geochemical correlations with hotspots in the South-Atlantic and implications for the mantle source. *Earth and Planetary Science Letters*, 126(4):315-331. DOI: 10.1016/0012-821X(94)90115-5.
- Veksler, I.V., Nielsen, T.F.D., Sokolov, S.V., 1998. Mineralogy of crystallized melt inclusions from Gardiner and Kovdor ultramafic alkaline complexes: implications for carbonatite genesis. *Journal of Petrology*, 39:2015-2031. <https://doi.org/10.1093/petroj/39.11-12.2015>.
- White, B.S., Wyllie, P.J. 1992. Solidus reactions in synthetic lherzolite-H₂O-CO₂ from 20–30 kbar, with applications to melting and metasomatism. *Journal of Volcanology and Geothermal Research*, 50(1-2):117-130. DOI: 10.1016/0377-0273(92)90040-K.
- Woolley, A.R., Bailey, D.K. 2012. The crucial role of lithospheric structure in the generation and release of carbonatites: geological evidence. *Mineralogical Magazine*, 76(2):259-270. DOI: 10.1180/minmag.2012.076.2.02.
- Wyllie, P.J., Lee, W.J. 1998. Model system controls on conditions for formation of magnesiocarbonatite and calciocarbonatite magmas from the mantle. *Journal of Petrology*, 39(11-12):1885-1893.

5. Nd-Sr-Hf ISOTOPES AND U-Pb AGES OF MESOPROTEROZOIC TRÊS ESTRADAS ALKALINE-CARBONATITE COMPLEX, BRAZIL: IMPLICATIONS FOR SUL-RIOGRANDENSE SHIELD EVOLUTION AND RODINIA BREAK-UP

Cimara Francisca Monteiro^{a,b}, Ítalo Lopes de Oliveira^a, José Affonso Brod^{a,c}, Elton Luiz Dantas^a, Carlos Eduardo Ganade de Araujo^d, Érico Natal Pedro Zacchi^a, Reinhardt Adolfo Fuck^a

^a Universidade de Brasília, Instituto de Geociências, Campus Darcy Ribeiro, Asa Norte, Brasília, DF. Brazil, Postal Code: 70.910-900.

^b Serviço Geológico do Brasil (SGB-CPRM), Centro de Desenvolvimento Tecnológico (CEDES), Setor Bancário Norte, Brasília, DF, Brazil. Postal Code: 70.040-904.

^c Universidade Federal de Goiás, Faculdade de Ciências e Tecnologia, Campus Aparecida de Goiânia, Setor Conde dos Arcos, Aparecida de Goiânia, GO, Brazil. Postal Code: 74.968-755

^d Serviço Geológico do Brasil (SGB-CPRM), Centro de Desenvolvimento Tecnológico (CEDES), Rio de Janeiro, RJ, Brazil. Postal Code: 22.290-255.

Corresponding author: cimara.monteiro@cprm.gov.br

ABSTRACT

The first occurrence of Mesoproterozoic carbonatite in the Rio de la Plata Craton - RDPC indicates extensional event prior to the opening of the Charrua Ocean. Nd-Sr-Hf Isotopic and U-Pb on zircon geochronological data are presented for the Três Estradas Alkaline-Carbonatite Complex - TEC, located in southernmost Brazil. The complex consists predominantly of ultramafic rocks, carbonatites and, subordinate, deformed fenitized syenites metamorphosed under greenschist to amphibolite facies conditions. U-Pb ages between $1,110 \pm 4.8$ Ma and $1,123 \pm 15$ Ma, respectively derived from a dolomite metacarbonatite and an associated metasyenite, constrain the TEC emplacement timing. The Nd-Sr-Hf isotopic signatures indicate that the TEC rocks were derived from a heterogeneous mantle, isotopically depleted in Sm-Nd and slightly depleted to enriched in Rb-Sr, with little influence of ancient crust and that these rocks are derived from the same source of parental magma probably submitted to

intense metasomatism. The Nd-Sr isotopic signatures and crystallization ages of the TEC allow correlating it to the carbonatitic intrusions of the Alkaline provinces of Ontario and Grenville, Canada, in Laurentia, associated with the Keweenawan magmatic event (1.11-1.09 Ga), to which extension efforts would be related causing ruptures in RDPC edge and Laurentia, probably juxtaposed in that time interval. According to paleogeographic reconstructions of Rodinia, the Kalahari Craton would only have joined Laurentia and the RDPC at 1,050 Ma. Around 920 Ma there is the generation of an oceanic crust in the Rio de la Plata Craton with the installation of the Charrua Ocean and the beginning of the formation of the Dom Feliciano Belt, concluded at 540 Ma, with peak deformation and metamorphism at 650-630 Ma.

Keywords: Três Estradas, carbonatite, Sul-Riograndense Shield, Rio de la Plata Craton, Rodinia.

5.1. INTRODUCTION

During the 1960s, with the discovery of the active Oldoinyo Lengai carbonatite volcano, Tanzania (Dawson, 1962), carbonatites started to be firmly recognized as derived from magmatic sources. Experimental evidence has demonstrated that carbonatites can be generated by a variety of processes, involving both primary carbonatitic magmas and products derived by either fractional crystallization or liquid immiscibility from carbonated silicate magmas (Bell *et al.*, 1999, 2004; Bell, 2001), characterizing, therefore, a group of rocks with multiple origins (Mitchell, 2005). Despite a large number of carbonatites worldwide (527 in Woolley & Kjarsgaard, 2008), only about 30 of the currently known occurrences are Mesoproterozoic in age (Oliveira *et al.*, 1975; Drüppel *et al.*, 2006; Woolley & Kjarsgaard, 2008; Yang *et al.*, 2011; Ray *et al.*, 2013; Ashwal *et al.*, 2016; Downes *et al.*, 2016; Rossoni *et al.*, 2017; Simon *et al.*, 2017; Ranta *et al.*, 2018).

Alkaline rocks and carbonatites (ARC's) occur in several geological environments over time, preferably in stable intra-plate cratonic areas and in the early stages of divergent margin evolution (i.e., continental rifting) (Bailey, 1974; Wooley, 1989; Bell *et al.*, 1999). On the other hand, deformed alkaline rocks and carbonatites (DARC's), which form a small subset of ARC's (<10%), are often related to complex evolution in collisional environments (Burke *et al.*, 2003; 2008; Burke & Khan, 2006; Attoh *et al.*, 2007; Ashwal *et al.*, 2016).

Bailey (1974) and Woolley & Bailey (2012) emphasized the recurrence of carbonatite magmatism in space and time, using old weakness zones and other lineaments, as noted in Malawi, Greenland, Ontario, SW Quebec, and Northern Europe (Kola Peninsula) (Woolley & Bailey, 2012). Burke *et al.* (2003) noted the same pattern concerning DARC's associated with suture zones and raise the hypothesis that ARC's are indicative of a lithospheric extension episode whereas DARC's record the deformational event. This implies the possibility to date the beginning and the end of a Wilson Cycle (Burke & Khan, 2006) and use DARC's to map old collisional zones as well. However, Attoh *et al.* (2007) demonstrated, based on geochronological studies of DARC's in the Pan African suture zone of the Dahomeyide Orogen, West Africa, that these rocks cannot always be used to constrain the beginning of a Wilson Cycle, as DARC's are not necessarily related to earlier intrusions associated with rifting of the lithosphere.

Syn-tectonic carbonatites, including DARC's, are placed in the Earth's crust during the evolution of mobile belts (Lapin *et al.*, 1999). Syn-tectonic carbonatites stand out for their linear morphology, emplaced along deep fault zones, and, in general, extend to tens of kilometers, sometimes reaching more than 100 km (Levin *et al.*, 1978). An example of syn-tectonic carbonatite in South America was reported by Lapin *et al.* (1999) for the Paleoproterozoic carbonatite complex of Angico dos Dias, NE Brazil. Other examples cited by the authors are the Chernigov and Tatarskaya carbonatites, both in Russia.

In this article, we report the first whole-rock Nd and Sr isotopic data, U-Pb zircon geochronology, and Lu-Hf isotopes on zircon for a deformed alkaline-carbonatite complex that occurs in southern Brazil, metamorphosed under greenschist to amphibolite facies conditions. Due to its geological uniqueness, the occurrence of the Três Estradas Alkaline-Carbonatite Complex (TEC) allows inferring geotectonic conditions for understanding the evolution of the Sul-Riograndense shield in the context of the South American Platform. Our field relations data suggest that TEC is emplaced in an extensional tectonic environment prior to the formation of the Charrua Ocean in the Rio de la Plata Craton, by the end of the Mesoproterozoic.

5.2. GEOLOGICAL SETTINGS

The TEC is situated in the southern portion of the Dom Feliciano Belt, a Neoproterozoic orogen (Hartmann *et al.*, 2007, 2008; Philipp *et al.*, 2016, 2018; Toni *et al.*, 2020), more

precisely in the Taquarembó Terrane, a remnant of the Archean to the Paleoproterozoic basement of the Rio de la Plata Craton (Chemale Jr., 2000; Girelli *et al.*, 2018). This terrane is located in the southwestern Sul-Riograndense Shield (SRS) and represents the northward extension of the Nico Pérez Terrane of central Uruguay (e.g. Bossi & Campal, 1992; Bossi & Cingolani, 2009). The TEC intrudes basic to acid gneisses that are assigned to the Santa Maria-Chico Granulitic Complex, considered the main geological unit of the SRS.

Hartmann *et al.* (2007, 2008) individualized the main SRS units, based on rock associations, tectonic features, geochemical and isotopic signatures, and aerial geophysics. While the Taquarembó Terrane represents part of the reworked Rio de la Plata Craton (Nardi & Hartmann, 1979), the São Gabriel and Tijucas terranes and Pelotas Batholith are allochthonous Neoproterozoic units (**Figure 5.1**). Archean tectonic fragments are found in the Taquarembó Terrane as protolith of the Santa Maria-Chico Granulitic Complex in addition to a set of ortho- and paragneisses metamorphosed under amphibolite facies conditions, generated in an orogenic environment (Chemale Jr., 2000).

Hartmann *et al.* (2008) obtained metamorphic U-Pb ages on zircon of $2,035 \pm 9$ Ma and $2,006 \pm 3$ Ma in granodioritic gneiss and granulite from the Santa Maria-Chico Granulite Complex, respectively, which are in agreement with the U-Pb ages on zircon of $2,022 \pm 18$ Ma and $2,031 \pm 40$ Ma reported by Hartmann (1987) for basic and intermediate granulites, respectively. The U-Pb ages on zircon obtained in protoliths from rocks dated by Hartmann *et al.* (2008) were $2,366 \pm 8$ Ma for the gneiss protolith and $2,489 \pm 6$ Ma for the granulite protolith, slightly less than the interval ($>2,510$ - $2,555$ Ma) of Sm-Nd ages obtained by Hartmann (1987). More recently, Girelli *et al.* (2018) reported comparable, early Paleoproterozoic U-Pb ages on zircon for the Santa Maria-Chico protoliths.

Tectonically juxtaposed to the Taquarembó Terrane along the Ibaré Lineament, is the São Gabriel Terrane. This terrane was formed mainly by Neoproterozoic juvenile accretion, with lithotectonic associations of passive margin and retro-arc environments, ophiolites, and magmatic arcs made up of volcano-sedimentary successions and plutonic rocks (Babinski *et al.*, 1996; Hartmann *et al.*, 2007, 2008; de Lena *et al.*, 2014; Hartmann *et al.*, 2019; Cerva-Alves *et al.*, 2020).

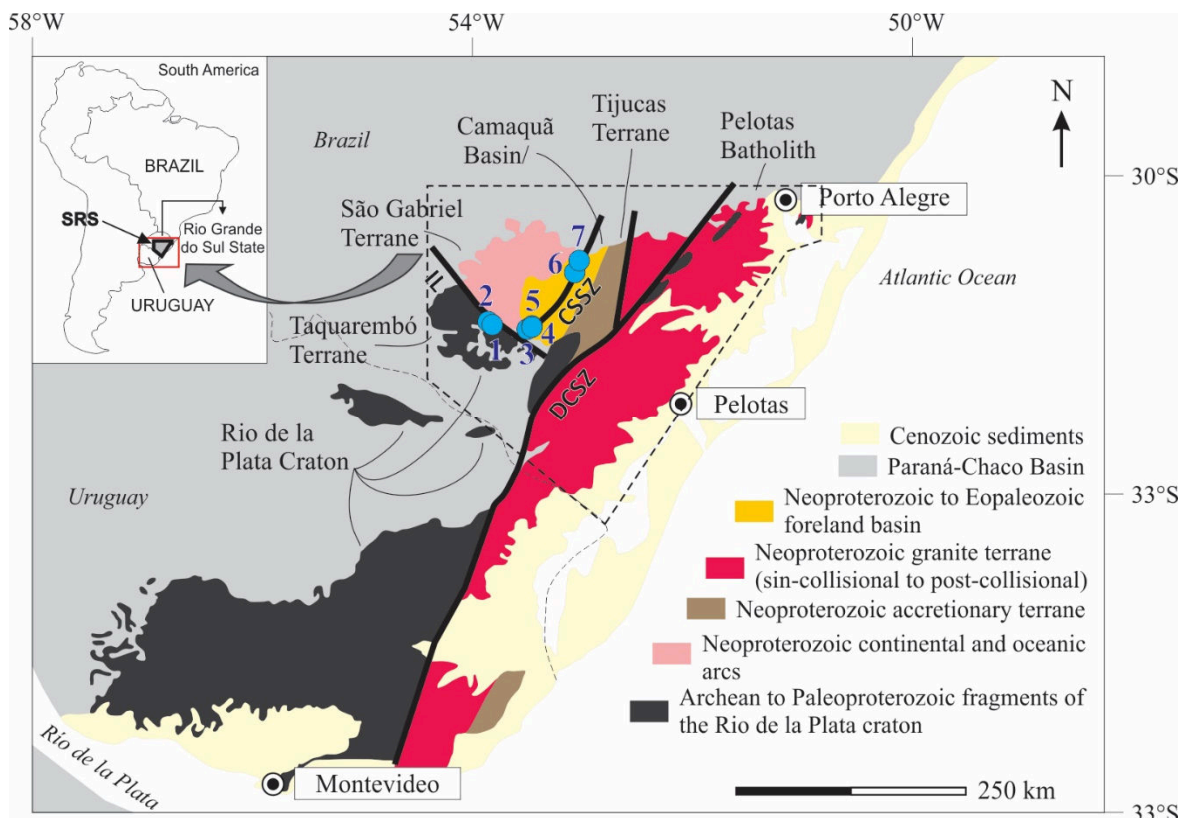


Figure 5.1 - Geological map of the main units of the SRS (dashed boundary), Brazil and Uruguay, showing the locations of carbonatites discovered in southern Brazil (modified from Hartmann *et al.*, 2007). Carbonatite: 1 – Três Estradas; 2 – Santa Clara; 3 – Porteira; 4 – Joca Tavares; 5 – Santa Inês; 6 – Passo Feio; e, 7 – Picada dos Tocos (also called by Aguiar Resources Ltd, holder of the mining right, as Mato Grande Carbonatite). IL – Ibaré Lineament; CSSZ – Caçapava do Sul Shear Zone; DCSZ – Dorsal de Canguçu Shear Zone.

5.2.1. CARBONATITES OF THE SUL-RIOGRANDENSE SHIELD

In total, seven carbonatites are known in the SRS as a result of recent mapping and mineral exploration projects, including the TEC (Toniolo *et al.*, 2010) (**Figure 5.2**). The Santa Clara, Passo Feio and Picada dos Tocos carbonatites share geochemical signatures, petrological associations and structural features with the TEC, but for the Santa Clara carbonatite, data are yet to be published. The Passo Feio and Picada dos Tocos carbonatites intrude the Passo Feio Complex, which has a minimum age of 803 Ma determined by Lopes (2014). This complex borders on the syn-tectonic Caçapava do Sul Granite showing a U-Pb age on zircon of 561 ± 6 Ma according to Leite *et al.* (1998), which is coincident with the U-Pb age of 562 ± 8 Ma obtained by Remus *et al.* (2000). Both Passo Feio and Picada dos Tocos carbonatites are in the geological context of the Neoproterozoic São Gabriel Terrane, while the Santa Clara carbonatite intrudes the same Paleoproterozoic rocks as TEC. The Picada dos Tocos (Rocha *et al.*, 2013; Cerva-Alves, 2017; Cerva-Alves *et al.*, 2017) and Passo Feio (Rocha *et al.*, 2013;

Cerva-Alves, 2017; Cerva-Alves *et al.*, 2017; Morales *et al.*, 2019) are composed of pink-colored calcite carbonatite, followed by late-stage white dolomite carbonatite, both occurring as deformed tabular bodies concordant with the schistosity and folds of the hosting rocks. Cerva-Alves *et al.* (2017) obtained a U-Pb zircon crystallization age of 603.2 ± 4.5 Ma for the Picada dos Tocos carbonatite, placing it in the context of a post-collisional environment of dominant transpressive tectonism.

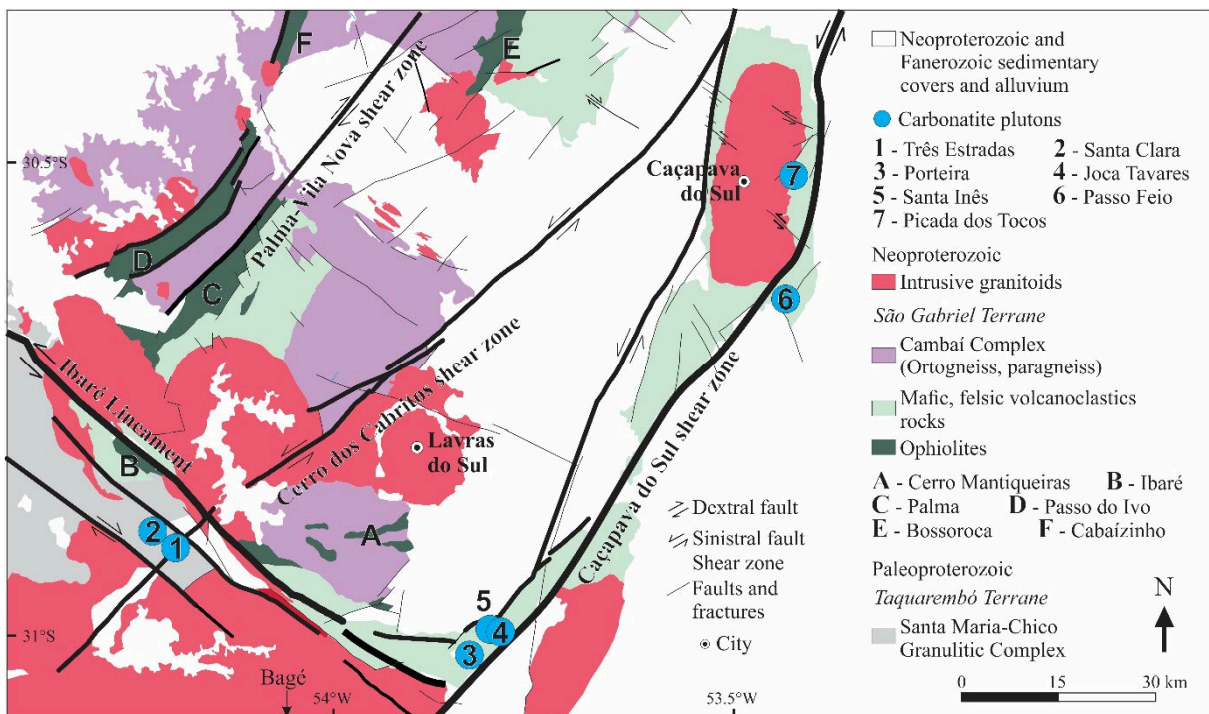


Figure 5.2 - Distribution of carbonatites discovered in Southern Brazil (modified from Ramgrab *et al.*, 2004; Silva *et al.*, 2004) regarding the structural configuration of the SRS. Carbonatites: 1 - Três Estradas; 2 - Santa Clara; 3 - Porteira; 4 - Joca Tavares; 5 - Santa Inês; 6 - Passo Feio; and, 7 - Picada dos Tocos (also called Mato Grande by Agua Resources Ltd, holder of the mining rights).

The Joca Tavares (Toniolo *et al.*, 2010), Porteira (Aguia Resources Ltd., 2013), and Santa Inês (Aguia Resources Ltd., 2014) carbonatites are poorly studied. These three carbonatites are similar to each other, with Joca Tavares being the one with more available data. The Joca Tavares carbonatite has an oval to circular shape, and is emplaced close to the contact between the Ediacaran sedimentary rocks of the Cerro do Bugio Group (Camaquã Basin - Paim *et al.*, 2000) and the Arroio Marmeiro Formation. In general, it presents a weak magnetometric response, despite the strong magnetic anomalies generally related to breccias associated with carbonatites. In outcrop, no deformation is observed and the presence of siltstone xenoliths in the Joca Tavares carbonatite is very common, indicating that this body probably has a maximum Ediacaran age.

5.2.1.1. TRÊS ESTRADAS ALKALINE-CARBONATITE COMPLEX

The TEC is emplaced in gneisses of the Santa Maria-Chico Granulitic Complex (**Figure 5.3**). Neoproterozoic granites occur at the southeast of the TEC and undeformed trachybasalt, tephrite and basanite dikes cross-cut the older rocks. The latter are observed only in drill cores. Metric quartz veins cut all units.

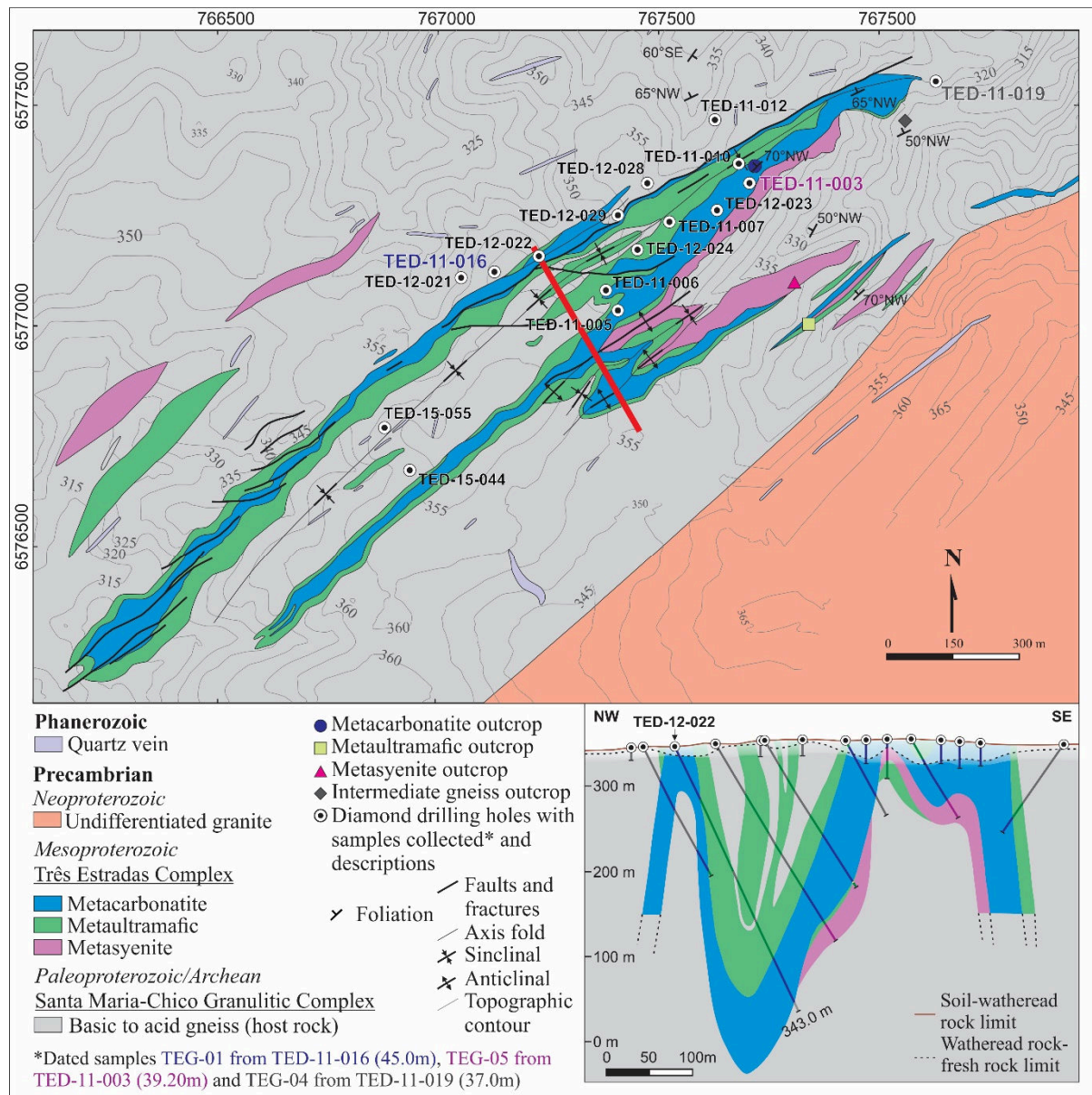


Figure 5.3 - Geological map at 1:10.000 of the TEC with sample locations and schematic NW-SE geological section perpendicular to the complex (Aguia Resources Ltd., 2018). Datum SAD-69, zone 21S.

The TEC forms a slightly undulating hill with its central portion showing the highest elevations (~ 365 m) and the NE and SW parts the lowest ones (~ 315 m) (**Figure 5.4A**). The

TEC has a linear shape, extending for up to 2.35 km along strike ($N50^{\circ}$ - 60° E) and 400 m in width, dipping mainly to the NW. On the surface, it occurs as small, localized, outcrops (**Figures 5.4B e 5.4C**) with apparent foliation.

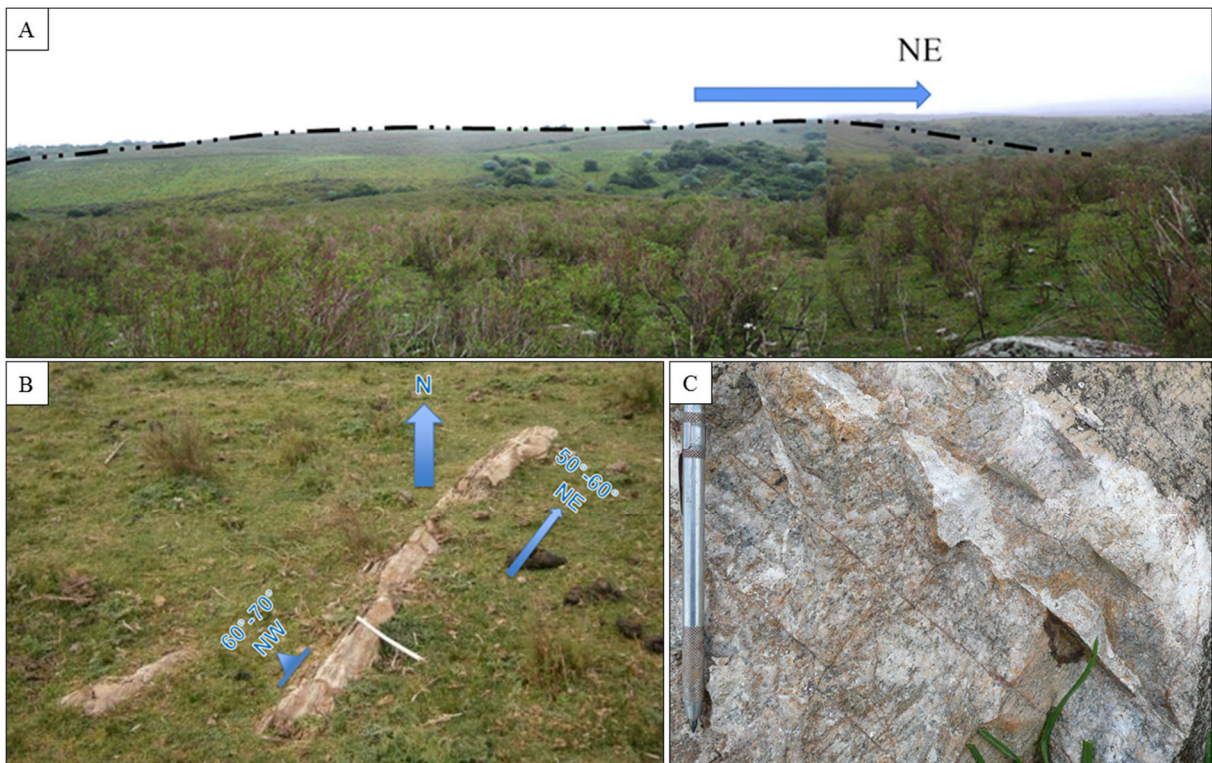


Figure 5.4 - A: Geomorphological expression of the NE portion of the TEC. In the center of the photo, in its highest portion, there are quartz veins that are the core of this elevation. The body continues for another 1.5 km toward SW; B: Typical outcrop of metacarbonatite found in the TEC. Coordinates: 767.719E / 6.577.362N, zone 21S, datum SAD-69; C: Weathered facies of the TEC foliated metacarbonatite.

Drill core samples revealed that the TEC complex is composed of grey calcite metacarbonatites, white to pink calcite metacarbonatites (**Figure 5.5A**) and white to grey calcite metacarbonatites (**Figure 5.5B**). These rocks are foliated, showing parasitic folds, and millimeter- to centimeter-wide bands of hornblende-rich and biotite-rich metaultramafic rocks. To a lesser extent, white dolomite metacarbonatite may occur intercalated with bands of metaultramafic composition rich in actinolite (**Figure 5.5C**). The dominant metacarbonatites are associated with minor metasyenite (**Figure 5.5D**) and metaultramafic rocks (**Figure 5.5E**). The presence of other magmatic phases related to the crystallization of phoscorites and magnetitites was considered insignificant in terms of the individualization of new phases.

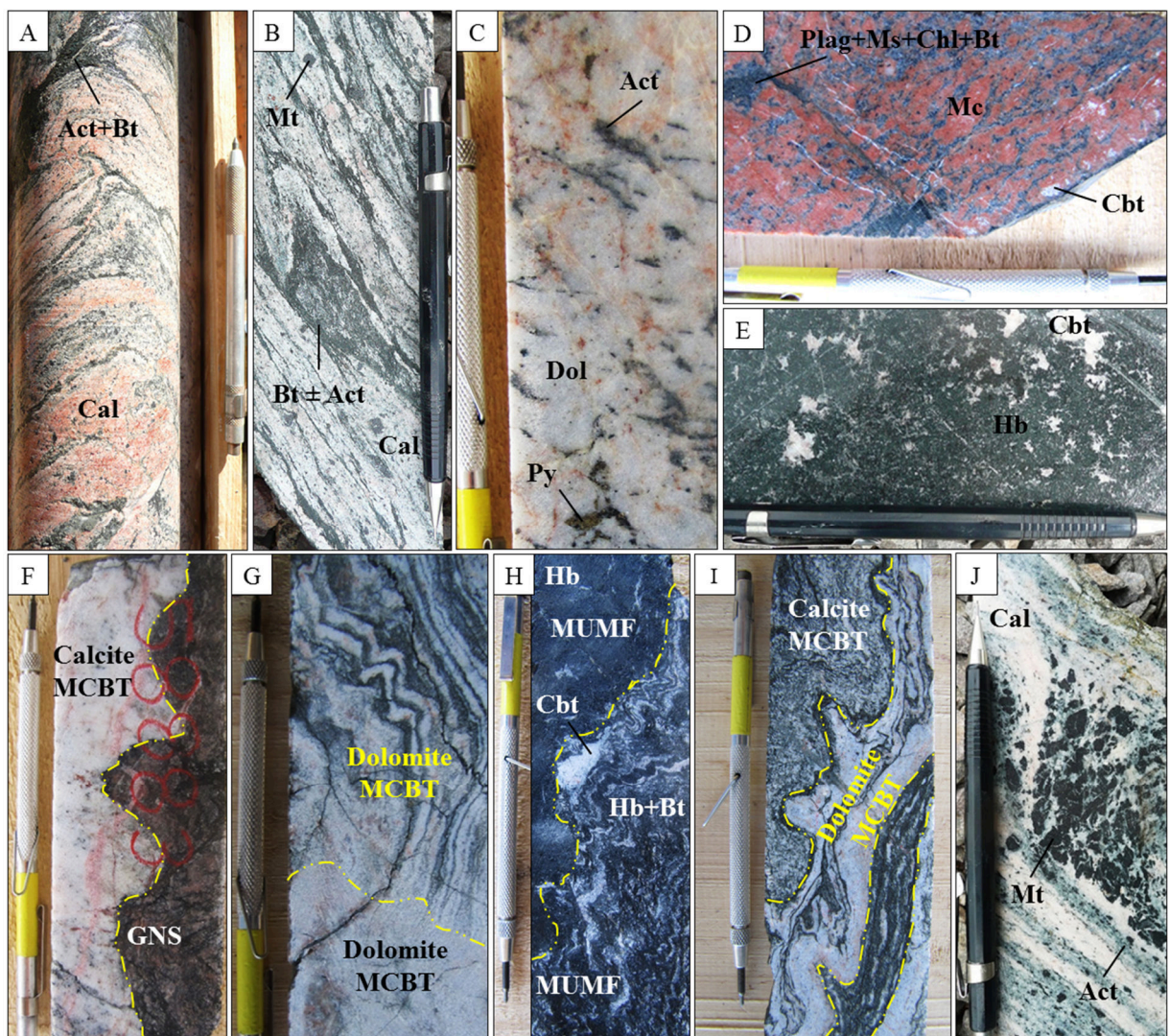


Figure 5.5 - Representative core samples of the TEC. A: Pink, foliated calcite metacarbonatite intercalated with millimetric bands of biotite-rich metaultramafic rock; B: White to grey, foliated calcite metacarbonatite, with intercalations of millimetric to centimetric bands of biotite-rich metaultramafic rock; C: Dolomite metacarbonatite characterized by the occurrence of disseminated actinolite in the middle of dolomite crystals (sample 58871, borehole TED-12-022, 38.00 m depth); D: Metasyenite core sample with fractures filled with carbonates (sample 59264, borehole TED-12-023, 57.00 m depth); E: Recrystallized metaultramafic rock with pockets of white carbonate and apatite; F: Intrusion of calcite metacarbonatite in the gneiss country-rock (GNS, borehole TED-12-022, 49.30 m depth); G: Late-stage dolomite metacarbonatite cross-cutting early-stage dolomite metacarbonatite interbedded with centimeter-thick metaultramafic bands (borehole TED-12-029, 191.20 m depth); H: Contact between distinct magmatic facies of metaultramafic rocks, one less evolved with little amount of carbonate and the other more differentiated, with carbonate bands; I: Contact between dolomite metacarbonatite and calcite dolomite facies showing flow banding; J: Aggregate of rotated magnetite crystals in calcite metacarbonatite (borehole TED-11-005, 24.80 m depth).

The TEC rocks are recrystallized and metamorphosed at greenschist to amphibolite facies, occasionally preserved of the tectonic deformation with flow foliation and banding (**Figure 5.5I**). The TEC is also characterized by the alternation of different phases and pulses of metacarbonatite and metaultramafic rocks, with a predominance of the former in an intricate

contact-relationship (**Figures 5.5F, 5.5G, 5.5H and 5.5I**). Deformation is evidenced by gneissic banding and protomylonitic foliation. Magnetite aggregates are commonly rotated (**Figure 5.5J**), as well as pyrite crystals, in metacarbonatite and metaultramafic rocks. K-feldspar crystals in metasyenite may also form sigmoidal and delta structures. Parasitic folds of varying types frequently occur as well (**Figure 5.5G and 5.5H**).

5.2.1.2. STRUCTURAL GEOLOGY OF THE TRÊS ESTRADAS ALKALINE-CARBONATITE COMPLEX

The TEC intruded probable extension zone in the Mesoproterozoic and currently coincides with the location of the Cerro dos Cabritos Fault Zone, nearby the intersection with the Ibaré Lineament (**Figure 5.2**). The sinistral Cerro dos Cabritos Transcurrent Shear Zone strikes N35°-45°E, orthogonal to the probably coeval Ibaré Lineament, which may represent its conjugate fault.

The Ibaré Lineament shows a NW-SE trend with general dextral movement. It is a crustal-scale discontinuity zone exposed to approximately 60 km that separates the Neoproterozoic Palma Metamorphic Terrane, located toward NE of the lineament, from the Archean to Paleoproterozoic Santa Maria-Chico Complex, in the SW portion. The Ibaré Lineament behaves as a transform fault and lateral ramp of an early Neoproterozoic asymmetric transpressive orogen, represented by low-grade supracrustal rocks, ophiolites and magmatic arcs thrust over the Rio de la Plata Craton (Fragoso-César, 1991; Toniolo *et al.*, 2007).

The schematic geological sections indicate that the main portion of the TEC complex forms a tight synclinal fold, with both flanks dipping dominantly toward the NW, the SE flank dipping less (50°-60°) than the NW flank (75°-85°). At the core of the folded structure are the metaultramafic rocks surrounded by metacarbonatites and with metasyenite being restricted to the outer portion of the SE flank. Later brittle fractures and faults cut across the entire complex.

All the TEC units exhibit gneissic banding and strong sinistral shearing (N50°-60°E, sub vertical), involving the main carbonatite body and its host rocks. Protomylonitic foliation, isoclinal parasitic folds, micro-faults and fault-breccias are also present.

5.3. PETROGRAPHY OF THE TRÊS ESTRADAS ALKALINE-CARBONATITE COMPLEX

5.3.1. METAULTRAMAFIC ROCKS

The metaultramafic rocks occur as centimetric to decametric, deformed or not, alternating bands observed in **Figure 5.5**. Outcrops of metaultramafic rocks are very rare, but when found, they occur in the form of small strongly magnetic blocks *in situ*, often with dark green color and medium to coarse grain size.

The metaultramafic rocks are composed of varying amounts of hornblende (45-60%), carbonate (5-25%), biotite (3-25%), titanite (1-25%), apatite (2-20%), magnetite (3-15%), plagioclase (1-5%) and pyrite (up to 5%) (**Figure 5.6A**). Hornblende occurs as granoblastic to nematoblastic aggregates of subhedral crystals, oriented or not, with the local presence of porphyroblasts. Interstitial carbonate (mainly calcite) are more frequent in foliated rocks than in the non-deformed ones. Similarly, biotite occurs preferentially in most deformed rocks as millimetric lamellae with minor alteration to chlorite. Apatite occurs as aggregates of euhedral to subhedral sub-millimetric crystals. Titanite occurs commonly as subhedral to anhedral sub-millimetric to millimetric crystals and occasionally as centimetric porphyroblasts. Magnetite occurs as millimetric crystals and locally intergrown with pyrite or altered to hematite. Plagioclase forms sparse, submillimetric, subhedral to anhedral, granoblastic aggregates. Pyrite, chalcopyrite, quartz and ilmenite occur as secondary minerals. The protolith probably was an alkaline pyroxenite or hornblendite, but cannot be well defined due to the high degree of recrystallization. No igneous pyroxene relics were found.

Distinct facies of metaultramafic rocks have been recognized based on their mineralogical composition, ranging from amphibole-rich, carbonate-poor terms to intercalations of amphibole- and biotite-rich bands with carbonate and rich-apatite bands or pockets. Contact relationships between the metaultramafic rocks with other rock types of the TEC and also with the wall-rocks show, in general, minor alteration marked by biotitization or carbonation. Secondary carbonate veins and venules commonly occur in the metaultramafic rocks.

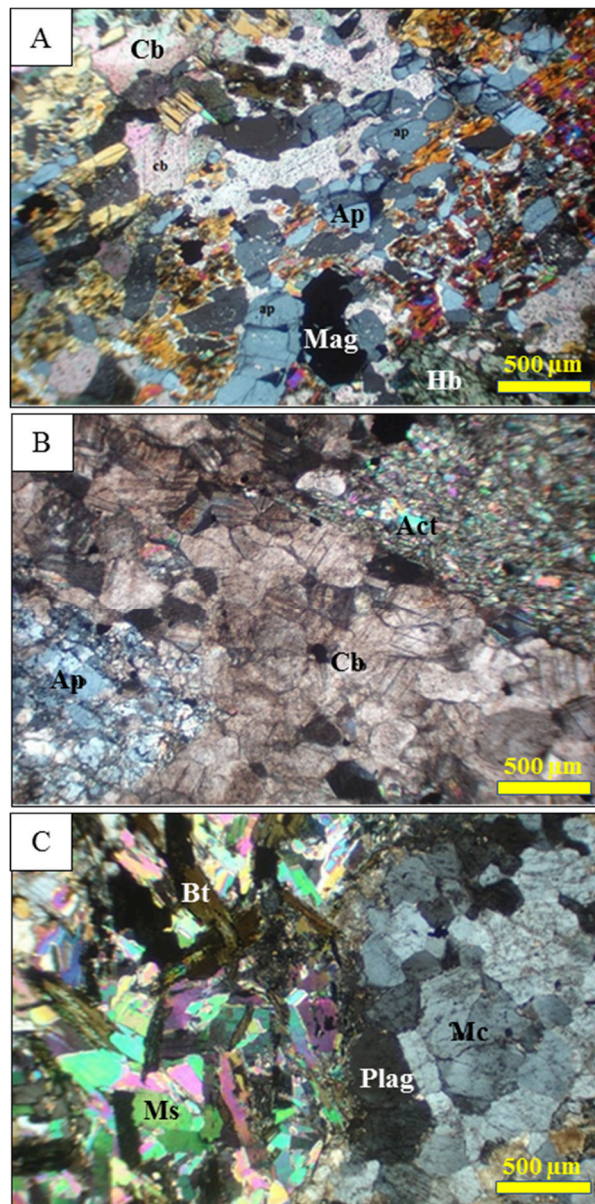


Figure 5.6 - A: Photomicrograph of apatite and carbonate-rich metaultramafic rock (sample 53408, borehole TED-11-007, 44.58 m depth). Mineralogy (sample TEP-12): hornblende (Hb) - 45%; carbonate (Cb) - 20%; apatite (Ap) - 18%; magnetite (Mt) - 4%; biotite-chlorite - 3%; ilmenite - 1.5%; titanite - 1% and pyrite - 1%; B: Photomicrograph of dolomite metacarbonatite (sample 54205, borehole TED-11-016, 77.28 m depth). Mineralogy (sample TEP-25): carbonate (Cb) - 57%; apatite (Ap) - 15%; actinolite (Act) - 14%; pyrite - 8%; ilmenite - 3%; magnetite - 2%; biotite - 1%; titanite, hematite and xenotime (?) – Tr; C: Photomicrograph of metasyenite (sample 53137, borehole TED-11-003, 40.00 m depth). Mineralogy (sample TEP-08): microcline (Mc) - 45%; muscovite (Ms) - 24%; plagioclase (Plag) - 20%; chlorite - 8%; biotite (Bt) - 2%; opaques - 0.7%; titanite - 0.3%; hornblende, carbonate, apatite and rutile – Tr.

5.3.2. METACARBONATITE

Metacarbonatite crops out locally as *in situ* blocks. These rocks are medium- to coarse-grained and exhibit, in general, white, pink, or gray colors. It is composed of variable amounts

of carbonates, apatite, biotite, actinolite, hornblende and chlorite, with titanite, quartz, xenotime, allanite, zircon and microcline in trace amounts and pyrite, chalcopyrite, ilmenite, hematite and millerite as secondary minerals (**Figure 5.6B**). Two distinct carbonatite facies were identified: calcite metacarbonatite and dolomite metacarbonatite. The contact relationships indicate that calcite metacarbonatites were emplaced before dolomite metacarbonatites. Calcite metacarbonatites, including the varieties magnesian- and silicate-rich calcite metacarbonatites, dominate in the TEC complex. Dolomite metacarbonatites occur in a subordinate amount and are rarely exposed, being observed essentially in the drill cores.

Calcite metacarbonatites are composed of carbonates (20-85%), biotite (1-25%), apatite (4-19%), titanite (4-16%), plagioclase (5-15%), magnetite (2-15%), actinolite (1-5%) and pyrite (up to 5%). The main phases occur as subhedral to euhedral crystals whereas accessory minerals are subhedral to anhedral. Carbonates are predominantly calcite, occurring as oriented granoblastic aggregates. Biotite occurs as oriented lamellae and may be replaced by chlorite. Titanite is often included in biotite. Apatite typically shows fractures filled with carbonates. Plagioclase, when present, also appears oriented. Magnetite, actinolite and pyrite commonly occur as disseminated crystals. Microcline, xenotime, allanite, chalcopyrite, ilmenite and hematite are accessory phases.

Dolomite metacarbonatites are composed of dolomite (65-90%), apatite (6-22%), actinolite (up to 20%), magnetite (3-7%) and pyrite (up to 5%). All the minerals vary from euhedral to anhedral crystals. Dolomite forms oriented granoblastic aggregates. Apatite may occur as aggregates or as diffuse bands. Actinolite usually occurs as prismatic crystals. Magnetite and pyrite occur disseminated or may be associated in some fractures. Xenotime, chalcopyrite, ilmenite and hematite are accessory phases.

Phoscorite composed of dolomite, apatite and magnetite, containing up to 12.90 wt.% of P₂O₅ was identified in only a 1.45 m thick layer in only one borehole (TED-11-016, sample 54173), located near the central portion of the TEC complex.

The contact relationships between the distinct metacarbonatite facies and the other rock types of the complex show minor mineralogical changes toward biotite- and carbonate-rich portions. Similar relationships are also noted between the metacarbonatites and the host rocks. Secondary late-stage carbonate veins and venules cross-cut the main metacarbonatite facies.

5.3.3. METASYENITE

Metasyenite is a coarse-grained rock characterized by pinkish-red color and lack of magnetism. It is composed of microcline (45-50%), plagioclase (20-25%), muscovite (20-25%), biotite and chlorite (8-15%) (**Figure 5.6C**). Microcline occurs as centimeter-sized crystals with incipient kaolinization. Polygonal, millimeter-sized, crystals represent a second-generation product of metamorphic recrystallization. Muscovite occurs as oriented lamellae or diffuse bands. Plagioclase is wholly recrystallized, forming granoblastic aggregates displaying strong kaolinization. Biotite, partially replaced by chlorite, shows incipient orientation and is often associated with muscovite-rich bands.

At the contact with metacarbonatites, metasyenite may show fractures infilled by secondary carbonates. However, being restricted to the SE flank of the TEC structure, metasyenite is almost always in contact with metaultramafic rocks. Deformation is evidenced by rotated potassic feldspar porphyroclasts and foliation development. Locally, relics of the original igneous rock are still preserved.

In general, the igneous textures preserved in the TEC complex are characterized by minerals relics and structures from the original protoliths. Despite the strong deformation, some portions of the TEC are undeformed or show only incipient deformation. Sulfidation (pyrite and chalcopyrite), carbonation, biotitization, and potassification are the most common hydrothermal processes recorded in the TEC rocks. The latter is related to the metasomatism caused by the carbonatite intrusion. **Figure 5.7** displays a summary of the metamorphic assemblages identified in the TEC rocks.

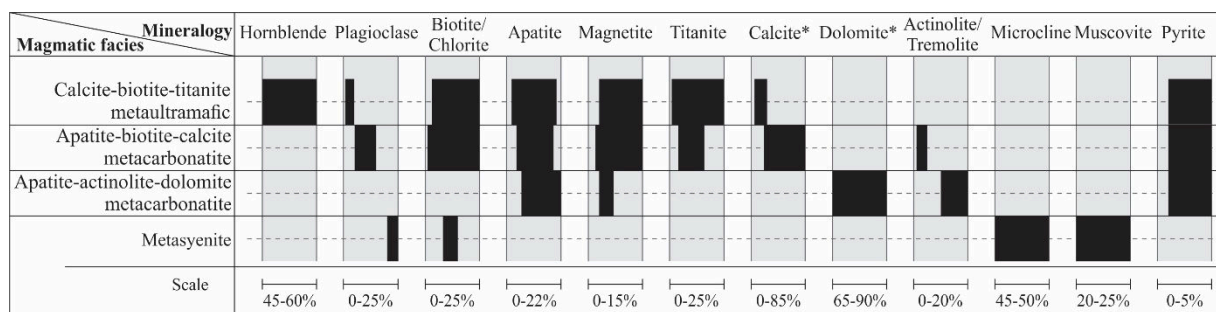


Figure 5.7 - Metamorphic assemblages of the main TEC units. *Main carbonate mineral.

5.4. MATERIALS AND METHODS

The TEC complex was mapped on a 1:10,000 based on the available outcrops and the subsurface geological information taken from drill core and reverse circulation drilling data. More than 5,000 m of borehole cores were described, mainly located in the central-northeast portion of the TEC. Thirty-one (31) thin-sections were produced at the University of Brasília Lamination Laboratory and described under a petrographic microscope. From this stage, samples were selected for geochronological and isotope investigations.

5.4.1. U-Pb AND Lu-Hf ON ZIRCON

Three samples were dated by U-Pb method: TEG-01 - metacarbonatite with 30 zircon crystals; TEG-04 - country-rock gneiss and TEG-05 - metasyenite, both with 29 zircon crystals each. Zircon crystals were analyzed with a laser ablation microprobe (New Wave UP213) coupled to a multi-collector ICP-MS (Neptune), at the Laboratory of Geochronological, Geodynamic and Environmental Studies at the Institute of Geosciences of the University of Brasília. The images of zircon crystals were obtained by backscattered electrons (BSE) and cathodoluminescence (CL), in a scanning electron microscope (SEM) brand GATAN, model Chroma CL, at the University of Brasília. Isotope data were acquired using static mode with a spot size of 30 μm . Laser operating conditions were adjusted according to the characteristics of the samples. The laser was operated with a fluency of 2.25 - 3.65 J/cm² and frequency of 10 Hz. The ablated material was carried by Ar (0.990-1.020 L/min) and He (0.44-0.45 L/min). The power of the laser was 1050 W. The detector arrangement consisted of a central Faraday cup and four Faraday collectors (L4, L3, H2, H4), each on the high side and low side of the center cup. The mass spectrometer was equipped with 3 ion counters (ICs, or multichannel ion counters MICs) (IC3, IC4, IC6). The isotopes were measured at the same time, as follows: L3 - ^{208}Pb , L4 - ^{206}Pb , H2 - ^{232}Th , H4 - ^{238}U , IC3 - ^{202}Hg , IC4 - ^{204}Pb and IC6 - ^{207}Pb . A detailed description of the analytical method can be found in Bühn *et al.* (2009).

Laser-induced elemental and instrumental mass fractionations were corrected by the primary reference zircon GJ-1 of 608.5 ± 1.5 Ma age (Jackson *et al.*, 2004). GJ-1 analyses were carried out after every 4 samples to correction in the TEG-01 and after every 8 samples in TEG-04 and TEG-05. To obtain the accuracy and precision of the laser results, the secondary

reference zircon 91500 of $1,063.4 \pm 0.6$ Ma age was used (Wiedenbeck *et al.*, 1995), along the day to verify analysis reproducibility. The external error was calculated after propagation of the errors of the GJ-1 mean and the individual sample zircon (or spot). During the TEG-01 sample analyses, the mean values obtained for the GJ-1 standard were $^{207}\text{Pb}/^{206}\text{Pb}=0.0055662 \pm 0.000056$ ($n=9$) and $^{206}\text{Pb}/^{238}\text{U}=0.09810 \pm 0.00066$ ($n=9$), with analytical precisions of $\pm 0.10\%$ and $\pm 0.68\%$, respectively. In the TEG-04 sample, the GJ-1 mean values were $^{207}\text{Pb}/^{206}\text{Pb}=0.05675 \pm 0.00041$ ($n=5$) and $^{206}\text{Pb}/^{238}\text{U}=0.0902 \pm 0.0021$ ($n=5$), with analytical precisions of $\pm 0.72\%$ and $\pm 2.3\%$, respectively. In the TEG-05 sample, the GJ-1 mean values were $^{207}\text{Pb}/^{206}\text{Pb}=0.05690 \pm 0.00031$ ($n=5$) and $^{206}\text{Pb}/^{238}\text{U}=0.0903 \pm 0.0031$ ($n=5$), with analytical precisions of $\pm 0.54\%$ and $\pm 3.4\%$, respectively. All the analytical precisions values were reported at 95% of confidence level (2σ). A compilation of secondary reference zircon 91500 values from all analytical sections in the course of this study yielded concordia ages of 1079 ± 18 Ma ($n=11$) and 1068 ± 10 Ma ($n=16$), which are in agreement with the recommended values. Blanks were measured before and after each sample analysis for blank correction.

Data reduction was performed using the Chronus software (Oliveira, 2015). The data evaluation took into account the contents of ^{204}Pb , errors of measured isotopic ratio and percentage of discordance. The corrected isotopic ratios along with the associated calculated ages were plotted using the Isoplot 4.15 software (Ludwig, 2012), also a supplement for Microsoft Excel.

Lu-Hf isotope ratios were also determined on zircon crystals from the samples TEG-01 ($n=7$), TEG-04 ($n=8$) and TEG-05 ($n=10$). Laser operating conditions are similar to the U-Pb method, modifying only the spot size (40 to 55 μm) and the fluency (3 to 4 J/cm^2). The detector arrangement consisted of a central Faraday cup and eight Faraday collectors, in which the following isotopes were analyzed: C - ^{177}Hf ; L1 - ^{176}Hf , ^{176}Lu , ^{176}Yb ; L2 - ^{175}Lu ; L3 - ^{173}Yb ; L4 - ^{171}Yb ; H1 - ^{178}Hf ; H2 - ^{179}Hf and H3 - ^{180}Hf . The detailed description of the methodology for isotope analysis of Lu-Hf on zircon crystals is presented by Matteini *et al.* (2010).

The primary reference zircon GJ-1 was also used as Lu-Hf standard, being analyzed before and after the zircon samples analysis. The mean value obtained for the GJ-1 during the course of this study was $^{176}\text{Hf}/^{177}\text{Hf}=0.28199 \pm 0.00011$ ($n=6$), with an analytical precision of 0.04% at 95% of confidence level (2σ). This value agrees with the GJ-1 certified value of $^{176}\text{Hf}/^{177}\text{Hf}=0.282000 \pm 0.000005$ (Morel *et al.*, 2008). Blanks were measured before and after

each sample analysis for blank correction. Additional information regarding the analyses of U-Pb and Lu-Hf can be found in **Tables 5.1 and 5.2**.

Table 5.1 - Additional information regarding U-Pb analyses (see also **Tables 5.3 to 5.5**).

Data report template (with modifications) from http://www.plasmage.org/recommendations
¹ Conversion factor from mV to CPS is 62500000
² Concentration uncertainty c.20%
³ Data not corrected for common-Pb
⁴ Not corrected for common-Pb
⁵ Discordance calculated as $(1 - (\frac{^{206}\text{Pb}}{^{238}\text{U} \text{ age}} / \frac{^{207}\text{Pb}}{^{206}\text{Pb} \text{ age}}))^*100$
Decay constants of Jaffey <i>et al.</i> (1971)

Table 5.2 - Additional information regarding Lu-Hf analyses (see also **Table 5.6**).

¹⁷⁶ Lu decay constant (1.867×10^{-11} /yr) of Söderlund <i>et al.</i> (2004)
Chondritic values of $^{176}\text{Hf}/^{177}\text{Hf} = 0.0336$ and $^{176}\text{Lu}/^{177}\text{Hf} = 0.282785$ (Bouvier <i>et al.</i> , 2008)
Present day values for depleted mantle model $^{176}\text{Hf}/^{177}\text{Hf} = 0.28325$ and $^{176}\text{Lu}/^{177}\text{Hf} = 0.0388$ (Griffin <i>et al.</i> , 2000; updated by Andersen <i>et al.</i> , 2008)
$^{176}\text{Lu}/^{177}\text{Hf}$ values for mafic and felsic crust are from Pietranik <i>et al.</i> (2008)
$^{176}\text{Lu}/^{177}\text{Hf}$ of 0,015 was used as an average value of the continental crust for calculating the crustal model age (Griffin <i>et al.</i> , 2002, 2004; Belousova <i>et al.</i> , 2006, 2010).
Ratio values $^{176}\text{Lu}/^{177}\text{Hf} = 0.03795$ and $^{176}\text{Hf}/^{177}\text{Hf} = 0.283158$ current to the juvenile crust (Dhuime <i>et al.</i> , 2012), as the crustal ratio $^{176}\text{Lu}/^{177}\text{Hf} = 0.0093$.

5.4.2. Sm-Nd-Sr ISOTOPES

Nd and Sr isotope ratios were determined for whole-rock samples of metacarbonatites (11), metaultramafic rocks (2), metasyenite (1) and gneiss country rock (1). The analyses were performed at the Laboratory of Geochronological, Geodynamic and Environmental Studies at the Institute of Geosciences of the University of Brasília (UnB) using a Thermo Scientific TRITON™ Plus Thermal Ionization Mass Spectrometry (TIMS) spectrometer, in static mode, equipped with nine Faraday cup collectors and a central electron multiplier.

The whole-rock samples were pulverized, weighed (50 to 100 mg), spiked with a mixed $^{149}\text{Sm}-^{150}\text{Nd}$ tracer, and then, dissolved in HF, HNO₃ and HCl in Savillex vials. Sm and Nd extractions were carried out by two-stage ion-exchange chromatography following the procedures described by Gioia & Pimentel (2000). In a first -stage, Teflon columns infilled with AG-50W-X8 100-200 mesh resin were used in a second-stage, infilled with LN-Spec 100-150 µm resin. Sr extraction was carried out using Teflon columns infilled with LN-Spec 50-

100 µm resin, being collected with HNO₃. Sm, Nd and Sr dry aliquots were loaded on a Re double-filament arrangement prior to evaporation.

The analytical precisions for ¹⁴³Nd/¹⁴⁴Nd and ⁸⁷Sr/⁸⁶Sr isotope ratios are better than ± 0.0005% (2σ), and 0.01% (2σ), respectively, based on repeated analyses of international rock standards BHVO-1 for Nd, with ¹⁴³Nd/¹⁴⁴Nd of 0.512989±0.000014 (compatible with values published, e.g., 0.512986±0.000009, Weis *et al.*, 2005), and NBS-987 for Sr, with ⁸⁷Sr/⁸⁶Sr of 0.71026±0.00001 (compatible with values published, around 0.71025, Thirlwall, 1991). The ¹⁴³Nd/¹⁴⁴Nd ratios were normalized to ¹⁴⁶Nd/¹⁴⁴Nd=0.7219, whereas the ⁸⁷Sr/⁸⁶Sr ratios were normalized to ⁸⁸Sr/⁸⁶Sr=8.375209. Nd-model ages (T_{DM} values) were calculated following DePaolo (1988).

Rb and Sr concentrations were determined by ICP-MS (digestion with lithium metaborate) in ALS Laboratory, Vancouver, Canada (ME-MS81 analytical package). The internal standards used, GRE-03 and GRE-04, were produced from Tanzanian carbonatites by Geostats Pty Ltd (Australia). Blanks used during the analyses were prepared by ACME Analytical Laboratories (Vancouver) with medium values of Rb and Sr of 0.13 ppm and 0.09 ppm, respectively.

5.5. RESULTS

5.5.1. U-Pb AND Lu-Hf ON ZIRCON

To determine the crystallization age of the TEC and its host rocks, 3 samples were analyzed by the U-Pb LA-MC-ICPMS method on zircon: (1) a dolomite metacarbonatite TEG-01; (2) a metasyenite TEG-05; and, (3) a quartz-feldspar gneiss (country rock) TEG-04. Sample TEG-01 is a dolomite metacarbonatite composed of dolomite, apatite, actinolite, and minor calcite, with magnetite and titanite as accessory minerals. The rock shows incipient foliation and some metaultramafic bands. Secondary carbonate segregations (veins) and reddish carbonate veins also may occur (**Figure 5.8A**). Thirty (30) zircon crystals were analyzed. These are, in general, small (~200 µm), well faceted, with a well-defined core and in some cases, rims (**Figure 5.9A**). The rims of the zircon crystals are partially recrystallized, with a yellowish color and yielded the same age as the cores.

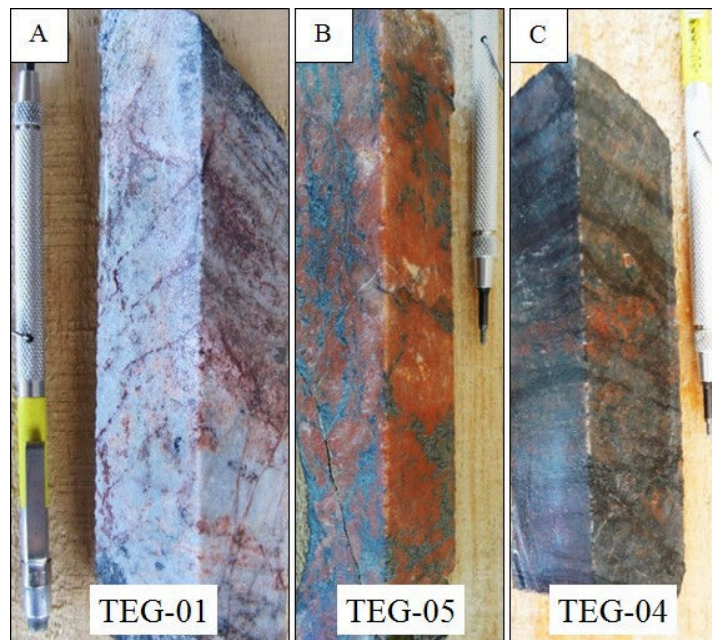


Figure 5.8 - Hand specimens of the samples dated by U-Pb. A: Dolomite metacarbonate (borehole TED-11-016, 45.0 m depth); B: Metasyenite (borehole TED-11-003, 39.20 m depth); C: Quartz-feldspar gneiss (borehole TED-11-019, 37.0 m depth).

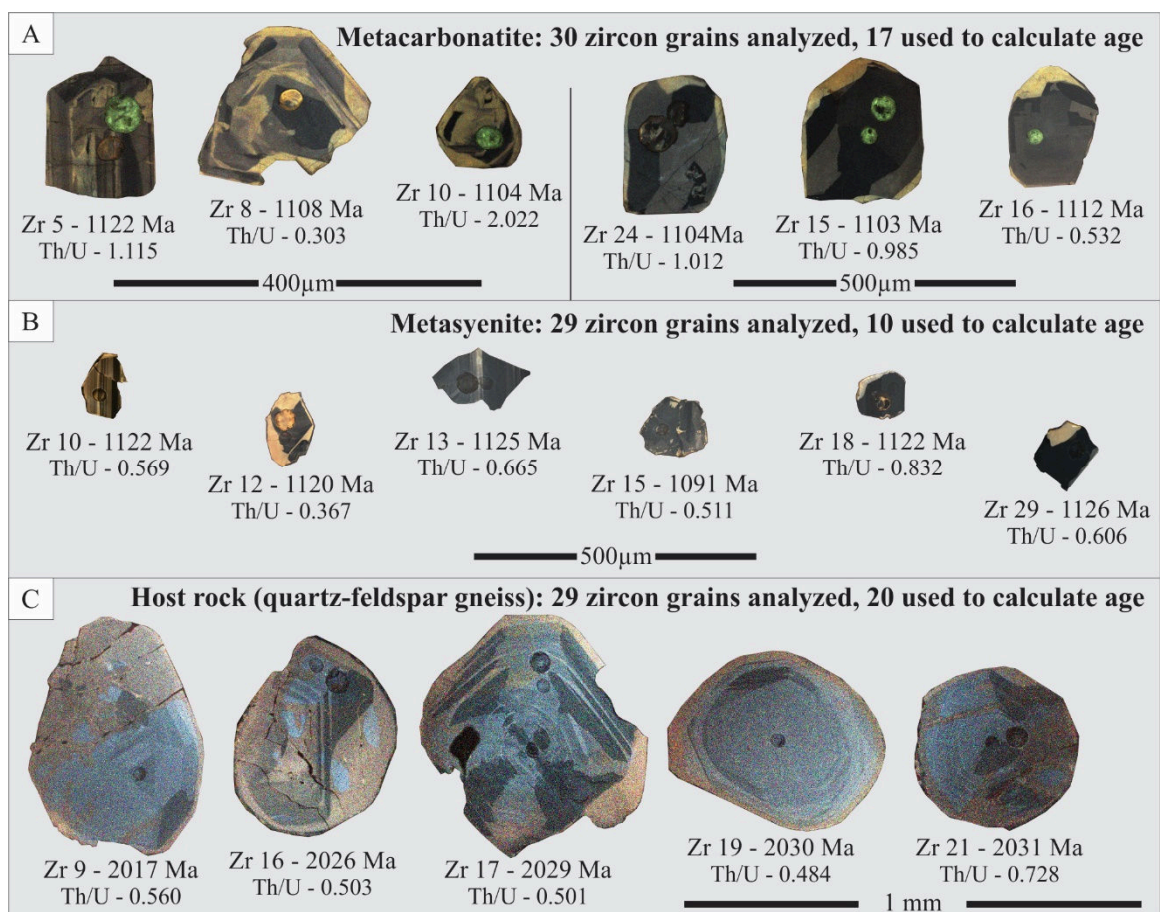


Figure 5.9 - Cathodoluminescence images of zircon crystals analyzed by U-Pb. A: Dolomite metacarbonate; B: Metasyenite; C: Quartz-feldspar gneiss.

Analyses of 17 zircon crystals were used for calculating the TEG-01 age. The others were rejected due to high analytical errors and/or high discordance (**Table 5.3**). The U-Pb age (upper intercept) obtained for the dolomite metacarbonatite (TEG-01) is $1,110 \pm 4.8$ Ma (**Figure 5.10A**). A 2,089 Ma crystal was interpreted as inheritance of the host gneiss of the Santa Maria-Chico Granulitic Complex. The Th/U ratio of 17 zircon crystals ranged from 0.3 to 2.0, that is, greater than the ratio of 0.1 considered by Rubatto and Gebauer (2000), Hoskin & Black (2000) and Belousova *et al.* (2002) for the separation of metamorphic (<0.1) and igneous zircon crystals (>0.1). According to Rubatto (2017), however, metamorphic zircon does not always have a low Th/U ratio. This author suggests that metamorphic zircon crystals with Th/U ratios >0.1 may be as a result of the chemical composition of the rock as well as of the high and ultra-high temperatures (>900°C) reached during the peak of metamorphism in granulite facies, which is recorded in the Santa Maria-Chico Granulitic Complex (Hartmann *et al.*, 2008).

Sample TEG-05 is a fenitized metasyenite with stretched and rotated alkali feldspar crystals (**Figure 5.8B**). Twenty-nine (29) zircon crystals were analyzed. These are small (~ 150 µm), subhedral to euhedral, with core not always clearly differentiated. The rims of the zircon crystals tend to be yellowish in color and partially recrystallized (**Figure 5.9B**). The analyzed zircon crystals do not show any significant differences between the ages of the outer zones and the core.

Only 10 zircon crystals were able to be used for calculating the TEG-05 age. The other analyses were rejected due to the high analytical errors, degree of discordance, and excess of common lead (**Table 5.4**). An upper intercept age of $1,123 \pm 15$ Ma was obtained for TEG-05 sample, which is in agreement with the dolomite metacarbonatite age (**Figure 5.10B**). The Th/U ratio of the 10 zircon crystals range between 0.37 and 1.3, suggesting an igneous origin (Rubatto & Gebauer, 2000; Hoskin & Black, 2000; Belousova *et al.*, 2002).

TEG-04 is a gneiss characterized by alternation of felsic (quartz-feldspar) and mafic (amphibole and biotite) bands, with localized potassic alteration and carbonate veins (**Figure 5.8C**). Twenty-nine (29) zircon crystals were analyzed. These are large (~ 0.5 mm), idiomorphic or sub-rounded, with well-defined cores (gray in color) and recrystallized rims (pinkish brown in cathodoluminescence) (**Figure 5.9C**). Fractures are also noted in some crystals. No significant difference was found between the cores and the recrystallized rims of the analyzed zircon crystals.

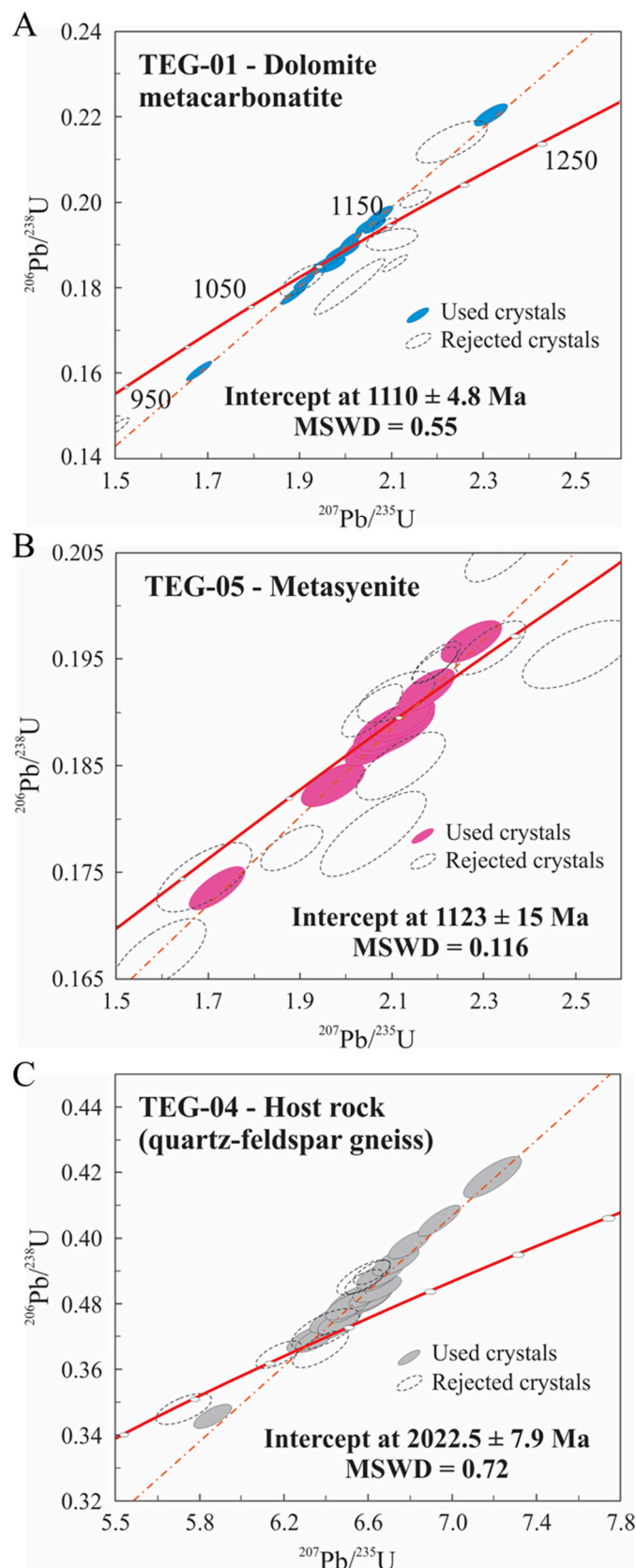


Figure 5.10 - A: U-Pb upper intercept age in $1,110.0 \pm 4.8 \text{ Ma}$ obtained for dolomite metacarbonate; B: U-Pb upper intercept age in $1,123.0 \pm 15 \text{ Ma}$ obtained for metasyenite. C: U-Pb upper intercept age in $2,022.5 \pm 7.9 \text{ Ma}$ obtained for quartz-feldspar gneiss country rock. In all the graphics, the dashed ellipses represent the rejected zircon crystals.

Twenty (20) zircon crystals were used for calculating the TEG-04 age. The other analyses were rejected due to high analytical errors and high discordance (**Table 5.5**). The Th/U ratio of the 20 zircon crystals range between 0.427 and 0.830. This average ratio greater than 0.1 might be interpreted as indicating an igneous origin. However, it is necessary to consider the high metamorphic grade of the studied rock (Rubatto, 2017). Besides, zircon crystals derived from acid rocks commonly have Th/U ratios higher than 0.1. A U-Pb age of $2,022.5 \pm 7.9$ Ma (**Figure 5.10C**) was obtained for the TEG-04 gneiss, which is attributed to the Santa Maria-Chico Granulitic Complex.

Lu-Hf isotopes on zircon crystals from the samples TEG-01, TEG-04 and TEG-05 are reported in **Table 5.6**. Dolomite metacarbonatite zircon crystals show values of $\epsilon_{\text{Hf}}(t)$ and Hf model ages (T_{DM}) varying between -0.49 and 2.66 and between 1.49 and 1.62 Ga, respectively. In the metasyenite, the values of $\epsilon_{\text{Hf}}(t)$ in analyzed zircon crystals vary between -0.08 and 5.72 and the Hf model ages (T_{DM}) vary between 1.40 and 1.62 Ga. As expected, the gneiss host rock zircon crystals show very contrasting values, with $\epsilon_{\text{Hf}}(t)$ varying between -7.10 and -4.73 and Hf model ages (T_{DM}) varying between 2.54 and 2.63 Ga.

Table 5.3 - U-Pb analyses of dolomite metacarbonatite zircon crystals (TEG-01).

CHRONUS Version 2.0.0-alpha.3		Data for Wetherill plot ^a										Ages ^b								
Identifier	206* (%)	204Pb cps	206Pb mV ^c	Th/U	206Pb/204Pb	1s%	207Pb/206Pb	1s %	207Pb/235U	1s %	206Pb/238U	1s %	Rho	207Pb/206Pb	2s abs	206Pb/238U	2s abs	207Pb/235U	2s abs	% U-Pb disc ^d
004-ZR01	0.0076	1	0.0033	2.003	204176	4.10	0.07693	0.50	2.013	0.89	0.1897	0.63	0.71	1119	20	1120	13	1120	12	-0.04
010-ZR05	0.0107	2	0.0026	1.115	145394	8.01	0.07705	0.67	1.981	1.02	0.1865	0.67	0.66	1122	27	1102	14	1109	14	1.79
015-ZR08	0.0035	1	0.0073	0.303	438815	5.03	0.07649	0.38	2.083	0.92	0.1975	0.75	0.82	1108	15	1162	16	1143	13	-4.88
017-ZR10	0.0071	2	0.0038	2.022	218286	5.12	0.07633	0.57	2.319	1.01	0.2203	0.75	0.74	1104	23	1283	18	1218	14	-16.28
018-ZR11	0.0039	2	0.0066	0.721	393300	3.93	0.07656	0.33	2.085	0.80	0.1975	0.63	0.78	1110	13	1162	13	1144	11	-4.71
021-ZR12	0.0039	1	0.0064	0.653	398881	2.14	0.07634	0.31	2.057	0.75	0.1954	0.58	0.77	1104	12	1150	12	1134	10	-4.19
022-ZR13	0.0018	1	0.0141	1.115	878216	1.91	0.07704	0.21	2.022	0.68	0.1903	0.53	0.78	1122	9	1123	11	1123	9	-0.07
023-ZR14	0.0012	1	0.0180	0.539	1289056	12.49	0.07669	0.19	1.983	0.62	0.1875	0.46	0.74	1113	7	1108	9	1110	8	0.47
024-ZR15	0.0026	1	0.0094	0.985	585604	2.24	0.07631	0.28	1.959	0.84	0.1862	0.69	0.83	1103	11	1101	14	1101	11	0.24
027-ZR16	0.0036	1	0.0068	0.532	427043	2.47	0.07664	0.28	2.017	0.71	0.1908	0.54	0.76	1112	11	1126	11	1121	10	-1.25
028-ZR17	0.0049	1	0.0052	1.670	316790	4.17	0.07658	0.43	1.996	0.87	0.1890	0.65	0.75	1110	17	1116	13	1114	12	-0.51
029-ZR18	0.0024	1	0.0101	0.932	633597	2.23	0.07641	0.22	1.923	0.78	0.1826	0.64	0.83	1106	9	1081	13	1089	10	2.24
034-ZR21	0.0014	1	0.0182	1.169	1135155	3.59	0.07637	0.20	2.023	0.77	0.1921	0.64	0.83	1105	8	1133	13	1123	10	-2.53
039-ZR24	0.0022	1	0.0111	1.012	694209	3.53	0.07633	0.25	1.950	0.72	0.1852	0.56	0.78	1104	10	1095	11	1098	10	0.75
040-ZR25	0.0054	2	0.0048	1.290	286149	4.94	0.07699	0.32	2.073	0.76	0.1953	0.57	0.76	1121	13	1150	12	1140	10	-2.57
042-ZR27	0.0029	5	0.0099	0.432	534044	8.49	0.07610	0.33	1.702	1.04	0.1622	0.91	0.88	1098	13	969	16	1009	13	11.71
047-ZR30	0.0030	1	0.0085	0.850	523578	3.07	0.07678	0.29	1.903	0.98	0.1798	0.86	0.88	1116	12	1066	17	1082	13	4.47
Data not used in calculating age																				
009-ZR04	0.0078	2	0.0033	1.328	198280	5.01	0.07395	0.44	1.503	1.09	0.1474	0.93	0.85	1040	18	887	15	932	13	14.75
011-ZR06	0.0089	1	0.0028	3.337	174768	0.92	0.07773	0.63	2.151	1.00	0.2007	0.68	0.68	1140	25	1179	15	1165	14	-3.44
016-ZR09	0.0075	1	0.0035	0.458	207272	4.23	0.07779	0.50	2.086	0.88	0.1944	0.62	0.71	1142	20	1145	13	1144	12	-0.33
041-ZR26	0.0173	1	0.0013	2.022	89295	16.46	0.07563	1.65	2.232	2.28	0.2140	1.53	0.67	1085	66	1250	35	1191	32	-15.19
046-ZR29	0.0120	1	0.0021	0.652	128783	1.52	0.07608	1.06	1.908	1.75	0.1819	1.34	0.77	1097	42	1077	27	1084	23	1.82
Unused data due to high disagreement																				
005-ZR02	0.0147	4	0.0020	1.351	106065	9.00	0.07695	1.26	1.405	2.53	0.1324	2.17	0.86	1120	50	802	33	891	30	28.42
006-ZR03	0.0058	1	0.0044	0.585	266693	13.26	0.07525	1.37	1.014	4.17	0.0977	3.91	0.94	1075	55	601	45	711	42	44.10
012-ZR07	0.0086	30	0.0059	0.662	180576	18.72	0.07964	1.46	2.101	1.76	0.1913	0.90	0.51	1188	57	1129	19	1149	24	5.00
035-ZR22	0.0408	182	0.0579	0.104	37925	31.00	0.08235	0.27	2.108	0.82	0.1856	0.68	0.83	1254	11	1098	14	1151	11	12.45
036-ZR23	0.0372	1	0.0007	0.140	41824	5.48	0.07862	1.74	1.446	2.49	0.1334	1.74	0.70	1163	68	807	26	908	30	30.57
045-ZR28	0.0073	4	0.0039	0.755	212973	17.00	0.08083	0.79	2.008	2.54	0.1802	2.39	0.94	1217	31	1068	47	1118	34	12.27
Older data (crustal contamination?)																				
033-ZR20	0.0015	1	0.0160	1.016	1003046	7.89	0.12937	0.36	6.662	0.92	0.3735	0.76	0.83	2089	13	2046	27	2068	16	2.10
Unused data due to high analytical error																				
030-ZR19	0.0197	1	0.0013	11.706	79380	3.64	0.07970	1.11	0.482	7.49	0.0438	7.40	0.99	1190	43	277	40	399	49	76.75

Table 5.4 - U-Pb analyses of metasyenite zircon crystals (TEG-05).

CHRONUS Version 2.0.0-alpha.3		Data for Wetherill plot ^d										Ages ^d								
Identifier	206* (%)	204Pb cps	206Pb mV ¹	Th/U	206Pb/204Pb	1s%	207Pb/206Pb	1s %	207Pb/235U	1s %	206Pb/238U	1s %	Rho	207Pb/206Pb	2s abs	206Pb/238U	2s abs	207Pb/235U	2s abs	% U-Pb disc ⁵
007-ZR4	0.0108	12	0.0030	0.634	143445	17.41	0.07715	0.66	1.996	0.96	0.1877	0.60	0.62	1125	26	1109	12	1114	13	1.46
015-ZR10	0.0206	11	0.0015	0.569	75193	16.41	0.07704	0.69	2.089	1.01	0.1967	0.65	0.64	1122	27	1157	14	1145	14	-3.13
017-ZR12	0.0110	9	0.0029	0.367	140548	12.68	0.07696	0.64	1.986	0.96	0.1871	0.62	0.64	1120	25	1106	13	1111	13	1.30
018-ZR13	0.0183	19	0.0030	0.665	84552	22.93	0.07713	0.65	2.017	0.93	0.1897	0.56	0.60	1125	26	1120	12	1121	13	0.45
020-ZR15	0.0371	21	0.0024	0.511	41840	28.74	0.07585	0.64	1.822	1.06	0.1742	0.75	0.71	1091	25	1035	14	1053	14	5.12
026-ZR18	0.0131	16	0.0036	0.832	118493	16.21	0.07702	0.58	2.042	0.96	0.1923	0.67	0.70	1122	23	1134	14	1130	13	-1.06
034-ZR24	0.0245	11	0.0019	1.302	63149	17.80	0.07677	0.79	1.944	1.13	0.1836	0.72	0.64	1115	31	1087	14	1096	15	2.56
035-ZR25	0.0247	13	0.0019	0.647	62730	17.77	0.07697	0.73	2.005	1.13	0.1889	0.78	0.69	1120	29	1115	16	1117	15	0.43
036-ZR26	0.0496	13	0.0010	0.651	31202	19.24	0.07712	1.04	2.007	1.41	0.1888	0.87	0.62	1124	41	1115	18	1118	19	0.87
039-ZR29	0.0211	12	0.0025	0.606	73284	19.80	0.07717	0.79	2.017	1.11	0.1895	0.68	0.61	1126	31	1119	14	1121	15	0.61
Data not used in calculating age																				
004-ZR1	0.0103	12	0.0042	0.739	149819	14.27	0.07630	0.39	2.049	0.84	0.1947	0.65	0.77	1103	16	1147	14	1132	11	-4.00
006-ZR3	0.0010	9	0.0068	0.810	1487396	83.34	0.07632	0.38	2.046	0.79	0.1944	0.59	0.74	1103	15	1145	12	1131	11	-3.79
013-ZR8	0.0199	14	0.0027	0.704	77685	18.06	0.07545	0.58	1.978	1.11	0.1901	0.87	0.78	1080	23	1122	18	1108	15	-3.86
019-ZR14	0.0238	15	0.0023	0.692	65025	20.32	0.07734	0.82	1.891	1.19	0.1773	0.77	0.65	1130	33	1052	15	1078	16	6.89
024-ZR16	0.0824	13	0.0005	0.474	18817	18.73	0.07575	1.38	1.741	2.13	0.1666	1.58	0.74	1089	55	993	29	1024	27	8.74
025-ZR17	0.0450	14	0.0012	0.585	34426	20.01	0.07591	1.06	2.004	1.40	0.1915	0.83	0.59	1093	42	1129	17	1117	19	-3.35
029-ZR21	0.0527	16	0.0012	0.520	29444	21.02	0.07461	1.40	1.795	1.89	0.1745	1.22	0.64	1058	56	1037	23	1044	25	1.98
038-ZR28	0.0298	9	0.0015	1.063	51868	18.27	0.07796	0.76	2.107	1.20	0.1960	0.85	0.71	1146	30	1154	18	1151	16	-0.69
Unused data due to high disagreement																				
009-ZR6	0.0105	10	0.0013	0.517	147769	51.69	0.07880	1.07	2.010	1.61	0.1850	1.14	0.71	1167	42	1094	23	1119	22	6.27
010-ZR7	0.0372	11	0.0011	0.579	41662	16.22	0.08170	1.40	2.201	1.80	0.1954	1.07	0.59	1238	54	1151	23	1181	25	7.08
014-ZR9	0.0292	14	0.0016	0.522	52989	17.34	0.07495	0.86	2.124	1.39	0.2055	1.03	0.74	1067	34	1205	23	1157	19	-12.91
033-ZR23	0.0497	11	0.0010	0.518	31186	16.87	0.08037	1.17	1.979	1.91	0.1786	1.46	0.77	1206	46	1059	29	1109	26	12.17
Unused data due to high analytical error																				
005-ZR2	0.0921	13	0.0005	0.282	16810	15.80	0.07778	2.81	2.060	3.89	0.1921	2.67	0.68	1141	110	1133	55	1136	53	0.74
016-ZR11	0.1582	14	0.0004	0.487	9793	19.80	0.07774	2.98	1.994	3.92	0.1860	2.52	0.64	1140	116	1100	51	1114	52	3.54
030-ZR22	0.0992	16	0.0003	0.545	15620	50.63	0.07862	3.33	1.994	4.90	0.1839	3.58	0.73	1163	129	1088	71	1113	65	6.39
037-ZR27	0.0787	10	0.0006	0.757	19668	14.79	0.07613	2.09	2.010	2.97	0.1914	2.08	0.70	1098	83	1129	43	1119	40	-2.80
Unused data due to high ²⁰⁴ Pb																				
008-ZR5	5.5895	62	0.0003	6.743	279	7.56	0.14985	8.71	1.568	12.52	0.0759	8.98	0.72	2344	284	472	81	958	150	79.88
027-ZR19	1.4869	225	0.0035	1.912	1040	5.72	0.09104	1.77	2.569	1.92	0.2046	0.65	0.34	1447	66	1200	14	1292	28	17.08
028-ZR20	19.9007	619	0.0005	2.298	78	16.84	0.09988	14.14	1.057	14.87	0.0767	4.58	0.31	1622	485	477	42	732	149	70.61

Table 5.5 - U-Pb analyses of zircon crystals of the TEC quartz-feldspar gneiss host rock (TEG-04).

CHRONUS		Version 2.0.0-alpha.3								Data for Wetherill plot ⁴					Ages ⁴					
Identifier	206* (%)	204Pb cps	206Pb mV ¹	Th/U	206Pb/204Pb	1s%	207Pb/206Pb	1s %	207Pb/235U	1s %	206Pb/238U	1s %	Rho	207Pb/ 206Pb	2s abs	206Pb/ 238U	2s abs	207Pb/ 235U	2s abs	% U-Pb disc ⁵
005-ZR02	0.0107	12	0.0045	0.493	140910	19.65	0.12392	0.48	6.813	0.92	0.3987	0.69	0.75	2013	17	2163	25	2087	16	-7.43
007-ZR04	0.0095	21	0.0085	0.699	159391	33.21	0.12578	0.54	6.633	0.87	0.3825	0.57	0.66	2040	19	2088	20	2064	15	-2.35
008-ZR05	0.0101	12	0.0045	0.494	150443	15.52	0.12443	0.59	6.668	0.93	0.3886	0.61	0.66	2021	21	2116	22	2068	16	-4.74
013-ZR08	0.0099	9	0.0036	0.492	153224	15.03	0.12431	0.66	6.751	1.05	0.3939	0.73	0.69	2019	23	2141	26	2079	18	-6.03
014-ZR09	0.0052	6	0.0055	0.560	289719	23.88	0.12420	0.44	6.950	0.95	0.4058	0.76	0.80	2017	15	2196	28	2105	17	-8.84
017-ZR12	0.0084	11	0.0051	0.820	179697	16.65	0.12391	0.45	6.532	0.94	0.3823	0.74	0.79	2013	16	2087	26	2050	17	-3.66
024-ZR16	0.0089	13	0.0043	0.503	170344	13.84	0.12477	0.60	6.378	0.97	0.3707	0.67	0.69	2026	21	2033	23	2029	17	-0.36
025-ZR17	0.0099	17	0.0054	0.501	153781	23.23	0.12500	0.46	6.475	0.86	0.3757	0.62	0.73	2029	16	2056	22	2043	15	-1.34
026-ZR18	0.0121	12	0.0042	0.447	125511	16.00	0.12479	0.46	6.530	0.88	0.3795	0.65	0.74	2026	16	2074	23	2050	15	-2.36
027-ZR19	0.0095	10	0.0045	0.484	159431	14.08	0.12511	0.45	6.620	0.84	0.3838	0.61	0.72	2030	16	2094	22	2062	15	-3.13
028-ZR20	0.0090	12	0.0050	0.560	168614	14.59	0.12405	0.59	6.344	0.99	0.3709	0.71	0.71	2015	21	2034	25	2025	17	-0.91
029-ZR21	0.0051	8	0.0078	0.728	300173	12.48	0.12516	0.68	6.492	1.02	0.3761	0.66	0.65	2031	24	2058	23	2045	18	-1.34
030-ZR22	0.0123	12	0.0047	0.440	123268	17.88	0.12536	0.77	6.664	1.09	0.3855	0.68	0.62	2034	27	2102	24	2068	19	-3.35
033-ZR23	0.0096	11	0.0051	0.439	158536	16.17	0.12586	0.59	6.637	0.99	0.3824	0.70	0.71	2041	21	2088	25	2064	17	-2.29
034-ZR24	0.0109	15	0.0042	0.448	138642	15.46	0.12548	0.54	6.479	0.90	0.3745	0.62	0.69	2036	19	2050	22	2043	16	-0.73
035-ZR25	0.0131	14	0.0029	0.483	115593	13.31	0.12423	0.72	6.678	1.08	0.3898	0.72	0.66	2018	25	2122	26	2070	19	-5.17
036-ZR26	0.0134	10	0.0025	0.830	112724	13.92	0.12470	0.69	7.198	1.24	0.4186	0.96	0.77	2025	24	2254	36	2136	22	-11.34
037-ZR27	0.0115	17	0.0034	0.479	132395	12.96	0.12306	0.60	5.907	0.99	0.3481	0.69	0.70	2001	21	1926	23	1962	17	3.77
038-ZR28	0.0135	11	0.0033	0.427	112087	21.86	0.12421	0.63	6.455	1.03	0.3769	0.73	0.71	2018	22	2062	26	2040	18	-2.19
039-ZR29	0.0130	16	0.0043	0.505	116374	18.11	0.12447	0.73	6.534	1.09	0.3807	0.72	0.66	2021	26	2079	26	2050	19	-2.88
Data not used in calculating age																				
004-ZR01	0.0079	18	0.0051	0.516	191510	36.11	0.12335	0.53	6.579	0.90	0.3868	0.63	0.69	2005	19	2108	22	2056	16	-5.12
006-ZR03	0.0166	14	0.0038	0.490	91126	20.85	0.12320	0.49	6.617	0.86	0.3895	0.60	0.70	2003	18	2121	22	2062	15	-5.86
009-ZR06	0.0158	11	0.0029	0.536	96251	17.21	0.12283	0.75	6.174	1.12	0.3645	0.75	0.67	1998	26	2004	26	2001	20	-0.30
015-ZR10	0.0085	10	0.0043	0.476	178230	14.97	0.12293	0.78	6.576	1.25	0.3879	0.90	0.72	1999	28	2113	32	2056	22	-5.70
018-ZR13	0.0220	10	0.0018	0.493	68972	13.30	0.12624	0.85	6.372	1.36	0.3660	0.99	0.73	2046	30	2011	34	2028	24	1.73
019-ZR14	0.0260	10	0.0015	0.552	58449	17.54	0.12460	1.20	6.397	1.68	0.3723	1.12	0.66	2023	42	2040	39	2032	29	-0.85
Unused data due to high disagreement																				
010-ZR07	0.0438	56	0.0030	0.502	34765	35.27	0.11925	1.16	5.722	1.51	0.3480	0.89	0.59	1945	41	1925	30	1935	26	1.04
Unused data due to high analytical error																				
016-ZR11	0.0163	13	0.0036	0.479	92487	27.21	0.12517	0.85	7.118	1.90	0.4124	1.66	0.87	2031	30	2226	62	2126	34	-9.59
020-ZR15	0.0413	9	0.0009	0.495	36664	17.55	0.12560	1.88	6.779	2.71	0.3915	1.91	0.71	2037	66	2130	69	2083	47	-4.53

Table 5.6 - Lu-Hf isotopes on zircon crystals of the TEC rocks dated by the U-Pb method.

Sample/ spot	CHUR		DM		Sample (present-day ratios)				Sample (initial ratios)				Crust Model	Ages (Ga)	T _{DM} (Hf)
	U-Pb Age (Ma)	±2s (t)	¹⁷⁶ Hf/ ¹⁷⁷ Hf	¹⁷⁶ Hf/ ¹⁷⁷ Hf	¹⁷⁶ Hf/ ¹⁷⁷ Hf	±2SE	¹⁷⁶ Lu/ ¹⁷⁷ Hf	±2SE	¹⁷⁶ Hf/ ¹⁷⁷ Hf	epsilon Hf	±2SE	Mafic source	Felsic source	(Ga)	
TEG-01 (dolomite metacarbonate)															
003-ZR1	1110	19.94345959	0.282075	0.282431	0.282157	0.000061	0.000306	0.000001	0.282150	2.66	0.1				1.50
004-ZR5	1110	26.74874367	0.282073	0.282428	0.282108	0.000063	0.000227	0.000004	0.282103	1.06	0.0				1.56
005-ZR14	1110	7.433896573	0.282079	0.282435	0.282074	0.000104	0.000423	0.000001	0.282066	-0.49	0.0				1.62
006-ZR15	1110	11.33367108	0.282086	0.282443	0.282159	0.000048	0.000187	0.000001	0.282155	2.45	0.0				1.49
007-ZR17	1110	17.31528099	0.282081	0.282437	0.282141	0.000047	0.000286	0.000010	0.282135	1.91	0.1				1.52
008-ZR18	1110	8.856156456	0.282084	0.282441	0.282163	0.000063	0.000403	0.000010	0.282155	2.50	0.1				1.50
010-ZR24	1110	9.911857456	0.282085	0.282442	0.282136	0.000061	0.000259	0.000003	0.282131	1.61	0.0				1.53
TEG-04 (host rock gneiss)															
003-ZR7	2022.5	41.03251596	0.281542	0.281815	0.281344	0.000029	0.000039	0.000001	0.281343	-7.10	0.3	3.43	2.82	2.57	
004-ZR6	2022.5	26.47176022	0.281508	0.281776	0.281340	0.000029	0.000047	0.000001	0.281338	-6.03	0.3	3.37	2.80	2.58	
005-ZR13	2022.5	29.99181676	0.281477	0.281739	0.281337	0.000031	0.000033	0.000002	0.281335	-5.02	0.3	3.32	2.79	2.58	
006-ZR14	2022.5	42.26253472	0.281492	0.281756	0.281354	0.000027	0.000042	0.000001	0.281352	-4.94	0.2	3.30	2.77	2.56	
007-ZR16	2022.5	21.25526654	0.281490	0.281755	0.281337	0.000031	0.000046	0.000001	0.281335	-5.49	0.2	3.35	2.80	2.58	
008-ZR17	2022.5	16.17364698	0.281488	0.281752	0.281302	0.000033	0.000039	0.000000	0.281301	-6.66	0.1	3.45	2.86	2.63	
009-ZR20	2022.5	20.77189793	0.281497	0.281762	0.281366	0.000029	0.000052	0.000002	0.281364	-4.73	0.3	3.27	2.75	2.54	
010-ZR21	2022.5	23.93470321	0.281486	0.281750	0.281310	0.000036	0.000037	0.000000	0.281308	-6.33	0.1	3.42	2.85	2.62	
TEG-05 (metasyenite)															
003-ZR2	1123	109.8921862	0.282061	0.282414	0.282143	0.000072	0.000701	0.000027	0.282128	2.35	0.3				1.53
004-ZR4	1123	26.00773998	0.282072	0.282426	0.282098	0.000075	0.001335	0.000016	0.282070	-0.08	0.0				1.62
005-ZR6	1123	42.08244649	0.282045	0.282395	0.282125	0.000112	0.001042	0.000016	0.282102	2.05	0.1				1.57
006-ZR13	1123	25.70559064	0.282072	0.282427	0.282179	0.000053	0.001159	0.000006	0.282155	2.93	0.1				1.50
008-ZR11	1123	116.3811958	0.282062	0.282415	0.282167	0.000044	0.000117	0.000001	0.282165	3.64	0.4				1.48
009-ZR18	1123	23.14905275	0.282074	0.282429	0.282275	0.000098	0.001860	0.000118	0.282235	5.72	0.5				1.40
010-ZR17	1123	42.25618656	0.282092	0.282450	0.282137	0.000062	0.000811	0.000019	0.282120	0.97	0.1				1.55
013-ZR26	1123	41.28767988	0.282072	0.282427	0.282182	0.000063	0.001357	0.000014	0.282154	2.88	0.1				1.51
014-ZR28	1123	30.05685421	0.282058	0.282411	0.282137	0.000072	0.000571	0.000005	0.282125	2.36	0.1				1.54

5.5.2. WHOLE-ROCK Nd AND Sr ISOTOPES

Nd and Sr isotope compositions of 15 whole-rock samples are given in **Tables 5.7** and **5.8**. Samples of calcite metacarbonatite (7), dolomite metacarbonatite (4), metaultramafic rocks (2), metasyenite (1) and the country rock gneiss (1) were analyzed.

The $\epsilon_{\text{Nd}}(t)$ and $\epsilon_{\text{Sr}}(t)$ values, calculated for $t=1,110$ Ma in the case of dolomite metacarbonatite samples, vary between 0.14 and 0.55 for $\epsilon_{\text{Nd}}(t)$ and between -0.53 and 9.49 for $\epsilon_{\text{Sr}}(t)$. The same age was used to calculate $\epsilon_{\text{Nd}}(t)$ and $\epsilon_{\text{Sr}}(t)$ for calcite metacarbonatite and metaultramafic rocks, as a function of their field relationships. Calcite metacarbonatite samples showed $\epsilon_{\text{Nd}}(t)$ ranging from -0.37 to 4.44 and metaultramafic rocks yielded $\epsilon_{\text{Nd}}(t)$ between 0.96 and 2.42. The $\epsilon_{\text{Sr}}(t)$ values for the same rocks are dominantly negative and vary between -5.16 and 10.69 for the calcite metacarbonatite samples and from -15.05 to -4.11 for the metaultramafic rocks. The $\epsilon_{\text{Nd}}(t)$ and $\epsilon_{\text{Sr}}(t)$ values obtained for the metasyenite were -0.58 and -3.95, respectively, for $t=1,123$ Ma.

Table 5.7 - Sm-Nd isotopes from TEC rocks.

Sample	Rock	Sm _{ID} (ppm)	Nd _{ID} (ppm)	147Sm/ 144Nd	143Nd/144Nd ± 2SE (measured)	143Nd/144Nd ± 2SE (initial)	ϵ_{Nd} (0)	ϵ_{Nd} (t) ^a	Age (Ga) U-Pb	T _{DM} (Ga)
TEG-01	Dolomite metacarbonatite	40.713	201.960	0.1219	0.512100+/-19	0.511212+/-19	-10.49	0.14	1.11	1.55
TEG-02	Calcite metacarbonatite	32.818	193.036	0.1028	0.512141+/-17	0.511392+/-17	-9.69	3.67	1.11	1.23
TEG-03	Metaultramafic	30.718	146.535	0.1267	0.512252+/-19	0.511329+/-19	-7.53	2.42	1.11	1.37
TEG-04	Intermediate gneiss (host rock)	3.242	22.166	0.0884	0.511159+/-17	0.509982+/-17	-28.85	-0.72	2.023	2.28
TEG-05	Metasyenite	4.947	27.927	0.1071	0.511948+/-14	0.511159+/-14	-13.45	-0.58	1.123	1.55
TEG-07	Calcite metacarbonatite	33.830	190.688	0.1072	0.512200+/-11	0.511419+/-11	-8.54	4.18	1.11	1.20
TEG-08	Metaultramafic	100.854	483.371	0.1261	0.512173+/-26	0.511254+/-26	-9.06	0.96	1.11	1.50
TEG-11	Calcite metacarbonatite	5.593	30.697	0.1101	0.512021+/-9	0.511219+/-9	-12.03	0.27	1.11	1.49
TEG-12	Calcite metacarbonatite	65.545	333.594	0.1188	0.512172+/-19	0.511307+/-19	-9.09	1.99	1.11	1.39
TEG-13	Calcite metacarbonatite	75.829	349.690	0.1311	0.512274+/-9	0.511319+/-9	-7.10	2.23	1.11	1.41
TEG-14	Dolomite metacarbonatite	54.147	235.672	0.1389	0.512239+/-4	0.511227+/-4	-7.78	0.43	1.11	1.62
TEG-15	Dolomite metacarbonatite	42.022	223.259	0.1138	0.512062+/-12	0.511233+/-12	-11.24	0.55	1.11	1.48
TEG-16	Calcite metacarbonatite	62.994	339.211	0.1123	0.512004+/-16	0.511186+/-16	-12.36	-0.37	1.11	1.55
TEG-17	Calcite metacarbonatite	81.666	491.401	0.1005	0.512164+/-16	0.511432+/-16	-9.25	4.44	1.11	1.18
TEG-18	Dolomite metacarbonatite	19.125	95.657	0.1209	0.512104+/-6	0.511223+/-6	-10.41	0.36	1.11	1.53

ID – Isotopic dilution.

^a Calculation of $\varepsilon_{\text{Nd}}(t)$ based on DePaolo (1988). $\varepsilon_{\text{Nd}}(t) = [(\frac{^{143}\text{Nd}}{^{144}\text{Nd}_{(i)}}/\frac{^{143}\text{Nd}}{^{144}\text{Nd}_{\text{CHUR}(T)}})-1]*10000$. ^{147}Sm decay constant (λ_{Sm}) of $6.54 \times 10^{-12} \text{ yr}^{-1}$. Constants $^{143}\text{Nd}/^{144}\text{Nd}_{\text{CHUR}} = 0.512638$ and $^{147}\text{Sm}/^{144}\text{Nd}_{\text{CHUR}} = 0.1967$ (Hamilton *et al.*, 1983).

Nd model ages (T_{DM}) calculated for the same ages mentioned above vary between 1.18 and 1.55 Ga for calcite metacarbonatite samples, between 1.48 and 1.62 Ga for dolomite metacarbonatite samples and between 1.37 and 1.50 Ga for the metaultramafic rocks. The metasyenite sample yielded an Nd model age (T_{DM}) of 1.55 Ga.

Table 5.8 - Rb-Sr data from TEC rocks.

Sample	Rock	Rb _{CA} (ppm)	Sr _{CA} (ppm)	⁸⁷ Rb/ ⁸⁶ Sr	⁸⁷ Sr/ ⁸⁶ Sr ± 2SE (measured)	⁸⁷ Sr/ ⁸⁶ Sr ± 2SE (initial)	$\varepsilon_{\text{Sr}}(0)$	$\varepsilon_{\text{Sr}}(t)$ ^b	Age (Ga) U-Pb
TEG-01	Dolomite metacarbonatite	28.4	3400	0.0242	0.703550+/-10	0.703174+/-11	-13.48	-0.20	1.11
TEG-02	Calcite metacarbonatite	3.4	3380	0.0029	0.702870+/-10	0.702825+/-10	-23.14	-5.16	1.11
TEG-03	Metaultramafic	34.50	789	0.1265	0.704100+/-10	0.702130+/-22	-5.68	-15.05	1.11
TEG-04	Intermediate gneiss (host rock)	20.70	1255	0.0477	0.705450+/-10	0.704087+/-17	13.48	28.39	2.023
TEG-05	Metasyenite	82.90	2270	0.1056	0.704560+/-10	0.702895+/-19	0.85	-3.95	1.123
TEG-07	Calcite metacarbonatite	5.20	5480	0.0027	0.703140+/-10	0.703097+/-10	-19.30	-1.29	1.11
TEG-08	Metaultramafic	10.70	908	0.0341	0.703430+/-10	0.702899+/-11	-15.19	-4.11	1.11
TEG-11	Calcite metacarbonatite	2.80	5560	0.0015	0.703540+/-10	0.703517+/-10	-13.63	4.69	1.11
TEG-12	Calcite metacarbonatite	25.50	4280	0.0172	0.703110+/-10	0.702842+/-10	-19.73	-4.92	1.11
TEG-13	Calcite metacarbonatite	7.30	3730	0.0057	0.703190+/-10	0.703102+/-10	-18.59	-1.22	1.11
TEG-14	Dolomite metacarbonatite	0.70	3250	0.0006	0.703160+/-20	0.703150+/-20	-19.02	-0.53	1.11
TEG-15	Dolomite metacarbonatite	2.80	5010	0.0016	0.703880+/-10	0.703855+/-10	-8.80	9.49	1.11
TEG-16	Calcite metacarbonatite	16.00	5600	0.0083	0.703290+/-10	0.703161+/-10	-17.18	-0.38	1.11
TEG-17	Calcite metacarbonatite	20.40	3400	0.0174	0.704210+/-10	0.703940+/-10	-4.12	10.69	1.11
TEG-18	Dolomite metacarbonatite	1.00	6310	0.0005	0.703510+/-10	0.703503+/-10	-14.05	4.48	1.11

CA – Rb and Sr concentrations determined by ICP-MS.

^b Calculation of $\varepsilon_{\text{Sr}}(t)$ based on Papanastassiou & Wasserburg (1969). $\varepsilon_{\text{Sr}}(t) = [(\frac{^{87}\text{Sr}}{^{86}\text{Sr}_{(i)}}/\frac{^{87}\text{Sr}}{^{86}\text{Sr}_{\text{BSE}(T)}})-1]*10000$. ^{87}Rb decay constant (λ_{Rb}) of $1.393 \times 10^{-11} \text{ yr}^{-1}$. Constant $^{87}\text{Sr}/^{86}\text{Sr}_{\text{BSE}(0)} = 0.7045$ e $^{87}\text{Rb}/^{86}\text{Sr}_{\text{BSE}(0)} = 0.0842$ (DePaolo & Wasserburg, 1976).

5.6. DISCUSSION

5.6.1. AGE OF CARBONATITE MAGMATISM IN THE SUL-RIOGRANDENSE SHIELD

A Mesoproterozoic age is proposed for the Três Estradas complex based on the U-Pb zircon ages determined for samples of dolomite metacarbonatite ($1,110 \pm 4.8$ Ma) and metasyenite ($1,123 \pm 15$ Ma) samples. All analyzed zircon crystals provided Mesoproterozoic

ages, except for one crystal with Paleoproterozoic age (2,089 Ma) in the dolomite metacarbonatite sample, which is interpreted as inherited from the country rocks. Therefore, the Mesoproterozoic age obtained in this study represents the crystallization age of the TEC rocks.

The TEC complex is emplaced in the Paleoproterozoic rocks of the Santa Maria-Chico Granulitic Complex, with a U-Pb zircon age of $2,022.5 \pm 7.9$ Ma. This age is similar, within uncertainty, with the ages of metamorphism reported by Hartmann *et al.* (2008) as $2,035 \pm 9$ Ma and $2,006 \pm 3$ Ma and by Girelli *et al.* (2018) as $2,055 \pm 55$ Ma for these rocks.

The similarity between the TEC and the Picada dos Tocos carbonatite is mentioned by Monteiro *et al.* (2016), Cerva-Alves *et al.* (2017), Anzolin *et al.* (2019) and Laux *et al.* (2019). However, different ages were obtained by zircon U-Pb dating in rocks of both carbonatite complexes.

Cerva-Alves *et al.* (2017) obtained U-Pb zircon ages of 603 ± 4.5 Ma for the Picada dos Tocos carbonatite using only 4 zircon crystals among 8 analyzed in total. Besides, zircon crystals older than 621 Ma were not found by the authors.

The Picada dos Tocos carbonatite is intrusive in metavolcano-sedimentary rocks attributed to the Passo Feio Complex. Remus *et al.* (2000) proposed a Neoproterozoic age and complex sedimentary provenance with Archean, Paleoproterozoic, Mesoproterozoic (only 1 grain) and Neoproterozoic detrital zircon grains for the Passo Feio Complex. Lopes (2014) dated four metasedimentary rock samples from the same unit and identified 4 populations of detrital zircon crystals with U-Pb ages ranging between 803 and 3,637 Ma. Their PF-03 sample, located near the Passo Feio carbonatite intrusion, is a garnet-staurolite-muscovite-biotite schist with detrital U-Pb zircon ages between 803 ± 43 Ma and $3,054 \pm 10$ Ma, with a peak at 850 Ma. Therefore, the Passo Feio carbonatite should have an Upper Neoproterozoic age. Cerva-Alves *et al.* (2017) interpreted the age of 603.2 ± 4.5 Ma of the Picada dos Tocos carbonatite in the context of post-collisional Ediacaran environment, with dominant transpressive tectonism and magmatism marked by shoshonitic affinity.

Laux *et al.* (2019) performed 16 analyses on 8 zircon crystals, all with corroded edges, and obtained a concordant age of ca. 233 Ma for the Três Estradas metacarbonatite by the U-Pb zircon method. However, there is no record of a ductile tectonic process after the agglutination of the Gondwana supercontinent, which occurred around 540 Ma (e.g. Chemale

Jr., 2000). An alternative to justify this age would be a new carbonatite intrusion into an older, probably Mesoproterozoic intrusive complex. However, so far, there is no evidence of such a process.

Based on all the data, it is possible to conclude that the Três Estradas, Picada dos Tocos, Passo Feio, and Santa Clara carbonatites are compositionally and texturally very similar, but may result from different carbonatite magmatic events that took place in the SRS at different times, probably taking advantage of deep fault zones. The Joca Tavares and Porteira carbonatites also may represent a distinct event of emplacement. The recurrence of carbonatite activity in the same area is recorded globally, such as in the Kola Province (Russia and Finland), in the Ontario and SW Quebec regions (Canada), and in the East African Rift system (Woolley & Bailey, 2012).

5.6.2. GENESIS AND EVOLUTION OF TEC

Currently, the most accepted hypothesis based on radiogenic (Sr, Nd and Pb) and stable isotope evidence (C and O) suggests that carbonatites are derived ultimately from deep asthenospheric mantle sources (Bell & Tilton, 2001; Bell *et al.*, 2004). Indeed, the Nd and Sr isotope signatures of carbonatites and oceanic island basalts (OIB) are comparable, suggesting mantle sources with similar evolutions (Bell & Blenkinsop, 1989). However, the lithospheric mantle plays a crucial role in the genesis of carbonatite magmas, especially within the continental lithosphere (Woolley & Bailey, 2012).

The isotopes and geochronological data obtained in this study indicate that TEC is an alkaline-carbonatite complex, originally composed of calcite and dolomite carbonatites, alkaline ultramafic rocks and syenites, all genetically related. $\epsilon_{\text{Nd}}(t)$ and $^{87}\text{Sr}/^{86}\text{Sr}$ show that only slight differences occur between metacarbonatites and metaultramafic rocks (**Figure 5.11**), supporting the interpretation that these rocks are cogenetic and probably derived from the same parental magma. The close spatial and temporal relationships observed between carbonatites and alkaline silicate rocks worldwide strongly indicates that carbonatites are intimately associated with alkaline silicate magmas (Gittins, 1989; Winter, 2001). Furthermore, the genesis of carbonated silicate magmas is the result of variations in temperature, in pressure and/or in the contents of H_2O and CO_2 (and other volatiles such as S, F and Cl) in the mantle (Winter, 2001). Therefore, it is suggested that the parental magma that gave rise to the TEC is

derived from partial melting of either the metasomatized SCLM (sub-continental lithospheric mantle) or the enriched asthenosphere beneath the SRS.

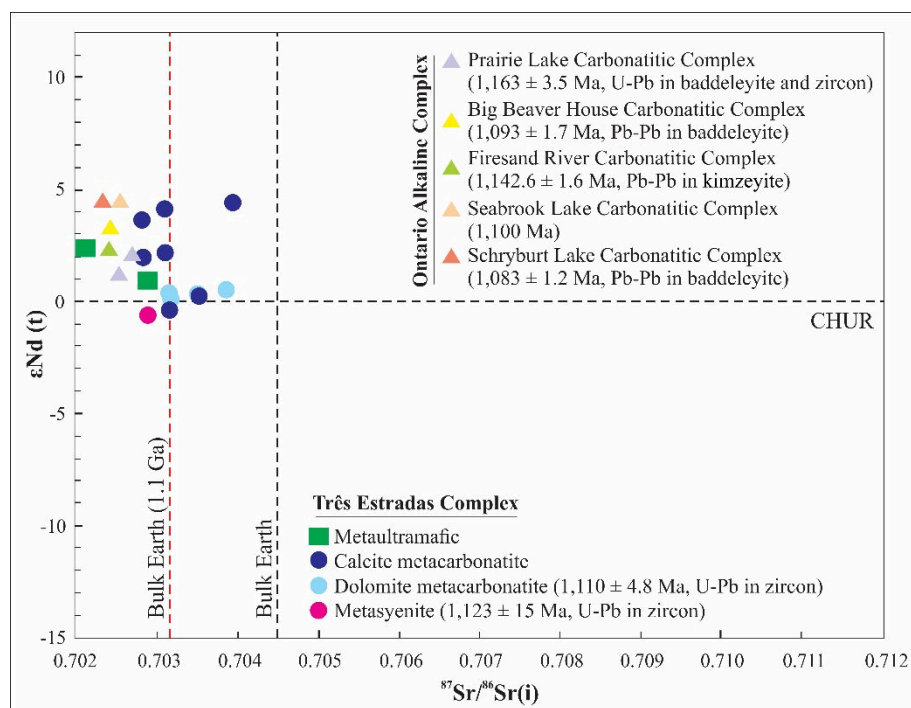


Figure 5.11 - $\epsilon_{\text{Nd}}(t)$ versus $^{87}\text{Sr}/^{86}\text{Sr}_{(\text{i})}$ for metacarbonatites, metaultramafic rocks and metasyenite from the TEC complex. Also plotted are the isotope compositions of Mesoproterozoic Canadian carbonatites (Rukhlov & Bell, 2010; Bell & Blenkinsop, 1987). Bulk Earth composition from Rollinson (1993).

Carbonatites derive from magmas extremely enriched in incompatible elements, including very low Sm/Nd ratios (Andersen, 1987). However, the positive $\epsilon_{\text{Nd}}(t)$ values seem to be contradictory with the trace elements contents since it should reflect a depleted mantle source (Andersen, 1987; Kogarko *et al.*, 2010). Even extremely low partial melting rates of a depleted mantle source cannot explain such contradiction, and then, mantle metasomatism is required (Kogarko *et al.*, 2010). But, such metasomatism should occur a short time before magma generation otherwise the isotopic signature of the depleted source will be significantly changed by the low Sm/Nd ratios from the metasomatic fluids or melts (Roden & Murty, 1985; Andersen, 1987; Kogarko *et al.*, 2010). Therefore, positive $\epsilon_{\text{Nd}}(t)$ values suggest that the difference between the ages of the events that generated the mantle metasomatism and the partial melting of the source for the generation of the parental magma of the TEC carbonatites was relatively short.

The negative correlation between the $\epsilon_{\text{Nd}}(t)$ values and the Nd model ages (T_{DM} values) may indicate minor contamination by the continental crust, which is corroborated by the

occasional occurrence of zircon xenocrysts inherited from the country rocks (**Figure 5.12**). However, binary mixing modelling (**Figure 5.13**) required between 30 and 80% of crustal contamination with the local Paleoproterozoic gneisses to explain the Nd-Sr isotope signatures in the TEC. Therefore, although one inherited zircon crystal attests to some wall-rock assimilation, the unlikely high contamination rates indicate that most of the Nd-Sr isotope variations in the rocks of TEC may reflect a heterogeneous mantle source.

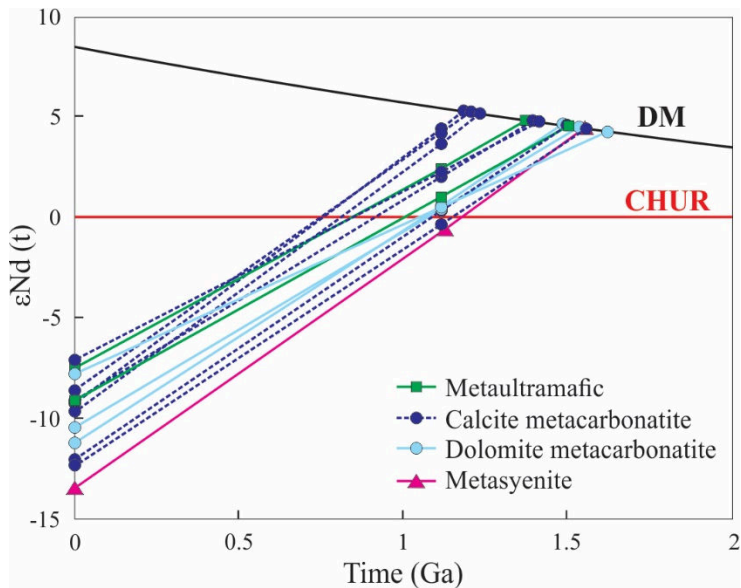


Figure 5.12 - Nd isotope evolution versus time for the TEC rocks.

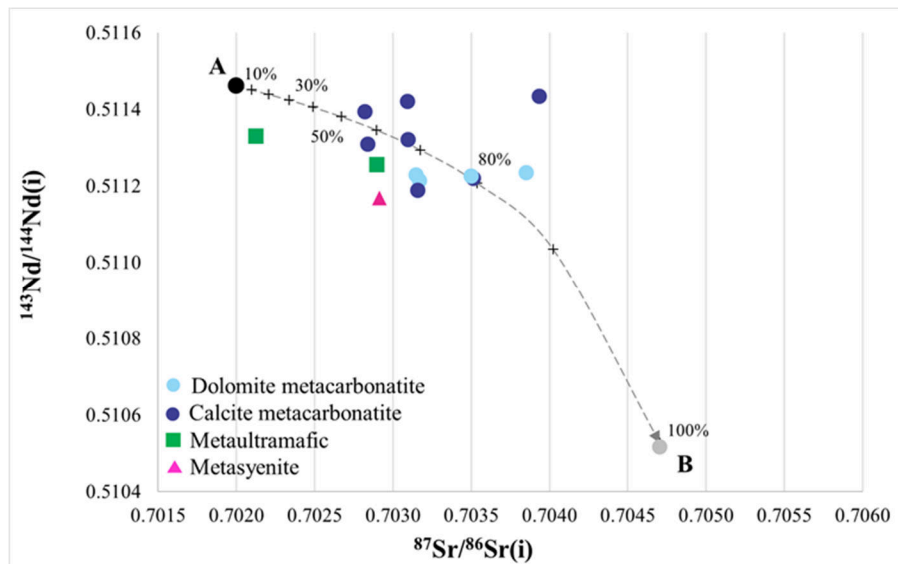


Figure 5.13 - Simple binary mixing modelling showing that the Nd and Sr isotope variations in the TEC complex probably reflects a heterogeneous mantle source signature, possibly with some minor contamination of older continental crust. A - A hypothetical parental magma with 3800 ppm Sr and 238 ppm Nd (average of the TEC rocks); B - Nd and Sr isotope compositions of the country-rock gneiss (TEG-04) calculated at 1.1 Ga. The mixture curve was calculated using well-known equations of mixtures of two components as in Faure (2001).

The TEC parental magma is derived from an isotopically depleted mantle source in terms of Sm-Nd and slightly depleted in terms of Rb-Sr (**Figure 5.11**). Similar variations in $\epsilon\text{Nd(t)}$ values, but with slightly lower $^{87}\text{Sr}/^{86}\text{Sr}$ ratios, were observed in the Mesoproterozoic Canadian carbonatites (1.2 and 1.0 Ga), suggesting a possible correlation between these carbonatites and the TEC. The range of ϵNd values obtained for TEC metacarbonatites is also similar to the Bull's Run carbonatite in South Africa (Ashwal *et al.*, 2016) and the Bayan Obo carbonatite in China (Yang *et al.*, 2011). This implies that the mantle sources of all these carbonatite complexes were depleted, possibly due to previous magma extraction events in the mantle. In contrast, the carbonatite complexes of Spitskop in South Africa (Harmer, 1999), Newania in India (Ray *et al.*, 2013) and Cummins Range in Australia (Downes *et al.*, 2016) were derived from much more enriched sources, despite the comparable ages with TEC (**Figure 5.14**). Nd and Sr isotope signature similar to the TEC has also been reported for other Proterozoic carbonatites of different ages, such as Planalto da Serra in Brazil, Saint Honoré, Burritt Island, Iron Island and Spanish River in Canada and Siilinjärvi in Finland, in contrast to Angico dos Dias in Brazil.

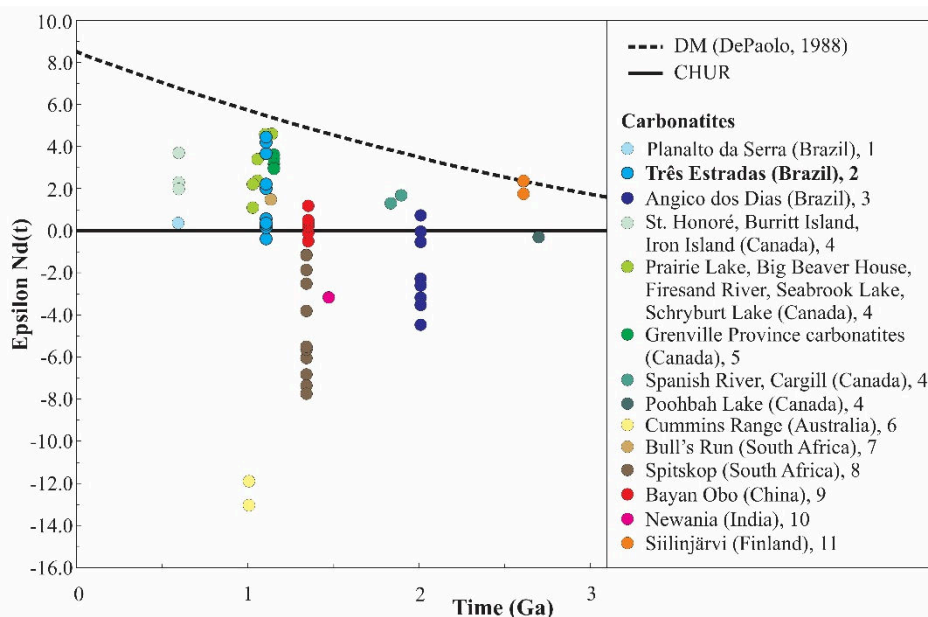


Figure 5.14 - $\epsilon\text{Nd(t)}$ variation for different Proterozoic carbonatites in the world. Sources of data: 1 - De Min *et al.* (2013); 2 - This work; 3 - Antonini *et al.* (2003); 4 - Bell & Blenkinsop (1987); 5 - Moecher *et al.* (1997); 6 - Downes *et al.* (2016); 7 - Ashwal *et al.* (2016); 8 - Harmer (1999); 9 - Yang *et al.* (2011); 10 - Ray *et al.* (2013); 11 - Tichomirowa *et al.* (2006).

The Sr evolution lines suggest at least two distinct mantle sources for the Canadian and Fennoscandia carbonatites (**Figure 5.15**), one depleted and the other enriched, with intermittent

mixing between them along with 3.0 Ga (Bell & Simonetti, 2010). Interestingly, the Sr isotope ratios of the TEC metacarbonatites vary in a similar range of the Canadian and Fennoscandia carbonatites. Therefore, the resemblance of Sr isotope signatures between the TEC and the Mesoproterozoic Canadian carbonatites also suggest a possible correlation, such as noted for the Nd isotopes.

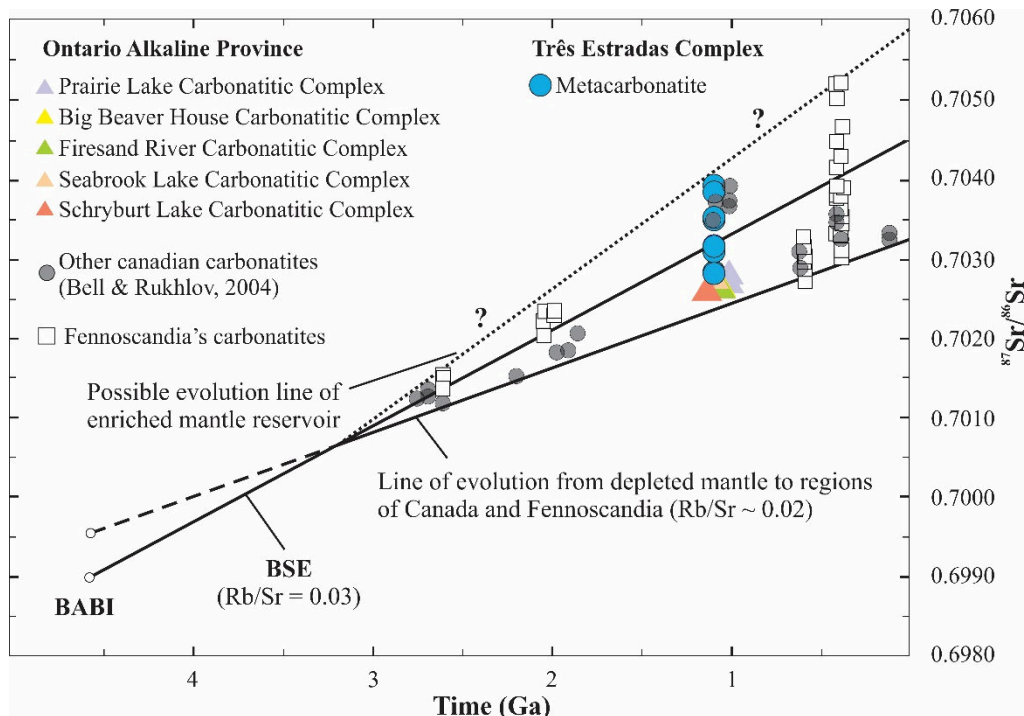


Figure 5.15 - $^{87}\text{Sr} / ^{86}\text{Sr}$ ratio variation versus time for the Canadian, Fennoscandian and TEC carbonatites (Modified from Bell & Simonetti, 2010).

Dominantly positive $\epsilon\text{Hf}(t)$ values on zircon (the same crystals used for U-Pb age determination) for metacarbonatite and metasyenite also indicates a depleted mantle source, corroborating the Nd and Sr isotope data. Variations in the Hf isotope compositions, like in the Nd isotopes, may indicate a heterogeneous source or some minor interaction between the magma and the country rocks (**Figure 5.16**). Negative ϵHf values from zircon crystals of the host gneiss suggest a crustal source for these rocks (**Table 5.6**).

Based on the Nd, Sr and Hf isotope evidence, we suggest that the TEC almost certainly derived from a parental carbonated silicate magma originated by partial melting of a heterogeneous metasomatized mantle source during the Mesoproterozoic, remarkably isotopically similar to Canadian carbonatites. The TEC complex emplaced along a deep crustal-scale fault zone with a minimum Mesoproterozoic age, coinciding with the Cerro dos Cabritos

Transcurrent Shear Zone and probably reactivated in the Neoproterozoic. Heterogeneous deformation and greenschist to amphibolite facies metamorphism are identified, but ages were not defined. The folding and faulting of the Três Estradas Carbonatite may be related to deformation generated in the final stages of the agglutination of Rodinia, in Mesoproterozoic, or to one of the three major deformational events: the Passinho Event at 900 Ma (Hartmann *et al.*, 2000), the São Gabriel Event (750-690 Ma) or the Dom Feliciano Event (640-590 Ma) (Chemale Jr., 2000).

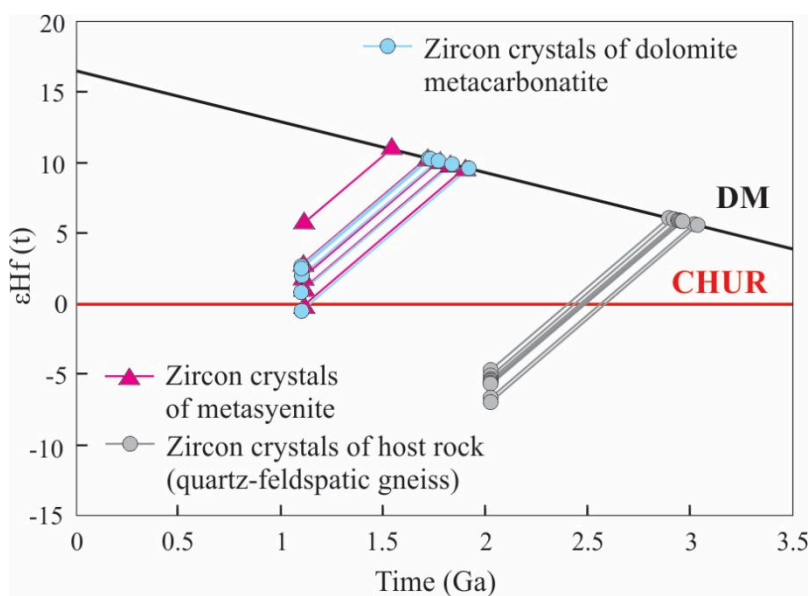


Figure 5.16 - ϵHf vs. time for the TEC complex and its host rocks.

5.6.3. IMPLICATIONS FOR THE GEOTECTONIC EVOLUTION OF THE SUL-RIOGRANDENSE SHIELD

All carbonatites in the SRS, including the TEC complex, are situated next to two deep shear zones. The Ibaré Lineament is a dextral transcurrent fault that separates the Archean-Paleoproterozoic Taquarembó Terrane, considered as a fragment of the Rio de la Plata Craton, from the Neoproterozoic São Gabriel Terrane, which represents a juvenile arc accretion (Hartmann *et al.*, 2007, 2008). The Caçapava do Sul shear zone system represents the boundary between the São Gabriel Terrane and the Neoproterozoic Tijucas Terrane, located toward the east of this fault system (Chemale Jr., 2000) (Figure 5.2). According to Chemale Jr. (2000), at the end of the Mesoproterozoic, the SRS probably behaved as a stable cratonic block for the Greenville or Kibaran orogenesis (1.2-1.0 Ga). These compressional events have been

identified in adjacent geotectonic terranes such as in the Sierra Pie de Palo region (Argentina), and in the Namaqualand and Natal mobile belts (South Africa). The paleogeographic reconstruction proposed by Li *et al.* (2008) suggests that the Kalahari Craton joined Laurentia and the Rio de la Plata Craton only after 1,050 Ma.

The carbonatite magmatism of the TEC at the end of the Mesoproterozoic suggests an extensional event in the Rio de la Plata Craton at approximately 1.11 Ga (**Figure 5.17A**). Hartmann *et al.* (2019) recorded the first occurrences of ophiolites originating in the Proto-Adamastor Ocean (named Charrua Ocean by Fragoso César (1991), Chemale Jr. (2000) and Philipp *et al.* (2016)) at 920 Ma (**Figure 5.17B**). Hartmann *et al.* (2019) proposed that such proto-ocean marked the rifting of the Rodinia supercontinent in the SRS region and the separation of the Rio de la Plata and Kalahari cratons. This hypothesis is corroborated by Arena *et al.* (2016) that registered U-Pb ages of 923 ± 3 Ma and 892 ± 3 M in the Cerro Mantiqueiras ophiolite and Ibaré ophiolite zircon crystals, respectively. However, Fragoso-César (1991), Chemale Jr. (2000), and Philipp *et al.* (2016) considered that such interpretation is not supported by evidence at the Kalahari Craton. The oldest rift-related dykes (Gannakouriep dykes) in the Kalahari Craton were dated at 833 ± 2 Ma (Frimmel *et al.*, 2001) and the rift to drift transition (i.e. generation of oceanic crust) only started at 740 Ma (Gaucher *et al.*, 2009). Philipp *et al.* (2016) suggested that another block, rather than the Kalahari Craton, should be involved and suggest that it could be the Nico Pérez Terrane (or part of it), which is represented in the SRS by the Encantadas Microcontinent.

After 920 Ma, the generation and growth of the oceanic crust gave rise to the development of subduction zones between 880 and 750 Ma, building up an oceanic island arc represented by the Passinho Arc, and oceanic to continental arcs, between 750 and 700 Ma, which together comprise the São Gabriel Terrane (Hartmann *et al.*, 2007, 2008) (**Figure 5.17C**). Between 700 and 680 Ma, the São Gabriel Terrane was added to the passive margin of the Rio de la Plata Craton (**Figure 5.17D**). The intrusions of late-tectonic granites and the formation of a new magmatic arc, represented in the SRS by the Pelotas Batholith (Hartmann *et al.*, 2007, 2008), which is considered part of the larger Arachania paleocontinent, took place between ca. 670 and 530 Ma (Gaucher *et al.*, 2009; Basei *et al.*, 2011; Frimmel *et al.*, 2011; Will *et al.*, 2019) (**Figure 5.17D**). Between 650 and 630 Ma, intense syn-tectonic calc-alkaline magmatism, as well as the peak of metamorphism, occurred in the Pelotas Batholith. The

development of the Ibaré, Caçapava do Sul and Dorsal de Canguçu deep shear zones also occurred at the time (Philipp *et al.*, 2016; Will *et al.*, 2009) (**Figure 5.17E**).

The final orogenetic stages of the SRS evolution took place between 630 to 540 Ma. This period was marked by late to post-orogenic magmatism and the establishment of the suture zones (Chemale Jr., 2000) (**Figure 5.17F**). Between 615 and 610 Ma, felsic alkaline magmatism represented by the Piquiri Syenite was recorded in the Pelotas Batholith, suggesting an enriched mantle source contribution to the batholith formation (Philipp *et al.*, 2003) (**Figure 5.17F**). A similar age was obtained by Cerva-Alves *et al.* (2017) in the Picada dos Tocos carbonatite (603.2 ± 4.5 Ma). This carbonatite is located in the São Gabriel Terrane, west of the Pelotas Batholith (**Figure 5.17F**), and it is also associated with a post-collisional environment. Although the similar ages do not mean that the Piquiri Syenite and the Picada dos Tocos carbonatite are genetically related, both may be related to the same thermal event responsible for triggering the partial melting of the enriched mantle. The final stabilization of the continental crust in the SRS occurred at ca. 540 Ma (Chemale Jr., 2000; Hartmann *et al.*, 2007).

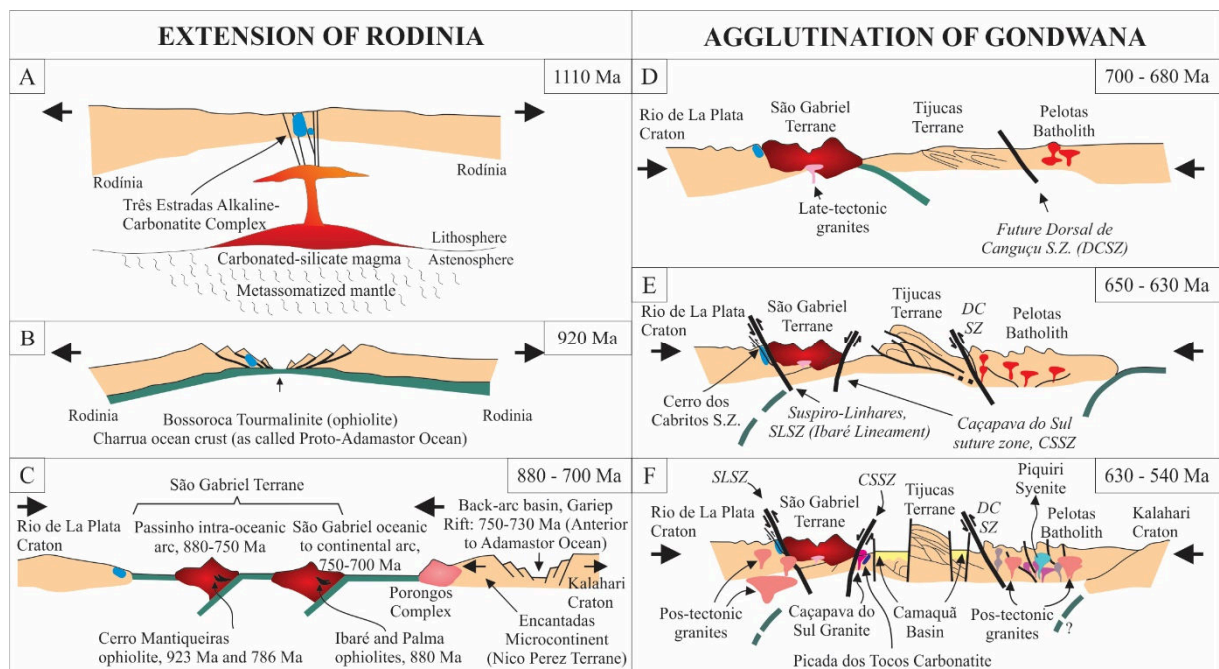


Figure 5.17 - Geotectonic evolution of the SRS from Mesoproterozoic to Neoproterozoic (Modified from Hartmann *et al.*, 2007; 2019).

5.6.4. CONTRIBUTION TO THE PALEOGEOGRAPHIC RECONSTRUCTION OF THE RODINIA SUPERCONTINENT

Several orogenic belts were formed globally between 1,300 and 900 Ma, resulting in the final agglutination of the Rodinia Supercontinent (Ernst *et al.*, 2008). It is difficult to locate the Rio de la Plata Craton in the context of this supercontinent because of the limited amount of preserved Mesoproterozoic terranes, the available paleomagnetic data and the fact that a large part of the Mesoproterozoic mobile belts was strongly reworked in the formation of the Andean Cordillera (Aleman & Ramos, 2000; Ramos, 2005). The positions of the Amazonian-Rio de la Plata and Congo-Kalahari cratons vary substantially in the different models, demonstrating the controversial nature of Rodinia reconstructions (Torsvik, 2003).

Tohver *et al.* (2006) considered the Amazonian Craton unique in South America, showing direct connection with Laurentia. Based on paleomagnetic data, the latitudinal variations of Laurentia and the São Francisco-Congo Craton (SFC), these authors place the Rio de la Plata Craton next to the SFC and suggest that the latter was located 1,500-3,000 km further south to Laurentia at 1,100-1,000 Ma. Tohver *et al.* (2006) cited geological evidence found in the literature that reinforces the interpretation of the separate evolutions of the SFC and Laurentia during Rodinia times, such as the Cariris Velhos Belt, located in the northern São Francisco Craton, recording dominantly extensional processes (Brito Neves *et al.*, 2000) in clear contrast to the collisional history of the Grenville Orogen in Laurentia.

Li *et al.* (2008) present a synthesis of knowledge regarding the amalgamation and breakup of the Rodinia Supercontinent and the subsequent assembly of Gondwana, based on paleomagnetic data and geological correlations. As opposed to Tohver *et al.* (2006), Li *et al.* (2008) and Gaucher *et al.* (2009, 2011) place the Rio de la Plata Craton juxtaposed to Laurentia at 1,100 Ma and the Kalahari Craton next to both only after 1,050 Ma (**Figure 5.18**). The similarity of U-Pb ages and Nd-Sr isotope compositions between the TEC complex and the carbonatites from the Ontario Alkaline Province and the Grenville Province in Canada, reinforce this hypothesis.

The main rifting event in Rodinia probably took place between 825 Ma and 740 Ma due to the presence of a mantle superplume, formed beneath the supercontinent after its agglutination (Li *et al.*, 2003). However, extensional events associated with back arcs, mantle plumes and other possible rifting events are reported as coeval with the late-stages of the

Rodinia amalgamation (Li *et al.*, 2003; Ernst *et al.*, 2018; Rukhlov & Bell, 2010). Noteworthy is the Keweenawan magmatism (1,110–1,090 Ma), marked by major basalt volcanism related to an intracontinental rift, and the Abitibi dyke swarm (1,160–1,140 Ma), comprising dykes associated with a mantle plume, both events occurring in Laurentia (Ernst *et al.*, 2008; Rukhlov & Bell, 2010) (**Table 5.9**).

The data presented herein, showing an 1,110 Ma emplacement age for the TEC, suggest that, after the early phases of the Grenville Orogeny in Laurentia (Shawinigan phase, 1,200–1,150 Ma; Bartholomew & Hatcher, 2010), an extensional event was recorded in both Laurentia and Rio de la Plata Craton. Furthermore, gabbros dated at $1,193 \pm 8$ Ma by Santos *et al.* (2017) provide additional evidence of extensional basic magmatism affecting the core of the Rio de la Plata Craton in the Stennian. In southern Brazil, the extensional event allowed for decompression and partial melting of the mantle, generating carbonated alkaline silicate magmas that ascended through a deep crustal-scale fracture zone near the edge of the Rio de la Plata Craton. A smaller extensional event, the precursor of the large Keweenawan magmatism, was probably responsible for triggering the mantle melting and continental crust fracturing.

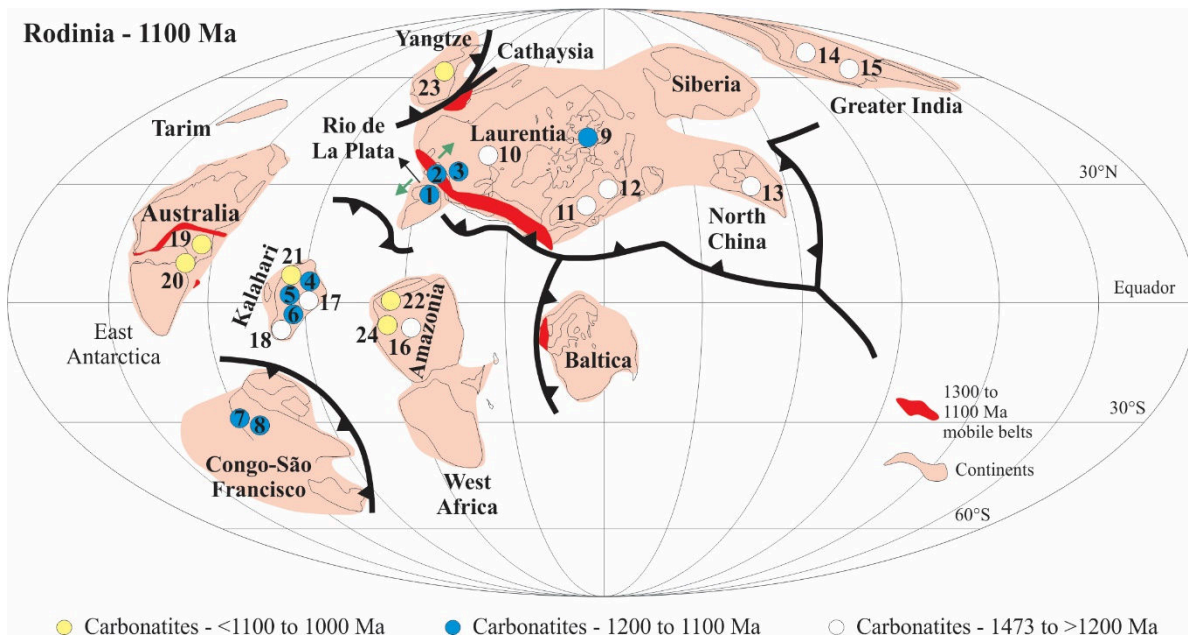


Figure 5.18 - Paleogeographic reconstruction of Rodinia at 1,100 Ma with three age groups of carbonatites (Modified from Li *et al.*, 2008). The position of carbonatites is random. 1 - Três Estradas, Brazil: 1,110 Ma (this work); 2 - Carbonatites from the Grenville Province, Canada: 1,155 Ma (Moecher *et al.*, 1997); 3 - Carbonatites from Ontario Alkaline Province (Praire Lake, Big Beaver House, Firesand River, Seabrook Lake, Schryburt Lake), Canada: 1,140 to 1,030 Ma (Bell, & Blenkinsop, 1987); 4 - Bull's Run, South Africa: 1,134 Ma (Ashwal *et al.*, 2016); 5 - Goudini, South Africa: 1,190 Ma (Verwoerd, 2008); 6 - Premier Mine, South Africa: 1,200 Ma

(Wooley & Kjarsgaard, 2008); 7 - Epembe, Namibia: 1,184 Ma (Simon *et al.*, 2017); 8 - Swartbooisdrif, Angola: 1,140 a 1,120 Ma (Drüppel *et al.*, 2006); 9 - Kalix área, Sweden: 1,142 Ma; 10 - Mountain Pass, USA: 1,415 Ma (Wooley & Kjarsgaard, 2008); 11 - Grønnedal-Íka, Greenland: 1,300 Ma (Ranta *et al.*, 2018); 12 - Igaliq, Greenland: 1,238 Ma (Wooley & Kjarsgaard, 2008); 13 - Bayan Obo, China: 1,354 Ma (Yang *et al.*, 2011); 14 - Newania, India: 1,473 Ma (Ray *et al.*, 2013); 15 - Elchuru, India: 1,242 Ma (Wooley & Kjarsgaard, 2008); 16 - Seis Lagos, Brazil: 1,328 Ma (Rossoni *et al.*, 2017); 17 - Spitskop, South Africa: 1,341 Ma (Harmer, 1999); 18 - Stukpan, South Africa: 1,357 Ma (Wooley & Kjarsgaard, 2008); 19 - Cummins Range, Australia: 1,009 Ma (Downes *et al.*, 2016); 20 - Gifford Creek, Australia: 1,075 Ma (Pirajno *et al.*, 2014); 21 - Glenover, South Africa: 1,000 Ma; 22 - Twareitau, Guyana: 1,025 Ma; 23 - Yenachang, China: 1,048 Ma (Wooley & Kjarsgaard, 2008); 24 - Mutum, Brazil: 1,026 Ma (Oliveira *et al.*, 1975). Younger carbonatites with positions 19 to 23 estimated in relation to Laurentia at 1,000 Ma.

Table 5.9 - Summary of major tectono-magmatic events related to carbonatites (Rukhlov & Bell, 2010).

Age (Ga)	Event	Tectonic configuration	Terrane
2.75 - 2.70	Abitibi - Wawa	Mantle plume? - Continental rift	Superior
2.70 - 2.61	Mikkelvik, Siilinjärvi, Sakharijök, Skjölungen, Keivy	Continental rift - mantle plume	Kola-Karelia-W. Tromso, E. Greenland
2.20 - 1.89	Polmak - Pechenga	Continental Rift - Break	Kola-Karelia
1.89 - 1.87	Circum - Superior	Mantle plume - Continental rift	Superior
1.16 - 1.14	Gardar - Abitibi	Mantle plume - break	N. Atlantic - Superior
1.11 - 1.09	Keweenawan	Continental Rift - Break	Laurentia
0.62 - 0.56	Central Iapetus	Continental Rift - Break	E. Laurentia-Baltica
0.38 - 0.36	Late Devonian	Mantle plume - Continental rift	E. European Platform
0.37 - 0.35	Cordilleran	Continental rifted margin	Foreland-Omineca Belts

Randomly plotting the Mesoproterozoic carbonatites on ancient continents in the paleogeographic reconstruction of Rodinia at 1,100 Ma proposed by Li *et al.* (2008) point out that carbonatites with ages between 1,200 and 1,000 concentrated on the left side of **Figure 5.18**. This arrangement encompasses the São Francisco-Congo, Australia, Rio de la Plata, Yangtze and partially Laurentia, Amazonia and Kalahari continents. Older carbonatites, with ages between 1,473 and 1,328 Ma tend to be placed mainly on the right side of **Figure 5.18**, including the North China, Greater India and partially Laurentia (Greenland), Amazonia and Kalahari continents. This temporal and spatial distribution of the Mesoproterozoic carbonatites may shed some new light on the formation of carbonatite magmas throughout the Rodinia supercontinent in future studies.

5.7. CONCLUSIONS

The isotope and geochronological data presented in this study for the Três Estradas Alkaline-Carbonatite Complex sheds light on the Mesoproterozoic evolution of the SRS. The

TEC consists of carbonatites, alkaline ultramafic rocks and syenites metamorphosed under greenschist to amphibolite facies conditions. These rocks were affected by ductile deformation between approximately 1100 Ma and 540 Ma during one or more deformational events. U-Pb LA-MC-ICPMS dating on zircon crystals of dolomite metacarbonatite and metasyenite provided ages of $1,110 \pm 4.8$ Ma and $1,123 \pm 15$ Ma, respectively, placing the TEC complex in a restricted set of carbonatites of Mesoproterozoic age worldwide.

$\epsilon_{\text{Nd}}(t)$ and $^{87}\text{Sr}/^{86}\text{Sr}$ ratios show very similar isotope signatures for the metacarbonatites and the metaultramafic rocks, supporting the hypothesis of these rocks being cogenetic and derived from the same parental magma. $\epsilon_{\text{Hf}}(t)$ values of zircon crystals coupled with whole rock Nd and Sr isotope signatures indicate that the TEC rocks are derived dominantly from a heterogeneous metasomatized mantle source, with some minor influence of old continental crust. The magmatism almost certainly occurred shortly after the time of mantle metasomatism. Radiogenic isotope compositions of the TEC rocks also point out that portions of an isotopically-depleted mantle rich in CO₂ occurred under the Rio de la Plata Craton.

The Mesoproterozoic Três Estradas Carbonatite also records partial melting of the mantle generated by extensional efforts in the Rio de la Plata Craton. Such efforts, prior to the Keweenawan magmatic event (1,110 to 1,090 Ma) recorded in Laurentia, were probably responsible for the development of a deep fracture zone at the edge of the Rio de la Plata Craton, reactivated later and causing the deformation of TEC rocks between the Mesoproterozoic and the end of the Neoproterozoic. The isotope and age similarities between the TEC and the carbonatites from the alkaline provinces of Ontario and Grenville, in Canada, support the hypothesis that the Rio de la Plata Craton and Laurentia were together at the end of the Mesoproterozoic, during the formation of the Rodinia Supercontinent.

ACKNOWLEDGEMENTS

The authors would like to thank Aguia Resources Ltd mining company for supporting field work, accessing core samples, and for assigning petrography data, to the Laboratório de Estudos Ambientais e Geodinâmicos from the Instituto de Geociências of the Universidade de Brasília for geochronological and isotopic analyses and to the Centro de Desenvolvimento Tecnológico (CEDES) of the Serviço Geológico do Brasil-CPRM. This study was financed in

part by the Coordenação de Aperfeiçoamento de Pessoal de Nível Superior - Brasil (CAPES) - Finance Code 001. ELD and RAF thank INCT Estudos Tectônicos (CNPq-CAPES-FAPDF) for financial support and CNPq for research fellowship. We thank Professor Márcio M. Pimentel (*in memorian*) for his contributions and Dr. Rodrigo R. Adôrno for English text formatting. We finally thank the two anonymous reviewers that contributed significantly to enhance the final version of this paper.

REFERENCES

- Aguia Resources Ltd. 2013. New phosphate discovery in southern Brazil. 5p. <http://aguiaresources.com.au/2013/01/21/new-phosphate-discovery-in-southern-brazil/>.
- Aguia Resources Ltd. 2014. Annual Report. 74p. http://aguiaresources.com.au/site/wp-content/uploads/11202014_agr_final_full_annual_report_20142.pdf.
- Aguia Resources Ltd. 2016. Aguia signs option agreement on property adjacent Três Estradas and secures new carbonatite occurrence. 3p. <https://www.asx.com.au/asxpdf/20160608/pdf/437rv1w13f05f8.pdf>.
- Aguia Resources Ltd. 2018. Três Estradas Phosphate Project, Rio Grande do Sul, Brazil. Preparado por Millcreek Mining Group. 591p. <http://aguiaresources.com.au/site/wp-content/uploads/Tres-Estradas-JORC-Report-4.11.18.pdf>.
- Aleman, A., Ramos, V.A., 2000. Northern Andes. In: Cordani, U.G., Milani, E.J., Thomaz Filho, A., Campos, D.A. (Eds.). Proceedings of the 31st International Geological Congress on The Tectonic Evolution of South America. Rio de Janeiro, pp. 453-480.
- Andersen, T. 1987. Mantle and crustal components in a carbonatite complex, and the evolution of carbonatite magma: REE and isotopic evidence from the Fen Complex, Southeast Norway. Chemical Geology, 65(2):147-166. DOI: 10.1016/0168-9622(87)90070-4.
- Andersen, O.B., Knudsen, P., Berry, P., Kenyon, S. 2008. The DNSC08 ocean-wide altimetry derived gravity field. In: Europe Geoscience Union, Vienna.
- Antonini, P., Comin-Chiaromonti, P., Gomes, C.B., Censi, P., Riffel, B.F., Yamamoto, E. 2003. The Early Proterozoic carbonatite complex of Angico dos Dias, Bahia State, Brazil: geochemical and Sr-Nd isotopic evidence for an enriched mantle origin. Mineralogical Magazine, 67(5):1039-1057. DOI 10.1180/0026461036750142.
- Anzolin, H.M., Dani, N., Remus, M.V.D., Ribeiro, R.R., Nunes, A.R., Ruppel, K.M.V. 2019. Apatite multi-generations in the Três Estradas Carbonatite, Southern Brazil: physical and chemistry meaning and implications to phosphate ore quality. Brazilian Journal of Geology, 49(2): 17p. DOI: 10.1590/2317-4889201920180092.
- Arena, K.R., Hartmann, L.A., Lana, C. 2016. Evolution of neoproterozoic ophiolites from the southern Brasiliano Orogen revealed by zircon U-Pb-Hf isotopes and geochemistry. Precambrian Research, 285:299-314. DOI: 10.1016/j.precamres.2016.09.014.
- Ashwal, L. D., Patzelt, M., Schmitz, M. D., Burke, K. 2016. Isotopic evidence for a lithospheric origin of alkaline rocks and carbonatites: an example from southern Africa. Canadian Journal Earth Sciences, 53(11):1216-1226. DOI 10.1139/cjes-2015-0145.

- Attoh, K.; Corfu, F.; Nude, P.M. 2007. U-Pb zircon age of deformed carbonatite and alkaline rocks in the Pan-African Dahomeyide suture zone, West Africa. *Precambrian Research*, 155(3-4):251-260. DOI 10.1016/j.precamres.2007.02.003.
- Babinski, M., Chemale Jr., F., Hartmann, L.A., Van Schmus, W.R., da Silva, L.C. 1996. Juvenile accretion at 750-700 Ma in Southern Brazil. *Geology*, 24(5):439-442. DOI: 10.1130/0091-7613(1996)024<0439:JAAMIS>2.3.CO;2.
- Bailey, D.K. 1974. Continental rifting and alkaline magmatism. In: Sorensen, H., (ed.). *The alkaline rocks*. John Wiley and Sons, New York, pp. 148-159.
- Bartholomew, M.J., Hatcher Jr, R.D. 2010. The Grenville orogenic cycle of southern Laurentia: Unraveling sutures, rifts, and shear zones as potential piercing points for Amazonia. *Journal of South American Earth Sciences*, 29(1):4-20. DOI: 10.1016/j.jsames.2009.08.007.
- Basei, M.A.S., Peel, E., Sánchez Bettucci, L., Preciozzi, F., Nutman, A.P. 2011. The basement of the Punta del Este Terrane (Uruguay): an African Mesoproterozoic fragment at the eastern border of the South American Río de la Plata Craton. *International Journal of Earth Sciences*, 100(2-3):289-304. DOI: 10.1007/s00531-010-0623-1.
- Bell, K. 2001. Carbonatites: relationship to mantle plume activity. In: Buchan, K.L., Ernst, R.E., (eds). *Mantle Plumes: Their Identification Through Time*. Geological Society of America Special Publications, 352:267-290. DOI 10.1130/0-8137-2352-3.267.
- Bell, K., Blenkinsop, J. 1987. Archean depleted mantle: Evidence from Nd and Sr initial isotopic ratios of carbonatites. *Geochimica et Cosmochimica Acta*, 51(2):291-298. DOI 10.1016/0016-7037(87)90241-9.
- Bell, K., Blenkinsop, J. 1989. Neodymium and strontium isotope geochemistry of carbonatites. In: Bell, K. (ed.). *Carbonatites: Genesis and Evolution*. Chapman & Hall, London, U.K. pp. 278-300.
- Bell, K., Castorina, F., Lavecchia, G., Rosatelli, G., Stoppa F. 2004. Is there a mantle plume below Italy? *EOS, Transactions American Geophysical Union*, 85(50):541-546. DOI: 10.1029/2004EO500002.
- Bell, K., Kjarsgaard, B.A., Simonetti, A. 1999. Carbonatites Into the twenty-first century. *Journal of Petrology*, 39(11-12):1839-1845. DOI: 10.1093/petroj/39.11-12.1839.
- Bell, K., Simonetti, A. 2010. Source of parental melts to carbonatites-critical isotopic constraints. *Mineralogy and Petrology*, 98(1):77-89. DOI: 10.1007/s00710-009-0059-0.
- Bell, K., Tilton, G.R. 2001. Nd, Pb and Sr isotopic compositions of East African carbonatites: evidence for mantle mixing and plume inhomogeneity. *Journal of Petrology*, 42(10):1927-1945. DOI: 10.1093/petrology/42.10.1927.
- Belousova, E.A., Griffin, W.L., O'Reilly, S.Y. 2006. Zircon crystal morphology, trace element signatures and Hf isotope composition as a tool for petrogenetic modelling: examples from eastern Australian granitoids. *Journal of Petrology*, 47(2):329-353. DOI: 10.1093/petrology/egi077.
- Belousova, E.A., Griffin, W.L., O'Reilly, S.Y., Fisher, N.J. 2002. Igneous zircon: trace element composition as an indicator of source rock type. *Contributions to Mineralogy and Petrology*, 143(5):602-622. DOI: 10.1007/s00410-002-0364-7.
- Belousova, E., Kostitsyn, Y.A., Griffin, W.L., Begg, G.C., O'Reilly, S.Y., Pearson, N.J. 2010. The growth of the continental crust: constraints from zircon Hf-isotope data. *Lithos*, 119(3-4):457-466. DOI: 10.1016/j.lithos.2010.07.024.
- Bossi, J., Campal, N., 1992. Magmatismo y tectónica transcurrente durante el Paleozoico Inferior en Uruguay. In: Gutierrez- Marco, J.G., Saavedra, J., Rabano, I. (Editors): *Paleozoico Inferior de Iberoamérica*. Universidad de Extremadura, Mérida, pp 343- 356.

- Bossi, J., Cingolani, C.A. 2009. Extension and general evolution of the Rio de la Plata Craton. In: Gaucher, C., Sial, A.N., Halverson, G.P., Frimmel, H.E. (Eds.), Neoproterozoic-Cambrian tectonics, global change and evolution: a focus on southwestern Gondwana. Developments in Precambrian Geology, 16:73-85. DOI: 10.1016/S0166-2635(09)01604-1.
- Bouvier, A., Vervoort, J.D., Patchett, P.J. 2008. The Lu-Hf and Sm-Nd isotopic composition of CHUR: Constraints from unequilibrated chondrites and implications for the bulk composition of terrestrial planets. Earth and Planetary Science Letters, 273(1-2):48-57. DOI: 10.1016/j.epsl.2008.06.010.
- Brito Neves, B.B., Santos, E.J., Van Schmus, W.R., 2000. Tectonic history of the Borborema province, northeastern Brazil. In: Cordani, U.G., Milani, E.J., Thomaz Filho, A., Campos, D.A. (Eds.), Tectonic Evolution of South America, 31st International Geological congress. Rio de Janeiro, pp. 151–182.
- Bühn, B., Pimentel, M.M., Matteini, M., Dantas, E.L. 2009. High spatial resolution analysis of Pb and U isotopes for geochronology by laser ablation multi-collector inductively coupled plasma mass spectrometry (LA-MC-ICP-MS). In: Anais da Academia Brasileira de Ciências, 81(1):1-16. DOI: 10.1590/S0001-37652009000100011.
- Burke, K., Ashwal, L.D., Webb, S.J. 2003. New way to map old sutures using deformed alkaline rocks and carbonatites. Geology, 31(5):391-394. DOI: 10.1130/0091-7613(2003)031<0391:NWTMOS>2.0.CO;2.
- Burke, K., Khan, S., 2006. Geoinformatic approach to global nepheline syenite and carbonatite distribution: testing a Wilson cycle model. Geosphere, 2(1):53-60. DOI: 10.1130/GES00027.1.
- Burke, K., Khan, S.D., Mart, R.W. 2008. Grenville Province and Montereigan carbonatite and nepheline syenite distribution related to rifting, collision, and plume passage. Geology, 36(12):983-986. DOI: 10.1130/G25247A.1.
- Cerva-Alves, T. 2017. Geologia dos carbonatitos ediacaranos de Caçapava do Sul, Rio Grande do Sul, Brasil. *Unpublished MSc Thesis*, Universidade Federal do Rio Grande do Sul, 99p.
- Cerva-Alves, T., Remus, M.V.D., Dani N., Basei, M.A.S. 2017. Integrated field, mineralogical and geochemical characteristics of Caçapava do Sul alvirkite and beforsite intrusions: A new Ediacaran carbonatite complex in southernmost Brazil. Ore Geology Reviews, 88:352-369. DOI: 10.1016/j.oregeorev.2017.05.017.
- Cerva-Alves, T., Hartmann, L.A., Remus, M.V.D., Lana, C. 2020. Integrated ophiolite and arc evolution, southern Brasiliano Orogen. Precambrian Research, 341:105648. DOI: 10.1016/j.precamres.2020.105648.
- Chemale Jr., F. 2000. Evolução Geológica do Escudo Sul-rio-grandense. In: Holz, M. De Ros, L.F. (eds). Geologia do Rio Grande do Sul. Porto Alegre, CIGO/UFRGS. pp. 13-52.
- Dawson, J.B. 1962. Sodium carbonate lavas from Oldoinyo Lengai, Tanganyika. Nature, 195:1075-1076. DOI: 10.1038/1951075a0.
- De Lena, L.O.F., Pimentel, M.M., Philipp, R.P., Armstrong, R., Sato, K. 2014. The evolution of the Neoproterozoic São Gabriel juvenile terrane, southern Brazil based on high spatial resolution U-Pb ages and $\delta^{18}\text{O}$ data from detrital zircons. Precambrian Research, 247:126-138. DOI: 10.1016/j.precamres.2014.03.010.
- De Min, A., Hendriks, B., Slejko, F., Comin-Chiaromonti, P., Girardi, V., Ruberti, C., Gomes, C.B., Neder, R.D., Pinho, F.C. 2013. Age of ultramafic high-K rocks from Planalto da Serra (Mato Grosso, Brazil). Journal of South American Earth Sciences, 41:57-64. DOI 10.1016/j.jsames.2012.06.10.
- DePaolo, D.J. 1988. Neodymium Isotope Geochemistry. Springer-Verlag, Heidelberg. 187p.

- DePaolo, D.J., Wasserburg, G.J. 1976. Inferences about magma sources and mantle structure from variations of $^{143}\text{Nd}/^{144}\text{Nd}$. *Geophysical Research Letters*, 3(12):743-746. DOI: 10.1029/GL003i012p00743.
- Dhuime, B., Hawkesworth, C.J., Cawood, P.A. & Storey, C.D. 2012. A change in the geodynamics of continental growth 3 billion years ago. *Science*, 335(6074):1334-1336. DOI: 10.1126/science.1216066.
- Downes, P.J., Dunkley, D.J., Fletcher, I.R., McNaughton, N.J., Rasmussen, B., Lynton Jaques, A., Verrall, M., Sweetapple, M.T. 2016. Zirconolite, zircon and monazite-(Ce) U-Th-Pb age constraints on the emplacement, deformation and alteration history of the Cummins Range Carbonatite Complex, Halls Creek Orogen, Kimberley region, Western Australia. *Mineralogy and Petrology*, 110:199-222. DOI 10.1007/s00710-015-0418-y.
- Drüppel, K., Wagner, T., Boyce, A.J. 2006. Evolution of sulfide mineralization in ferrocarbonatite, Swartbooisdrif, Northwestern Namibia: constraints from mineral compositions and sulfur isotopes. *The Canadian Mineralogist*, 44(4):877-894. DOI: 10.2113/gscanmin.44.4.877.
- Ernst, R.E., Wingate, M.T.D., Buchan, K.L., Li, Z.X. 2008. Global record of 1600–700 Ma Large Igneous Provinces (LIPs): Implications for the reconstruction of the proposed Nuna (Columbia) and Rodinia supercontinents. *Precambrian Research*, 160(1-2): 159-178. DOI: 10.1016/j.precamres.2007.04.019.
- Faure, G. 2001. Origin of igneous rocks: the isotopic evidence. Springer-Verlag. 516pp. DOI: 10.1007/978-3-662-04474-2.
- Fragoso-César, A.R.S. 1991. Tectônica de Placas no Ciclo Brasiliense: as orogenias dos cinturões Dom Feliciano e Ribeira no Rio Grande do Sul. Unpublished PhD Thesis, IGC-USP, São Paulo, 367 pp.
- Frimmel, H.E., Zartman, R.E. and Späth, A., 2001. Dating Neoproterozoic continental break-up in the Richtersveld Igneous Complex, South Africa. *The Journal of Geology*, 109(4):493-508. DOI: 10.1086/320795.
- Frimmel, H.E., Basei, M.A.S., Gaucher, C., 2011. Neoproterozoic geodynamic evolution of SW-Gondwana: a southern African perspective. *International Journal of Earth Sciences*, 100(2):323-354. DOI: 10.1007/s00531-010-0571-9.
- Fuck, R.A., Brito Neves, B.B., Schobbenhaus C. 2008. Rodinia descendants in South America, *Precambrian Research*, 160:108–126. DOI 10.1016/j.precamres.2007.04.018.
- Gaucher, C., Frimmel, H.E., Germs, G.J.B. 2009. Tectonic events and palaeogeographic evolution of southwestern Gondwana in the Neoproterozoic and Cambrian. In: Gaucher, C., Sial, A.N., Halverson, G.P., Frimmel, H.E. (Editors): *Neoproterozoic-Cambrian Tectonics, Global Change and Evolution: a focus on southwestern Gondwana*. Developments in Precambrian Geology, 16, Elsevier, pp. 295-316.
- Gaucher, C., Frei, R., Chemale Jr., F., Bossi, J., Martínez, G., Chiglino, L., Cernuschi, F. 2011. Mesoproterozoic evolution of the Río de la Plata Craton in Uruguay: at the heart of Rodinia? *International Journal of Earth Sciences*, 100(2):273-288. DOI: 10.1007/s00531-010-0562-x.
- Gioia, S.M.C.L., Pimentel, M.M., 2000. Sm-Nd isotopic method in the Geochronology Laboratory of University of Brasília. *Anais da Academia Brasileira de Ciências*, 72(2):219-245. DOI: 10.1590/S0001-3765200000200009.
- Gioia, S.M.C.L., Hollanda, M.H., Pimentel, M.M. 1999. Aplicação das resinas RE-spec e Sr-spec na Geoquímica Isotópica. In: *Anais do V Congresso de Geoquímica dos Países de Língua Portuguesa & VII Congresso Brasileiro de Geoquímica*, Porto Seguro, pp. 218-220.
- Girelli, T.J., Chemale Jr., F., Lavina, E.L.C., Laux, J.H., Bongiolo, E.M., Lana, C. 2018. Granulite accretion to Rio de la Plata Craton, based on zircon U-Pb-Hf isotopes: Tectonic implications for

- Columbia Supercontinent reconstruction. *Gondwana Research*, 56:105-118. DOI: 10.1016/j.gr.2017.12.010.
- Gittins, J. 1989. The origin and evolution of carbonatite magmas. In: Bell, K. (ed.). *Carbonatites: Genesis and Evolution*. Chapman & Hall, London, U.K. pp. 580-600.
- Griffin, W.L., Pearson, N.J., Belousova, E., Jackson, S.E., O'Reilly, S.Y., Van Achterberg, E., Shee, S.R. 2000. The Hf isotope composition of cratonic mantle: LAM-MC-ICPMS analysis of zircon megacrysts in kimberlites. *Geochimica et Cosmochimica Acta*, 64(1):133-147. DOI: 10.1016/S0016-7037(99)00343-9.
- Griffin, W.L., Wang, X., Jackson, S.E., Pearson, S.E., O'Reilly, S.Y., Xu, X.S., Zhou, X.M. 2002. Zircon chemistry and magma genesis, SE China: in-situ analysis of Hf isotopes, Tonglu and Pingtan Igneous Complexes. *Lithos*, 61(3):237–269. DOI: 10.1016/S0024-4937(02)00082-8.
- Griffin, W. L., Belousova, E., Shee, S.R., Pearson, N.J., O'Reilly, S. 2004. Archean crustal evolution in the northern Yilgarn Craton: U-Pb and Hf isotope evidence from detrital zircons. *Precambrian Research*, 131(3-4):231-282. DOI: 10.1016/j.precamres.2003.12.011.
- Hamilton, P.J., O'Nions, R.K., Bridgwater, D. Nutman, A., 1983. Sm-Nd studies of Archaean metasediments and metavolcanics from West Greenland and their implications for the Earth's early history. *Earth Planetary Science Letters*, 62(2):263-272. DOI: 10.1016/0012-821X(83)90089-4.
- Harmer, R.E. 1999. The Petrogenetic Association of Carbonatite and Alkaline Magmatism: Constraints from the Spitskop Complex, South Africa. *Journal of Petrology*, 40(4):525-548. DOI: 10.1093/petroj/40.4.525.
- Hartmann, L.A. 1987. Isócrona Sm-Nd de 2,1 Ga em minerais de duas amostras do Complexo Granulítico Santa Maria Chico, RS. In: *Anais do I Congresso Brasileiro de Geoquímica*, pp. 105-111.
- Hartmann, L.A., Leite, J.A.D., Silva, L.C., Remus, M.V.D. Advances in SHRIMP geochronology and their impact on understanding the tectonic and metallogenic evolution of southern Brazil. *Australian Journal of Earth Sciences*, 47(5):829-844. DOI: 10.1046/j.1440-0952.2000.00815.x.
- Hartmann, L.A., Chemale Jr., F., Philipp R.P. 2007. Evolução geotectônica do Rio Grande do Sul no Pré-Cambriano. In: *50 Anos de geologia no Rio Grande do Sul*. Editora Comunicação e Identidade, Porto Alegre, 97-123p.
- Hartmann, L. A., Liu, D., Wang, Y., Massonne, H. J., & Santos, J. O. S. 2008. Protolith age of Santa Maria Chico granulites dated on zircons from an associated amphibolite-facies granodiorite in southernmost Brazil. *Anais da Academia Brasileira de Ciências*, 80(3):543-551. DOI: 10.1590/S0001-37652008000300014.
- Hartmann, L. A., Werle, M., Michelin, C.R.L., Lana, C., Queiroga, G.N., Castro, M.P., Arena, K.R. 2019. Proto-Adamastor ocean crust (920 Ma) described in Brasiliano Orogen from coextensive zircon and tourmaline. *Geoscience Frontiers*, 10(4):1623-1633. DOI: 10.1016/j.gsf.2018.09.018.
- Hoskin, P.W.O., Black, L.P. 2000. Metamorphic zircon formation by solid-state recrystallization of protolith igneous zircon. *Journal of Metamorphic Geology*, 18(4):423-439. DOI: 10.1046/j.1525-1314.2000.00266.x.
- Jackson, S.E., Pearson, N.J., Griffin, W.L., Belousova, E.A. 2004. The application of laser ablation-inductively coupled plasma-mass spectrometry to in situ U-Pb zircon geochronology. *Chemical Geology*, 211(1-2):47-69. DOI: 10.1016/j.chemgeo.2004.06.017.
- Jaffey, A.H., Flynn, K.F., Glendenin, L.E., Bentley, W.C., Essling, A.M. 1971. Precision measurements of half-lives and specific activities of ^{235}U and ^{138}U . *Physical Review C*, 4:1889-1906. DOI: 10.1103/PhysRevC.4.1889.

- Kogarko, L.N., Lahaye, Y., Brey, G.P. 2010. Plume-related mantle source of super-large rare metal deposits from the Lovozerovo and Khibina massifs on the Kola Peninsula, Eastern part of Baltic Shield: Sr, Nd and Hf isotope systematics. *Mineralogy and Petrology*, 98(1): 197-208. DOI: 10.1007/s00710-009-0066-1.
- Lapin, A.V., Iwanuch, W., Ploshko, V.V. 1999. Carbonatitos lineares de cinturões móveis: uma síntese. *Revista Brasileira de Geociências*, 29(4):483-490.
- Laux, J.H., Toniolo J.A., Sander A., Pinto L.G.R., Parisi G., Senhorinho E.M. 2019. Seria 233 ma a idade do Carbonatito Três Estradas - Rio Grande do Sul? In: *Anais do IV Simpósio Brasileiro de Metalogenia*, Gramado, p. 36.
- Leite, J.A., Hartman, L.A., Mcnaughton, N.J., Chemale Jr, F. 1998. SHRIMP U/Pb zircon geochronology of Neoproterozoic juvenile and crustal-reworked terranes in southernmost Brazil. *International Geology Review*, 40(8):688-705. DOI: 10.1080/00206819809465232.
- Li, Z.X., Li, X.H., Kinny, P.D., Wang, J., Zhang, S., Zhou, H., 2003. Geochronology of Neoproterozoic syn-rift magmatism in the Yangtze Craton South China and correlations with other continents: evidence for a mantle superplume that broke up Rodinia. *Precambrian Research*, 122(1-4):85-109. DOI: 10.1016/S0301-9268(02)00208-5.
- Li, Z.X., Bogdanova, S.V., Collins, A.S., Davidson, A., De Waele, B., Ernst, R.E., Fitzimons, I.C.W., Fuck, R.A., Gladkochum, D.P., Jacobs, J., Karlstrom, K.E., Lu, S., Natapov, L.M., Pease, V., Pisarevsky, S.A., Thrane, K., Vernikovsky, V. 2008. Assembly, configuration, and break-up history of Rodinia: a synthesis. *Precambrian Research*, 160(1-2):179-210. DOI: 10.1016/j.precamres.2007.04.021.
- Levin, V.Y., Roncson, B.M., Levin, I.A. 1978. Carbonatites in Ilmen-Vishnovie Gory Alkaline Province, Urais. *Doklady Akademii Nauk SSSR*, 240(4):930-933 (in Russian).
- Lopes, C.G. 2014. Análises de U-Pb por LA-ICP-MS e SHRIMP em zircões detriticos do Complexo Passo Feio, Terreno São Gabriel: implicações geotectônicas para a evolução do Cinturão Dom Feliciano. *Unpublished MSc Thesis*, Universidade Federal do Rio Grande do Sul, Porto Alegre, 51p.
- Ludwig, K.R. 2012. User's Manual for Isoplot 3.75: A geochronological toolkit for Microsoft Excel. Berkeley Geochronology Center Special Publication, 5. 75p.
- Luzardo, R., Fernandes, L.A.D. 1990. Análise estrutural do Lineamento de Ibaré. *Acta Geológica Leopoldensia*, 13:25-36.
- Matteini, M., Dantas, E.L., Pimentel, M.M., Bühn, B. 2010. Combined U-Pb and Lu-Hf isotope analyses by laser ablation MC-ICP-MS: methodology and applications. *Anais da Academia Brasileira de Ciências*, 82(2):479-491. DOI: 10.1590/S0001-37652010000200023.
- Mitchell, R.H., 2005. Carbonatites and carbonatites and carbonatites. *Canadian Mineralogist*, 43(6):2049-2068. DOI: 10.2113/gscanmin.43.6.2049.
- Moecher, D.P., Anderson, E.D., Cook, C.A., Mezger, K. 1997. The petrogenesis of metamorphosed carbonatites in the Grenville Province, Ontario. *Canadian Journal of Earth Sciences*, 34(9):1185-1201. DOI: 10.1139/e17-095.
- Monteiro, C.F., Toniolo, J.A., Bastos Abram M. 2016. Carbonatitos associados ao Escudo Sul-Riograndense, Rio Grande do Sul. In: Bastos Abram M. *Projeto Fosfato Brasil – Parte II*, CPRM, Salvador.
- Morales, B.A.A., Almeida, D.P.M., Koester, E., Rocha, A.M.R., Dorneles, N.T., Rosa, M.B., Martins, A.A. 2019. Mineralogy, whole-rock geochemistry and C, O isotopes from Passo Feio Carbonatite, Sul-Riograndense Shield, Brazil. *Journal of South American Earth Sciences*, 94:102-208. DOI: 10.1016/j.jsames.2019.05.024.

- Morel, M.L.A., Nebel, O., Nebel-Jacobsen, Y.J., Miller, J.S., Vroon, P.Z. 2008. Hafnium isotope characterization of the GJ-1 zircon reference material by solution and laser-ablation MC-ICPMS. *Chemical Geology*, 255(1-2):231-235. DOI: 10.1016/j.chemgeo.2008.06.040.
- Nardi, L.V.S., Hartmann, L.A. 1979. O Complexo Granulítico Santa Maria Chico do Escudo Sul-riograndense, *Acta Geologica Leopoldensia*, 6:45-75.
- Oliveira, A.D.S., Fernandez, C.A.C., Issler, R.S., Abreu, A.S., De Montalvao, R.M.G., Teixeira, W. 1975. Folha NA.21 Tumucumaque e parte da Folha NB.21; geologia, geomorfologia, pedologia, vegetação e uso potencial da terra. Levantamento de Recursos Minerais, Vol. 9. Projeto RADAMBRASIL, Departamento Nacional de Produção Mineral. Rio de Janeiro. 370pp.
- Oliveira, F.V. 2015. Chronus: Um novo suplemento para a redução de dados U-Pb obtidos por LA-MC-ICPMS. *Unpublished MSc Thesis*, Universidade de Brasília, Brazil. 91 pp.
- Paim, P.S.G., Chemale, Jr., F., Lopes, R.D.C., 2000. A Bacia do Camaquã. In: Holz, M., De Ros, L.F. (Eds.), *Geologia do Rio Grande do Sul*, CIGO/UFRGS, Porto Alegre, pp. 231-274.
- Papanastassiou, D.A., Wasserburg, G.J. 1969. Initial Sr isotopic abundances and the resolution of small time differences in the formation of planetary objects. *Earth and Planetary Sciences Letters*, 5:361-376. DOI: 10.1016/S0012-821X(68)80066-4.
- Philipp, R.P., Machado, R., Chemale Jr, F. 2003. Reavaliação e Novos Dados Geocronológicos (Ar/Ar, Rb/Sr e Sm/Nd) do Batólito Pelotas no Rio Grande do Sul: Implicações Petrogenéticas e Idade de Reativação das Zonas de Cisalhamento. *Revista do Instituto de Geociências – USP*, 3:71-84.
- Philipp, R.P., Pimentel, M.M., Chemale Jr., F. 2016. Tectonic evolution of the Dom Feliciano belt in Southern Brazil: geological relationships and U–Pb geochronology. *Brazilian Journal of Geology*, 46(1):83-104. DOI: 10.1590/2317-4889201620150016.
- Philipp, R.P., Pimentel, M.M., Basei, M.A.S. 2018. The Tectonic Evolution of the São Gabriel Terrane, Dom Feliciano Belt, Southern Brazil: The Closure of the Charrua Ocean. In: Siegesmund S., Basei M., Oyhantçabal P., Oriolo S. (eds) *Geology of Southwest Gondwana. Regional Geology Reviews*. Springer, Cham, pp 243-265. DOI: 10.1007/978-3-319-68920-3_10.
- Pietranik, A.B., Hawkesworth, C.J., Storey, C.D., Kemp, A.I.S., Sircombe, K.N., Whitehouse, M.J., Bleeker, W. 2008. Episodic, mafic crust formation from 4.5 to 2.8 Ga: New evidence from detrital zircons, Slave craton, Canada. *Geology*, 36(11):875-878. DOI: 10.1130/G24861A.1.
- Pirajno, F. 2015. Intracontinental anorogenic alkaline magmatism and carbonatites, associated mineral systems and the mantle plume connection. *Gondwana Research*, 27(3):1181-1216. DOI: 10.1016/j.gr.2014.09.008.
- Pirajno, F., González-Álvarez, I., Chen, W., Kyser, K.T., Simonetti, A., Leduc, E., leGras, M. 2014. The Gifford Creek Ferrocyanite Complex, Gascoyne Province, Western Australia: Associated fenitic alteration and a putative link with the ~1075 Ma Warakurna LIP. *Lithos*, 202-203:100-119. DOI: 10.1016/j.lithos.2014.05.012.
- Ramos, V.A. 2005. The Proterozoic-early Paleozoic margin of Western Gondwana. *Gondwana* 12, Mendoza, Abstracts 304.
- Ramgrab, G.E., Wildner, W., Lopes, R.C., Favilla, C.A.C., Silva, M.A.S., Sachs, L.L.B., Silva, V.A., Batista, I.H. 2004. Folha SH.22-Porto Alegre. In: Schobbenhaus, C., Gonçalves, J.H., Santos, J.O.S., Abram, M.B., Leão Neto, R., Matos, G.M.M., Vidotti, R.M., Ramos, M.A.B., Jesus, J.D.A. de. (eds.). *Carta Geológica do Brasil ao Milionésimo, Sistema de Informações Geográficas*. Programa Geologia do Brasil. CPRM, Brasília. CD-ROM.
- Ranta, E., Stockmann, G., Wagner, T., Fusswinkel, T., Sturkell, E., Tollesen, E., Skelton, A. 2018. Fluid–rock reactions in the 1.3 Ga siderite carbonatite of the Grønnedal–Íka alkaline complex,

- Southwest Greenland. Contributions to Mineralogy and Petrology, 173:78 26p. DOI: 10.1007/s00410-018-1505-y.
- Ray, J.S., Pande, K., Bhutani, R., Shukla, A.D., Rai V.K., Kumar, A., Awasthi, N., Smitha, R.S., Panda, D.K. 2013. Age and geochemistry of the Newania dolomite carbonatites, India: implications for the source of primary carbonatite magma. Contributions to Mineralogy and Petrology, 166:1613-1632. DOI 10.1007/s00410-013-0945-7.
- Remus, M.V.D., Hartmann, L.A., McNaughton, N.J., Groves, D.I., Fletcher, I.R. 2000. The link between hydrothermal epigenetic copper mineralization and the Caçapava Granite of the Brasiliano Cycle in Southern Brazil. Journal of South American Earth Sciences, 13(3):191-216. DOI: 10.1016/S0895-9811(00)00017-1.
- Rocha, A.M.R., Dorneles, N.T., Gindri, M.D., Vargas, J.M., Alves, T.C., Benetti F.A. 2013. Descoberta dos carbonatitos Picada dos Tocos e Passo Feio e o potencial para fosfato e ETR's, Caçapava do Sul, Rio Grande do Sul. In: Anais do III Simpósio Brasileiro de Metalogenia, Gramado.
- Roden, M.F., Murthy, V.R. 1985. Mantle Metasomatism. Annual Review of Earth and Planetary Sciences, 13:269-296. DOI: 10.1146/annurev.ea.13.050185.001413.
- Rollinson, H.R. 1993. Using geochemical data: evaluation, presentation, interpretation. Longman, New York. 352 p.
- Rossoni, M.B., Bastos Neto, A.C., Souza, V.S., Marques, J.C., Dantas, E., Botelho, N.F., Giovannini, A.L., Pereira, V.P. 2017. U-Pb zircon geochronological investigation on the Morro dos Seis Lagos Carbonatite Complex and associated Nb deposit (Amazonas, Brazil). Journal of South American Earth Sciences, 80:1-17. DOI: 10.1016/j.jsames.2017.09.021.
- Rubatto, D. 2017. Zircon: The metamorphic mineral. Reviews in Mineralogy and Geochemistry, 83:261-295. DOI 10.2138/rmg.2017.83.09.
- Rubatto, D., Gebauer, D. 2000. Use of Cathodoluminescence for U-Pb Zircon dating by ion microprobe: Some examples from the Western Alps. In: Pagel, M., Barbin, V., Blanc, P., Ohnenstetter, D. (Eds.). Cathodoluminescence in geosciences, 373–400 pp. Berlin Heidelberg: Springer. DOI 10.1007/978-3-662-04086-7.
- Rukhlov, A.S., Bell, K., 2010. Geochronology of carbonatites from the Canadian and Baltic Shields, and the Canadian Cordillera: clues to mantle evolution. Mineralogy and Petrology, 98(1):11-54. DOI: 10.1007/s00710-009-0054-5.
- Sadowski G.R. & Bettencourt J.S. 1996. Mesoproterozoic tectonic correlation between east Laurentia and the western border of the Amazon Craton. Precambrian Research, 76(3-4):213-227. DOI: 10.1016/0301-9268(95)00026-7.
- Santos, J.O.S., Chernicoff, C.J., Zappettini, E.O., McNaughton, N.J., Greau, Y. 2017. U-Pb geochronology of Martín García, Sola, and Dos Hermanas Islands (Argentina and Uruguay): Unveiling Rhyacian, Statherian, Ectasian, and Stenian of a forgotten area of the Río de la Plata Craton. Journal of South American Earth Sciences, 80:207-228. DOI: 10.1016/j.jsames.2017.09.029.
- Silva, M.A.S., Favilla, C.A.C., Wildner, W., Ramgrab, G.E., Lopes, R.C., Sachs, L.L.B., Silva, V.A., Batista, I.H., 2004. Folha SH.21-Uruguaiana. In: Schobbenhaus, C., Gonçalves, J.H., Santos, J.O.S., Abram, M.B., Leão Neto, R., Matos, G.M.M., Vidotti, R.M., Ramos, M.A.B., Jesus, J.D.A. de. (eds.). Carta Geológica do Brasil ao Milionésimo, Sistema de Informações Geográficas. Programa Geologia do Brasil. CPRM, Brasília. CD-ROM.
- Simon, S.J., Wei, C., Ellmies, R., Yang, H., Tamehe, L.S. 2017. New SIMS U-Pb age on zircon from the Epembe carbonatite dyke, NW Namibia: Implications for Mesoproterozoic evolution of carbonatites at the southern margin of the Congo Craton. Journal of African Earth Sciences, 135:108-114. DOI: 10.1016/j.jafrearsci.2017.08.011.

- Söderlund, U., Jonathan Patchett, P., Vervoort, J.D., Isachsen, C.E. 2004. The ^{176}Lu decay constant determined by Lu-Hf and U-Pb isotope systematics of Precambrian mafic intrusions. *Earth and Planetary Science Letters*, 219:311-324. DOI 10.1016/j.jafrearsci.2017.08.011.
- Thirlwall, M.F. 1991. Long-term reproducibility of multicollector Sr and Nd isotope ratio analysis. *Chemical Geology*, 94:85-104. DOI: 10.1016/0168-9622(91)90002-E.
- Tichomirowa, M., Grosche, G., Götze, J., Belyatsky, B.V., Savva, E.V., Keller, J., Todt, W. 2006. The mineral isotope composition of two Precambrian carbonatite complexes from the Kola Alkaline Province – Alteration versus primary magmatic signatures. *Lithos*, 91(1-4):229-249. DOI: 10.1016/j.lithos.2006.03.019.
- Toni, G.B., Bitencourt, M.F., Nardi, L.V.S., Florisbal, L.M., Almeida, B.S., Geraldes, M. 2020. Dom Feliciano Belt orogenic cycle tracked by its pre-collisional magmatism: The Tonian (ca. 800 Ma) Porto Belo Complex and its correlations in southern Brazil and Uruguay. *Precambrian Research*, 342:105702. DOI: 10.1016/j.precamres.2020.105702.
- Toniolo, J.A., Gil, C.A.A., Sander, A. 2007. Metalogenia das bacias neoproterozoicas-eopaleozooicas do Sul do Brasil: Bacia do Camaquã. CPRM, Porto Alegre. 154p.
- Toniolo, J.A., Gil, C.A.A., Sander, A. 2007. Metalogenia das bacias neoproterozoicas-eopaleozooicas do Sul do Brasil: Bacia do Camaquã. CPRM, Porto Alegre, 154p.
- Toniolo, J.A., Parisi, G.N., Grazia, C.A., Reischl, J.L. 2010. Prospecção de fosfato na região de Três Estradas, Lavras do Sul, RS. In: IV Simpósio de Exploração Mineral, Ouro Preto.
- Tohver, E., Van der Pluijm, B.A., Van der Voo, R., Rizzotto, G., Scandolara, J.E. 2002. Paleogeography of the Amazon craton at 1–2 Ga: early Grenvillian collision with the Llano segment of Laurentia. *Earth Planetary Science Letters*, 199(1):185–200. DOI: 10.1016/S0012-821X(02)00561-7.
- Tohver, E., D’Agrella-Filho, M.S., Trindade, R.I.F. 2006. Paleomagnetic record of Africa and South America for the 1200–500 Ma interval, and evaluation of Rodinia and Gondwana assemblies. *Precambrian Research*, 147(3-4):193-222. DOI: 10.1016/j.precamres.2006.01.015.
- Torsvik, T.H. 2003. The Rodinia Jigsaw Puzzle. *Science*, 300(5624):1379-1381. DOI: 10.1126/science.1083469.
- Verwoerd, W.J. 2008. The Goudini Carbonatite Complex, South Africa: a re-appraisal. *The Canadian Mineralogist*, 46(4):825-830. DOI: 10.3749/canmin.46.4.825.
- Weis, D., Kieffer, B., Maerschalk, C., Pretorius, W., Barling, J. 2005. High-precision Pb-Sr-Nd-Hf isotopic characterization of USGS BHVO-1 and BHVO-2 reference materials. *Geochemistry Geophysics Geosystems*, 6(2):1-10. DOI: 10.1029/2004GC000852.
- Wiedenbeck, M., Allé, P., Corfu, F., Griffin, W.L., Meier, M., Oberli, F., Von Quadt, A., Roddick, J.C., Spiegel, W. 1995. Three natural zircon standards for U-Th-Pb, Lu-Hf, trace element and REE analyses. *Geostandards Newsletter*, 19(1):1-23. DOI: 10.1111/j.1751-908X.1995.tb00147.x.
- Will, T., Gaucher, C., Ling, X.X., Li, X.H., Li, Q.L., Frimmel, H.E. 2019 Neoproterozoic magmatic and metamorphic events in the Cuchilla Dionisio Terrane, Uruguay, and possible correlations across the South Atlantic. *Precambrian Research*, 320:303-322. DOI: 10.1016/j.precamres.2018.11.004.
- Winter, J.D. 2001. An introduction to igneous and metamorphic petrology. Prentice Hall Upper Saddle River, New Jersey. 669p.
- Woolley, A.R., Bailey, D.K. 2012. The crucial role of lithospheric structure in the generation and release of carbonatites: geological evidence. *Mineralogical Magazine*, 76(2):259-270. DOI: 10.1180/minmag.2012.076.2.02.

- Woolley, A.R., Kjarsgaard, B.A. 2008. Paragenetic types of carbonatites as indicated by the diversity and relative abundances of associated silicate rocks: evidence from a global database. *The Canadian Mineralogist*, 46(4):741-752. DOI: 10.3749/canmin.46.4.741.
- Yang, K.F., Fan, H.R., Santosh, M. Hu, F.F., Wang, K.Y. 2011. Mesoproterozoic mafic and carbonatitic dykes from the northern margin of the North China Craton: Implications for the final breakup of Columbia supercontinent. *Tectonophysics*, 498:1-10. DOI 10.1016/j.tecto.2010.11.015.
- Zaitsev, A., Bell, K. 1995. Sr and Nd isotope data of apatite, calcite and dolomite as indicators of the source and the relationships of phoscorites and carbonatites from the Kovdor massif, Kola peninsula, Russia. *Contributions to Mineralogy and Petrology*, 121:324-335. DOI:10.1007/BF02688247.

6. CONCLUSÕES

Os dados geoquímicos, isotópicos e geocronológicos inéditos para o Complexo Alcalino-Carbonatítico Três Estradas apresentados nessa tese de doutorado permitiram contribuir para a compreensão da evolução geotectônica do ESRG. As principais conclusões obtidas são apresentadas a seguir.

- A idade de cristalização do CTE é Mesoproterozoica com idades U-Pb em zircão de $1.110 \pm 4,8$ Ma e 1.123 ± 15 Ma obtidas em dolomita metacarbonatito e metassienito, respectivamente. Os gnaisses encaixantes são compatíveis com o Complexo Granulítico Santa Maria-Chico e tiveram idade U-Pb em zircão de $2.022 \pm 7,9$ Ma, interpretada como a idade de metamorfismo do complexo de acordo com a literatura científica.
- $\varepsilon_{\text{Nd}}(t)$ e $^{87}\text{Sr}/^{86}\text{Sr}$ de calcita e dolomita metacarbonatitos, rochas metaultramáficas e metassienitos mostram valores muito próximos, reforçando relações geológicas de campo que sugerem que essas rochas sejam cogenéticas, e, portanto, podem ser agrupadas quanto à nomenclatura formal como Complexo. Dado os tipos de rochas que constituem o Complexo, a classificação dessa unidade como complexo alcalino-carbonatítico é pertinente.
- As semelhanças texturais e padrões geoquímicos similares entre o metacarbonatito do CTE e os carbonatitos Picada dos Tocos ($603,2 \pm 4,5$ Ma, U-Pb em zircão) e Passo Feio (idade neoproterozoica sugerida) sugerem que estas três intrusões tenham se originado a partir da fusão de uma fonte sustentadamente semelhante e submetida a processos petrogenéticos similares. A diferença de aproximadamente 500 milhões de anos entre essas intrusões sugere que manto astenosférico tenha sido recorrentemente fundido para a geração dessas rochas.
- Os valores de $\varepsilon_{\text{Hf}}(t)$ positivos em zircão de metacarbonatito e metassienito e as baixas razões isotópicas $^{147}\text{Sm}/^{144}\text{Nd}$ em rocha total nessas rochas e em rochas metaultramáficas indicam origem do CTE a partir de fonte mantélica metassomatizada isotopicamente empobrecido.
- A correlação negativa entre $\varepsilon_{\text{Nd}}(t)$ e idades modelo $T_{\text{DM}}(\text{Nd})$ associada à esporádica ocorrência de xenocristal de zircão herdado da rocha encaixante em dolomita

metacarbonatito permitem inferir pequena contaminação crustal dos líquidos que originaram o CTE.

- As idades de derivação mantélica das rochas do CTE mostram elevada variação, conforme as idades modelo $T_{DM}(Nd)$. Dolomita metacarbonatitos teriam derivado primeiramente (1,48 a 1,62 Ga), seguidos por rochas metaultramáficas (1,37 a 1,50 Ga) e calcita metacarbonatitos (1,18 a 1,55 Ga).
- O metassomatismo do manto a partir do qual foram formadas as rochas do CTE ocorreu provavelmente em tempo muito próximo ao início de sua fusão parcial, dado que razões $^{147}\text{Sm}/^{144}\text{Nd}$ herdadas de manto metassomatizado são baixas e os valores εNd são positivos. O que se esperaria de um manto não metassomatizado seriam razões $^{147}\text{Sm}/^{144}\text{Nd}$ elevadas que, com o passar do tempo, em função do decaimento isotópico, gerariam então εNd negativos.
- O manto metassomatizado é rico em ETR, elementos incompatíveis e voláteis, assinaturas essas, herdadas por carbonatitos, tal como se observa no CTE.
- As assinaturas geoquímicas de elementos menores e ETR evidenciam que processos petrogenéticos complexos atuaram para a formação das rochas do CTE. Cristalização fracionada e imiscibilidade de líquidos a partir de mesmo magma parental com composição silicática e enriquecido em CO_2 são propostos como processos predominantes, incluindo metassomatismo gerado pela percolação de fluidos ricos em K e Na provenientes da intrusão de carbonatitos.
- A cristalização fracionada do magma parental é evidenciada pelo fracionamento cada vez mais acentuado de elementos incompatíveis e ETR partindo de rochas ultramáficas mais primitivas (MUMF-1) até calcita carbonatitos mais evoluídos (CMC-2), provavelmente formados pela cristalização residual do líquido que formou as rochas ultramáficas. A imiscibilidade teria sido o processo responsável pela geração de dolomita carbonatitos dados os seus padrões espelhados de Sr, P, Nd e Ta e razões inversas Nb/Ta e Zr/Hf (<1).
- A liberação de fluidos ricos em K e Na por carbonatitos provocou extenso metassomatismo com desenvolvimento de fenitos potássicos e sódicos e biotitização/glimeritização de rochas ultramáficas. Tantos as rochas encaixantes

quanto as rochas do CTE foram submetidas à cloritização de anfibólios e biotitas e sulfetação com formação de pirita e calcopirita.

- As assinaturas isotópicas Nd-Sr, C-O e idades U-Pb do CTE são similares às assinaturas de carbonatitos de mesma idade encontrados na Província Alcalina de Ontário, Canadá, relacionados ao evento extensional Keweenawan (1.110-1.090 Ma) e à geração do enxame de diques Abitibi (1.160-1.140 Ma), ambos associados a processos de rifteamento intracontinental. Com base nesses dados, reforça-se, portanto, a teoria de que o Cráton Rio de la Plata e Laurentia estiveram conectados ao final do Mesoproterozoico, durante a construção do supercontinente Rodinia. Nessa configuração, o CTE teria intrudido zona de fratura antiga associada a algum processo extensivo.
- O CTE indica, portanto, a provável ocorrência de manto astenosférico metassomatizado, heterogêneo, isotopicamente empobrecido em Sm/Nd e levemente empobrecido em Rb/Sr, e rico em CO₂, elementos incompatíveis e ETR, formado sob o Cráton Rio de la Plata. A fusão parcial desse manto gerou magmas silicáticos carbonatados entre 1,18 e 1,62 Ga, culminando na cristalização do CTE por volta de 1,1 Ga. O CTE foi alojado na crosta continental, possivelmente durante evento extensional mesoproterozoico, previamente à formação de crosta oceânica, espacialmente próxima, iniciada em 920 Ma no ESRG. Foi metamorfizado em fácies xisto verde a anfibolito e submetido à deformação heterogênea em pelo menos dois eventos no fechamento dos supercontinentes Rodinia e Gondwana, no final do Mesoproterozoico e Neoproterozoico, respectivamente, com preservação local de foliação e bandamento de fluxo ígneo.
- As idades distintas entre o Carbonatito Picada dos Tocos e o CTE sugerem idades diferentes de repetição de magmatismo carbonatítico, gerado a partir de mesma fonte de manto astenosférico ao longo do tempo em zonas de falhas/fraturas antigas nesse escudo. No mínimo uma terceira idade de magmatismo carbonatítico, mais jovem, relacionada aos carbonatitos Joca Tavares, Porteira e Santa Inês é sugerida nesta tese.
- Mineralizações em fosfato, considerando teor de corte acima ou igual a 3% P₂O₅, são observadas em todos os sete carbonatitos do ESRG, revelando o potencial

mineral dessas intrusões carbonatíticas para a ocorrência de depósitos de fosfato, tal como o identificado no CTE.

- O principal controle das intrusões carbonatíticas são as zonas de falha/fratura profundas. As concentrações de fosfato estão relacionadas tanto a cristalização fracionada, quanto a imiscibilidade de líquidos, que se mostraram processos petrogenéticos eficientes para concentração de apatita.

REFERÊNCIAS BIBLIOGRÁFICAS

- Aguia Resources Ltd. 2013. Key phosphate tenements granted at Três Estradas South and Joca Tavares in southern Brazil. 5p. <http://aguiaresources.com.au/site/wp-content/uploads/20130501.pdf>
- Aguia Resources Ltd. 2014. Annual Report. 74p. http://aguiaresources.com.au/site/wp-content/uploads/11202014_agr_final_full_annual_report_20142.pdf.
- Aguia Resources Ltd. 2016. Aguia signs option agreement on property adjacent Três Estradas and secures new carbonatite occurrence. 3p. <https://www.asx.com.au/asxpdf/20160608/pdf/437rv1w13f05f8.pdf>.
- Aguia Resources Ltd. 2017. Aguia ramps up exploration of targets surrounding Três Estradas. 10p. <https://www.openbriefing.com/AsxDownload.aspx?pdfUrl=Report%2FComNews%2F20171108%2F01919003.pdf>
- Aguia Resources Ltd. 2018a. Três Estradas Phosphate Project, Rio Grande do Sul, Brazil. Preparado por Millcreek Mining Group. 591p. <http://aguiaresources.com.au/site/wp-content/uploads/Tres-Estradas-JORC-Report-4.11.18.pdf>.
- Aguia Resources Ltd. 2018b. Auger drilling at Mato Grande Carbonatite returns highly encouraging assay results. 10p. <https://www.asx.com.au/asxpdf/20180116/pdf/43qv68mcy7gcvq.pdf>.
- Aguia Resources Ltd., 2019. Rio Grande Projects. Disponível em <http://aguiaresources.com.au/projects/rio-grande/>. Acesso em 01/09/2020.
- Anzolin, H.M. 2015. Mineralogia e Geoquímica do Perfil de Intemperismo do Carbonatito Três Estradas. Trabalho de Conclusão de Curso, Universidade Federal do Rio Grande do Sul, Porto Alegre, 116 p.
- Anzolin, H.M., Dani, N., Remus, M.V.D., Ribeiro, R.R., Nunes, A.R., Ruppel, K.M.V. 2019. Apatite multi-generations in the Três Estradas Carbonatite, Southern Brazil: physical and chemistry meaning and implications to phosphate ore quality. Brazilian Journal of Geology, 49(2): 17p. DOI: 10.1590/2317-4889201920180092.
- Ashwal, L. D., Patzelt, M., Schmitz, M. D., Burke, K. 2016. Isotopic evidence for a lithospheric origin of alkaline rocks and carbonatites: an example from southern Africa. Canadian Journal Earth Sciences, 53(11):1216-1226. DOI 10.1139/cjes-2015-0145.
- Attoh, K.; Corfu, F.; Nude, P.M. 2007. U-Pb zircon age of deformed carbonatite and alkaline rocks in the Pan-African Dahomeyide suture zone, West Africa. Precambrian Research, 155(3-4):251-260. DOI 10.1016/j.precamres.2007.02.003.
- Babinski, M., Chemale Jr., F., Hartmann, L.A., Van Schmus, W.R., da Silva, L.C. 1996. Juvenile accretion at 750-700 Ma in Southern Brazil. Geology, 24(5):439-442. DOI: 10.1130/0091-7613(1996)024<0439:JAAMIS>2.3.CO;2.
- Bailey, D.K. 1974. Continental rifting and alkaline magmatism. In: Sorensen, H., (ed.). The alkaline rocks. John Wiley and Sons, New York, pp. 148-159.
- Bailey, D.K. 1987. Mantle metasomatism - perspective and prospect. In: Fitton, J.G., Upton, B.G.J. (eds.). Alkaline igneous rocks. Geological Society Special Publications 30:1-13. The Geological Society, London.

- Bailey, D.K. 1993. Carbonate magmas: Journal of the Geological Society, 150(4):637-651. DOI: 10.1144/gsjgs.150.4.0637.
- Barbosa, E.S.R. 2009. Mineralogia e petrologia do Complexo Carbonatítico-Foscorítico de Salitre – MG. Tese de Doutorado, Universidade de Brasília, Brasília, 432p.
- Bardina, N.Y., Popov, V.S., 1994. Fenites: systematics, formation conditions and significance for crustal magma genesis. Zapiski Vseross. Mineral. Obshcheswa, 113:485-497.
- Barker, D.S. 1989. Field relations of carbonatites. In: Bell, K. (ed.). Carbonatites: Genesis and Evolution. Chapman & Hall, London, U.K. p.38-69.
- Bell, K., (ed). 1989. Carbonatites: Genesis and Evolution. Chapman & Hall, London, U.K.
- Bell, K. 2001. Carbonatites: relationship to mantle plume activity. In: Buchan, K.L., Ernst, R.E., (eds). Mantle Plumes: Their Identification Through Time. Geological Society of America Special Publications, 352:267-290. DOI 10.1130/0-8137-2352-3.267.
- Bell, K., Simonetti, A. 1996. Carbonatite magmatism and plume activity: implications from the Nd, Pb and Sr isotope systematics of Oldoinyo Lengai. Journal of Petrology, 37(6):1321-1339. DOI: 10.1093/petrology/37.6.1321.
- Bell, K., Tilton, G.R. 2001. Nd, Pb and Sr isotopic compositions of East African carbonatites: evidence for mantle mixing and plume inhomogeneity. Journal of Petrology, 42(10):1927-1945. DOI: 10.1093/petrology/42.10.1927.
- Bell, K., Kjarsgaard, B.A., Simonetti, A. 1999. Carbonatites Into the twenty-first century. Journal of Petrology, 39(11-12):1839-1845. DOI: 10.1093/petroj/39.11-12.1839.
- Bell, K., Castorina, F., Lavecchia, G., Rosatelli, G., Stoppa F. 2004. Is there a mantle plume below Italy? EOS, Transactions American Geophysical Union, 85(50):541-546. DOI: 10.1029/2004EO500002.
- Biondi, J.C. 2003. Processos metalogenéticos e os depósitos minerais brasileiros. Oficina de textos. SP. 528p.
- Bitencourt, M.F., 1983. Geologia, petrologia e estrutura dos metamorfítos da região e Caçapava do Sul, RS. Dissertação de mestrado, Universidade Federal do Rio Grande do Sul, Porto Alegre, 161 p.
- Bossi, J., Campal, N., 1992. Magmatismo y tectónica transcurrente durante el Paleozoico Inferior en Uruguay. In: Gutierrez- Marco, J.G., Saavedra, J., Rabano, I. (Editors): Paleozoico Inferior de Iberoamérica. Universidad de Extremadura, Mérida, pp 343- 356.
- Bossi, J., Cingolani, C.A. 2009. Extension and general evolution of the Rio de la Plata Craton. In: Gaucher, C., Sial, A.N., Halverson, G.P., Frimmel, H.E. (Eds.), Neoproterozoic-Cambrian tectonics, global change and evolution: a focus on southwestern Gondwana. Developments in Precambrian Geology, 16:73-85. DOI: 10.1016/S0166-2635(09)01604-1.
- Brod, J.A., Gibson, S.A., Thompson, R.N., Junqueira-Brod, T.C., Seer, H.J., De Moraes, L.C., Boaventura, G.R., 2000. The kamafugite-carbonatite association in the Alto Paranaíba Igneous Province (APIP) southeastern Brazil. Revista Brasileira de Geociências, 30(3):408-412.
- Brod, J.A., Ribeiro, C.C., Gaspar, J.C., Junqueira-Brod, T.C., Barbosa, E.S.R., Riffel, B.F., Silva, J.F., Chaban, N., Ferrari, A.L.D. 2004. Excursão 1: Geologia e Mineralizações dos Complexos Alcalino-

- Carbonatíticos da Província Ígnea do Alto Paranaíba. In: 42 Congresso Brasileiro de Geologia, Araxá, Guias de Excursões. 1-29. (CD-ROM).
- Brod, J. A., Junqueira-Brod, T.C., Gaspar, J.C., Petrinovic, I.A., Valente, S.C., Corval, A. 2013. Decoupling of paired elements, crossover REE patterns, and mirrored spider diagrams: Fingerprinting liquid immiscibility in the Tapira alkaline-carbonatite complex, SE Brazil. Journal of South American Earth Sciences, 41:41-56. DOI: 10.1016/j.jsames.2012.04.013.
- Brøgger, W.C. 1921. Die Eruptivegesteine des Kristianiagebietes. IV. Das Fengebiet in Telemarken, Norwegen. Norske Vidensk. Skrift. Mat-Naturv. Kl. 1920, 408p.
- Brooker, R.A. 1995. Carbonatite genesis: the role of liquid immiscibility to 25 kb. PhD thesis, University of Manchester, Manchester.
- Brooker, R.A. 1998. The effect of CO₂ saturation on immiscibility between silicate and carbonate liquids: an experimental study. Journal of Petrology, 39(11-12):1905-1915. DOI: 10.1093/petroj/39.11-12.1905.
- Burke, K., Ashwal, L.D., Webb, S.J. 2003. New way to map old sutures using deformed alkaline rocks and carbonatites. Geology, 31(5):391-394. DOI: 10.1130/0091-7613(2003)031<0391:NWTMOS>2.0.CO;2.
- Burke, K., Khan, S., 2006. Geoinformatic approach to global nepheline syenite and carbonatite distribution: testing a Wilson cycle model. Geosphere, 2(1):53-60. DOI: 10.1130/GES00027.1.
- Burke, K., Khan, S.D., Mart, R.W. 2008. Grenville Province and Monteregian carbonatite and nepheline syenite distribution related to rifting, collision, and plume passage. Geology, 36(12):983-986. DOI: 10.1130/G25247A.1.
- Cerva-Alves, T. 2017. Geologia dos carbonatitos ediacaranos de Caçapava do Sul, Rio Grande do Sul, Brasil. *Unpublished MSc Thesis*, Universidade Federal do Rio Grande do Sul, 99p.
- Cerva-Alves, T., Remus, M.V.D., Dani N., Basei, M.A.S. 2017. Integrated field, mineralogical and geochemical characteristics of Caçapava do Sul alvikite and beforsite intrusions: A new Ediacaran carbonatite complex in southernmost Brazil. Ore Geology Reviews, 88:352-369. DOI: 10.1016/j.oregeorev.2017.05.017.
- Chemale Jr., F. 2000. Evolução Geológica do Escudo Sul-rio-grandense. In: Holz, M. De Ros, L.F. (eds). Geologia do Rio Grande do Sul. Porto Alegre, CIGO/UFRGS. pp. 13-52.
- Chemale Jr., F., Hartmann, L.A., Silva, L.C. 1995a. Stratigraphy and Tectonism of Precambrian to Early Paleozoic units in Southern Brazil and Uruguay - Excursion Guidebook. Acta Geologica Leopoldensia 43:4-115.
- Chemale Jr., F., Hartmann, L.A., Silva L.C. 1995b. Stratigraphy and Tectonism of Brasiliano Cycle in Southern Brazil. Communs. Geologica Survey of Namibia 10:151-166.
- Comin-Chiaromonti, P., Gomes, C.B., Castorina, F., di Censi, P., Antonini, P., Furtado, S., Ruberti, E., Scheibe, L.F. 2002. Geochemistry and geodynamic implications of Anitapolis and Lages alkaline-carbonatite complexes, Santa Catarina State, Brazil. Revista Brasileira de Geociências, 32(1):43-58. DOI: 10.25249/0375-7536.20023214358.

- Costa, A.F.U., Shukowsky, W., Fernandes, L.A.D., Nardi, L.V.S., Bitencourt, M.F.A.S. 1995. Modelamento gravimétrico 3D do Complexo Granítico de Caçapava do Sul, RS. In: Anais do III Congresso Internacional da Sociedade Brasileira de Geofísica, Rio de Janeiro, p.753-758.
- Costanzo, A., Moore, K.R., Wall, F., Feely, M. 2006. Fluid inclusions in apatite from Jacupiranga calcite carbonatites: evidence for a fluid-stratified carbonatite magma chamber. *Lithos*, 91(1-4):208–228. DOI: 10.1016/j.lithos.2006.03.047.
- Daly, R.A. 1914. Igneous Rocks and Their Origin. McGraw-Hill, New York, N.Y.
- Dawson, J.B. 1962. Sodium carbonate lavas from Oldoinyo Lengai, Tanganyika. *Nature*, 195:1075-1076. DOI: 10.1038/1951075a0.
- Dobson, D.P., Jones, A.P., Rabe, R., Sekine, T., Kurita, K., Taniguchi, T., Kondo, T., Kato, T., Shimomura, O., Urakawa, S. 1996. In-situ measurement of viscosity and density of carbonate melts at high pressure. *Earth and Planetary Science Letters*, 143(1-4):207-215. DOI: 10.1016/0012-821X(96)00139-2.
- Downes, H., Wall, F., Demény, A., Szabo, C. 2012. Continuing the carbonatite controversy: preface. *Mineralogical Magazine*, 76(2):255-257. DOI: 10.1180/minmag.2012.076.2.01.
- Downes, P.J., Dunkley, D.J., Fletcher, I.R., McNaughton, N.J., Rasmussen, B., Lynton Jaques, A., Verrall, M., Sweetapple, M.T. 2016. Zirconolite, zircon and monazite-(Ce) U-Th-Pb age constraints on the emplacement, deformation and alteration history of the Cummins Range Carbonatite Complex, Halls Creek Orogen, Kimberley region, Western Australia. *Mineralogy and Petrology*, 110:199-222. DOI 10.1007/s00710-015-0418-y.
- Drüppel, K., Wagner, T., Boyce, A.J. 2006. Evolution of sulfide mineralization in ferrocarbonatite, Swartbooisdrif, Northwestern Namibia: constraints from mineral compositions and sulfur isotopes. *The Canadian Mineralogist*, 44(4):877-894. DOI: 10.2113/gscanmin.44.4.877.
- Eggler, D.H. 1989. Carbonatites, primary melts, and mantle dynamics. In: Bell, K. (ed.). *Carbonatites: Genesis and Evolution*. Chapman & Hall, London, U.K. p.561-579.
- Elliott, H.A.L., Wall, F., Chakhmouradian, A.R., Siegfried, P.R., Dahlgren, S., Weatherley, S., Finch, A.A., Marks, M.A.W., Dowman, E., Deady, E. 2018. Fenites associated with carbonatite complexes: A review. *Ore Geology Reviews*, 93:38-59. DOI: 10.1016/j.oregeorev.2017.12.003.
- Frantz, J.C., McNaughton, N.J., Marques, J.C., Hartmann, L.A., Botelho, N.F., Caravaca, G. 2003. SHRIMP U-Pb zircon ages of granitoids from southernmost Brazil: constrains on the temporal evolution of the Dorsal de Canguçu Transcurrente Shear Zone and Eastern Dom Feliciano belt. In: IV South American Symposium on Isotope Geology, Salvador, BA. Short Papers 1:174-177.
- Ganade de Araujo, C.E., Rubatto, D., Hermann, J., Cordani, U.G., Caby, R., Basei, M.A.S., 2014. Ediacaran 2,500-km-long synchronous deep continental subduction in the West Gondwana Orogen. *Nature Communications*, 5, 5198, p.1-8. DOI: 10.1038/ncomms6198.
- Gibson, S.A., Thompson, R.N., Leonardos, O.H., Dickin, A.P., Mitchell, J.G. 1995. The Late Cretaceous impact of the Trindade mantle plume: evidence from largevolume, mafic, potassic magmatism in SE Brazil. *Journal of Petrology*, 36(1):189-229. DOI: 10.1093/petrology/36.1.189.
- Girelli, T.J., Chemale Jr., F., Lavina, E.L.C., Laux, J.H., Bongiolo, E.M., Lana, C. 2018. Granulite accretion to Rio de la Plata Craton, based on zircon U-Pb-Hf isotopes: Tectonic implications for

- Columbia Supercontinent reconstruction. *Gondwana Research*, 56:105-118. DOI: 10.1016/j.gr.2017.12.010.
- Gittins, J. 1978. Some observations on the present status of carbonatite studies. In Proc. First Int. Symp. on Carbonatites (Poços de Caldas, Brazil). Ministério das Minas e Energia – Departamento Nacional da Produção Mineral p.107-115.
- Gittins, J. 1989. The origin and evolution of carbonatite magmas. In: Bell, K. (ed.). Carbonatites: Genesis and Evolution. Chapman & Hall, London, U.K. pp. 580-600.
- Gittins, J., Harmer, R. 1997. What is ferrocarbonatite? A revised classification. *Journal of African Earth Sciences*, 25(1):159-168. DOI: 10.1016/S0899-5362(97)00068-7.
- Gittins, J., Harmer, R.E., Barker, D.S. 2005. The bimodal composition of carbonatites: reality or misconception? *Lithos*, 85(1-4):129-139. DOI: 10.1016/j.lithos.2005.03.023.
- Goulart, R.V., Remus, M.V.D., Reis, R.S. 2013. Composição isotópica de Sr, C e O e geoquímica de ETRs das rochas carbonáticas do Bloco São Gabriel, Rio Grande do Sul. *Pesquisas em Geociências*, 40(1):75-97.
- Goulart, A.R. 2014. Geologia e petrografia do Picrito do Boqueirão e sua correlação com outras rochas maficas-ultramáficas no SW do Escudo Sul-Riograndense. Trabalho de Conclusão de Curso de Graduação em Geologia - Universidade Federal do Rio Grande do Sul, Porto Alegre, 85p.
- Harmer, R.E., Gittins, J. 1998. The case for primary, mantled-derived carbonatite magma. *Journal of Petrology*, 39(11-12):1895-1903. DOI: 10.1093/petroj/39.11-12.1895.
- Hartmann, L.A. 1987. Isócrona Sm-Nd de 2,1 Ga em minerais de duas amostras do Complexo Granulítico Santa Maria Chico, RS. In: I Congresso Brasileiro de Geoquímica, Porto Alegre, pp. 105-111.
- Hartmann, L.A. 1998. Deepest exposed crust of Brazil – Geochemistry of Paleo-proterozoic depleted Santa Maria Chico granulites. *Gondwana Research*, 1(3-4):331-341. DOI: 10.1016/S1342-937X(05)70849-2.
- Hartmann, L.A., Chemale Jr., F., Philipp R.P. 2007. Evolução geotectônica do Rio Grande do Sul no Pré-Cambriano. In: 50 Anos de geologia no Rio Grande do Sul. Editora Comunicação e Identidade, Porto Alegre, 97-123p.
- Hartmann, L. A., Liu, D., Wang, Y., Massonne, H. J., & Santos, J. O. S. 2008. Protolith age of Santa Maria Chico granulites dated on zircons from an associated amphibolite-facies granodiorite in southernmost Brazil. *Anais da Academia Brasileira de Ciências*, 80(3):543-551. DOI: 10.1590/S0001-37652008000300014.
- Heinrich, E.W. 1966: The Geology of Carbonatites. Rand McNally & Co., Chicago, Illinois.
- Heinrich, E.W. 1985: Infinite variations on a fenite theme. Indian Mineral., Sukheswala p.151-162.
- Herz, N. 1977. Timing of spreading in the South Atlantic: information from Brazilian alkalic rocks. *Geological Society of America Bulletin*, 88(1):101-112. DOI: 10.1130/0016-7606(1977)88<101:TOSITS>2.0.CO;2.
- Jones, A.P., Genge, M., Carmody, L. 2013. Carbonate melts and carbonatites. *Reviews in Mineralogy & Geochemistry*, 75(1):289-322. DOI: 10.2138/rmg.2013.75.10.

- Jost, H., Bitencourt, M.F. 1980. Estratigrafia e tectônica de uma fração da faixa de dobramentos Tijucas no Rio Grande do Sul. *Acta Geologica Leopoldensia*, 11(7):27-59.
- Junqueira-Brod, T.C., Gaspar, J.C., Brod, J.A., Jost, H., Barbosa, E.S.R., Kafino, C.V. 2005. Emplacement of Kamafugite Lavas from the Goiás Alkaline Province, Brazil: Constraints from whole-rock simulations. *Journal of South American Earth Sciences*, 18(3-4):323-335. DOI: 10.1016/j.jsames.2004.11.001.
- Kalt, A., Hegner, E., Satir, M. 1997. Nd, Sr and Pb isotopic evidence for diverse lithospheric mantle sources of East African Rift carbonatites. *Tectonophysics*, 278(1-4):31-45. DOI: 10.1016/S0040-1951(97)00093-0.
- Kapustin, Y.L. 1980. The mineralogy of carbonatites. Amerind Publ Co, New Delhi, India.
- Kogarko, L.N., Kononova, V.A., Orlova, M.A., Woolley, A.R. 1995. The Alkaline Rocks and Carbonatites of the World. 2. Former USSR. Chapman & Hall, London, U.K.
- Kresten, P. 1988. The chemistry of fenitization: examples from Fen, Norway. *Chemical Geology*, 68(3-4):329-349. DOI: 10.1016/0009-2541(88)90030-7.
- Kresten, P., Troll, V.R. 2018. The Alnö Carbonatite Complex, Central Sweden. Springer, Cham, Switzerland. p.1-53. DOI: 10.1007/978-3-319-90224-1.
- Lapin, A.V., Iwanuch, W., Ploshko, V.V. 1999. Carbonatitos lineares de cinturões móveis: uma síntese. *Revista Brasileira de Geociências*, 29(4):483-490.
- Lapin, A.V., Ploshko, V.V. 1988. Tipos morfológico-formacionais e regimes geológico-tectônicos de formação de carbonatitos. *Izv. Akad. Nauk. SSSR, Ser. Geol.* 1:66-73 (em russo).
- Laux, J.H., Toniolo J.A., Sander A., Pinto L.G.R., Parisi G., Senhorinho E.M. 2019. Seria 233 ma a idade do Carbonatito Três Estradas - Rio Grande do Sul? In: Anais do IV Simpósio Brasileiro de Metalogenia, Gramado, p. 36.
- Le Bas, M.J. 1981. Carbonatite magmas. *Mineralogical Magazine*, 44(334):133-140. DOI: 10.1180/minmag.1981.044.334.02.
- Le Bas, M. J. 1987. Nephelinites and carbonatites. In: Fitton, J. G. & Upton, B. G. J. (eds) *Alkaline Igneous Rocks*. Geological Society, London, Special Publication 30, 85–94.
- Le Bas, M.J., 2008. Fenites associated with carbonatites. *The Canadian Mineralogist*, 46(4):915-932. DOI: 10.3749/canmin.46.4.915.
- Le Maitre, R.W. (ed). 2002. *Igneous Rocks: A Classification and Glossary of Terms: Recommendations of the International Union of Geological Sciences, Subcommission on the Systematics of Igneous Rocks*. Cambridge University Press, Cambridge, 2º ed., 256p.
- Lee, W.J., Wyllie, P.J. 1994. Experimental data bearing on liquid immiscibility, crystal fractionation, and the origin of calciocarbonatites and natrocarbonatites. *International Geology Review*, 36(9):797-819. DOI: 10.1080/00206819409465489.
- Lee, W.J., Wyllie, P.J. 1997. Liquid Immiscibility in the Join NaAlSiO₄-NaAlSi₃O₈-CaCO₃ at 1 GPa: Implications for Crustal Carbonatites. *Journal of Petrology*, 38(9):1113-1135. DOI: 10.1093/petroj/38.9.1113.

- Lee, W.J., Wyllie, P.J. 1998. Petrogenesis of carbonatite magmas from mantle to crust, constrained by the system CaO-(MgO+FeO*)(Na₂O+K₂O)-(SiO₂+Al₂O₃+TiO₂)-CO₂. *Journal of Petrology* 39(3):495–517. DOI: 10.1093/petro/39.3.495.
- Leite, J.A., Hartman, L.A., Mcnaughton, N.J., Chemale Jr, F. 1998. SHRIMP U/Pb zircon geochronology of Neoproterozoic juvenile and crustal-reworked terranes in southernmost Brazil. *International Geology Review*, 40(8):688-705. DOI: 10.1080/00206819809465232.
- Levin, V.Y., Roncnson, B.M., Levin, I.A. 1978. Carbonatitos da Província Alcalina de Ilmen-Vishnovie Gory, nos Urais. *Doklady Akademii Nauk SSSR*, 240(4):930-933 (em russo).
- Lopes, C.G. 2014. Análises de U-Pb por LA-ICP-MS e SHRIMP em zircões detriticos do Complexo Passo Feio, Terreno São Gabriel: implicações geotectônicas para a evolução do Cinturão Dom Feliciano. Dissertação de mestrado, Universidade Federal do Rio Grande do Sul, Porto Alegre, 51p.
- Martinez, G.A. 2019. Caracterização petrográfica e geoquímica das rochas glimeríticas do complexo alcalino-carbonatítico Três Estradas, Lavras do Sul, RS. Trabalho de Conclusão de Curso de Graduação em Geologia - Universidade Federal do Rio Grande do Sul, Porto Alegre, 73p.
- Mitchell, R.H. 1995. Kimberlites, Orangeites and Related Rocks. Plenum Press, New York, N.Y.
- Mitchell, R.H., 2005. Carbonatites and carbonatites and carbonatites. *Canadian Mineralogist*, 43(6):2049-2068. DOI: 10.2113/gscanmin.43.6.2049.
- Monteiro, C.F., Toniolo, J.A., Bastos Abram M. 2016. Carbonatitos associados ao Escudo Sul-Riograndense, Rio Grande do Sul. In: Bastos Abram M. Projeto Fosfato Brasil – Parte II, CPRM, Salvador.
- Morales, B.A.A., Almeida, D.P.M., Koester, E., Rocha, A.M.R., Dorneles, N.T., Rosa, M.B., Martins, A.A. 2019. Mineralogy, whole-rock geochemistry and C, O isotopes from Passo Feio Carbonatite, Sul-Riograndense Shield, Brazil. *Journal of South American Earth Sciences*, 94:102-208. DOI: 10.1016/j.jsames.2019.05.024.
- Nardi, L.V.S., Hartmann, L.A. 1979. O Complexo Granulítico Santa Maria Chico do Escudo Sul-riograndense, *Acta Geologica Leopoldensia*, 6:45-75.
- Nasraoui, M. and Bilal, E. (2000) Pyrochlores from the Lueshe carbonatite complex (Democratic Republic of Congo): a geochemical record of different alteration stages. *Journal of Asian Earth Sciences*, 18(2):237-251. DOI: 10.1016/S1367-9120(99)00056-5.
- Nelson, D.R., Chivas, A.R., Chappell, B.W., McCulloch, M.T. 1988. Geochemical and isotopic systematics in carbonatites and implications for the evolution of ocean-island sources. *Geochimica et Cosmochimica Acta* 52(1):1-17. DOI: 10.1016/0016-7037(88)90051-8.
- Notholt, A.J.G. 1979. The economic geology and development of igneous phosphate deposits in Europe and the USSR. Vol 74, pp. 339-350.
- Olafsson, M., Egger, D.H. 1983. Phase relations of amphibole, amphibole-carbonate, and phlogopite-carbonate peridotite: petrologic constraints on the asthenosphere. *Earth and Planetary Science Letters*, 64(2):305-315. DOI: 10.1016/0012-821X(83)90212-1.
- Oliveira, A.D.S., Fernandez, C.A.C., Issler, R.S., Abreu, A.S., De Montalvao, R.M.G., Teixeira, W. 1975. Folha NA.21 Tumucumaque e parte da Folha NB.21; geologia, geomorfologia, pedologia,

- vegetação e uso potencial da terra. Levantamento de Recursos Minerais, Vol. 9. Projeto RADAMBRASIL, Departamento Nacional de Produção Mineral. Rio de Janeiro. 370pp.
- Paim, P.S.G., Chemale, Jr., F., Lopes, R.D.C., 2000. A Bacia do Camaquã. In: Holz, M., De Ros, L.F. (Eds.), Geologia do Rio Grande do Sul, CIGO/UFRGS, Porto Alegre, pp. 231-274.
- Parisi, G.N., Toniolo, J.A., Grazia, C.A., Pinto, L.G. 2010. Prospecção de fosfato no Rio Grande do Sul. *In: Anais do 45º Congresso Brasileiro de Geologia*, Belém.
- Philipp, R.P., Pimentel, M.M., Chemale Jr., F. 2016. Tectonic evolution of the Dom Feliciano belt in Southern Brazil: geological relationships and U–Pb geochronology. *Brazilian Journal of Geology*, 46(1):83-104. DOI: 10.1590/2317-4889201620150016.
- Philipp, R.P., Pimentel, M.M., Basei, M.A.S. 2018. The Tectonic Evolution of the São Gabriel Terrane, Dom Feliciano Belt, Southern Brazil: The Closure of the Charrua Ocean. In: Siegesmund S., Basei M., Oyhantçabal P., Oriolo S. (eds) *Geology of Southwest Gondwana. Regional Geology Reviews*. Springer, Cham, pp 243-265. DOI: 10.1007/978-3-319-68920-3_10.
- Puustinen, K. 1969. The Carbonatite of Siilinjärvi in the Precambrian of Eastern Finland: A preliminary report. Technical University, Department of mining and metallurgy, Otaniemi, Finlândia.
- Ranta, E., Stockmann, G., Wagner, T., Fusswinkel, T., Sturkell, E., Tollesen, E., Skelton, A. 2018. Fluid–rock reactions in the 1.3 Ga siderite carbonatite of the Grønnedal–Íka alkaline complex, Southwest Greenland. Contributions to Mineralogy and Petrology, 173:78 26p. DOI: 10.1007/s00410-018-1505-y.
- Ray, J.S., Pande, K., Bhutani, R., Shukla, A.D., Rai V.K., Kumar, A., Awasthi, N., Smitha, R.S., Panda, D.K. 2013. Age and geochemistry of the Newania dolomite carbonatites, India: implications for the source of primary carbonatite magma. Contributions to Mineralogy and Petrology, 166:1613-1632. DOI 10.1007/s00410-013-0945-7.
- Remus, M.V.D., Hartmann, L.A., McNaughton, N.J., Groves, D.I., Fletcher, I.R. 2000. The link between hydrothermal epigenetic copper mineralization and the Caçapava Granite of the Brasiliano Cycle in Southern Brazil. *Journal of South American Earth Sciences*, 13(3):191-216. DOI: 10.1016/S0895-9811(00)00017-1.
- Ribeiro, M., Teixeira, C.A.S. 1970. Datações de rochas do Rio Grande do Sul e sua influência nos conceitos estratigráficos e geotectônicos locais. *Iheringia, Série Geologia* 3:109-120.
- Ribeiro, M., Fantinel, L.M. 1978. Associações petrotectônicas do Escudo Sul-rio-grandense: Tabulação e distribuição das associações petrotectônicas do Rio Grande do Sul. *Iheringia, Série Geológica* 5:19-54.
- Ribeiro, M. 1980. Geossuturas do Escudo do Rio Grande do Sul. *In: Anais do 31º Congresso Brasileiro de Geologia*, Balneário Camboriú.
- Rocha, A.M.R., Dorneles, N.T., Gindri, M.D., Vargas, J.M., Alves, T.C., Benetti F.A. 2013. Descoberta dos carbonatitos Picada dos Tocos e Passo Feio e o potencial para fosfato e ETR's, Caçapava do Sul, Rio Grande do Sul. *In: Anais do III Simpósio Brasileiro de Metalogenia*, Gramado.
- Rossoni, M.B., Bastos Neto, A.C., Souza, V.S., Marques, J.C., Dantas, E., Botelho, N.F., Giovannini, A.L., Pereira, V.P. 2017. U-Pb zircon geochronological investigation on the Morro dos Seis Lagos Carbonatite Complex and associated Nb deposit (Amazonas, Brazil). *Journal of South American Earth Sciences*, 80:1-17. DOI: 10.1016/j.jsames.2017.09.021.

- Rukhlov, A.S., Bell, K., 2010. Geochronology of carbonatites from the Canadian and Baltic Shields, and the Canadian Cordillera: clues to mantle evolution. *Mineralogy and Petrology*, 98(1):11-54. DOI: 10.1007/s00710-009-0054-5.
- Rundqvist, D.V.; Gillen C. 1997. Precambrian ore deposits of the east European and Siberian cratons. Elsevier Science. 456 p.
- Ruppel, K.M.V. 2016. Geotermometria da clorita no Lineamento de Ibaré (RS). Trabalho de Conclusão de Curso de Graduação em Geologia - Universidade Federal do Rio Grande do Sul, Porto Alegre, 95p.
- Rusakov, N.F. and Kravchenko, G.L., 1986. Structure of the Chernigov carbonatite intrusion. *Geologicheskii zhurnal*, no. 4, p. 112-118.
- Senhorinho, E. M. 2012. Controle estrutural dos carbonatitos do Rio Grande do Sul: análise de produtos de sensoriamento remoto e aerogeofísicos. Trabalho de Conclusão de Curso de Graduação em Geologia - Universidade Federal do Rio Grande do Sul, Porto Alegre, 180p.
- Silva A.B.; Liberal G.S.; Issa Filho A.; Rodrigues C.S.; Riffel B.F. 1987. Depósito de fosfato em carbonatito pré-cambriano Angico dos Dias- BA. Sociedade Brasileira de Geologia, Núcleo da Bahia, Salvador, 15 p. (inédito).
- Simandl, G.J., Paradis, S. 2018. Carbonatites: related ore deposits, resources, footprint, and exploration methods. *Applied Earth Science*, 127(4):123-152. DOI: 10.1080/25726838.2018.1516935.
- Simon, S.J., Wei, C., Ellmies, R., Yang, H., Tamehe, L.S. 2017. New SIMS U-Pb age on zircon from the Epembe carbonatite dyke, NW Namibia: Implications for Mesoproterozoic evolution of carbonatites at the southern margin of the Congo Craton. *Journal of African Earth Sciences*, 135:108-114. DOI: 10.1016/j.jafrearsci.2017.08.011.
- Shand, S.J. 1943. *Eruptive Rocks*. J. Wiley & Sons, New York, N.Y.
- Sharygin, I.S., Litasov, K.D., Shatskiy, A., Safonov, O.G., Golovin, A.V., Ohtani, E., Pokhilenko, N.P. 2017. Experimental constraints on orthopyroxene dissolution in alkali carbonate melts in the lithospheric mantle: Implications for kimberlite melt composition and magma ascent. *Chemical Geology*, 455:44-56. DOI: 10.1016/j.chemgeo.2016.09.030.
- Tappe, S., Foley, S.F., Jenner, G.A., Kjarsgaard, B.A. 2005. Integrating ultramafic lamprophyres into the IUGS classification of igneous rocks: rationale and implications. *Journal of Petrology* 46(9):1893-1900. 10.1093/petrology/egi039.
- Thivierge, S., Roy, D.-W., Chown, E.H. et Gauthier, A., 1983. Évolution du complexe alcalin de St.-Honoré (Québec) après sa mise en place. *Mineralium Deposita*, 18:267-283. DOI: 10.1007/BF00206214.
- Thompson, R.N., Gibson, S.A. 1991. Subcontinental mantle plumes, hot spots and pre-existing thinspots. *Journal of the Geological Society, London* 148:973-977. DOI: 10.1144/gsjgs.148.6.0973.
- Toni, G.B., Bitencourt, M.F., Nardi, L.V.S., Florisbal, L.M., Almeida, B.S., Geraldes, M. 2020. Dom Feliciano Belt orogenic cycle tracked by its pre-collisional magmatism: The Tonian (ca. 800 Ma) Porto Belo Complex and its correlations in southern Brazil and Uruguay. *Precambrian Research*, 342:105702. DOI: 10.1016/j.precamres.2020.105702.

- Toniolo, J.A., Parisi, G.N., Grazia, C.A., Reischl, J.L. 2010. Prospecção de fosfato na região de Três Estradas, Lavras do Sul, RS. In: IV Simpósio de Exploração Mineral, Ouro Preto.
- Toniolo, J.A., Remus, M.D., Parisi, G.N., Dani, N. 2013. Dois eventos carbonatíticos temporalmente distintos no RS: tipos linear e central. In: Anais do VIII Simpósio Sul-brasileiro de Geologia, Porto Alegre-RS, Sociedade Brasileira de Geologia.
- Toyoda, K., Horiuchi, H., Tokonami, M. 1994. Dupal anomaly of Brazilian carbonatites - geochemical correlations with hotspots in the South-Atlantic and implications for the mantle source. *Earth and Planetary Science Letters*, 126(4):315-331. DOI: 10.1016/0012-821X(94)90115-5.
- Tuttle, O.F., Gittins, J. 1966. Carbonatites. John Wiley & Sons, New York, N.Y.
- VanDecar, J.C., James, D.E., Assumpção, M. 1995. Seismic evidence for a fossil mantle plume beneath South America and implications for plate driving forces. *Nature*, 378:25-31. DOI: 10.1038/378025a0.
- Verplanck, P.L., Van Gosen, B.S., Seal, R.R., McCafferty, A.E., 2014. A deposit model for carbonatite and peralkaline intrusion-related rare earth element deposits. In: *Mineral Deposit Models for Resource Assessment*. No. 2010-5070-J in *Scientific Investigations*. U.S. Geological Survey, p.1-58.
- Wall, F. & Zaitsev, A. N. (eds). 2004. Phoscorites and Carbonatites from Mantle to Mine: the Key Example of the Kola Alkaline Province. The Mineralogical Society Series nº 10, 498p. London: The Mineralogical Society of Great Britain and Ireland.
- Winter, J.D. 2001. An introduction to igneous and metamorphic petrology. Prentice Hall Upper Saddle River, New Jersey. 669p.
- Woolley, A.R. 1982. A discussion of carbonatite evolution and nomenclature, and the generation of sodic and potassic fenites. *Mineralogical Magazine*, 46(338):13-17. DOI: /10.1180/minmag.1982.046.338.03
- Woolley, A.R. 1987. The Alkaline Rocks and Carbonatites of the World. 1. North and South America. British Museum (Natural History), London, U.K.
- Woolley, A.R. 2001. The Alkaline Rocks and Carbonatites of the World. 3. Africa. The Geological Society, London, U.K.
- Woolley, A.R. 2003: Igneous silicate rocks associated with carbonatites: their diversity, relative abundances and implications for carbonatite genesis. *Periodico di Mineralogia*, 72:9-17.
- Woolley, A.R. 2019. Alkaline Rocks and Carbonatites of the World, Part 4: Antarctica, Asia and Europe (excluding the former USSR), Australasia and Oceanic Islands. The Geological Society, London, U.K.
- Woolley, A.R., Kempe, D.R.C. 1989. Carbonatites: nomenclature, average chemical composition. In: Bell, K. (ed.). *Carbonatites: Genesis and Evolution*. Chapman & Hall, London, U.K. p.1-14.
- Woolley, A.R., Kjarsgaard, B.A. 2008. Paragenetic types of carbonatites as indicated by the diversity and relative abundances of associated silicate rocks: evidence from a global database. *The Canadian Mineralogist*, 46(4):741-752. DOI: 10.3749/canmin.46.4.741.

- Woolley, A.R., Bailey, D.K. 2012. The crucial role of lithospheric structure in the generation and release of carbonatites: geological evidence. *Mineralogical Magazine*, 76(2):259-270. DOI: 10.1180/minmag.2012.076.2.02.
- Wyllie, P.J. 1989. Origin of carbonatites: evidence from phase equilibrium studies. In: Bell, K. (ed.). *Carbonatites: Genesis and Evolution*. Chapman & Hall, London, U.K. p.500-545.
- Wyllie, P.J., Tuttle, O.F. 1960: The system CaO–CO₂–H₂O and the origin of carbonatites. *J. Petrol.* 1(1):1-46. DOI: 10.1093/petrology/1.1.1.
- Yang, K.F., Fan, H.R., Santosh, M. Hu, F.F., Wang, K.Y. 2011. Mesoproterozoic mafic and carbonatitic dykes from the northern margin of the North China Craton: Implications for the final breakup of Columbia supercontinent. *Tectonophysics*, 498:1-10. DOI 10.1016/j.tecto.2010.11.015.
- Yuhara, M., Hirahara, Y., Nishi, N., Kagami, H. 2005. Pb-Sr, Sm-Nd ages of the Phalaborwa Carbonatite Complex, South Africa. *Polar Geoscience*, 18:101-113.
- Zharikov, V.A., Pertsev, N.N., Rusinov, V.L., Callegari, E., Fettes, D.J., 2007. Metasomatism and metasomatic rocks. In: Recommendations by the IUGS Subcommision of the Systematics of Metamorphic Rocks. British Geological Survey.
- Ziebell, A. 2013. Caracterização geoquímica do Meta-carbonatito Três Estradas (Lavras do Sul) pelo método de fluorescência de raios-X portátil. Trabalho de Conclusão de Curso de Graduação em Geologia - Universidade Federal de Pelotas, Pelotas.